

UNIVERSITÉ DU QUÉBEC À MONTRÉAL

CU-AU SKARN MINERALIZATIONS OF THE ARCHEAN EAST SULLIVAN
STOCK, ABITIBI GREENSTONE BELT, QUEBEC, CANADA

THESIS
PRESENTED
AS PARTIAL REQUIREMENT
OF THE MASTERS OF EARTH SCIENCES

BY
FLORENT BIGOT

FEVRIER 2021

UNIVERSITÉ DU QUÉBEC À MONTRÉAL

LES MINÉRALISATIONS A CU-AU DE TYPE SKARN DU STOCK DE EAST
SULLIVAN, CEINTURE DE ROCHES VERTES DE L'ABITIBI, QUÉBEC,
CANADA

MÉMOIRE

PRÉSENTÉ

COMME EXIGENCE PARTIELLE
DE LA MAÎTRISE EN SCIENCES DE LA TERRE

PAR

FLORENT BIGOT

FEVRIER 2021

UNIVERSITÉ DU QUÉBEC À MONTRÉAL
Service des bibliothèques

Avertissement

La diffusion de ce mémoire se fait dans le respect des droits de son auteur, qui a signé le formulaire *Autorisation de reproduire et de diffuser un travail de recherche de cycles supérieurs* (SDU-522 – Rév.10-2015). Cette autorisation stipule que «conformément à l'article 11 du Règlement no 8 des études de cycles supérieurs, [l'auteur] concède à l'Université du Québec à Montréal une licence non exclusive d'utilisation et de publication de la totalité ou d'une partie importante de [son] travail de recherche pour des fins pédagogiques et non commerciales. Plus précisément, [l'auteur] autorise l'Université du Québec à Montréal à reproduire, diffuser, prêter, distribuer ou vendre des copies de [son] travail de recherche à des fins non commerciales sur quelque support que ce soit, y compris l'Internet. Cette licence et cette autorisation n'entraînent pas une renonciation de [la] part [de l'auteur] à [ses] droits moraux ni à [ses] droits de propriété intellectuelle. Sauf entente contraire, [l'auteur] conserve la liberté de diffuser et de commercialiser ou non ce travail dont [il] possède un exemplaire.»

REMERCIEMENTS

Je voudrais tout d'abord remercier mon directeur de maîtrise Michel Jébrak, Professeur émérite (UQAM), de m'avoir fait confiance tout au long de ce long et ambitieux projet. Je le remercie pour son encadrement, ses précieux conseils et son apport scientifique qui ont permis de mener à bien cette maîtrise. Je le remercie également pour son soutien et pour les nombreuses possibilités qu'il m'a offertes de présenter mes travaux dans de nombreux congrès et conférences.

Je tiens à remercier l'ensemble du personnel d'Alexandria Minerals et plus particulièrement Philippe Berthelot pour son accueil chaleureux, et nos conversations enrichissantes sur la géologie de Val-d'Or. Merci de m'avoir ouvert les portes d'Alexandria et de m'avoir fait découvrir le métier de géologue d'exploration.

Un grand merci également à Pierre-Etienne Mercier géologue d'Alexandria, pour m'avoir formé et pris sous son aile lors de mes passages dans la Compagnie.

Un grand merci à Marc Choquette (U. Laval), Audrey Lavoie (UQAC), Robert Creaser (U. Alberta) et Jean-François Hélie (UQAM) pour leur aide dans les analyses et l'acquisition de données respectivement à la microsonde, au LA-ICPMS, pour la datation de la molybdénite et les isotopes de la calcite.

Un grand merci également à MITACS, CONSOREM, DIVEX pour m'avoir octroyé des financements et permis de mener à terme cette maîtrise.

Une pensée également pour tous les géologues, professeurs et spécialistes qui ont apporté un regard complémentaire sur le sujet, et tout particulièrement à Lucie Mathieu, Stéphane De Souza, Pierre Pilote, Mehmet Taner.

Enfin je tiens également à remercier ma Maman qui a toujours été là pour moi ainsi que mon petit frère Clément, et bien évidemment ma compagne Crystal qui m'a accompagnée et soutenue tout au long de ces années d'étude.

AVANT-PROPOS

Ce mémoire est rédigé sous la forme d'un article scientifique qui sera soumis à la revue *Economic Geology* sous le titre *Cu-Au Skarn Mineralizations of the Archean East-Sullivan Stock, Abitibi Greenstone Belt, Quebec, Canada*. Sa présentation diffère des mémoires habituellement présentés à l'UQAM du fait de l'utilisation de l'anglais pour la rédaction et du positionnement des figures et des tableaux à la fin de l'article. Michel Jébrak, le directeur de maîtrise, est co-auteur de cet article. Ce format de mémoire a été choisi car il donne l'opportunité de transmettre de nouvelles connaissances à la communauté scientifique à l'échelle internationale.

TABLE DES MATIÈRES

AVANT-PROPOS	iv
LISTE DES FIGURES.....	vii
LISTE DES TABLEAUX.....	ix
LISTE DES ABRÉVIATIONS, DES SIGLES ET DES ACRONYMES	x
RÉSUMÉ	xii
ABSTRACT.....	xiv
INTRODUCTION GENERALE	1
CHAPITRE I CU-AU SKARN MINERALIZATIONS OF THE ARCHEAN EAST-SULLIVAN STOCK, ABITIBI GREENSTONE BELT, QUEBEC, CANADA.....	7
1.1 Introduction.....	7
1.2 Regional geology.....	9
1.3 Geologic setting of the Val-d’Or district.....	10
1.3.1 Stratigraphy.....	10
1.3.2 Plutonism	11
1.3.3 Economic geology.....	12
1.4 Sampling and analytical techniques.....	14
1.5 Geology of the East Sullivan Stock.....	15
1.5.1 Petrography of the ESS	15
1.5.2 Geochemistry of intrusive rocks	18
1.5.2.1 East Sullivan Stock	18
1.5.2.2 Associated porphyry dikes	20
1.5.3 Alteration in the East Sullivan Stock	21
1.5.3.1 Potassic alteration.....	21

1.5.3.2	Phyllic alteration	22
1.5.3.3	Propylitic alteration.....	23
1.5.4	Mineralization in the intrusion	23
1.5.4.1	Cu-Mo ± Au porphyry style mineralization.....	23
1.5.4.2	Cu-Mo vug-associated mineralization	25
1.6	Exoskarn in the Héva Formation	26
1.6.1	Skarn host rocks	26
1.6.2	Hornfels and metasomatism area	27
1.6.3	Ore gangue mineralogy	30
1.6.3.1	Garnet.....	30
1.6.3.2	Magnetite.....	31
1.6.3.3	Amphibole.....	33
1.6.3.4	Epidote	34
1.6.3.5	Carbon and oxygen isotope on calcite	35
1.6.4	Cu-Au-Ag skarn mineralization in Héva Formation.....	36
1.7	Thermometry of the East Sullivan skarn system	38
1.7.1	Zircon	38
1.7.2	Amphibole.....	39
1.7.3	Biotite.....	40
1.7.4	Chlorite.....	43
1.8	Discussion.....	44
1.8.1	Skarn or VMS ?.....	44
1.8.2	Archean intrusion-related Cu-Au-Ag skarn formation	45
1.8.3	Cu-Au-Mo porphyry mineralizations.....	47
1.8.4	Magma fertility.....	49
1.8.5	ESS emplacement.....	51
1.8.6	ESS magma evolution.....	52
1.8.7	Regional implication	54
1.8.8	Comparisons with other skarn deposits.....	57
1.9	Conclusion	60
	BIBLIOGRAPHIE	102
	CONCLUSION GENERALE.....	126
	APPENDICE A DETAILED ANALYTICAL METHODS	128
	APPENDICE B SUPPLEMENTARY DATA.....	134

LISTE DES FIGURES

Figure	Page
Figure 1.1 Geology of the Abitibi greenstone belt.....	62
Figure 1.2 Simplified geologic map of the East-Sullivan Stock area, South-East of Val-d'Or	63
Figure 1.3 Cross-section, geological, geophysical map and cross-section of the East-Sullivan intrusion' south border.	65
Figure 1.4 Hand specimen photographs of samples of the East-Sullivan porphyry facies	67
Figure 1.5 Major element geochemistry plots for rocks of the East Sullivan intrusive suite.....	69
Figure 1.6 Normalized trace element abundances of the East-Sullivan facies	71
Figure 1.7 Hand specimen photographs and photomicrographs of alteration	72
Figure 1.8 Drill core logs with geochemical profiles of selected elements and ratios for mineralized zone.	74
Figure 1.9 Hand specimen photographs and photomicrographs of mineralized phase and zone within the ESS and in the Héva Formation.....	76
Figure 1.10 Paragenetic sequence diagram of the ESS skarn mineralization.....	78
Figure 1.1 Hand specimen photographs and photomicrographs of host rock, hornfels and skarn from Héva Formation.....	79

Figure 1.12 Composition of representative mineral from the south border of the ESS.	81
Figure 1.13 Photomicrographs, backscattered electron (BSE) images, and electron microprobe analysis profiles for representative garnets	83
Figure 1.14 Multi-element box and whisker plots of trace elements analyzed by LA-ICP-MS of igneous and hydrothermal magnetite. Multielement variation diagrams for hydrothermal magnetite	84
Figure 1.15 Schematic model of the East-Sullivan Stock and related intrusions emplacement in the Val d'Or district.....	86
Figure 1.16 Extended trace element for Lamaque, Triangle and ESS intrusions profiles normalized to chondrites from McDonough and Sun (1995).....	87

LISTE DES TABLEAUX

Tableau	Page
Tableau 1.1 Whole-rock major elements composition for the East-Sullivan Stock and associated rocks	88
Tableau 1.2 Trace element abundances determined by solution ICP-MS for rocks of the area	89
Tableau 1.3 Re-Os data and model ages for molybdenite from E.S.S Cu-Mo-Au porphyry mineralization.....	92
Tableau 1.4 Microprobe Analyses of Amphiboles	93
Tableau 1.5 Microprobe Analyses of Epidote.....	95
Tableau 1.6 Microprobe Analyses of Mica.....	96
Tableau 1.7 Microprobe Analyses of Chlorite.....	98
Tableau 1.8 Carbon and oxygen isotopic composition of calcite veins from ESS skarn.....	99
Tableau 1.9 Estimation of temperature for different phases in ESS and associated skarn.....	100
Tableau 1.10 Comparison with other skarn occurrences	101

LISTE DES ABRÉVIATIONS, DES SIGLES ET DES ACRONYMES

APFU: Atom per formula unit

CIPW: Norm used for the calculation of normative mineralogy of a rock sample based on quantitative chemical analysis

ESS: East-Sullivan stock

EP: Early porphyry

HFSE: High-field-strength elements (Zr, Hf, Nb, Ta, Ti, P, U, Th)

HREE: Heavy rare earth elements (Er, Tm, Yb, Lu)

ICP-MS: Inductively coupled plasma mass spectrometry is a type of mass spectrometry that uses an Inductively coupled plasma to ionize the sample to detect metals and several non-metals at very low concentrations (ppb)

IP: Intermediate porphyry

LA-ICP-MS: Laser ablation inductively coupled plasma mass spectrometry

LILE: Large ion lithophile elements (Cs, Rb, K, Ba, Sr)

LOI: Loss on ignition

LREE: Light rare earth elements (La, Ce, Pr, Nd)

LP: Late porphyry

MALI/ASI: Modified alkali-lime index / Aluminium saturation index

MP: Mineralized porphyry

MREE: Middle rare earth elements (Sm, Eu, Gd, Tb, Dy, Ho)

PPM: Part per million

PPB: Part per billion

QAP: Quartz, Alkali feldspar, Plagioclase ternary diagram used to classify igneous rocks

QFP: Quartz-feldspar porphyry diorite dike

REE: Rare earth elements (LREE, MREE, HREE)

WT%: Weight percent, corresponds to the proportion relative to total rock weight

RÉSUMÉ

Le district aurifère de Val-d'Or (mines Lamaque, Sigma, Goldex) représente l'archétype des minéralisations aurifères "orogéniques", liées aux circulations de fluides métamorphiques tardi-orogéniques. Cependant, près de ces gisements et indices bien connus, plusieurs minéralisations aurifères atypiques ont été découvertes. Certaines de ces minéralisations sont principalement concentrées au niveau de la bordure sud du pluton d'East-Sullivan, immédiatement au nord de la faille Cadillac au sud-est de la ville de Val-d'Or. La zone a été largement explorée depuis les années 1930 et a permis la découverte d'indices à $\text{Cu} \pm \text{Au} \pm \text{Mo}$ (Ducros Zone1 et 2) au niveau de la bordure sud du pluton d'East-Sullivan. La minéralisation à l'intérieur de l'intrusion peut être subdivisée en deux sous-types : porphyrique et disséminée en remplissage de géodes. Les deux sous-types sont caractérisés par de la chalcopyrite et de la pyrite avec une quantité variable de molybdénite contenues dans des faciès intrusifs porphyriques fortement altérés (principalement altération potassique et propylitique). Au cours des années 1960, une campagne d'exploration a permis de découvrir les zones Orenada 2 et 4, des gisements de type orogénique au sein de la faille Cadillac plus au sud. Dans le secteur du pluton d'East-Sullivan, les volcanites mafiques interstratifiées avec les filons-couches et les dykes gabbroïques de la Formation de Héva sont plissées et métamorphisées au faciès des schistes verts.

Le Stock d'East Sullivan est une suite intrusive composite comprenant des monzonites et des syénites et partage certaines affinités avec la famille des sanukitoïdes syn-Timiskaming. Cette suite porphyrique est reliée aux nombreuses intrusions tonalitiques et dioritiques des gisements Lamaque et Triangle situés au Nord-Est de l'intrusion. Elle pourrait avoir joué un rôle actif dans la formation de la minéralisation aurifère

orogénique de la zone. Au sud du contact de l'intrusion avec les volcanites, les 200 premiers mètres sont fortement altérées et bréchifiées et contiennent un second type de minéralisation à Cu ± Au ± Ag, découverte pour la première fois en 1938 (Oramaque Zone 3, Zone Hogg et Zone Porphyre), puis fréquemment dans la Formation de Héva jusqu'à récemment (Orenada Zone 5). Cette minéralisation se caractérise par des sulfures disséminés ou stockworks et des corps minéralisés massifs riches en sulfures de remplacement (chalcopyrite ± pyrite ± pyrrhotite), localement enrichis en or et associés à des assemblages calco-silicatés (principalement amphibole calcique, carbonate et épidote) et de la magnétite massive. Entre l'intrusion et la zone minéralisée, des zones à grenats associées à de la magnétite, épidote, des carbonates et des amphiboles ont été fréquemment rencontrées aux indices Orenada Zone 3 & 5, Hogg, Porphyre et Jolin. Les zones minéralisées forment au sud de l'intrusion des corridors subparallèles. Ce style de minéralisation est très similaire à la mine Akasaba, située à 10 km plus à l'est, qui a été interprétée comme un skarn. Le secteur du pluton d'East Sullivan est un cas exceptionnel de coexistence de minéralisation périplutonique (porphyre et skarn), volcanogène (mine East-Sullivan) et orogénique d'or et de cuivre dans la ceinture de l'Abitibi, reflétant la métallogénie or-cuivre développée dans la région.

Mots clés : Archéen, Abitibi, Cu-Au, intrusion, porphyre, skarn.

ABSTRACT

The gold-bearing district of Val-d'Or (Lamaque, Sigma, Goldex) represents the archetype of "orogenic" gold mineralizations related to circulation of late-orogenic metamorphic fluids. However, near these well-known deposits and showings, several atypical gold mineralizations have been discovered. These mineralizations are mainly concentrated at the southern edge of the East Sullivan Stock (ESS), immediately north of the Cadillac Break southeast of the town of Val-d'Or. The area has been extensively explored since the 1930s and has allowed the discovery of several Cu ± Au ± Mo showings (Ducros Zones 1 and 2) within the southern edge of the East Sullivan Stock. The mineralization within the intrusion can be subdivided into two sub-types: porphyry-style and vug filling. Both sub-types are characterized by chalcopyrite and pyrite with variable amounts of molybdenite hosted in strongly altered porphyritic intrusive facies (mainly potassic and propylitic alteration). During the 1960s, an exploration campaign allowed the discovery of Orenada Zones 2 and 4, which are orogenic type deposits within the Cadillac Break further south. In the East Sullivan Stock area, the mafic volcanics interbedded with sills and gabbroic dykes of the Héva Formation are folded and metamorphosed to greenschist facies.

The East Sullivan Stock is an intrusive composite suite composed of monzonites and syenites and it shares some affinities with the syn-Timiskaming sanukitoids family. The porphyry suite is related to the numerous tonalitic and dioritic intrusions associated with the Lamaque and Triangle deposits, located in the northeast of the intrusion. The ESS may have played an active role in the formation of the orogenic gold mineralization in the area. South of the contact of the intrusion with the volcanics, the first 200 meters of the volcanic rocks are strongly altered and brecciated. They host a

second type of mineralization (Cu ± Au ± Ag) first discovered in 1938 (Oramaque Zone 3, Zone Hogg and Zone Porphyre), and then frequently found in the Héva Formation until now (Orenada Zone 5). This mineralization is characterized by disseminated sulfide or stockworks and massive sulfide-rich replacement bodies (chalcopyrite ± pyrite ± pyrrhotite), locally enriched in gold associated with calc-silicate assemblages (mainly Ca-amphibole, carbonate, and epidote) and massive magnetite. Between the intrusion and the mineralized area, garnet zones associated with magnetite, epidote, carbonates, and amphiboles have been frequently encountered at Orenada Zones 3 and 5, Hogg, Porphyre and Jolin showings. Ore zones form sub-parallel corridors to the intrusion. This style of mineralization is very similar to the Akasaba mine, located 10 km further east, that has been interpreted as a skarn deposit. The East Sullivan pluton sector is an exceptional case of coexistence of periplutonic (porphyry and skarn), volcanogenic (East Sullivan mine) and orogenic gold and copper mineralization in the Abitibi belt, indicating the protracted gold-copper metallogeny in the area.

Keywords : Archean, Abitibi, Cu-Au, intrusion, porphyry, skarn

INTRODUCTION GENERALE

Le district aurifère de Val-d'Or (mines de Lamaque et Sigma) constitue l'archétype des minéralisations en or dite « orogéniques », reliées aux circulations de fluides métamorphiques à la fin des orogènes (Robert et Brown, 1986; Goldfarb et Groves, 2015). Cependant, il existe dans ce district des indices d'or qui présentent des caractéristiques différentes.

C'est le cas des projets Porphyre et Ducros, d'abord détenus par la compagnie Alexandria Minerals puis maintenant par la compagnie O3 Mining. Ces projets sont localisés à 7 kilomètres au sud-est de la ville de Val-d'Or. Le secteur de ces projets chevauche la limite sud de l'intrusion de East-Sullivan (Taner, 1996), en contact avec les roches volcaniques de la Formation de Héva. La zone de faille de Cadillac passe à 500 m au sud de l'intrusion. L'exploration de ce secteur a débuté au milieu des années 1930 avec la découverte des premiers indices de Cu et Au associés à des veinules de chalcopryrite dans l'intrusion de East Sullivan. Un deuxième type de minéralisation à $\text{Cu} \pm \text{Au} \pm \text{Ag}$ a été découvert en 1938 (Bubar and Beaudry, 1986; Bubar and Cooke, 1987) à 300 mètres au sud de l'intrusion (Oramaque Zone 3, Zone Hogg et Zone Porphyre), et fréquemment rencontré depuis dans la Formation de Héva (Orenada Zone 5, Carrier et al. (2004)). Ce dernier type de minéralisation est caractérisé par un assemblage à chalcopryrite \pm pyrrhotite \pm pyrite \pm magnétite contenu dans des assemblages calco-silicatés à actinolite-tremolite, grenat, carbonate et épidote. Durant les années 60, une dizaine de forages ont recoupé pour la première fois, à l'intérieur de l'intrusion, des minéralisations de style porphyrique à Cu-Mo-Au, associées à des zones d'altération potassique (Ducros Zone 1 & 2) (Bérubé, 1969). Par la suite,

l'exploration s'est principalement concentrée le long de la faille Cadillac avec la découverte des zones d'or orogénique Orenada 2 et 4 (Robert et al., 1990).

La minéralisation autour du pluton de East Sullivan présente des similitudes avec le gisement de l'ancienne mine Akasaba, localisé 6 km à l'est de l'intrusion. Le modèle métallogénique de la mine Akasaba a été discuté auparavant. On pensait initialement qu'il s'agissait d'un gisement stratiforme de type amas sulfuré, affecté par un métamorphisme de contact à épidote-hornblende-actinolite (Lebel, 1987). Cependant, Vorobiev (1998) a démontré que les faciès observés correspondent à ceux de skarns, et donc d'une minéralisation magmatique en relation avec une intrusion. Ces skarns auraient commencé par une phase prograde, marquée par le grenat, le clinopyroxène, l'épidote, la titanite et la magnétite ; suivie par une phase rétrograde à épidote, magnétite, hornblende, actinolite, biotite, chlorite, quartz, calcite (Vorobiev, 1998; Pilote et al., 2000).

Ces minéralisations périphériques sont associées à l'intrusion de East Sullivan, un pluton qui présente des caractéristiques particulières (Taner, 1996). En effet, il appartient à la famille du magmatisme sanukitoïde tel que défini par Laurent et al., (2014) et Moyen, (2019), syn-Timiskaming, magmatisme à l'origine de plusieurs importants gisements d'or (ex : Beattie, Robert (2001); Bigot and Jébrak (2015) et Lac Bachelor, Fayol and Jébrak (2017)). La présence de ces skarns, suivant la définition d'Einaudi and Burt (1982) et Meinert et al. (2005), posent donc une question fondamentale pour la métallogénie de l'or en Abitibi. Le modèle « orogénique » de l'or stipule que les minéralisations sont reliées directement au fonctionnement des grands accidents crustaux, avec des fluides métamorphiques (Robert et Brown, 1986; Goldfarb et Groves, 2015). Un modèle alternatif relierait les minéralisations à une première phase magmatique d'origine mantellique, suivie par des reprises structurales. L'étude du pluton de East Sullivan et des minéralisations associées permet de tester ces hypothèses, notamment concernant l'existence d'un possible lien entre les

minéralisations du pluton de East Sullivan et de Sigma-Lamaque, gisement typique orogénique, et donc sur la contribution du pluton à la métallogénie du district de Val-d'Or. Cette étude est donc susceptible de contribuer significativement à la compréhension métallogénique de l'or, en analysant les relations génétiques entre le plutonisme et les minéralisations en or.

L'objectif de ce projet de recherche est d'approfondir la compréhension métallogénique des minéralisations associées au pluton de East-Sullivan et de comprendre la signification du développement de porphyres à cuivre, molybdène et des skarns à cuivre et or dans le district de Val-d'Or. Pour cela ont été réalisés des travaux de terrain sur les décapages disponibles, des levés sur les forages, des échantillonnages tant de faciès intrusifs que de minéralisations, la réalisation de coupes, de plans pour comprendre la distribution de la minéralisation et des altérations, suivis d'études pétrographiques et minéralogiques au microscope électronique à balayage afin d'obtenir un aperçu des successions paragénetiques de la bordure Sud du pluton. L'interprétation des analyses des intrusifs associés (éléments majeurs et traces) a permis de réaliser une classification et de comprendre la pétrogenèse de l'intrusif, et notamment les relations entre les différents faciès et la minéralisation. Enfin l'étude en détail des minéraux d'altération à l'intérieur et à l'extérieur de l'intrusion a permis d'affiner le modèle génétique et le modèle de gisement dans la zone d'étude.

Ce mémoire est présenté sous la forme d'un article scientifique qui sera soumis dans une revue scientifique ayant pour thème la géologie économique. L'article a été rédigé par le premier auteur et le second auteur est Michel Jébrak, agissant en qualité de directeur de maîtrise. Son implication s'est faite par la génération du sujet, de pistes de recherches et des axes de réflexion, d'aide sur le terrain, du suivi de l'avancement du projet et de la rédaction. A cela il faut ajouter un travail de relecture et un soutien financier.

L'article introduit d'abord la problématique du projet de recherche et les principales questions du projet de recherche. Ensuite, une synthèse de la géologie régionale puis du district de Val-d'Or, comprenant la stratigraphie, le plutonisme et la géologie économique est présentée. Les techniques analytiques et une remarque quant à la terminologie employée dans l'article précédent l'étude de l'intrusion. Cette étude s'intéresse d'abord à la pétrographie et à la chronologie de mise en place du pluton, suivie de la géochimie détaillée des différents faciès ainsi que des dikes apparentés. Elle se poursuit par l'étude des différentes altérations observables dans l'intrusion ainsi que des minéralisations localisées dans la bordure sud de l'intrusion. Elle est suivie par une seconde étude concernant les formations environnantes, suivant un axe Nord-Sud depuis l'intrusion jusqu'aux éléments les plus éloignés. Elle s'intéresse aux roches hôtes et altérations associées aux minéralisations à Cu-Au-Ag dans le secteur de Val-d'Or, une des thématiques importantes de ce sujet de recherche. Une étude détaillée de la minéralogie est faite à la fin de cette partie suivie par une partie sur la thermométrie du système à l'aide de la minéralogie. Une discussion vient proposer une explication quant au lien entre les minéralisations observées, le district de Val-d'Or et l'intrusion de East-Sullivan. Un modèle génétique est proposé, ainsi que des comparaisons avec d'autres minéralisations similaires. La conclusion synthétise cet ensemble en mettant l'emphase sur les points clés du sujet d'étude et les avancées réalisées au cours du projet.

Des données complémentaires sont données dans les appendices à la suite de l'article. Elles comprennent le détail des méthodes analytiques employées dans l'article ; respectivement l'analyse des roches totales, les analyses des minéraux à la microsonde, la datation de la molybdénite par la méthode Re/Os, et enfin l'analyse des isotopes de l'oxygène et du carbone sur des échantillons de carbonates, et enfin l'analyse des magnétites par ablation laser. A la suite de ces méthodes, une série de tableaux a également été insérée, contenant les données complètes des analyses réalisées figurant dans ce projet. Le lecteur peut y trouver respectivement la liste des échantillons utilisés,

leur localisation et une brève description, les analyses complètes des plagioclases, grenats, amphiboles, biotites et chlorites, et enfin le détail des analyses des matériaux de référence utilisés pour la calibration des analyses de magnétites par ablation laser.

Références

- Bigot, L. and Jebrak, M. (2015). Gold Mineralization at the syenite-hosted Beattie Gold deposit, Duparquet, Neoproterozoic Abitibi belt, Canada. *Economic Geology*, 110, 315-335.
- Bubar, D. S. and Beaudry, C. (1986). *Geological Compilation Report, Oramaque Property, Bourlamaque Twp., Quebec*. Unpublished private report for Aur Resources Inc.
- Bubar, D. S. and Cooke, D. R. (1987). *Report on the 1987 Diamond drilling program, Oramaque Property, Project 410, Bourlamaque Tp, Quebec*. (Vol. GM47650 Ministère de l'Énergie et des Ressources naturelles du Québec). Aur Resources Inc.
- Carrier, A., Savard, C. and Berthelot, P. (2004). *Resultats de la campagne d'exploration, Hiver 2003-2004, propriété Orenada, projet 17407, Canton Bourlamaque, Québec*. (Vol. GM462121 Ministère de l'Énergie et des Ressources naturelles du Québec). Alexis Minerals Corporation.
- Einaudi, M. T. and Burt, D. M. (1982). Introduction Terminology, Classification, and Composition of Skarn Deposits. *Economic Geology*, 77, 745-754.
- Fayol, N. and Jébrak, M. (2017). Archean Sanukitoid Gold Porphyry Deposits: A New Understanding and Genetic Model from the Lac Bachelor Gold Deposit, Abitibi, Canada. *Economic Geology*, 112(8), 1913-1936. doi: 10.5382/econgeo.2017.4534

- Goldfarb, R. J. and Groves, D. I. (2015). Orogenic gold: Common or evolving fluid and metal sources through time. *Lithos*, 233, 2-26. doi: 10.1016/j.lithos.2015.07.011
- Laurent, O., Martin, H., Moyen, J. F. and Doucelance, R. (2014). The diversity and evolution of late-Archean granitoids: Evidence for the onset of “modern-style” plate tectonics between 3.0 and 2.5Ga. *Lithos*, 205, 208-235. doi: 10.1016/j.lithos.2014.06.012
- Lebel, J. (1987). *Gîtologie de la mine d'or Akasaba, Abitibi, Québec*. (Msc thesis). Ecole Polytechnique, Montréal.
- Meinert, L., Dipple, G. M. and Nicolescu, S. (2005). World Skarn Deposits. *Economic Geology, 100th Anniversary Volume*, 299-336.
- Moyen, J.-F. (2019). Archean granitoids: classification, petrology, geochemistry and origin. *Geological Society, London, Special Publications*. doi: 10.1144/sp489-2018-34
- Pilote, P. (2000). *Géologie de la région de Val d'Or, sous-province de l'Abitibi volcanologie physique et évolution métallogénique*. (Ministère des Ressources naturelles du Québec) (Vol. MB 2000-09).
- Robert, F. (2001). Syenite-associated disseminated gold deposits in the Abitibi greenstone belt, Canada. *Mineralium Deposita*, 36, 503-516
- Robert, F., Brommecker, R. S. and Bubar, D. (1990). The Orenada Zone 4 Deposit: Deformed veine-type gold mineralization within the Cadillac tectonic zone, SE of Val-d'Or. *Institut Canadien des mines et de la métallurgie, Spécial 43*, 255-268.
- Robert, F. and Brown, A. C. (1986). Archean gold-bearing quartz veins at the Sigma Mine, Abitibi Greenstone belt, Quebec. Part I. Geologic relations and formation of the veins system. *Economic Geology*, 81, 578-592.

CHAPITRE I

CU-AU SKARN MINERALIZATIONS OF THE ARCHEAN EAST-SULLIVAN STOCK, ABITIBI GREENSTONE BELT, QUEBEC, CANADA

1.1 Introduction

The Neoproterozoic Abitibi greenstone belt, located in the southeastern part of the Superior Province of Canada, is well known as hosting several multi-million ounce Archean gold deposits (Poulsen et al., 2000; Goldfarb et al., 2005; Gosselin and Dubé, 2005; B. Dubé, and Gosselin, 2007; B. Dubé, et al., 2015; Monecke et al., 2017; Poulsen, 2017). These precious and base metal deposits are distributed between Au-Cu-Zn volcanogenic massive sulfide deposits, komatiite-associated Ni-Cu-(PGE) deposits within the different volcanic assemblages of the Abitibi, and numerous gold camps located along the Larder Lake-Cadillac (e.g., Kirkland Lake, Matachewan, Malartic and Val-d'Or) and the Destor-Porcupine fault zones (e.g., Timmins-Porcupine, Duparquet; Monecke et al., 2017 and references therein). Most of the gold deposits belong to the orogenic clan (Robert et al., 2005), whereas some gold deposits share common characteristics with magmatic-hydrothermal gold systems (Sillitoe, 1991; Robert and Poulsen, 1997; Robert, 2001; Groves et al., 2003) and are recognized to be spatially associated with or related to intrusions (e.g., B. Dubé, et al. 2015), with an inferred genetic link between mineralization and magmatic-hydrothermal fluids for some of these deposits (Cameron and Hattori, 1987; Robert, 2001; Bigot and Jébrak, 2015; Fayol and Jébrak, 2017; Mériaud and Jébrak, 2017; Nadeau, 2019 and references

therein). A number of these deposits are associated with ~2680 to 2670 Ma alkaline to subalkaline porphyritic syenite to quartz monzonite intrusions. They have been defined as syenite-associated disseminated gold deposits in the vicinity of sedimentary Timiskaming-type basins developed along major fault zones (Robert, 2001).

The East Sullivan Stock (ESS) is located on the north side of the Cadillac-Larder Lake fault zone and in the vicinity of the town of Val-d'Or. The district has been considered archetypal of orogenic gold deposits since the pioneering work of Robert and Brown (1986a). However, several atypical mineralized zones have been recognized, including Cu-Au-Mo zones developed within the ESS and Cu-Au-Ag zones associated with magnetite and calc-silicate replacement assemblages in the Héva Formation. The Cu-Au-Ag mineralized zones forms subparallel corridors to the south border of the ESS, associated with garnet-magnetite-epidote-carbonates-amphibole zones.

This contribution presents new petrographic and geochemical data for the Archean ESS and its surrounding formations. This study focuses on the southern border of the intrusion and provides a relative chronology and an explication of the relationships between the various porphyritic facies of the ESS. Using drill core logging, geologic field work, mineral compositions, stable isotopes, as well as lithochemical data and Re-Os molybdenite geochronology, we propose a new interpretation of the atypical copper-gold mineralization and associated hydrothermal alterations in this area. The specific objectives of this study are to determine the link between the ESS and: (1) the Cu-Au mineralizations; (2) the gold mineralization in the Val-d'Or district; and (3) other similar mineralized systems associated with Neoproterozoic plutons.

The composition and mutual associations of the alteration and their distribution with respect to the mineralization inside and outside the intrusion demonstrate the presence of an uncommon Cu-Au skarn-type mineralization associated with porphyry-style Cu-Mo-Au zones along the southern border of the ESS. This stock therefore played an

active role in the hydrothermal system, the formation of favorable conduits for the magmatic-hydrothermal fluid circulation, and metasomatism. Gold mineralization in the Val-d'Or district appears partly from magmatic origin.

1.2 Regional geology

The Abitibi Subprovince consists of a large Archean greenstone belt located in the southern part of the Superior Province in the Canadian Shield (Card and Ciesielski, 1986; Card, 1990; Monecke et al., 2017). The belt is bounded by the Mesoproterozoic Grenville Province on the east and the Kapuskasing uplift in the western Ontario area (Figure 1.1). This subprovince is mainly composed of continuous metavolcanic and metasedimentary belts cored by large magmatic domains, mainly granitoids alternating with east-trending formations of turbiditic wackes (Ayer et al., 2002).

Several major E-W trending fault zones truncate the supracrustal rocks and intrusions of the Abitibi Greenstone Belt (Figure 1.1). In the southern part of the belt, the Porcupine-Destor and the Cadillac-Larder Lake fault zones (CLLFZ) delimit the Timmins-Val-d'Or gold belt (Robert et al., 2005). The CLLFZ is a major and complex crustal structure, separating the supracrustal rocks of the Pontiac and Abitibi subprovinces in Quebec (Daigneault et al., 2002; Thurston et al., 2008). The suture is interpreted as a succession of faults segments (Rafini, 2014; Bedeaux et al., 2017), mainly northerly dipping, but variation of strike and dip occurs between the fault segments. These variations are the consequence of multiple stages during the formation of the CCLFZ with accretions of various original structures (Robert, 1989; Rafini, 2014; Bedeaux et al., 2017; Poulsen, 2017). The Pontiac Subprovince ($<2682.7 \pm 1.9$ Ma; Mortensen and Card 1993) is mainly composed of metasedimentary rocks intruded by late-tectonic granitic intrusions. The regional metamorphism in the Abitibi Greenstone Belt occurred around 2660 Ma (Hanes et al., 1992; Robert et al., 2005; Tremblay et al.,

2020) and is at subgreenschist facies to locally amphibolite facies at the fringes of late tectonic intrusions (Dimroth et al., 1983; Faure, 2015)

1.3 Geologic setting of the Val-d'Or district

The Val-d'Or district (Figure 1.2) is part of the Southern Volcanic Zone (Chown et al., 1992). This volcano-sedimentary sequence is composed of mafic and felsic volcanic and volcanoclastic rocks of the Malartic and Louvicourt Groups, both of Neoproterozoic age (2714 ± 2 Ma to 2704 ± 2 Ma; Wong et al., 1991; Pilote et al., 1998 and 1999), and levels of sedimentary rocks (<2687 Ma; Mortensen and Card, 1993; Davis, 2002) of the Cadillac Group (Pilote et al., 2015).

1.3.1 Stratigraphy

The oldest volcanic rocks of the area, the Jacola Formation (Figure 1.2), is composed of an assemblage of mafic and locally ultramafic units and corresponds to the upper part of the Malartic Group. The Louvicourt Group further south overlies the previous formations and is represented by the Val-d'Or and the Héva Formations, two distinct volcanic cycles. The Val-d'Or Formation (2704 - 2705 Ma; Wong et al. 1991; Machado and Gariépy 1992; Pilote et al. 1998) in contact with the Malartic Group (Figure 1.2), is composed of submarine lavas and volcanoclastics, mainly intermediate to mafic in the north and more intermediate towards the south. The volcanic rocks exhibit a transitional to calc-alkaline affinity (Desrochers et al., 1996). The younger Héva Formation (2702 ± 1 Ma; Pilote et al. 2000) contains mafic to intermediate volcanoclastics, pyroclastics and numerous dikes and syngenetic gabbro sills disturbing the small sedimentary levels. An horizon of spherulitic dacite characterizes the base all along the Héva Formation over 20km (Scott et al., 2002). These volcanoclastic deposits were followed by several episodes of sedimentation corresponding locally to the Cadillac Group (2688 Ma, Davis 1991) and the Pontiac

Group (~2685 Ma, Davis 2002; De Souza et al. 2017; 2682.7 ± 1.9 Ma Mortensen and Card 1993). The Cadillac Group is composed of thin bands of wackes, pelites and polymictic conglomerates separated from the Pontiac sandstones and pelites by the Piché Group ($>2709.5 \pm 2$ Ma, Pilote et al. 2014). The Piché Group rocks, predominantly intermediate to ultramafic, are highly deformed and mainly expose bands of talc-chlorite-carbonate schist, but cumulate textures characteristic of ultramafic rocks can be observed in preserved areas. South of the ESS, the CLLFZ is developed within the Piché Group, but also encompasses some of the rocks of the Cadillac Group in the Orenada area (Robert, 1989), where the volcano-sedimentary formations are mainly oriented E-W and dip steeply to the north.

1.3.2 Plutonism

Several intrusive rocks intersect the volcanic rocks in the area. The largest on the north side of the ESS is the synvolcanic Bourlamaque Pluton (2700 ± 1 Ma; Wong et al. 1991) consisting of intrusive phases of diorite to quartz diorite composition (Campiglio and Darling, 1976; Jébrak et al., 1991; Lemarchand, 2012). A large proportion of the intrusive rocks intrudes the Val-d'Or Formation and presents in the west of the ESS a dioritic to tonalitic composition with an age between 2704 ± 1 Ma (Wong et al., 1991) in the Sigma-Lamaque zone and 2684 ± 1.2 Ma (J. Dubé, 2018) for the most recent dikes in the Triangle zone (Figure 1.2). To the east, the intrusions are mostly porphyry diorite sills interspersed in the volcanites such as the Dunraine sill. Monzonitic intrusions such as the Sabourin and Calahan plutons in the vicinity of the old Akasaba mine intersect the volcanic sequences in the southern part of the Val-d'Or area. The East Sullivan intrusion (2684 ± 1 Ma; Pilote et al. 1999), a composite circular stock intrudes the central part of the area, north of the CLLFZ (Figure 1.2). The composite stock of calc-alkaline composition (Taner, 1996; Pilote et al., 2000) displays strongly altered porphyry phases of interpreted dioritic to monzonitic composition (Norman,

1943; Assad, 1958). Finally, Paleoproterozoic NE-SW diabase dikes record the youngest plutonic event in the district.

1.3.3 Economic geology

The Val-d'Or district is historically known for the Sigma-Lamaque gold complex, an archetype of mesothermal gold deposits (Robert and Poulsen, 1997). The Sigma and Lamaque mines, located at the eastern limit of the city of Val-d'Or, are hosted in the volcanic rocks of the Val-d'Or Formation (Figure 1.2). Since the discovery of the Lamaque mine in 1923, the cumulative production exceeded 10 Moz from 1935 to 2008 (Sauvé et al., 1993; J. Dubé, 2018), mainly from large quartz-carbonate-tourmaline vein systems spatially associated with shear zones (Robert and Brown, 1986a). The Val-d'Or Formation is also known to host some volcanogenic massive sulfide deposits such as the East Sullivan deposit, which is adjacent to the ESS, and from which was produced 15 Mt of ore grading 1.07% Cu, 4.0% Zn, 7.92 g/t Ag and 0.27 g/t Au from 1949 to 1966 (Lavoie, 2003).

The southern edge of the ESS also hosts many mineralized occurrences (Figure 1.2 and Figure 1.3A). The first discoveries of gold showings in the area between the ESS and the CLLFZ were made in 1923 (Bayne, 1985), in the Héva Formation (Orenada Zone 1, Mid-Canada South Zone). Gold was extracted at the Mid-Canada mine, which produced 89,269 t of ore at 2.26 g/t Au and 1.7 g/t Ag until 1983 (Bayne, 1985; Khobzi et al., 1986), and at the Orenada Zone 4 with a production of 20,418 t of ore at 1.85 g/t Au (Gagnon and David, 1982). The Orenada Zone (formally Zones 2 and 4) consists of two generations of auriferous quartz-tourmaline-albite-carbonate-arsenopyrite veins in the rocks south of the ESS, within the CLLFZ (Robert et al., 1990). Gold-bearing veins have been observed in high strain zones in all rock formations between the ESS and the Pontiac Group, but they occur mainly in the volcanoclastic rocks in the Cadillac Group. In the 2018 resource estimate for Orenada Zones 2 and 4, total indicated resources were estimated at 3,754,000 t of ore at 1.61 g/t Au for a total of 194,533 oz

(Savard et al., 2018). Minor gold occurrences are also found within the ESS in quartz veins or shear zones.

In addition to the gold mineralization, the study area hosts several copper showings associated with other metals such as gold, silver, or molybdenum. All these mineralized zones are associated with strong positive magnetic geophysical anomalies (Figure 1.3B). These copper showings, subject of this study, may be classified by their position relative to the ESS: 1) within the intrusion and in the contact area with the Héva Formation; 2) outside the intrusion and contained by Malartic Group volcanic rocks. The first type of mineralization, discovered in 1968 (Bérubé, 1969), mainly consists of a broad zone of $\text{Cu} \pm \text{Mo} \pm \text{Au}$ mineralization (Ducros Zones 1 and 2) contained in the porphyritic facies of the ESS. This Cu mineralization in the intrusion can be subdivided into two sub-types: porphyry-style and in vug-filling or replacement. Both sub-types are characterized by chalcopyrite and pyrite with variable amounts of molybdenite.

The second type of mineralization of $\text{Cu} \pm \text{Au} \pm \text{Ag}$ was first discovered in 1938 (Bubar and Beaudry, 1986; Bubar and Cooke, 1987), 300 meters south of the intrusion (Oramaque Zone 3, Zone Hogg and Zone Porphyre), and then frequently found in the Héva Formation (Orenada Zone 5; Carrier et al. 2004). This mineralization is characterized by disseminated sulfides or stockworks and massive sulfide-rich replacement bodies (chalcopyrite \pm pyrrhotite \pm pyrite \pm magnetite) hosted in hydrothermally altered rocks of the Héva Formation by calc-silicate association (mainly Ca-amphibole, carbonate, and epidote). Between the ESS and the mineralized area, garnet-rich zones associated with epidote, carbonates, amphibole, and magnetite have frequently been encountered (Orenada Zones 3 and 5). This $\text{Cu} \pm \text{Au} \pm \text{Ag}$ mineralization has been described and interpreted as a probable skarn (Carrier et al., 2004) similar to the Akasaba deposit 6 km further east, also interpreted as a skarn (Vorobiev, 1998).

1.4 Sampling and analytical techniques

Mineralized and hydrothermally altered zones, as well as their host rocks, were examined in drill core except for two rocks obtained from the single accessible outcrop, due to the poorly exposed area. Samples, locations, and analyses are listed in Appendix Table B1. Thirty representative samples from the area were selected for petrographic observations using polarized and reflected light microscopy. Thirty-two samples were selected for whole-rock geochemical and trace element analysis in order to document the chemical and mineralogical variations proximal to, distal to, and within the intrusion. Analyses were performed by ICP-AES, XRF and ICP-MS (sixty-five elements were analyzed) following lithium metaborate/tetraborate fusion and dilute nitric acid digestion. Determination of the concentration of F and titration of Fe was also performed on five samples from the ESS. Ten calcite-rich samples from the Héva Formation in the skarn zone were selected for $\delta^{13}\text{C}$ and $\delta^{18}\text{O}$ determination. One sample of molybdenite from a quartz-carbonate-biotite-chalcopyrite-molybdenite vein from the ESS was collected for Re-Os dating. Almost all thin sections were used for microprobe mineral analysis to identify textural and chemical variations in the hydrothermally altered rocks, mineralized zones and the least altered protoliths. Average mineral compositions are given in Table 1.4-1.7, and the full dataset is provided in the Appendices Table B2-B6. A selection of magnetite grains from inside the ESS and surrounding mineralized rocks was also analyzed by LA-ICP-MS analysis. Detailed analytical methods are described in Appendix 1. Complete analyses for magnetite are given in Appendix Table B4, and the LA-ICP-MS dataset calibration is provided in the Appendix Table B8.

1.5 Geology of the East Sullivan Stock

The ESS was formerly known as the Center Post Intrusion due to its central position in the Bourlamaque Township (Bérubé, 1974). It owes its current name to the former East Sullivan mine located in its western part. For the purposes of this article the East Sullivan Stock name, or ESS, will be retained. The ESS is not well exposed at the surface but is distinct on geophysics images as a composite magnetic zone surrounded by a highly magnetic halo in contact with the Val-d'Or and Héva Formations' volcanic rocks (Figure 1.3B). The stock is roughly circular with a slightly larger radius from east to west (5 km) than north-south (4 km) and covers an area of 16.2 km². The intrusion has a steep northern contact against the Val-d'Or Formation rocks, a contact inclined at 85° east on the western side in the vicinity of the old East Sullivan mine and an uncertain inclination in the east side. The southern contact against the Héva Formation dips north at 60° (Bérubé, 1974; Taner, 1996) with an unclear transition between the intrusion and the mafic volcanic rocks. This transition corresponds to a mixture of intensely silicified, altered and fractured rocks with numerous apophyses and dikes cutting through the strongly altered surrounding rocks of the Héva Formation (Figure 1.3C).

1.5.1 Petrography of the ESS

In the study area, the ESS is composed of three main intrusive phases which have undergone several phases of hydrothermal alteration. These were distinguished based on their mineralogy and texture, and their relative age was determined from crosscutting relationships. These three phases are, from oldest to youngest: early (EP), intermediate (IP) and late (LP) porphyries (Figure 1.4A-D).

The EP is a porphyritic micro-grained facies (Figure 1.4A) that composes most of the pluton and occupies the central part of it. It is also the only facies available in outcrop

(Figure 1.4E). The EP contains altered megaphenocrysts of albitic composition (An1.5-3) (Appendix Table A2) in a microcrystalline matrix. The mostly euhedral phenocrysts may have a preferential orientation and often contain epidote, apatite, and Fe-Mg minerals inclusions. Sodium cobaltinitrite staining on the samples showed a pervasive yellow coloration which suggests a strong presence of K-minerals in the fine-grained matrix. Lack of quartz is characteristic of the EP facies. Clusters of coarse accessory minerals composed of an assemblage of abundant euhedral to subhedral apatite (200-700 μm), magnetite (200-500 μm), titanite (100 μm) and fine biotite (300-100 μm) are distributed throughout the massive porphyritic rock. Zircon grains are present as biotite inclusion emphasized by their characteristic pleochroic radiation halos. Few minute grains of euhedral pyrite and magnetite are quite frequent in the matrix.

The IP includes numerous facies, all of which have a porphyritic texture. The intermediate phases all have in common the presence of Fe-Mg minerals clusters, giving them a cumulo-phyrlic texture (Figure 1.4B-C) or even glomeroporphyritic when the clusters are essentially composed of biotite. IP facies show textural continuity with the early phase by the progressively decreasing abundance of the albite megaphenocrysts and the increasing grain size in the matrix with formation of smaller plagioclase phenocrysts (500 μm to 1cm). These plagioclase crystals present similar compositions (An1.5-3) but systematically have a core highlighted by the presence of small epidote grains and irregular boundaries. Preserved areas show that the core has a richer calcic composition (An10-13). Unlike the EP facies, IP facies contain generally between 1 and 5% interstitial quartz (100-500 μm) with frequent undulose extinction and interlobate grain boundaries. Pseudomorphs can be observed near the Fe-Mg clusters with complete replacement of original minerals, probably hornblende amphiboles, by quartz, biotite, and epidote assemblages. Accessory minerals consist of euhedral apatite (200-800 μm), coarse euhedral to subhedral titanite (100 μm -1cm) and anhedral magnetite grains (<200 μm).

The IP facies can be subdivided based on their spatial distribution and association with mineralization. The facies in the northern part of the intrusion (IP1) is barren and is not associated with any known mineralized occurrence (Figure 1.4B). IP1 is the texturally closest phases to EP with coarse-grained texture but with a much larger amount of phenocrysts (up to 70% modal). IP1 dominates in the northern part of the stock in contact with the Val-d'Or Formation but has also been observed in the southeastern part of the intrusion. Contact between IP1 and EP seems to be gradual. The southern porphyries (IP2) are associated with copper and molybdenum mineralization. IP2 forms a belt along the southern contact between EP and the Héva Formation and frequently cuts the EP facies (Figure 1.3C; Figure 1.4F).

The LP facies (Figure 1.4D) occur mainly as dikes intersecting the EP and IP facies (Figure 1.3C; Figure 1.4G). LP facies exhibits a coarse-grained texture roughly equigranular and locally aplitic. The composition of plagioclase phenocrysts ranges between albite and oligoclase with interlobate grain boundaries. From core to rim, the calcicity of zoned plagioclase crystals varies from An₂₀₋₁₀ to An₀₋₁, respectively. Oscillatory zoning is also outlined by epidote inclusions, with epidote being more abundant in cores. The zoned grains could suggest that oligoclase was the primary composition of the plagioclase in LP. K-feldspars are usually rimming plagioclase phenocrysts with frequent perthite unmixing, but they also locally consist of subhedral interstitial crystals. Some euhedral to subhedral albite plagioclases (An_{0.5-1}) are also present with polysynthetic twinning often distinguishable. The LP is the only phase to present large interstitial quartz (up to 10% modal) (Figure 1.4D) with frequent undulose extinction and coarse (500-1000 μm) euhedral to subhedral hornblende (Figure 1.4D) in least altered samples. Small masses of anhedral magnetite and euhedral titanite (<500 μm) associated with rare euhedral apatite grains (500 μm -800 μm) are disseminated between the phenocrysts. The presence of neograins, recrystallization textures such as sutured grain boundaries and frequent undulose extinction of quartz grains indicate that the ESS underwent some subsequent strain.

Pale gray dikes are also frequent in the border zone of the intrusion. These dikes are texturally similar to the ESS (Figure 1.4H) and crosscut the IP, the Val-d'Or Formation west of the ESS, and the Héva Formation south and east of the ESS (Figure 1.3C; Figure 1.4I). They exhibit a porphyritic texture with euhedral to subhedral plagioclase (1 to 10 mm), in a fine to medium grayish matrix that makes up to 30 to 50% of the mode. Plagioclase is commonly altered to sericite and epidote. The matrix is mainly quartzo-feldspathic in composition. Ferro-magnesian minerals occur as clusters of amphibole and biotite that are frequently altered to chlorite and associated with minor amounts of ilmenite grains (<200 μm), anhedral titanite (anatase) and euhedral to subhedral apatite (300-500 μm).

1.5.2 Geochemistry of intrusive rocks

1.5.2.1 East Sullivan Stock

Geochemical data for the ESS porphyry suites rocks are presented in Tables 1.1 and 1.2 and Figures 1.5 and 1.6. Nomenclature of ESS rocks has never been constant in the literature (diorite-syenite-monzonite; Assad 1958; Bérubé 1974, Taner 1996, Mercier and Berthelot 2017) due to the presence of alteration disturbing the concentration of major elements, commonly mobile during metamorphism and alteration (Kerrick and Wyman, 1996 and references therein). Lack of outcrop for the majority of the facies and the different sampling campaigns did not allow a consensus to be reached by previous authors. The rocks of the ESS suite have SiO_2 contents of 55 to 66 wt%, ranging from an intermediate to felsic composition. Least altered samples have LOI values <1.5 wt%. Major (Al_2O_3 , Fe_2O_3 , MgO , CaO) and minor oxides (TiO_2 , P_2O_5) are negatively correlated with SiO_2 (Figure 1.5A-B, Table 1.2). The whole rock compositions of the ESS porphyry rocks reported by Taner (1996) (mainly EP facies) and Mercier and Berthelot (2017) show similar values and a good correlation with the samples from this study. However, the P_2O_5 concentration reported by Taner (1996) for EP facies show more dispersion in bivariate Harker diagrams and are lower (0.05-

0.5 wt%) than the P_2O_5 concentration from this study (0.46-0.53) (Figure 1.5B). The correlations are consistent with differentiation from early (EP) to more advanced and late facies (LP). The use of silica in discrimination diagrams is often problematic due to mobility of this element influenced by the alteration processes. The presence of quartz veins and veinlets in the samples (carefully avoided in this work) should be considered when interpreting the results. Despite these challenges, the amount of silica in samples seems to be reliable with chemical fractionation and with the relative chronology observed. However, the K_2O contents exhibit a more scattered pattern and a weak negative correlation with SiO_2 (Table 1.2). This may be related to a possible presence of K-minerals related to the hydrothermal alteration in the samples analyzed. The alteration box plot from Large et al. (2001) (Figure 1.5C) and the alkali/alumina ratio diagram from Davies and Whitehead (2006) (Figure 1.5D) suggest that the rocks are relatively fresh despite a weak phyllic alteration (Davies and Whitehead, 2010), confirmed in thin sections by the presence of muscovite partially replacing plagioclase phenocrysts in EP facies. This explains the dispersion of K_2O values in the EP samples. The fluorine content of the samples decreases from 900 ppm for EP to 600 ppm for LP. There is a significant difference in the quantity of fluorine between the intermediate facies of the north (IP1: 900 ppm) and the south (IP2: 500 ppm), consistent with the strong similarities between EP and IP1.

Classification based on calculation of normative minerals determined with the CIPW calculation for porphyry rocks of the East-Sullivan suite, suggests a monzonite to syenite composition (Figure 1.5E) in the QAP diagram (Streckeisen, 1974) modified by Le Maitre (1976). The composition is consistent with the classification based on immobile or less mobile elements (Winchester and Floyd, 1977) (Figure 1.5F). Using the criteria of Frost et al. (2001) and Frost and Frost (2008) for granitoids classification, ESS rocks show a subtle alkalic affinity (MALI: $Na_2O + K_2O - CaO$ of 3.2 to 8.7 for 55 to 66 wt% SiO_2) and a metaluminous composition ($AI > 1$ and ASI 0.85-1) in agreement with minerals observed in thin sections and CIPW classification.

In addition, ESS porphyry rocks are typically rich in Ba (>1000 ppm) and Sr (>1300 ppm) and characterized by variable concentrations of transition elements V (50-150 ppm), Cr (20-30 ppm), Co (3-12 ppm), Ni (4-12 ppm) and Sc (4-10 ppm). Base metals and especially Mo, Cu, Sb are in variable amounts, increasing in facies in association with the mineralizations.

Chondrite-normalized rare earth element (REE) (McDonough and Sun, 1995) profiles (Figure 1.6A) show similar parallel patterns for the rocks of the ESS. All facies exhibit light and medium rare earth element enrichments (LREE, MREE) with a strong fractionation expressed by $La_{(N)}/Yb_{(N)}$ ranging from 13 to 15 except for IP2 from the southern border with a lower fractionation ($La_{(N)}/Yb_{(N)}$ ranging from 9.7 to 13). Porphyritic rocks have flat or slightly negative Eu anomalies with Eu/Eu^* ranging from 0.80 to 1.1, where $Eu/Eu^* = Eu_{chondrite}/([Sm_{chondrite} \times Gd_{chondrite}]^{0.5})$ and a pattern for heavy rare earth elements (HREE) that is mostly flat. Total REE content decreases from EP facies to LP facies. REE profiles are consistent with the structural relationships seen in outcrop, establishing a relative chronology between co-magmatic facies with the youngest phase EP.

Primitive mantle-normalized (Hofmann, 1988) extended trace element patterns (Figure 1.6B) are characterized by strong to moderate enrichment for the large ion lithophile elements (LILE: Ba, Rb, Th, K and Sr), low concentrations of high field strength elements (HFSE: Nb, Ta, Zr, Hf and Ti), with strong negative Nb, Ta, Ti characteristic anomalies. This pattern remains largely similar between the ESS facies.

1.5.2.2 Associated porphyry dikes

In the bivariate Harker diagrams, the pale grey porphyry dikes composition is correlated to the ESS composition except for the Al_2O_3 contents (Figure 1.5A-B). Classification ranges between monzodiorites to granodiorites (Figure 1.5E). The content of Ba (<600 ppm), Sr (<650 ppm), Cr (110 ppm) and Ni (46 ppm) differs from

ESS rocks, but the content in transition elements and base metals remains equivalent for most geochemical elements.

REE normalized profiles (McDonough and Sun, 1995) for the grey dikes show a similar and parallel pattern to the ESS rocks (Figure 1.6A) with strong REE fractionation expressed by $La_{(N)}/Yb_{(N)}$ ranging from 16.1 to 16.7, Eu anomalies ranging from 0.84 to 0.87 and a flat pattern for HREE. The same behavior is observed in normalized extended trace element patterns (Figure 1.6B) (Hofmann, 1988) with enrichment in LILE, low concentration of HFSE and strong negative Nb, Ta and Ti anomalies.

All these characteristics suggest a link between the grey dikes and the ESS. Similar dikes have been encountered in the vicinity of the Sigma-Lamaque and Triangle deposits where an age of 2694 ± 2 Ma was obtained (Wong et al., 1991). Nevertheless, south of the ESS no dating is available for these dikes and mutual cross-cutting between the intrusions is lacking. The trace element patterns and the geochemical signature of the grey dikes instead suggest a magmatic affinity with the ESS.

1.5.3 Alteration in the East Sullivan Stock

The ESS is characterized by several overlapping hydrothermal alteration envelopes of variable intensity. The different types of alteration do not seem to be related to a specific facies of the intrusion considering the variations observed within the same rock phases. Three main characteristic assemblages of decreasing temperature in the intrusion have been identified: (1) potassic with biotite-microcline-quartz-magnetite assemblage; (2) phyllic with sericite-quartz \pm pyrite assemblage; and (3) propylitic represented by epidote \pm chlorite \pm calcite assemblage.

1.5.3.1 Potassic alteration

The most common alteration of the intrusion is a potassic alteration expressed in all facies, and particularly intense in the southern part of the intrusion. Cobaltinitrite

staining highlights two forms of K-alteration: in cross-cutting veins (Figure 1.7A) made of microcline and biotite in association with granoblastic quartz; and pervasive (Figure 1.7B) in the matrix of porphyritic rocks with the formation of micro-grains of biotite and secondary K-feldspar. The latter is also found in interstitial filling or rimming the plagioclase crystals. Hydrothermal biotite resulting from K-alteration forms aggregates with K-feldspar and quartz and can sometimes form pseudomorphs of biotite in association with quartz after magmatic minerals (Figure 1.7C). The pseudomorphic replacement could be a phenomenon of biotitization of magmatic hornblende during the K-metasomatism (Brimhall et al., 1984).

1.5.3.2 Phyllic alteration

In all facies in association with the potassic alteration or in partial overprinting, a diffuse phyllic alteration is common and results in sericitization of orthoclase and feldspar-plagioclase with formation of secondary micaceous minerals in aggregates. Sericite can be abundant, obliterating primary magmatic assemblages in strong alteration areas (Figure 1. 7D-E) and associated in highly altered areas with calcite and actinolite. The phyllic-style alteration observed in the E.S.S is typical of a hydrothermal alteration with the lack of oriented sericite grains and the replacement of the feldspar plagioclase and orthoclase by micaceous minerals. In association with this alteration, euhedral pyrite grains can be observed and they locally form discontinuous pyritic zones in the area. Although generally subsequent to the potassium alteration, the phyllic alteration may be anterior in some areas (mainly EP facies). This overlap is evidenced by fresh intergranular microclines surrounding sericitized plagioclase and is interpreted in porphyry system as anomalous offsetting relationships (Seedorf and Einaudi, 2004). The overlap of sericite assemblages of moderate temperature by potassic assemblages of high temperatures involves a succession of hydrothermal fluids from successive porphyritic intrusions. This anomalous overlap of alterations in

the EP facies is consistent with geochemical observations, implying the establishment of a porphyritic co-magmatic suite to form the ESS.

1.5.3.3 Propylitic alteration

Biotites and amphiboles are frequently altered to chlorite following cleavages and giving rise to some isomorphs surrounded by small grains of titanium-bearing minerals (sphene and/or rutile) released by newly formed chlorite (Figure 1.7F). Propylitic alteration is dominated by epidote, common in the surrounding area and frequent in the intrusion. Epidotization mainly consists of fine-grained epidote inclusions associated with the more calcic portions of plagioclase laths (Figure 1.7G). Epidote can also form interstitial grains between feldspar and after Fe-Mg minerals. Small associated calcite veins are common with interstitial epidote. Epidotization may also form thin veins crosscutting the phenocrysts and matrix of EP rocks (Figure 1.7H). The crosscuts and overlaps of the original mineral assemblages by propylitic assemblages testify to a relatively late establishment of this alteration in the intrusion.

Another alteration causing frequent color changes in the pluton facies is hematization. Hematite is found along veins and veinlets as well as on some fracture planes, and it occurs as fracture-filling in the plagioclase, highlighting mineral zonation. Mostly diffuse in the intrusion, it may be locally intense in early facies (Figure 1.7I) and it is common to find carbonate-quartz vein or carbonate filling in highly hematized areas. Generally quite late in the system, hematization seems to predate the late hydrous alteration phase associated with chlorite replacement and vein.

1.5.4 Mineralization in the intrusion

1.5.4.1 Cu-Mo \pm Au porphyry style mineralization

Mineralization is associated with the intermediate porphyritic intrusion (IP2) (Figure 1.3C and Figure 1.4C) in area of variable potassic alteration, accompanied by

reddening of the rocks and numerous quartz veins. Widespread epidotization is frequent along the mineralized zone and pervasive magnetite is locally intense. Mineralization is essentially composed of pyrite and chalcopyrite forming a relatively continuous Cu-mineralization (Figure 1.8A) through the intermediate porphyry facies. Sulfides mainly occur as stringers, in fracture coatings (Figure 1.9A), locally in millimetric to centimetric clusters or associated with quartz-biotite or magnetite veins. Native copper (Figure 1.9B) was observed in intervals of higher-grade copper content (>0.2%). Scattered molybdenite grains are associated with the mineralization. Molybdenite may be relatively abundant when associated with quartz veins (Figure 1.9C) in high grade intervals forming Cu-Mo ore zones in the stock. These intervals (Figure 1.8A) show a correlation between Cu and Mo content as well as significant Te enrichment (>10 ppm). In the intrusion, gold and copper are well correlated in contrast to Au and Mo content.

This Cu-Mo mineralization also continues outside the intrusion, within the adjacent volcanic rocks of the Louvicourt Group. The contact area between the ESS and the volcanic rocks is characterized by an intensely brecciated zone composed of a heterogeneous mixture of centimetric to decametric fragments of mafic volcanics, porphyritic dikes and part of the intrusion. The contact is strongly magnetic, highly silicified and carries a chalcopyrite-molybdenite mineralization. In this area, indistinctly from the host rock, the mineralization is essentially composed of pyrite, chalcopyrite and molybdenite occurring as stringers, in fractures and disseminations, spatially associated with quartz and magnetite veins. The mineralization provides areas of anomalous molybdenite concentrations (up to 300 ppm), higher in IP2 than in the mafic rocks, and well correlated (Figure 1.8A) with the copper concentration (up to 0.3%). In the contact intervals, gold content remains relatively low (<0.1 g/t) and seems to not be correlated with the mineralization. However, these intervals have a significant tellurium enrichment -between 10 and 20 ppm- mainly contained within the mafic rocks, and well correlated with the iron content (up to 10%).

A sample of Cu-Mo \pm Au mineralization in the ESS was sampled for Re/Os dating. The sampled molybdenite grains, forming rich patches, were associated with a quartz vein in the intermediate porphyry facies (Figure 1.9C). The analyzed grains have relatively high Re contents (\sim 492 ppm, Table 1.3), which is common for molybdenite in porphyry-style Cu-Mo deposits (Sinclair et al., 2016). The model age of 2695 ± 12 Ma (within analytical and decay constant uncertainty) is in good agreement and overlaps the 2684 ± 1 Ma U-Pb age (Pilote et al., 1999) of the ESS.

1.5.4.2 Cu-Mo vug-associated mineralization

The historic higher-grade Cu-Mo (e.g., average of 0.22% Cu and 0.02% Mo over 170 meters in the 1960s; Mercier and Berthelot 2017) mineralized zones (Ducros Zones 1 and 2) are associated with a medium-grained intrusion with granular to porphyritic texture, chemically and petrographically strongly similar to IP2 (Figure 1.5-6) except for an enrichment in Cu and Mo (Table 1.2). The mineralized porphyry (MP) is located in the contact between the ESS and the Héva Formation near the surface (Figure 1.3C) and is probably eroded in its major part. The main textural difference between MP and IP2 in sharp contact (Figure 1.9D) is the high porosity of MP, with characteristic vugs accounting for 3 to 5% of the rock, filled by secondary minerals and mineralization (Figure 1.9E), which are common characteristics of episyenites (Suikkanen and Rämö, 2019). Filling minerals mainly consist of amphibole, epidote, apatite, anatase, magnetite, sulfides, and fine-grained secondary quartz. Secondary minerals form after primary ferromagnesian minerals, such as biotite altered to chlorite by pseudomorphic replacements. The mineralization is disseminated in the vuggy-intrusion and is composed of chalcopyrite in systematic association with epidote patches and variable actinolite content inside the vugs (Figure 1.9E). Planar contact surface between subhedral chalcopyrite and epidote indicates probable equilibrium crystallization. Although they fill the vugs, massive epidote patches can overlap and replace primary

minerals. These replacement areas have relatively higher chalcopyrite and magnetite contents.

1.6 Exoskarn in the Héva Formation

In the Héva Formation, mineralization is characterized by disseminated sulfide or stockworks and massive sulfide-rich replacement bodies (chalcopyrite \pm pyrite \pm pyrrhotite) locally enriched in gold. The mineralization is associated with calc-silicate assemblages (mainly Ca-amphibole, carbonate, and epidote) and massive magnetite. Mineralized zones form corridors sub-parallel to the ESS (e.g., Orenada Zone 5; Figure 1.3A and C). Between the intrusion and the sulfide-rich area, garnet zones associated with magnetite, epidote, carbonates, and amphiboles replaced the volcanic rocks of the Héva Formation. The term skarn is applied in the following sections to describe these metasomatic rocks composed of calc-silicates, magnetite, and carbonates assemblage as ore gangue, in replacement of rocks of the Héva Formation, in agreement with the definition of Einaudi and Burt (1982) and Meinert et al. (2005). Based on field and petrographic evidence and associations, a paragenetic sequence has been determined for the skarn system within the Héva Formation. The sequence is provided in Figure 10 and detailed in the following sections.

1.6.1 Skarn host rocks

In the south part of the ESS, rocks from the Héva Formation consist of massive to pillowed mafic flows, interdigitating and cross-cutting gabbroic sills and dikes, porphyritic dikes, and thin, finely laminated volcano-sedimentary horizons. All the rocks in the area have undergone one or more phases of hydrothermal alteration, induced by intrusive phases and regional metamorphism, which entails difficulties in the identification of primary textures and composition. In relatively preserved areas, the texture of gabbro is fine- to medium-grained with Fe-Mg mineral relicts and

feldspar-plagioclase. Iron oxides are omnipresent and are associated with Ti-minerals altered into leucoxene-anatase, giving a characteristic white patchy texture to the rock (Figure 1.11A). Epidote occurs in matrix and mainly in replacement after the Fe-Mg mineral relicts. In the matrix of the gabbro, epidote grains exhibit a low birefringence, similar to the clinozoisite habitus. The tuff horizons are grayish and show sedimentary features (Figure 1.11A). They have altered feldspar phenocrysts in a quartz-feldspar matrix, whereas epidote and amphibole are locally abundant. Chlorite pseudomorphs are formed during a late alteration event. These minerals of metamorphic origin reflect the regional metamorphism post ESS skarn formation in greenschist facies.

The Zr/TiO₂ vs Nb/Y diagram (Winchester and Floyd, 1977) (Figure 1.6F) indicates that the rocks described as gabbro or mafic volcanic have similar basalt to basalt-andesite composition. REE profiles (Figure 1.6; Table 1.2) for gabbro and mafic volcanic rocks are relatively flat (La_(N)/Yb_(N) ranging from 0.87 to 1.11) without a significant Eu anomaly (Eu/Eu* ranging from 0.91 to 0.98). The flat REE profiles, combined with the Th/Yb (0.11-0.13) and the Zr/Y (2.8-3.1) ratios (Ross and Bédard, 2009) are consistent for Archean mafic rocks with tholeiitic affinity and the tholeiitic character of volcanism south of Val-d'Or (Imreh, 1984; Scott et al., 2002).

1.6.2 Hornfels and metasomatism area

The mafic rocks of the Héva Formation were subjected to an intense silicification (Figure 1.11A) forming a halo of contact metamorphism around the intrusion and the numerous porphyritic dikes crossing the area (Figure 1.3C). Disseminated pyrite is common in altered rocks. The original composition of these rocks is difficult to identify due to the impoverishment in all the major elements, except for silica content (Table 1.2). Using the immobile elements, altered rocks have a rhyolitic to dacitic composition (Zr/TiO₂ ranging from 0.3 to 0.4 and Nb/Y ranging from 0.2 to 0.4). They show a slight enrichment in LILE with La_(N)/Yb_(N) ranging from 2.5 to 4.5 and a negative Eu anomaly (Eu/Eu* ranging from 0.60 to 0.80). In thin sections, the mineral composition of altered

rocks is dominated by granoblastic quartz grains (30-60 μm) associated with relicts of elongated plagioclase laths (Figure 1.11B). Plagioclase laths exhibit a composition of pure albite An_{2-3} (Appendix Table A2) and could result from the alteration of original plagioclase feldspars in the basalt. Albitization of earlier-formed plagioclase could explain the Eu negative anomalies of altered rocks. In addition to the quartz-feldspar matrix, fine disseminated magnetite, fibrous actinolite and epidote grains are common. Magnetite and epidote can occur as late veinlets or form massive clusters with chalcopyrite grains. Pseudomorphosis of Fe-Mg minerals by actinote-anatase-quartz-epidote occurs in strongly silicified areas (Figure 1.11C).

In addition to the contact metamorphism, rocks of the Héva Formation have undergone an intense metasomatism resulting in an overprint and replacement of the original composition by an assembly of Ca-minerals. The alteration zone is quite wide and extends over more than a hundred meters from the intrusion (Figure 1.3C). Alteration is mainly dominated by garnet, amphiboles, carbonates, epidote, and magnetite in variable proportions (Figure 1.11D-F). This calc-silicate assemblage can be observed through all lithologies, from thin veins to a complete replacement. The replacement seems to be dependent on rock type, with frequent complete replacement of the basalts and andesites (Figure 1.11D), while the metasomatism in laminated tuff layers seems to be concentrated in specific levels. Unlike the less altered area, where laminated units exhibit parallel thin laminations, the formation of calc-silicates have disturbed the laminations in the metasomatized area (Figure 1.11F). Gabbros are generally less altered with preserved sections exhibiting characteristic leucoxene (Figure 1.11A and E), but complete replacement also occurs. Indeed, a sulfide-magnetite rich zone hosted in a gabbro shows a complete disappearance of the original protolith for several meters, with only a few remnant grains of oxides, possibly relicts of original ilmenite.

Although the lithologies seem to influence the intensity of the replacement, it frequently extends from one unit to another, making the limits of the lithologies

difficult to interpret. In drilling and in some outcrops, the metasomatized zones occur in varying shades of red, green, black, and white, which are colors given by varying proportions of garnet, epidote, amphibole, magnetite and calcite. Garnets are easily identified by their red-brown to orange color and seem more abundant in lithologies close to the intrusion. In the silicified halo, garnet occurs in zoned veins with minor quartz in the core and a greenish band composed of epidote associated with small opaque minerals (chalcopyrite and pyrite) on the edges of the vein. Locally garnet veins can evolve to massive garnet-rich zones (Figure 1.11D). These garnets-rich zones exhibit frequent overlap and replacement by epidote and calcite. Complete replacement of the garnet core by epidote is common (Figure 1.11J-K). In these areas, disseminated chalcopyrite and pyrite are associated with epidote grains and locally may form thin veinlets. Iron oxides are frequently associated with sulfides and occur as disseminations, veins, and massive replacements in garnet-rich zones (Figure 1.11E) or in mineralized zones (Figure 1.9G-H). Calc-silicates can form banded monomineralic intervals of several centimeters in width with sharp transitions between the domains (Figure 1.11D-F). Metasomatism also occurs as epidote-amphibole stockwork and carbonate veinlets, mainly in mafic rocks. In areas of increased veining intensity, the stockworks can cause the formation of brecciated zones. The breccias are then composed of centimetric angular fragments of roughly similar size, without directional fabric or rotation in a green cement. The fragments are preserved from the alteration with distinguishable original textures. Epidote and amphibole compose the infilling material and are associated in large inter-fragment spaces with calcite pods and rare sulfides. Formation of these breccias is typical of a fluid-assisted brecciation (Jébrak, 1997). Toward the intrusion, metasomatized assemblages are intensely deformed and exhibit some ptigmatic features highlighting the influence of the stock.

1.6.3 Ore gangue mineralogy

Names given to gangue and minerals are based on electron microprobe analysis following the International Mineralogical Association recommendations (Whitney and Evans, 2009).

1.6.3.1 Garnet

Two types of garnet have been identified in the exoskarn area. Type 1 is located close to the stock, mainly in veins locally overlapping the silicified halo. Massive aggregates also occur (Figure 1.11D). In thin sections garnet is anhedral (100-500 μm), fragmented and exhibits frequent inclusions and is characterized by its orange color (Figure 1.11G). Garnet veins come along with K-feldspar, carbonates and quartz in vein core and magnetite-epidote on the walls (Figure 1.11G-J). Magnetite and some cavities (300-500 μm) can be interstitial to garnets. Replacement and overlap of K-feldspar and garnet veins by epidote and actinolite is common (Figure 1.11J-K). Type 2 garnet forms massive monomineralic zones. In thin sections, these garnets are lighter colored, euhedral (750 μm – 2 mm), and affected by trans-mineral fractures filled by actinolite and carbonates, and therefore appear early in the system as a prograde mineral (Figure 1.10). Some garnets exhibit a poikilitic core contrasting with inclusion-free rims (Figure 1.11L), which is a frequent variation in garnet associated with skarn deposits (Vlasova et al., 1985). Garnet grains of type 1 and 2 in the skarn area belong to the grossular-andradite solid solution ($\text{And}_{65-100}\text{Grs}_{0-35}\text{Py}_{0-1}\text{Sps}_{0-5}\text{Uva}_{0-0.2}$) (Figure 1.12A; Appendices Table B3), a characteristic garnet composition for Cu skarns (Einaudi et al., 1981; Meinert et al., 2005).

The garnets are frequently zoned, especially type 2 garnet. Garnet zoning is highlighted by inclusion trails and a subtle optical anisotropy, which are common characteristics of garnet in skarn deposits (Pollok et al., 2001). Oscillatory zoning is evident on BSE images (Figure 1.13). Oscillatory zoning is associated with compositional variations,

increasing andradite contents and decreasing grossular contents from core to rim. This content variation is expressed by chemical variation in Fe and Al content with Al-rich core and Fe content increasing outwards. Such chemical zoning is encountered in many skarn deposits and is the result of increasing fluid-rock interaction (Meinert et al., 2005). The increase in iron concentration in the outer mantle is also associated to an increase in the $\text{Fe}^{3+}/\text{Fe}^{2+}$ ratio (Appendices Table B3), and therefore reflects an increase in the oxidation state of the system. This zonation implies a fluctuation in the fluid activity responsible for the garnet formation, and reflects evolution of hydrothermal fluids in the skarn (Jamtveit et al., 1993) related to the intrusion. Some garnets also exhibit a significant fluctuation of the composition within the rim (Figure 1. 13C).

1.6.3.2 Magnetite

Magnetite is ubiquitous in the ESS area, both within the intrusion and in the skarn zone within the adjacent rocks of the Héva Formation. Based on petrographic observation, two types of magnetite have been identified: igneous and hydrothermal.

Igneous magnetite generally occurs as disseminated subhedral to anhedral grains or as irregular grain aggregates in all intrusive porphyritic rocks from the stock. Magnetite grains exhibit exsolution lamellae and are associated with mafic accessory minerals: hornblende (LP facies) and biotite. Titanite is frequently associated with grains of magnetite along the borders, fractures or as a replacement of the original exsolution lamellae.

Hydrothermal magnetite is abundant in the altered volcanic rocks of the Héva Formation, disseminated, in veins or associated with the skarn assemblage (Figure 1.11E and G). Magnetite forms relatively early in the system as shown by the garnet association, and the overlap of the magnetite grains by sulfides and retrograde minerals. The frequent epidote inclusions in magnetite grains as well as the equilibrium texture between magnetite, epidote and euhedral pyrites also testify to a late formation of the

magnetite during the retrograde stage. Overall, the magnetite appears at the end of the prograde stage and continues during the early part of the retrograde stage, causing the mutual overlap observed both with prograde and retrograde minerals (Figure 1.10). In ore zones, hydrothermal magnetite is more abundant and occurs in veins, in massive replacement aggregates (Figure 1.9F-H), and locally in magnetite-dominated zones associated with pyrite, chalcopyrite, and rare pyrrhotite. Massive magnetite is locally replaced by pyrite and more frequently by chalcopyrite (Figure 1.9I). Hydrothermal magnetite also occurs as disseminated grains or as magnetite veinlets within the ESS in association with potassic alteration (Figure 1.9B).

Igneous and hydrothermal magnetite may be differentiated by their trace element content analyzed by LA-ICP-MS (Appendix Table A3). The location and setting of the samples are shown in Appendix Table A1. Box and whisker plots of trace elements concentrations (Figure 1.14A) show greater variability for igneous magnetite compared to hydrothermal magnetite. The variability may be due to the numerous mineral inclusions and exsolution. Na, Mg, Al, Si, K, Ca, Ti, V, Cr and Mn concentrations in both igneous and hydrothermal magnetite are higher than 100 ppm. Hydrothermal magnetite has average concentrations of Mg, Al, Si, Ca, Co, Ni, Cu, Ga, Sb, and W that are one order of magnitude higher than igneous magnetite. The concentration differences in hydrothermal magnetite compared to igneous magnetite, do not exceed more than one order of magnitude except for Y, Zr, Nb and Hf in very low concentrations, below or close to the detection limit. Magnetite formation is influenced by many physical and chemical parameters (e.g., fluid compositions, temperature, host rock, oxygen and sulfur fugacity; Nadoll et al. 2014 and references therein). Fairly similar composition testifies to an affinity between the two magnetite types and could suggest some similar conditions of crystallization, such as hydrothermal fluids composition originating from the ESS.

The composition of hydrothermal magnetite within the skarn mineralization (Cu-Au-Ag) have been compared to the composition of hydrothermal magnetite in association with worldwide mineralized Cu and Fe skarns (Huang et al., 2019 and references therein) in Figure 14B. The overall magnetite composition of the exoskarn is close to the median values of worldwide Cu and Fe skarns and remains inside the extremum values. As previously observed, the composition of hydrothermal magnetite exhibits a low dispersion of the values and therefore a homogeneous composition despite the various sample's localization. Tungsten content, however, is more variable, possibly due to small inclusions of scheelite in high grade zones.

Hydrothermal magnetite from this study displays some specificities: 1) a relative Mg depletion for magnetites associated with ore zone; 2) some Cr-rich values from magnetite in replacement of mafic rocks; 3) an overall low Zn and Co content as well as low Zr and Nb contents close to the detection limits; 4) a relative Ni, and V enrichment compared to the median values for some Cu-Fe skarn. These specificities are due to the large number of processes involved in skarn formation (c.f., Einaudi et al. 1981; Baker et al. 2004; Meinert et al. 2005) and mainly reflect the interaction of hydrothermal fluids with the skarn host rock. Despite this, the trend and composition of the hydrothermal magnetite associated with the Cu-Au-Ag mineralization are quite similar to the results obtained on hydrothermal magnetite associated with others Cu skarn deposits worldwide (e.g., McQueen and Cross 1998; Nadoll et al. 2014; Nadoll et al. 2015; Huang et al. 2019).

1.6.3.3 Amphibole

Amphibole structural formulas were determined following the International Mineralogical Association guidelines (Hawthorne et al., 2012) and using the spreadsheet of Locock (2014). Amphiboles all belong to the calcic amphibole series (Table 1.3; Appendices Table B4) and form a series between actinolite-tremolite and magnesio-hornblende (Figure 1.12B). The dominant amphibole is fibrous actinolite

which exhibits frequent decussate texture (Figure 1.11H-I) and is commonly associated with thermal contact metamorphism. Actinolite occurs systematically in the metasomatized area, forming monomineralic replacements in strongly skarnified zones. In mineralized zones, acicular tremolite is frequent in association with coarse epidote. Fibrous actinolite-tremolite surrounds and forms veinlets within most of the early minerals such as prograde garnet or K-feldspar veins (Figure 1.11H-L), and sometimes large crystals of epidote, thus it represents the retrograde phase (Figure 1.10). Composition of the actinolite shows limited variation ($\text{Si} = 7.5\text{-}7.9$, $X_{\text{Mg}} = 0.5\text{-}0.72$) and seems dependent on the variation of Fe and Al content (Table 1.4). Hornblende grains mainly occur in the alteration-preserved LP facies, but also occur associated with mineralization in both exoskarn and Cu-Mo ore zones. Hornblende in ore zones consists mainly of isolated grains (300-750 μm) interstitial to sulfides. Hornblende composition differs slightly between the exoskarn ($\text{Si} = 7.25\text{-}7.85$, $X_{\text{Mg}} = 0.55\text{-}0.65$) and the Cu-Mo ore zone within the intrusion ($\text{Si} = 7.36\text{-}7.71$, $X_{\text{Mg}} = 0.69\text{-}0.76$).

1.6.3.4 Epidote

Epidote, as for actinolite-tremolite, is a major component of the retrograde alteration of the skarn (Figure 1.10). Epidote occurs in veins, aggregates, and massive replacements. In highly metasomatized areas, epidote can replace up to 50% of the original rock. Generally, epidote occurs as small disseminated grains (<200 μm , Figure 1.11G), but in magnetite- and sulfide-rich areas, the grain size increases (av. of 300 μm and up to 1.5 mm, Figure 1.11I). These coarse-grained epidotes exhibit frequent prismatic optical zonation, sometimes associated with rare cleavage relicts. These features could suggest a formation by pseudomorphosis with preservation of cleavage and mineral zoning of the replaced mineral. Outside the mineralized zone, the epidote abundance is related to the amount of chalcopyrite, especially when it forms large aggregates of relatively small grains (<200 μm), as in the mineralized porphyry facies (MP).

Using the Franz and Liebscher (2004) classification, the sorosilicate minerals were all classified as epidote (Figure 1.12C). Epidote compositions are homogeneous (Table 1.5) and seem independent of the facies and position in the skarn system, i.e., there is no apparent composition variation between epidote in the exoskarn and in the MP facies. The large epidote crystals, however, exhibit a slight variability in Al and Fe between the borders and the core. This variability could be linked to the optical zonation.

1.6.3.5 Carbon and oxygen isotope on calcite

Carbonates are common in the ESS and in metasomatized zones. Carbonates analyzed during this study are exclusively calcite and belong to both the prograde and retrograde assemblages (Figure 1.10). The prograde calcite is relatively scarce and is mainly associated with garnet veins. The calcite grains are partially replaced by retrograde minerals. The retrograde calcite is more abundant and is found in fracture-filling and in crosscutting veins, mainly after garnets in skarn zone. In strongly altered zones, calcite occurs as enclosed coarse-grain, small pods (Figure 1.11L) or in large veins associated with epidote and actinolite.

Oxygen and carbon isotope ratios were obtained from retrograde calcite in skarn zones. The samples were collected from a garnet-rich zone (GAR), an andesite highly metasomatized and replaced by garnet-magnetite-actinolite-epidote (AAX) and a sulfide-magnetite-rich area (MT) (Table 1.8). GAR samples are the closest to the intrusion and MT is the most distant. Oxygen isotope ratios remain constant regardless of samples (av. $\delta^{18}\text{O}_{\text{SMOW}} = 11.3\text{‰}$) and fall within the range of isotope ratio for igneous rocks (Bowman, 1998). The carbon isotope ratio seems to be more dependent on the sample location (av. $\delta^{13}\text{C}_{\text{PDB}} = -5.3\text{‰}$, -4.3‰ and -3.7‰), the lowest $\delta^{13}\text{C}$ ratio values being obtained by those furthest from the intrusion, but remaining close to the values for igneous carbon isotope ratios. East Sullivan skarn calcite exhibits isotope ratios within the range reported from hydrothermal calcites of some Archean gold

deposits in the Superior Province, especially those obtained at the Lamaque mine (Kerrick, 1990 and references therein) and within the range reported for some worldwide skarn ores ($\delta^{13}\text{C}_{\text{PDB}} = -9$ to -4% and $\delta^{18}\text{O}_{\text{SMOW}} = 7$ to 14% ; Bowman, 1998).

1.6.4 Cu-Au-Ag skarn mineralization in Héva Formation

In addition to the Cu-Au-Mo mineralizations in the intrusion, the Héva Formation hosts some mineralized areas. These zones display massive pyrite-chalcopyrite and magnetite \pm pyrrhotite mineralization within actinolite-tremolite, epidote-rich retrograde replacement (Figure 1.9F-H). One of these zones was intersected in the vicinity of the Orenada Zone 5 showing (Figure 1.3) by drilling, and the associated log is provided in Figure 8B. The ore zone is hosted by mafic units and seems to follow the volcanic levels by forming lenses roughly parallel to the southern border of the stock (Figure 1.3C). However, the vertical extension of the zones is poorly constrained by lack of drilling and we assumed that some of these zones exhibit vertical continuities. Strong magnetic anomalies are associated with the high-grade area (Figure 1.3B). The ore zone comprises an average of 5% pyrite and 2 to 3% chalcopyrite \pm pyrrhotite in a magnetite-amphibole-epidote-calcite assemblage. Sulfide percentage can exceed 10% over decametric to metric sections (Figure 1.9H). Pyrite is subhedral to euhedral, and generally displays silicate and chalcopyrite inclusions and sometimes shows corroded borders by amphibole and epidote. Pyrite and magnetite display complex overlaps, replacement, and association (e.g., frequent equilibrium texture), which could suggest either a successive or a simultaneous formation of the minerals. Chalcopyrite is slightly later and is often associated with pyrite. Chalcopyrite grains occur around the pyrite grains, in crosscutting veins, in inclusions and more frequently in replacements of the pyrite (Figure 1.9I-J). These textural relationships demonstrate that, as for magnetite (see section 1.7.3.2), pyrite is intimately associated with copper mineralization, especially in the retrograde assemblages (Figure 1.10). No free gold was observed in the sulfide-rich zones, although some Au values reach up to 1.64g/t over 1 meter. Gold

comes in the form of electrum around the chalcopyrite grains (Figure 1.9K) and in tiny inclusions (<5 μm) in silicates.

Thereby, the main mineralized zones in the Heva skarn occurrence are systematically enriched in Au, Cu, Ag, Co, Bi and show a strong similar behavior between these elements (Figure 1.8B). The metal contents are well correlated with the amount of iron (up to 25%) and the percentage of sulfides (up to 8%). Some decametric intervals show strong continuous values in Au (>1g/t), Cu (>1%) and Ag (>10g/t). The Au/Ag ratio in the main zone is slightly variable and does not exceed 1:6. Tellurium concentration remains more or less constant within and outside the main zones (average of 15 ppm) throughout the different mafic lithologies, but decreases and disappears in the volcanic rocks. Zn and Ni content are low and rarely exceed 100 ppm. Higher Ni values may be associated with the local presence of minute (<15 μm) pentlandite and possible sphalerite grains within pyrite fractures. The highest copper values are associated with elevated indium values (>20 ppm), possibly incorporated in chalcopyrite due to the lack of Zn minerals.

Outside the mineralized zones, the relationships tend to be less visible between the metal contents, with Ag concentrations close to the detection limit (0.5 ppm) and Bi disappearance. Copper concentration is significantly lower with values between 100 and 200 ppm except for some small scattered ore zones. Sb and As values are low and do not exceed 10 ppm, and Pb remains undetectable outside the zones and does not exceed 10 ppm in the massive mineralization intervals, as with Mo (average of 2 ppm). The average Zn and Ni content remains around 30 ppm.

1.7 Thermometry of the East Sullivan skarn system

1.7.1 Zircon

Zircon saturation temperature can be obtained by the relationship of Watson and Harrison (1983) using zircon solubility, temperature, and major element composition of melt (whole rock analysis) following the rearranged equation of Miller et al. (2003):

$$T_{Zr} = 12,900 / [2.95 + 0.85M + \ln (496,000/Zr_{melt})],$$

where T is in kelvins; $M = [(Na + K + 2*Ca)/(Al*Si)]$, all elements in cation fraction, and Zr_{melt} is the Zr concentration in the whole rock. The Zr-saturation thermometer, based on the strong dependence of Zr concentration relative to temperature, is robust and can be used to estimate the temperature of the melt crystallization. Large variations in both the Zr concentration from whole-rock analysis and the M parameter, reflecting the zircon solubility of the melt, only incur small errors in the estimated temperature, i.e. $\pm 50^{\circ}C$ (Hanchar and Hoskin, 2003). Some elements such as F can also alter the behavior of magma, decreasing the solidus temperature as pointed out by Fayol and Jébrak (2017).

The Zr content of the ESS is relatively low, between 150 and 280 ppm, giving an average T_{Zr} value for all facies of $771^{\circ}C \pm 14^{\circ}C$ (Table 1.9). Average temperature decreases from early (EP) and intermediate facies (IP1, IP2), with similar average temperatures ($774^{\circ}C$), to the late (LP, $764^{\circ}C$) and mineralized facies (MP, $758^{\circ}C$) with slightly lower temperatures.

Granitoids with $T_{Zr} < 800^{\circ}C$ are interpreted as cold and inherited zircon-rich granitoids by (Miller et al., 2003). Temperature obtained for inheritance-rich granitoid is a maximum estimate of the initial magma temperature. The inheritance-rich granitoids

group is consistent with ESS rocks, particularly EP facies which contain numerous inherited zircons, noticeable on BSE images, and giving uninterpretable U-Pb ages.

1.7.2 Amphibole

Amphibole composition has been frequently used to estimate and constrain magmatic crystallization temperature (e.g., Erdmann et al. 2014). The Al-in-hornblende geothermometer of Ridolfi et al. (2009) can be applied on amphibole-bearing granites derived from calc-alkaline to alkaline magmas with high or low water content formed under moderately reduced to moderately oxidized conditions, consistent with the ESS parameters. Preserved magmatic hornblendes only occur in the LP facies and allow the geothermometer application. Following the equation of Ridolfi et al. (2009):

$$T (^{\circ}\text{C}) = -151.487\text{Si}^* + 2041;$$

where $\text{Si}^* = \text{Si} + ([^{4}\text{Al}]/15) - (2[^{4}\text{Ti}]) - ([^{6}\text{Al}]/2) - ([^{6}\text{Ti}]/1.8) + (\text{Fe}^{3+}/9) + (\text{Fe}^{2+}/3.3) + (\text{Mg}/26) + ([^{\text{B}}\text{Ca}]/5) + ([^{\text{B}}\text{Na}]/1.3) - ([^{\text{A}}\text{Na}]/15) + (\text{A}[]/2.3)$, with a deviation of $\pm 22^{\circ}\text{C}$, based on the classification scheme of Leake et al. (1997). LP amphiboles yield similar temperatures with a calculated average of $730 \pm 22^{\circ}\text{C}$ (Table 1.9).

The P-independent geothermometer of Putirka (2016) is based on the following equation:

$$T (^{\circ}\text{C}) = 1781 - 132.74[\text{Si}^{\text{Amp}}] + 116.6[\text{Ti}^{\text{Amp}}] - 69.41[\text{Fe}_t^{\text{Amp}}] + 101.62[\text{Na}^{\text{Amp}}],$$

where [X] are the indicated cations in amphibole on the basis of 23 O atoms, with a precision of $\pm 30^{\circ}\text{C}$. It produces a slightly higher temperature for LP crystallization, with an average of $752 \pm 14^{\circ}\text{C}$.

Temperatures obtained of the two amphibole geothermometers are in agreement with the previous zircon saturation temperature calculated for the late porphyry facies of the ESS and allow estimation of a crystallization temperature of LP facies between 705 and 759°C.

1.7.3 Biotite

Although mainly present in the ESS as primary minerals and associated with K-alteration as hydrothermal phases, biotites are also present in the volcanic facies of the Héva Formation outside the stock. Based on petrographic observations, the biotites can be divided into two main types: magmatic and hydrothermal. Magmatic biotites, frequently altered to chlorite, occur in intrusive rocks as euhedral to subhedral phenocrysts (500-1000 μm) exhibiting green to brown pleochroism (Figure 1.7F). Hydrothermal biotites occur as partially to completely chloritized and randomly oriented aggregates of fine-grained anhedral flakes (<100 μm). These biotites are observed both within the intrusion in potassic veins (Figure 1.7A) and in the groundmass of surrounding volcanic host rocks as part of the hydrothermal mineral assemblage (Figure 1.7C), frequently associated with titanium-bearing oxides. The composition of both types of biotite is roughly equivalent and plots close to the biotite-phlogopite fields' boundary (Figure 1.12D). Despite these textural differences, the FeO*-TiO₂-MgO triangular diagram of Nachit et al. (2005) indicates that all biotites plot in the field of re-equilibrated biotites in an intermediate trend between the magmatic and pure hydrothermal biotite fields (Figure 1.12E). The relatively constant X_{FeO} ratio ($X_{\text{FeO}} = 0.5$ to 0.6 , with $X_{\text{FeO}} = \text{FeO}^*/(\text{FeO}^* + \text{MgO})$ and FeO* as FeOt + MnO) associated with TiO₂ variation for each biotite independently of the facies indicates progressive hydrothermal re-equilibration (Nachit et al., 2005). Biotites are Mg-rich ($X_{\text{Mg}} = 0.50$ to 0.67) and exhibit variable halogen content: F varies from 0.32 to 1.74 wt% and Cl varies from 0.01 to 0.18 wt%. The highest F values (>1 wt%) are obtained for the biotites within IP facies, associated with Cu-Au-Mo mineralization

and in endoskarn. Biotite composition shows several correlations between the X_{Mg} ratio, oxide, and halogen content. X_{Mg} is positively correlated with F and Mg contents and negatively correlated with Ti, Fe and Al contents (Table 1.6, Appendix Table 1.A5). The link between X_{Mg} and Cl content is less clear but the lowest Cl values correspond to the highest X_{Mg} values. Incorporation of more F and less Cl in biotite with high X_{Mg} was described as the Fe-F and Mg-Cl avoidance principle by Munoz (1984). The biotite compositional variations in halogen and oxide contents from the southern border of the ESS are consistent with biotite composition in several porphyry Cu deposits (Selby and Nesbitt, 2000 and references therein). These results are also in agreement with those obtained by Taner et al. (1986) on biotite within the ESS.

The geothermometer of Henry et al. (2005) based on temperature and pressure dependence of Ti solubility in biotite, originally for biotite in graphitic and peraluminous metapelites, has frequently been applied on porphyry copper systems to obtain the temperature of magmatic-hydrothermal systems (e.g., Mercer and Reed 2013; Rezaei and Zarasvandi 2020 and references therein). The Henry et al. (2005) geothermometer can be applied with confidence on biotites from this study, considering that the formation temperatures of porphyritic systems (Sillitoe, 2010) can be compared with those of spatially associated skarn systems (Meinert et al., 2005), in addition of the correlation between the prograde-retrograde phases with potassic-sericite alterations. The temperature in Celsius can be obtained with the following equation:

$$T = ([\ln (Ti) - a - c(X_{Mg})^3]/b)0.333;$$

where $a = -2.3594$, $b = 4.6482 \times 10^{-9}$, $c = -1.7283$, $X_{Mg} = Mg/(Mg + Fe)$ and calibrated for $X_{Mg} = 0.275 - 1.000$, $Ti = 0.04 - 0.60$ apfu, $T = 480 - 800^\circ C$, and $P = 400 - 600$ MPa. Biotite compositions from the ESS area fall within the appropriated calibration range (Table 1.5). All biotite temperatures, regardless of their location and context, lie

within the range of 445°C to 613°C (average of 532°C \pm 35°C) (Table 1.9) with an estimated precision of \pm 24°C for temperatures below 600°C (Henry et al., 2005). The temperatures obtained should reflect re-equilibrated biotite conditions.

As pointed out by Mercer and Reed (2013), application of this thermometer to rocks associated with porphyry systems requires evaluation of whether chemical equilibrium was attained and preserved in biotites since several factors can lead to a chemical imbalance and therefore a poor temperature estimate. The common presence of chlorite after biotite in several analyzed grains can explain the relatively low temperature (Henry et al., 2005) determined in EP and for some biotites in IP (average of 490 \pm 16°C) and therefore cannot reflect the temperature of re-equilibrium crystallization. Temperatures obtained from biotite in ore zones (average of 570 \pm 7°C for exoskarn and average of 534 \pm 7°C for Cu-Mo endoskarn) are to be interpreted with caution due to the precipitation of several Fe-Ti minerals (e.g., chalcopyrite, pyrite, magnetite) which act as a buffer for TiO₂ and tend to drive the Ti and X_{Mg} content. Then, in LP facies (average of 530 \pm 20°C) biotite formed after hornblende may have inherited compositional heterogeneity from the original amphibole which is, however, not confirmed by the lack of scattering in Ti and Mg content in most grains (Table 1.4). However, the absence of Ti-saturating minerals (ilmenite or rutile) in the LP facies may result in significant underestimation of temperatures (Henry et al., 2005). Despite these restrictions, several temperatures calculated for biotites from the ESS can be interpreted with confidence because they respect the equilibrium and calibration conditions for this geothermometer, i.e., the presence of Fe-Ti oxides, the lack of chlorite replacement and biotites have a homogeneous composition. These biotites, mainly associated with IP2, provide a temperature for re-equilibrated biotite by post-magmatic hydrothermal fluids around 523 \pm 32°C, consistent with average potassic alteration of porphyry systems and equivalent prograde stage in skarn systems (e.g., Meinert et al. 2005; Richards 2011).

1.7.4 Chlorite

Chlorite occurs exclusively as an accessory phase, replacing biotite and amphibole, mainly within the ESS (Figure 1.7F and H), and represents a late hydrous retrograde phase of alteration. All analyzed chlorite grains are Mg-rich and correspond to pynchochlorite (Figure 1.11F). The grains exhibit compositional variations related to their respective association with the ESS facies, the mineralized and K-altered zones (Table 1.7). Chlorite composition shows X_{Fe} decreases from IP and LP facies ($X_{\text{Fe}} = 0.38\text{-}0.42$) to K-alteration zones ($X_{\text{Fe}} = 0.33\text{-}0.35$). The chlorites formed after biotite associated with Cu-Mo mineralization have intermediate X_{Fe} values ($X_{\text{Fe}} = 0.34\text{-}0.36$). The variation in X_{Fe} ratio corresponds to an increase in Fe and a decrease in Mg at the expense of Si. The potassium content of chlorites is very low and often below the detection limit (<0.05 apfu) in the ESS, and is slightly higher in the potassic alteration zones (up to 0.15 apfu). These ratio variations are consistent with bulk rock composition (Table 1.1) and protolith mineralogy, i.e., the greater availability of Al in the ESS and of K in the K-feldspar veinlets, and higher Mg content of chlorite replacing biotite. The dependence of the chlorite composition on host rock facies, and therefore on coexisting minerals, has been underlined by several authors (e.g., Caritat et al. 1993).

The chemical composition of chlorite, and variations in the occupation of crystalline sites, was used to estimate the temperature of the late hydrothermal event by several authors (Cathelineau and Nieva, 1985; Kranidiotis and MacLean, 1987; Jowett, 1991).

The results (Table 1.9) of the three geothermometers on the chlorites reveal similar average temperatures regardless of the method (average $273 \pm 18^\circ\text{C}$ to $284 \pm 26^\circ\text{C}$) in the study area. Calculated temperatures are slightly higher for chlorites that replace biotite in the intrusive phases (average 265 to 307°C), and in the Cu-Mo mineralization (average 281 to 297°C) than those for chlorite in K-alteration zones (average 245°C). This disparity is in agreement with compositional variation observed in chlorite depending on the position in the system (see section 1.6.3). The calculated temperatures

are considered as minimum temperatures for the late hydrous phase of hydrothermal alteration within the intrusion.

1.8 Discussion

1.8.1 Skarn or VMS ?

In the Superior Province, chalcopyrite and pyrite ores hosted by volcanic rocks are common. In the Abitibi greenstone belt, many of these mineralizations are associated with several well-known Au-Cu-Zn volcanogenic massive sulfide deposits contained in the Blake River Group (Monecke et al., 2017). Some of these deposits exhibit ore lenses consisting of massive magnetite, pyrrhotite and chalcopyrite, such as the West Ansil massive sulfide ore body in the Noranda central camp (Boucher et al., 2010). The mineralized zones are hosted by andesites and basalts of the Blake River Group and are underlain by the synvolcanic Flavrian Pluton. In addition, in the Noranda camp, the Cu-Au Ansil deposit located 2 km further north of the West Ansil ore body is associated with calc-silicate minerals originating from the metamorphic aureole produced by the trondhjemitic phases of the Flavrian intrusion (Galley et al., 2000a). In the Val-d'Or area, close to the western limit of the ESS, mineralized sulfide-rich Cu-Zn-Ag-Au zones of the East Sullivan deposit are also interpreted as VMS-type mineralization (Lavoie, 2003). It is also frequent to find an overprinting porphyry Cu-Mo-Au mineralization in numerous VMS camps (e.g., Galley et al. 2000b).

In contrast, magnetite-pyrite-chalcopyrite skarn-type mineralization remains an exception in the Superior Province. The only recognized occurrence is the Akasaba deposit, which is located 6 km southeast of the ESS, and was initially interpreted as a VMS deposit (Lebel, 1987). Therefore, the interpretation of the ESS associated mineralization and its classification could be equivocal. However, the successive potassic-phyllitic-propylitic alteration zones within the ESS and the adjoining Héva

Formation, as well as the paragenetic successions of the alteration and ore minerals, are not consistent with their formation by exhalative processes. The composition of hydrothermal magnetite and the calculated temperatures of the hydrothermal fluids by the biotite geothermometer are in favor of a magmatic-hydrothermal origin for the mineralization. In particular, the typical garnet oscillatory zoning and the replacement of the Héva Formation lithologies along the southern border of the ESS by calc-silicate minerals instead suggest the development of an intrusion-related skarn mineralization, in accordance with the definition of Burt (1977), Einaudi and Burt (1982) and Meinert et al. (2005). The ESS is the host of a porphyry-type mineralization within the IP phase in the southern part of the intrusion, in association with the skarn.

1.8.2 Archean intrusion-related Cu-Au-Ag skarn formation

Skarn assemblages in intrusion-related systems are usually formed by the reaction of intrusion-derived metasomatic fluids with surrounding carbonate rocks, including limestone, dolostone and marls (Meinert et al., 2005). These sedimentary carbonate rocks are, however, uncommon in the Archean cratons. Nevertheless, the presence of carbonates has been recognized in the Archean volcanic successions in greenstone belts, particularly in basaltic rocks, prone to carbonatization (Groves et al., 1988; Veizer et al., 1989). Nakamura and Kato (2004) suggested that the carbonate formations (i.e., calcite \pm ankerite \pm siderite) in basalts were the result of seafloor hydrothermal activity, from a reaction between CO₂ in the seawater and Ca from the oceanic crust. The Héva Formation, which hosts the Cu-Au-Ag skarn mineralization, is interpreted as a result of subaqueous effusive volcanism of tholeiitic composition, and to have formed in a rift setting (Scott et al., 2002). It could have undergone subseafloor carbonatization, but also carbonatization at a later time, prior to skarn formation. The verticalization of the volcanic structure would have allowed the vertical skarn development following the carbonate-enriched levels of the Héva Formation (Figure 1.3C). This lithological control could explain the restricted horizontal extent of the skarn and mineralization

development as well as the weak skarn zoning pattern from the intrusion to the distal metasomatized rocks. The skarn formation may also have been influenced by structural control (faults, shear zone, etc.) as evidenced in the nearby Akasaba deposit (Vorobiev, 1998), but the area lacks direct evidence of such control.

Three major stages of skarn formation have been identified based on field and mineralogical evidences:

Stage 1 is a high temperature metamorphism aureole (around 500-800°C) induced by the ESS, that preceded mineralization and the formation of skarn assemblages. It led to the formation of a metamorphic halo surrounding the ESS. This contact metamorphism is evidenced by several minerals, which are characteristic of the amphibolite facies in mafic rocks, such as hornblende, biotite, albite ± epidote. This halo is accompanied by an abundant silicification. However, this stage remains difficult to identify due to many local lithological variations in the Héva Formation, and therefore variations in the characteristic minerals of this stage. In addition, several minerals may belong to the late regional metamorphic assemblage (e.g., epidote, hornblende, actinolite, quartz).

Stage 2 is a prograde skarn stage dominated by garnet formation. During this stage, potassic metasomatism is associated with K-feldspar and biotite formation within the ESS and in the surrounding volcanic host rocks. The Ti-in-biotite thermometer provides a temperature of around $530 \pm 20^\circ\text{C}$ for both the prograde stage and potassium metasomatism within the intrusion. This stage was also accompanied by the evolution of the oxidation state of the fluids (i.e., increasingly oxidized hydrothermal fluid), resulting in a change in the garnet composition from grossular-andradite towards pure andradite. Magnetite and pyrite formed late within this stage of metasomatism. In addition to the garnet formation, the prograde stage is usually associated with the pyroxene formation (diopside-hedenbergite in Cu skarn).

Stage 3 corresponds to a retrograde alteration stage leading to the partial replacement of the prograde assemblages by hydrous phases. More specifically, epidote and calcite replace grossular garnet, and iron oxides, quartz, calcite and epidote replace andradite garnet. This stage was associated with circulation of a large quantity of fluids, as evidenced by the hydraulic breccias and the complete replacement of both the original photoliths and prograde minerals by hydrated minerals. Retrograde alteration is dominated by epidote and actinolite-tremolite, especially in the mineralized zone. The lack of prograde clinopyroxene within the studied samples may be due to complete retrogression to actinolite and tremolite, during this stage in the evolution of the hydrothermal system. Indeed, complete replacement of pyroxene and garnets by intense hydrolytic alteration occurs frequently in Cu skarn deposits (Einaudi, 1981). The deposition of magnetite and pyrite overlaps both stage 2 and stage 3, and was followed by the deposition of chalcopyrite and minor pyrrhotite, as well as quartz and calcite. Gold and silver are associated with this stage, as evidenced by the electrum association with chalcopyrite. Chloritization of biotite and amphibole occurs during the retrograde stage at a temperature of approximately $274 \pm 12^\circ\text{C}$. This temperature is consistent with a relatively late chloritization, since the retrogressive phase in most skarn deposits is initiated at approximately $350\text{-}400^\circ\text{C}$ (Meinert et al., 2005).

1.8.3 Cu-Au-Mo porphyry mineralizations

The Cu-Au-Mo mineralization in the ESS is closely related to potassic metasomatism. Quartz-chalcopyrite veins crosscut the K-feldspar-magnetite-biotite veins and indicate that copper was deposited relatively late with respect to potassic alteration. The potassic alteration formed at around 530°C , which is a maximum temperature for copper deposition. In many Cu-porphyry deposits, the precipitation of Cu-Fe sulfide and gold occurs between 550° and 350°C (Sillitoe, 2010). The concomitant Au-Cu precipitation is consistent with the strong correlation observed between these elements in the porphyry-style mineralization in the IP2 phase (Figure 1.12A). The bulk of the

Cu precipitation at the end of the potassic alteration, prior to the phyllic phase, coincides with the waning stages of garnet formation and the initiation of the retrograde stage in the skarn. The formation of Cu mineralization by fluid-rock interaction in the IP2 facies is evidenced by the abundant chalcopyrite content in fracture-filling as well as the increased rock fracturing in areas of the higher Cu content.

Molybdenite is restricted to the porphyry-style mineralization and is usually associated with abundant quartz veins postdating Cu-Fe sulfide deposition, which results in a weak correlation with the Cu and Au content. The molybdenite precipitation after the bulk of the Cu \pm Au precipitation (Sillitoe, 2010) explains the weak correlation of the Mo with the Cu and Au contents through the mineralized area (Figure 1.12A). The silver content is insignificant in the Cu-Mo-Au porphyry-style mineralization. This contrasts with the metal content of the skarn, where silver is more abundant (Figure 1.12B), and is well correlated with the Au-Cu content. This metal zoning is reported in porphyry Cu deposits centered on Cu-Mo-rich zones, and shows an outer margin with Zn-Pb and Au-Ag zones (Sillitoe, 2010).

The highest Cu \pm Mo grades are hosted in the syenitic MP facies. Quartz-sulfide veins are common, but most of the mineralization is disseminated in vugs through the MP facies. The vugs are filled by authigenic minerals and sulfides. The quartz is present in the altered rock not as magmatic quartz but rather as large late vug-filling minerals with numerous epidote and biotite inclusions. Chalcopyrite in the vugs is in systematic association with epidote patches and exhibit equilibrium texture with epidote grains. The chalcopyrite and epidote association contrasts with the Cu mineralization associated in quartz-chalcopyrite veins without epidote association. The MP facies is similar to episyenite formed by quartz dissolution under Na-K metasomatism (Cathelineau 1986; Jébrak and Doucet 2002; Suikkanen and Rämö 2019 and references therein). Quartz dissolution may result from the retrograde quartz solubility when fluids are cooling as rocks undergo a transition from ductile to brittle conditions (i.e.,

between $\sim 375\text{--}475^\circ\text{C}$ in porphyry systems; Monecke et al., 2018). This process results in increasing permeability in the silicate rocks with increased porosity and vein opening. Quartz dissolution is favorable to fluid flow and can substantially increase metal content (e.g., in Bingham Canyon Porphyry; Redmond and Einaudi 2010). This episyenitization process with vug formation may explain the formation of the Cu \pm Mo richer zones with an additional Cu \pm Mo enrichment in the porous porphyry rock (MP). This additional Cu-mineralization could be related to the evolution of the adjacent skarn zones in the Héva Formations, with formation of a local endoskarn favored by the prior episyenitization. Emplacement of the MP facies along the southern margin of the ESS, in contact with the skarn, as well as the common epidotization and presence of vugs, favors such an interpretation. Nevertheless, endoskarn formation in mineralized porphyry intrusions is uncommon (Meinert et al., 2005). Chang and Meinert (2004) highlighted the influence of the fluorine activity in the development and formation of endoskarn. A high fluorine content lowers the magma solidus temperature, favors chemical corrosion and dissolution in silicic rocks and influences the solubility of some metals. Biotite of the MP facies exhibits fluorine content moderately high, 0.85–1.71 wt.% compared to the mean value of about 0.7 wt.% F in biotite in granitic rocks (Bailey, 1977). Part of the fluorine can be released during biotite chloritization, lowering the actual content. Thus, the relatively high fluorine content documented in the biotites and in the ESS (500-900 ppm; Table 1.2) may have favored the vug formation and therefore the endoskarn development, resulting in additional Cu enrichment in the porphyry Cu-Mo mineralization area.

1.8.4 Magma fertility

Although the spatial association of the ESS with both Cu \pm Au \pm Ag and Cu \pm Au \pm Mo mineralized zones is demonstrated (Figure 1.15), the genetic link remains questionable. The ESS is a porphyritic metaluminous multiphased intrusion composed of monzonite and syenite, which are favorable lithologies for the formation of porphyry

and skarn Cu deposits (e.g., Meinert 1995; Sillitoe 2010). The slight alkaline affinity of the ESS is also consistent with the composition of some copper-porphyry systems (Seedorf et al., 2005).

An important parameter in the formation of copper mineralization is the oxidation state of the associated intrusion. Most of the Cu ± (Mo-Au) porphyries and magmatic-hydrothermal deposits such as skarns are formed by oxidized granitoids belonging to the magnetite-series (Ishihara, 1998; Meinert et al., 2005; Sillitoe, 2010; Sun et al., 2015). Although influenced by alteration, the ratio $\text{Fe}_2\text{O}_3/(\text{FeO}+\text{Fe}_2\text{O}_3)$ is an indicator of the intrusion oxidation state. The ESS displays a Fe speciation ratio ranging from 0.49 to 0.55 for all facies (Table 1). The intermediate facies (IP2) associated with mineralization shows the highest ratio and oxidation state. This oxidation state is also expressed in the ESS mineralogy by the absence of ilmenite, the presence of magmatic magnetite, as well as the presence of hematite in the system. In addition, the REE profiles for the ESS porphyritic facies do not display europium anomalies. This can be explained by the oxidized conditions of the parental magma (Drake and Weill, 1975). As constrained by the mineralogical composition of the ESS, the $f\text{O}_2$ lies between the fayalite-magnetite-quartz (FMQ) and the hematite-magnetite (HM) buffers.

The water content of the magma is another important parameter that controls exsolution of an aqueous volatile phase associated with the formation of a magmatic-hydrothermal mineralized system (Burnham, 1997; Richards, 2011). The ESS displays several magmatic hydrous phases such as biotite in all facies and hornblende in LP facies, a mineral indicator of high magmatic water content. More specifically, hornblende can only crystallize in liquids containing appreciable contents of water (>4 wt.%) (Naney, 1983; Ridolfi and Renzulli, 2011). The Sr/Y ratio for the least altered samples of the ESS and the lack of significant europium anomaly support this interpretation because hydrous magma tends to suppress plagioclase crystallization (Sisson and Grove, 1993).

The high magmatic water content of the ESS is also in agreement with differentiation being controlled in part by the fractionation of amphibole, as presented above.

In addition to the Cu-mineralization, Taner (1996) highlighted the gold potential of the ESS, presumably indicated by the alkaline nature of the intrusion. The association of gold with alkaline, oxidized magmatism and porphyry intrusions was evidenced by several authors (Cameron and Hattori, 1987; Sillitoe, 2000; Robert, 2001); and summarized by the -sanukitoid gold porphyry deposits- genetic model of Fayol and Jébrak (2017). The favorable conditions to form such gold deposits have been well constrained by the authors at Lac Bachelor Deposits: an alkaline-oxidized magmatism near crustal discontinuities emplaced in permeable host rocks favorable to the formation of gold mineralization. These conditions are shared by the ESS and could explain a part of the gold enrichment of the intrusion.

1.8.5 ESS emplacement

The abundant volcanic host rocks' fracturing and brecciation (i.e., Héva and Val-d'Or Formations) in drill cores and intense hydrothermal alteration associated with veining and stockwork formation attest to a shallow emplacement of the stock. The lack of magmatic foliation and ductile deformation evidence induced by the intrusion as well as the sharp contact between the intermediate ESS facies (IP) and the host rocks are also in agreement with a shallow emplacement. Shallow emplacement of intrusion are a common feature of Cu skarns (Meinert et al., 2005). The presence of coarse porphyritic textures and glomerocrysts in the ESS suggests a deep crystallization processes in a magmatic system dominated by a crystal mush (Cashman et al., 2017). In the upper part of the crust, the magma ascent may have been led by some crustal incident. Located 600m south of the intrusion, the crustal structure, or proto-CLLFZ, forming the southern border of the study area (Daigneault et al., 2002; Bedeaux et al., 2017) could have favored the emplacement and ascent of the ESS (>2684Ma) (Figure 1.15). Finally, the metasomatic halo developed in the vertical volcanic rock units

testifies of an emplacement after the deposition and tilting of the Héva and Val-d'Or Formations. The magma ascent toward its final emplacement was probably favored by the interface between these volcanic formations (Figure 1.15).

1.8.6 ESS magma evolution

According to the definition of Laurent et al. (2014) and Moyen (2019), the ESS displays the major geochemical and mineralogical characteristics of the sanukitoid rocks (see Section 1.6.1), especially the early and least differentiated facies, EP: 1) an average SiO₂ content of 56 wt.%, associated with high contents of ferromagnesian oxide content (FeO_t + MgO + MnO + TiO₂ >8 wt.%), and a metaluminous nature (Table 1.1); 2) high LILE content (av. Ba = 1000 ppm, av. Rb = 118 ppm and Sr >1500 ppm) conjugate with typical Nb, Ta, and Ti anomalies (Table 1.2 and Figure 1.6); 3) high REE content (av. ΣREE = 280 ppm) associated with a strong fractionation (La(N)/Yb(N) = 13.5) and small Eu anomaly (av. Eu/Eu* = 0.85) (Table 1.2 and Figure 1.6). However, except for V (av. = 130 ppm), the transition elements content (av. Ni = 10 ppm, av. Cr = 18 ppm) as well as Mg # (average of 0.4 ppm) are relatively low (Table 1.1 and Table 1.2) near the limits of sanukitoid definition fields (e.g., Stern and Hanson 1991; Martin et al. 2005). Nevertheless, the geochemistry of the intrusion reflects the sanukitoids mantle-crustal duality (Martin et al., 2005; Laurent et al., 2014). In addition, the sanukitoid magmas are hydrous and often oxidized (Moyen, 2019), such as for the ESS.

Sanukitoids are interpreted as being formed by interactions, in the mantle, between peridotite and an incompatible (both LILEs, including K, and HFSE) element-rich component, most probably TTG melts (Moyen 2019 and references therein), and therefore form mafic to intermediate parental magma rich in Mg, Ni, and Cr, mainly of dioritic composition (Stern and Hanson, 1991; Stevenson et al., 1999; Moyen, 2019). The absence of this parental mafic member in the ESS suite suggests that early facies (EP) is therefore not the parental magma but already represents an evolved magma.

One hypothesis would be that the EP and the ESS sanukitoid suite are formed by a differentiation process, which is in agreement with the documented relative chronology (EP to LP) and establishment of a comagmatic suite (i.e., parallel trace element patterns, common mineral assemblage). In addition, the lack of magmatic enclaves or other mingling and mixing features in the ESS, could support the fractional crystallization hypothesis. Moreover, fractional crystallization is commonly proposed to explain the evolved members of sanukitoid suites (e.g., Stern and Hanson, 1991). The differentiation process is usually controlled by amphibole and plagioclase (e.g., Stern and Hanson 1991; Laurent et al. 2014 and references therein.). This amphibole-controlled fractionation implies variations in some REEs during differentiation, since amphibole preferentially incorporates middle REEs over heavy REEs. These REE variations occurs in the porphyritic suite of the ESS (i.e., from early facies to late differentiated facies) with Sc and Y content, as well as Dy/Yb ratio decrease and simultaneous increasing La/Yb ratio (Table 1.2). These REE variations in the rocks of the ESS are in agreement with a process of differentiation controlled by fractionation of amphibole (cf. Feng and Kerrich 1992; Davidson et al., 2007). This amphibole fractionation control is consistent with the relatively low crystallization temperature estimated on zircon for the ESS (average of $771^{\circ}\text{C} \pm 14^{\circ}\text{C}$). In those conditions plagioclase and pyroxene, precursor of the amphibole by reaction-replacement (Smith, 2014), are not stable. The variation of the fluorine content between the ESS phases (Table 1.2) may also have influenced the differentiation process by reducing the viscosity in the fluorine-enriched porphyry facies (Manning, 1981). Nevertheless, this process alone fails to explain the increasing content for some compatible elements (e.g., Ni, Cr) between the early and late facies in the ESS (Table 1.2). Former studies have proposed an alternative explanation to the fractional crystallization model, such as the one of Stevenson et al. (1999) for sanukitoid suites of the Superior Province that show crustal assimilation during the magmatic differentiation (AFC). Binary mixing, as suggested by Moyen et al. (2001) may also explain the geochemistry of sanukitoid suites. The formation of the ESS sanukitoid suite is instead due to various mixing and

assimilation during the differentiation process from a deep mafic source, allowing an increase in some compatible elements following an alkaline differentiation suite (Lameyre and Bowden, 1982). This interplay of these multiple processes, involving the crystallization of mantle-derived magma and the mixing with felsic melts, mainly TTG, in increasing amounts during differentiation, is evidenced in the formation of numerous sanukitoid suites (Laurent et al., 2013; Moyen, 2019).

1.8.7 Regional implication

The ESS is located in the district of Val-d'Or in the heart of the prolific auriferous quartz-carbonate vein field (Robert, 1994), a vast hydrothermal system including the Sigma-Lamaque deposit. The Lamaque and Sigma mines represent the archetype of orogenic vein-hosted gold mineralization, as defined by Groves et al. (1998). These mineralizations are interpreted as being related to the circulation of syn- to late-orogenic metamorphic fluids along major structural discontinuities. The CLLFZ constitutes the first-order regional structural conduit for the transport of gold-bearing fluids in the Val-d'Or district (Neumayr et al., 2000; Beaudoin and Pitre, 2005; Goldfarb et al., 2005). These fluids are then redistributed along second- and third-order subsidiary discontinuities to form the gold deposits (Robert, 1994). The gold mineralization is contained in a vertically extensive vein system developed within an early porphyritic diorite, crosscut by feldspar porphyry dikes. The latter are themselves cut by steeply plunging diorite-tonalite chimneys (Robert and Poulsen, 1997). The Sigma-Lamaque hydrothermal system extends southeastward into the Triangle and Cheminée No. 4 deposits (J. Dubé, 2018), which are located 2 km from the northwestern limit of the ESS (Figure 1.2). J. Dubé, (2018) interprets the multiphased Lamaque and Triangle intrusions as comagmatic and synchronous based on the geochemical correlations, spatial association and U/Pb dating (2685 ± 1 to 2680.1 ± 4).

The trace element profiles of the Lamaque Cheminée Principale (Figure 1.16A) and Triangle diorite (Figure 1.16B) are remarkably similar to the one of the ESS. The

parallel profiles are characterized by strong to moderate LILE enrichment and characteristic negative Nb, Ta, Ti anomalies. Patterns of the melanocratic Triangle diorite and of the Amphibole Lamaque diorite remain largely indistinguishable from the ESS patterns. All of these intrusions do not show significant Eu anomaly, but show a strong REE fractionation (La(N)/Yb(N) ranging from 8.3 to 26). These characteristics associated with the similar distance between Lamaque vs Triangle and Triangle vs ESS are in favor of a comagmatic system. In addition, the crystallization age of the ESS (2684 ± 1 Ma; Pilote et al. 1999) overlaps with those of the Lamaque (2685 ± 3 Ma; Jemielita et al. 1989) and Triangle intrusions (2685 ± 1 to 2680.1 ± 4 ; J. Dubé, 2018) and supports the presence of a large igneous system including ESS, Lamaque and Triangle intrusions.

The metamorphic grade increases with depth at the Sigma mine, from epidote-chlorite-white mica assemblages in the upper part to epidote-chlorite-biotite assemblages below the 20th levels (800 m) in the wall rocks (andesite, porphyritic diorite and feldspar porphyry dikes) (Robert and Brown, 1986a). Hornblende appears below the 1500 m level in the porphyritic diorite (Robert and Brown, 1986a). This mineralogical zoning is interpreted as a metamorphic event postdating intrusion of the feldspar porphyry dikes (i.e., $<2694 \pm 2$ Ma; Robert and Brown, 1986a). The perpendicular intersection of the local verticalized stratigraphy by the two horizontal isogrades also may be related to an intrusion at depth. Emplacement of the ESS induced a thermal metamorphism in the vicinity of the intrusion and could extend to the Sigma-Lamaque area. The presence of hornblende was also evidenced in the Lamaque mine in diorite. In the Sigma mine, the presence of hornblende was restricted to the porphyritic diorite due to the absence of andesites and feldspar porphyry dike in the deeper levels of the mine (Robert and Brown, 1986a). However, this zonation, not yet observed in Triangle or Cheminée No4, could be related to some tectonic events (local fault displacement, variable erosion level...), therefore the interpretation of this metamorphic gradient remains questionable.

Lode-gold mineralization in the Val-d'Or district is interpreted to have been formed by two distinct events (Couture et al., 1994; Robert, 1994). The first event occurs prior to 2690 Ma and is affected by the main shortening event in the area (Feng and Kerrich, 1992; Daigneault et al., 2002; Bedeaux et al., 2017) and metamorphism in the west part of the Val-d'Or district (Couture et al., 1994). The younger second event postdates magmatism and is coeval with metamorphism, being younger than 2684 Ma and extending to circa 2600 Ma (Couture et al., 1994; Robert et al., 2005). This second event occurs in the Sigma-Lamaque deposit and Triangle plugs (J. Dubé, 2018), as well as in the eastern part of the Val-d'Or district (Couture et al., 1994). The Lamaque and Triangle intrusions are interpreted as pre-gold deposition (J. Dubé, 2018 and references therein) and as competent physical and chemical traps for orogenic gold vein formation. However, the Lamaque and Triangle association with the sanukitoid gold fertile ESS intrusion questions the role of the ESS in the formation of the gold system. The emplacement of the ESS between the CLLFZ and the Lamaque and Triangle intrusions may have favored the formation of an important plumbing system, allowing the circulation of orogenic fluids from the CLLFZ to the gold deposits of Sigma-Lamaque (Figure 1.15). This is supported by the crystallization age of the ESS (2684 ± 1 Ma), the Re/Os dating from this study on Molybdenite (2695 ± 12 Ma) associated with the ESS mineralization and the Triangle and Lamaque plugs (2685-2680 Ma). In addition, the magmatic gold contained in the ESS, due to its gold fertility, could have been remobilized and concentrated by the orogenic fluids from the CLLFZ associated with the second gold mineralization event. Overprinting a magmatic-hydrothermal system by an orogenic event is recognized in some Abitibi deposits such as at Hollinger-McIntyre and at the Dome deposit (Groves et al., 2003) or at the Wasamac deposit (Mériaud and Jébrak, 2017). A process of remobilization of the gold and possibly the copper from the ESS, could explain the vertical sulfide zoning observed at Sigma with an unusual abundance of chalcopyrite below 1300 m rather than pyrite (Robert and Brown, 1986b). At Sigma, a minor part of the gold is interpreted as contemporaneous of the chalcopyrite evidenced by their respective association and mutual intergrowth

(Robert and Brown, 1986b). This copper event may have been sourced from the Cu-enriched ESS intrusion. However, it remains equivocal because copper may also have been scavenged from local mafic rocks. This demonstrates the importance of dedicated studies on the gold-bearing fluids in the orogenic Sigma-Lamaque deposit as well as better constraining the gold timing mineralization.

1.8.8 Comparisons with other skarn deposits

The only known skarn occurrence in the Abitibi greenstone belt is the Akasaba deposit in the vicinity of the ESS (Vorobiev, 1998). It displays characteristics very similar to the ESS skarn system, especially calc-silicate mineral assemblages, metal and mineral zoning, host rock composition, paragenetic sequences, as well as the mineralization formation during the retrograde phase (i.e., mainly epidote and actinolite), and abundant magnetite (Table 1.10). Nevertheless, the Akasaba deposit exhibits some specificities like a structurally-controlled Au-rich zone dominated by pyrrhotite. Also, the extension of the calc-silicate alteration within the Héva Formation is controlled by local lithological variations with mineralized zones being mainly located within tuffs and volcanic breccia units (Vorobiev, 1998). However, a genetic relation with an intrusion has not been demonstrated at the Akasaba deposit. Vorobiev (1998) proposed an intermediate to felsic multiphase intrusion with sub-alkaline to alkaline affinity, such as the ESS or similar intrusion, to provide the hydrothermal fluids associated with the skarn mineralization development. The ESS was the ideal candidate, but the nearby Callahan and Sabourin intrusions (i.e., 2 and 4 km respectively, Figure 1.2), or fluids from an intrusion at depth, possibly of similar composition to the ESS, also may have contributed to the formation of the Akasaba deposit. These monzonitic porphyry plutons intrude the Héva Formation along the CLLFZ and with the ESS form an intrusive corridor parallel to the fault zone. However, the Callahan and Sabourin intrusions have not been the subject of dedicated studies and genetic relationships with the Akasaba deposit therefore remain to be demonstrated.

Apart from these occurrences, skarn-type deposits remain atypical in Archean rocks, unlike Phanerozoic rocks, which contain abundant skarn deposits (Einaudi, 1981; Dawson et al., 1995; Meinert et al., 2005). This Archean exception can be explained by a scarcity of carbonate rocks, different geodynamic contexts, the lack of fertile intrusions, as well as the erosion of ancient terranes. Nevertheless, several gold deposits in the Precambrian belt exhibit skarn-type alteration in areas of high-grade metamorphism (Meinert et al., 2005 and reference therein). Their Fe-rich mineralogy and reduced assemblages, as well as their geochemical resemblance to Phanerozoic Au-skarn, differ greatly from the ESS skarn mineralization. In addition, some of these skarn deposits are interpreted as having formed in deep hypozonal environments (e.g., 10-15 km at Nevorio Au-skarn in the Archean Yilgarn craton, Mueller (1997); Mueller et al. (2004)), distinct from the shallow environment proposed for the formation of the skarn associated with the ESS and modern Au-Cu-Fe skarn analogue.

Several Cu-Au skarn occurrences are documented in the Australian Eastern Goldfields Province within the Archean Yilgarn craton, and associated with the Mt. Shea intrusive complex (Table 1.10; Mueller 2007; Mueller et al. 2012). The skarns described as epidote endoskarn (Mueller et al., 2007) are formed between 2658 ± 3 and 2642 ± 6 Ma and located near the Boulder Lefroy and the Golden Mile strike-slip faults. These deposits contain epidote-calcite-chlorite-magnetite gangue (Hannan South) and epidote-actinolite-magnetite zones (Shea prospects), mineralized in pyrite and chalcopyrite, and which are similar to skarns related to the ESS. However, unlike the ESS skarn, prograde assemblages at Hannan South are poorly developed and are interpreted as having formed deeper in the crust. Nevertheless, a notable common feature with the ESS mineralization is the genetic relation of the Mt. Shea skarn with oxidized porphyry intrusions, which display affinities to Archean sanukitoids (Mueller, 2007). Mueller et al. (2007) also report the presence of an epidote-actinolite-calcite skarn in the Wallaby district associated with sanukitoid oxidized monzodioritic to syenitic intrusion. These sanukitoid intrusions and Cu-Au syenite associated deposits

(Mueller et al., 2007; Witt et al., 2018) are interpreted as equivalent to the Timiskaming-type syenites of Robert (2001). They exhibit fertility indicators similar to the ESS, including oxidized and hydrous magma similar to the Phanerozoic alkali-rich porphyry systems formed in post-subduction context (Witt et al., 2018).

Phanerozoic alkaline to sub-alkaline porphyry intrusions and associated Cu-Au deposits indeed provide a great analogue to these sanukitoid intrusions and particularly to the ESS. The numerous Cu-Au skarns in the Canadian Cordillera share several features with the ESS skarn mineralization, especially the Galore Creek porphyry copper deposit (Table 1.10; Enns et al. 1995; Micko et al. 2014). Located in the Intermontane Belt, the Galore Creek Cu-Au skarn is hosted by Upper Triassic volcanic and volcanic-derived rocks within the Stikinia terrane. Formed in a comparable orogenic context, the skarn mineralizations are associated with multiple porphyritic to equigranular, alkaline, monzonitic to syenitic intrusions similar to the ESS. The potassic and sericite alteration at Galore Creek as well as the calc-silicates minerals forming the skarn gangue are also comparable to those observed within the ESS. In addition, some porphyritic syenites exhibit mafic minerals replaced by aggregates of garnet and epidote in association with sulfides. Garnet and epidote also occur in vug fillings and are interpreted as resulting from metasomatism during the magma cooling (Enns et al., 1995). This alteration is reminiscent of the mineralized episyenite facies (MP) in the ESS. However, the general alteration pattern in the Galore Creek deposit is locally different, exhibiting complex overlap due to the many intrusive events in the area. Faults, breccias, and diatremes also have significant influence on the mineralizing process. Nevertheless, the ESS skarn mineralization appears to be a smaller Archean version of the Cu-Au Phanerozoic skarn deposits related to alkali-rich porphyry intrusions.

1.9 Conclusion

The ESS is an Archean monzonitic to syenitic porphyritic intrusive suite consisting of three major distinctive facies: early, intermediate, and late. The intrusion shares specific features with the gold-associated syn-Timiskaming sanukitoid group. The emplacement of the ESS crystallized at approximately 2684 Ma after the Héva and Val-d'Or Formation deformation and verticalization, erupted respectively between 2705 and 2702 Ma. The alkaline affinity of the ESS, in addition to its high oxidation state and the high-water content of the initial magma, are indicators of its potential to form Cu-(Au-Mo) porphyry-style mineralization. Three main characteristic alteration assemblages associated with the porphyry mineralization have been identified: (1) potassic with biotite-microcline-quartz-magnetite assemblage; (2) phyllic with sericite-quartz \pm pyrite assemblage; and (3) propylitic, represented by epidote \pm chlorite \pm calcite assemblage.

In addition, the carbonatized volcanic rocks surrounding and hosting the ESS enabled the development of a Cu-(Au-Ag) skarn mineralization, focused along the verticalized, prior to the emplacement of the ESS, volcanic strata. This setting restrained the zoning pattern usually observed in Phanerozoic Cu skarns. The skarn formed as a result of three main stages: 1) a high-temperature thermal event induced by the ESS emplacement; 2) a prograde hydrothermal stage dominated by garnet; and 3) a widespread retrograde stage leading to mineralization precipitation and destruction of the prograde stage with decreasing temperature. Episyenitization of the ESS intermediate facies allowed a local enrichment in Cu-Mo related to an endoskarn formation. The endoskarn may have been triggered by the relatively high fluorine content of the intermediate facies. The bulk of the copper deposition coincides with the transition between the prograde and retrograde stages in the exoskarn, as well as the waning stages of potassic alteration within the intrusion. This demonstrates the existence of Cu-Au skarn deposits in the Abitibi greenstone belt.

The ESS and associated skarn mineralization are contemporaneous of the crystallisation of the Lamaque and Triangle plugs that host the multimillion-ounce deposits currently mined. These intrusions form a large and prolific igneous system located between the CLLFZ and the city of Val-d'Or. This area displays therefore two distinct gold events: -the first plutonic-related associated to the ESS, the second related to a younger orogenic hydrothermal event associated with the regional metamorphism. This two events raise the question about either a common longstanding gold origin, or a possible remobilization of plutonic gold by orogenic fluids in the Val-d'Or district.

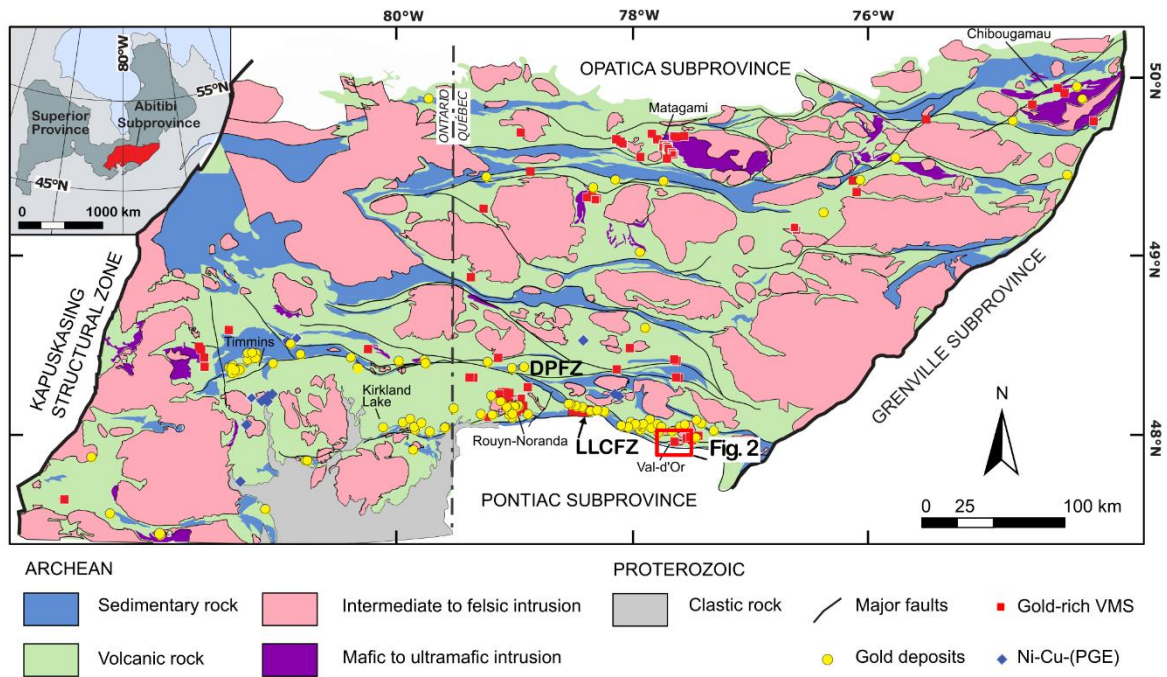
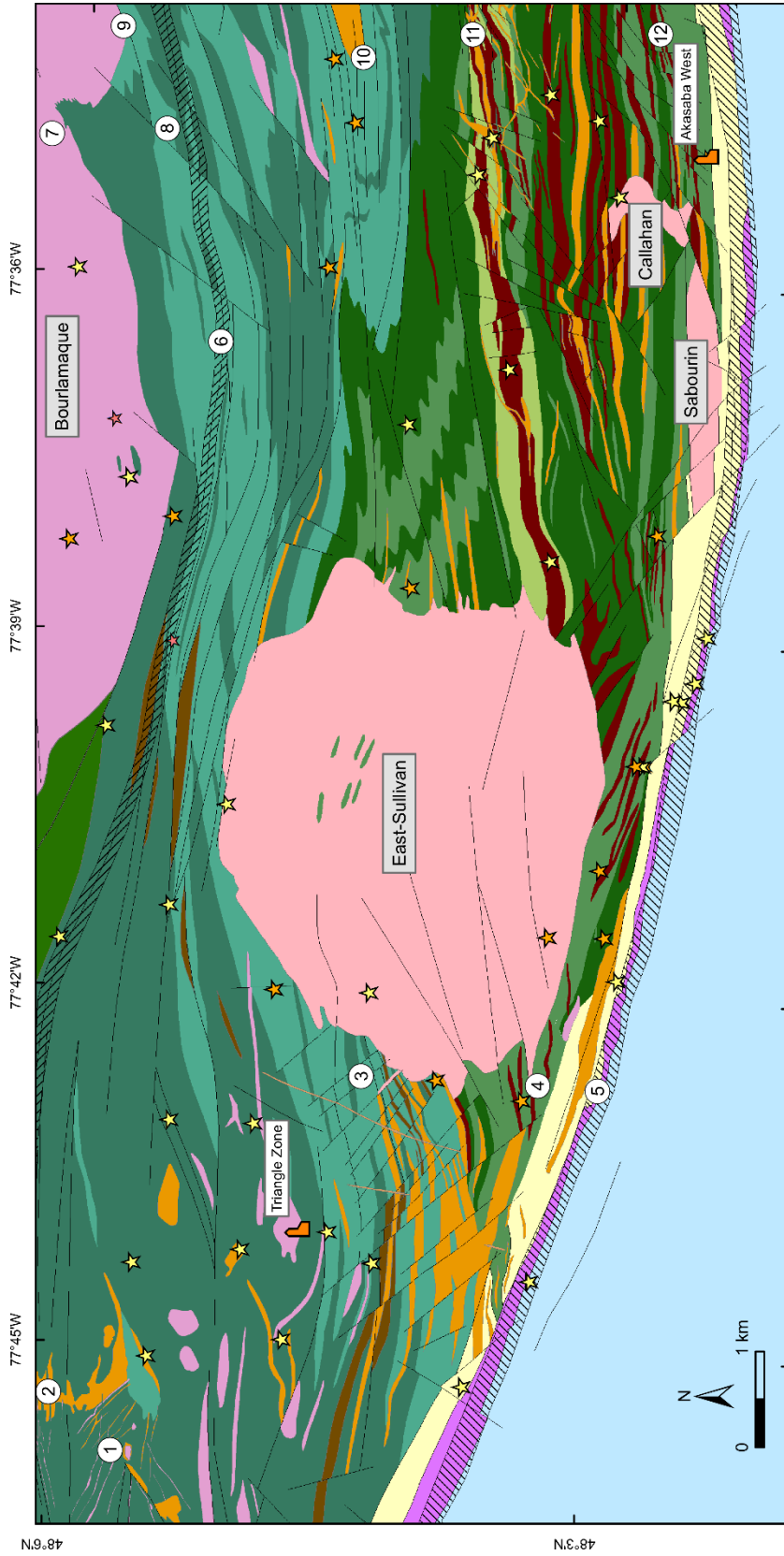


Figure 1.1 Geological map of the Abitibi greenstone belt showing the distribution of the main deposits. Inset shows the location of the Superior province; location of Figure 2 is marked by a red rectangle. Abbreviations: DPFZ = Destor-Porcupine Fault Zone, CLLFZ = Cadillac-Larder Lake Fault Zone. Modified from Mercier-Langevin *et al.* (2014)



Historical mines

- ① Lamaque
- ② Sigma
- ③ East Sullivan (Sullico)
- ④ Mid-Canada
- ⑤ Orenada (No.4)
- ⑥ Manitou-Barvue
- ⑦ Wrightbar
- ⑧ Quebec Manitou
- ⑨ d'Or Val (Beacon No.2)
- ⑩ Dumrairie
- ⑪ Simkar (Louvicoourt Gold Fields)
- ⑫ Akasaba

Fault Zone

- Cadillac
- Manitou
- Faults

Showings

- Au
- Cu
- Zn
- Active mines

Val d'Or Formation

- Mafic to intermediate volcanic rocks
- Volcanoclastics and intermediate to felsic volcanics
- Gabbro

Jacola Formation (Malaric Group)

- Basalt, mafic to intermediate volcanoclastics
- Intrusions
- Quartz diorite and tonalite
- Diorite
- Monzonite-Syenite

Proterozoic

- Diabase dike

Archean

- Pontiac Group**
- Wacke, pelite, sandstone
- Piché Group**
- Ultramafic and volcanic rocks
- Cadillac Group**
- Wacke, pelite, conglomerates
- Héva Formation (Louvicoourt Group)**
- Volcanoclastics and mafic to intermediate volcanic rocks
- Volcanoclastics and intermediate to felsic volcanics
- Spherulitic tuffite
- Gabbro

Figure 1.2 Simplified geologic map of the East-Sullivan Stock area and the main showings with the location of the mines. Geology is from Pilote *et al.* (2017) and this study.

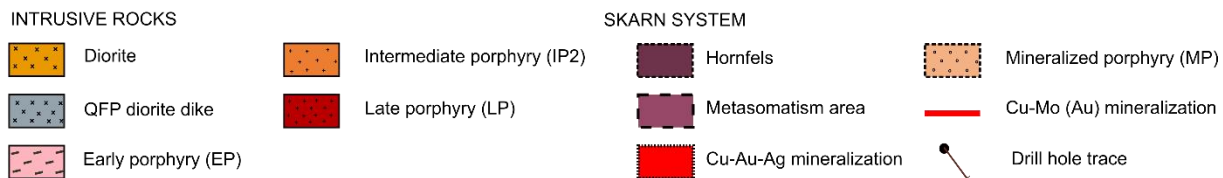
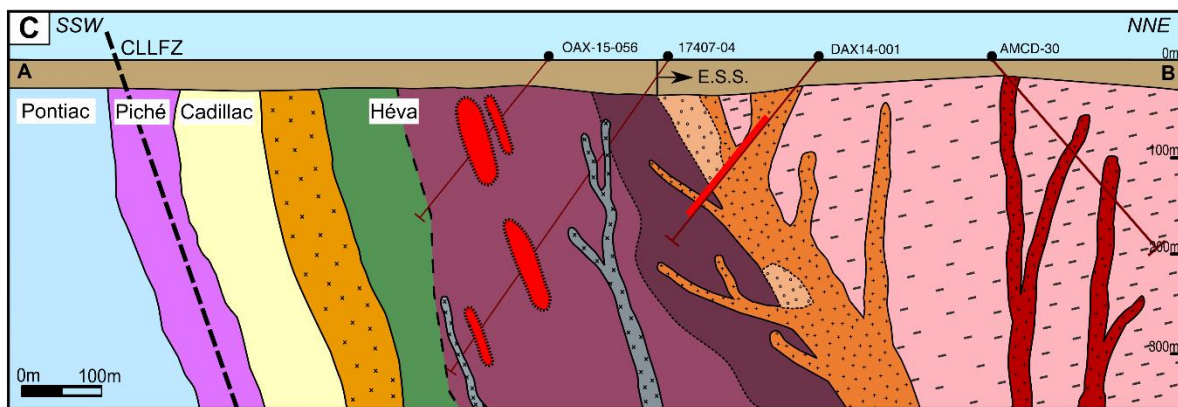
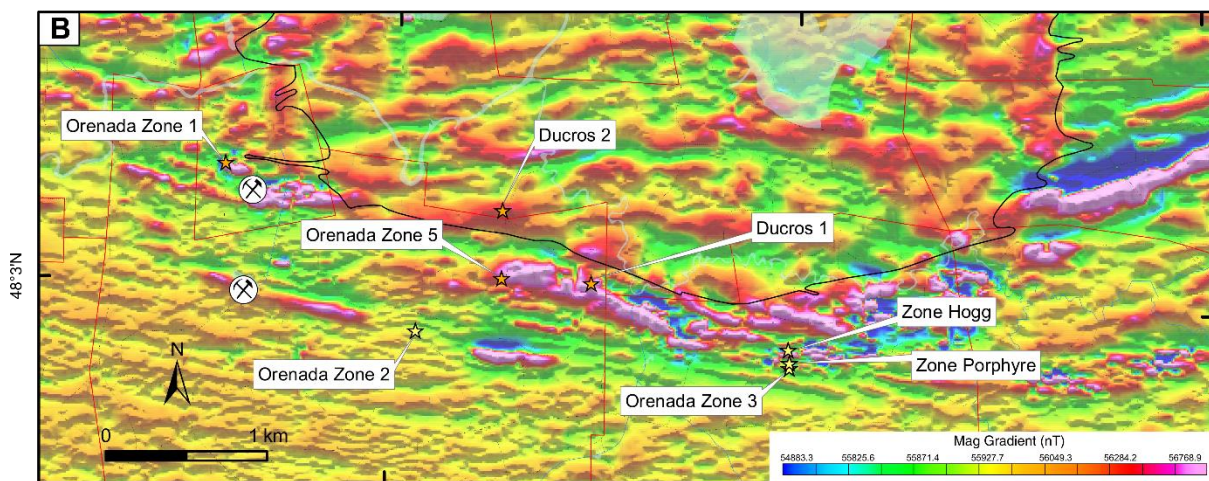
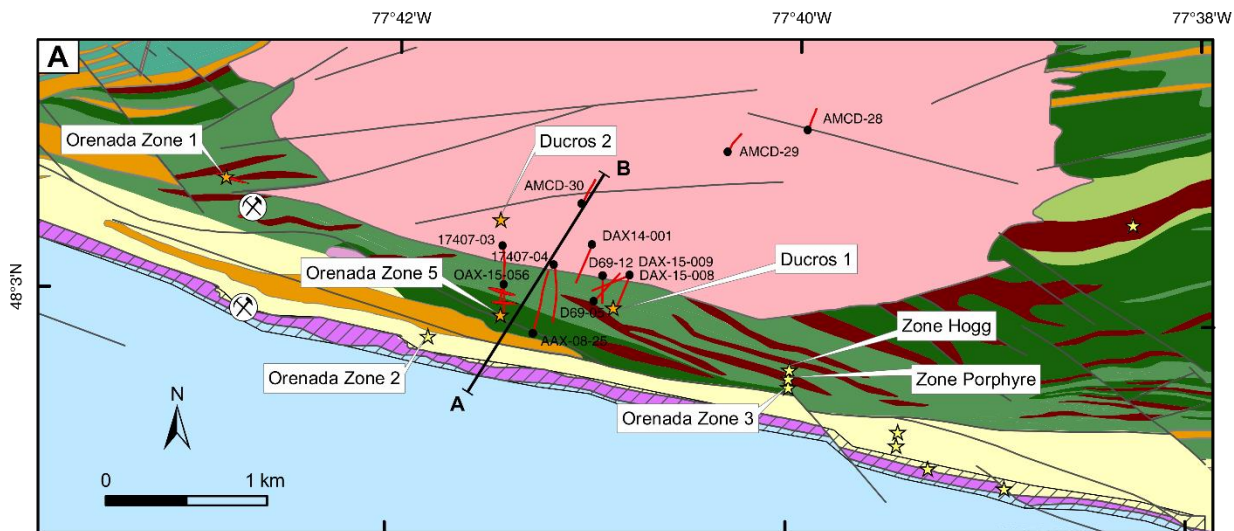


Figure 1.3 (A) Geological and (B) geophysical map of the East-Sullivan intrusion South border with location of the A-B cross section and main showings; (C) Geological cross section through the South border of the intrusion showing the ESS skarn system and related alteration area in the surrounding units; the ore zones are associated with highly altered corridors parallel to the E.S.S contact with the Héva Formation. See Figure 1.2 for the geological map legend. Abbreviations: CLLFZ = Cadillac-Larder Lake fault zone.

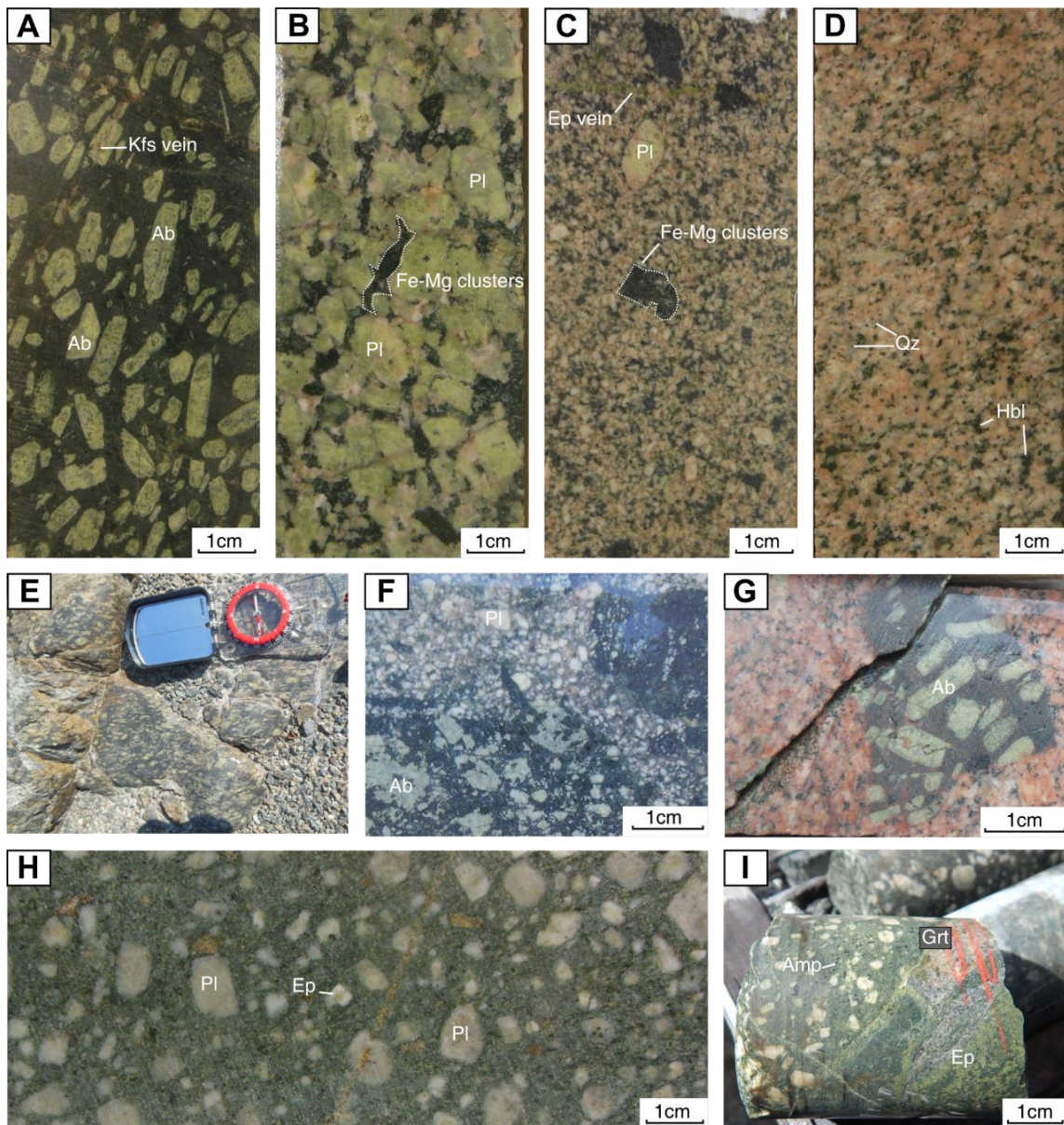


Figure 1.4 Hand specimen photographs of samples of East-Sullivan porphyry intrusions: (A) Early porphyry (EP) facies with altered megaphenocrysts of albite in a microcrystalline matrix, crosscut by K-feldspar veins (drill hole AMCD-28); (B) Intermediate porphyry (IP1) facies with megaphenocrysts of altered plagioclase and Fe-Mg clusters (drill hole 17407-03); (C) IP2 porphyry facies with a glomeroporphyritic texture and zoned plagioclase, cross-cut by an epidote vein (drill hole DAX-15-008); (D) Late porphyry (LP) phases with plagioclase, quartz and

hornblende (drill hole AMCD-28); (E) EP in outcrop; (F) EP crosscutting and partially digested by IP2; (G) EP enclave in LP dike, the reddish color is due to hematite; (H) Feldspar porphyry dike (drill hole AAX-08-025); (I) Skarn alteration in Héva formation crosscut by a feldspar porphyry dike. Abbreviations: Ab = albite; Amp = amphibole; Ep = epidote; Fe-Mg = ferromagnesian; Grt = garnet; Kfs= K-feldspar; Pl = plagioclase; Qz = quartz.

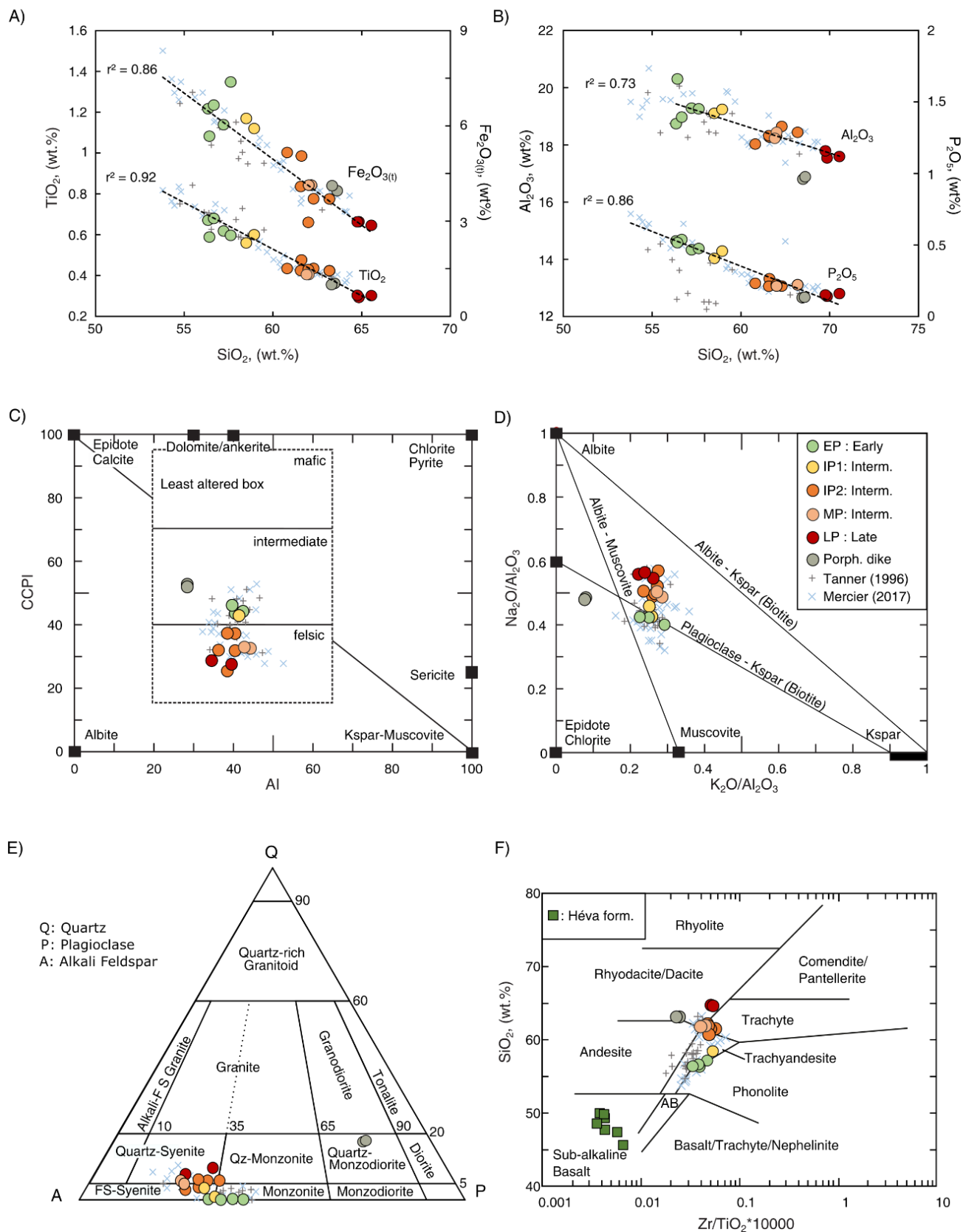
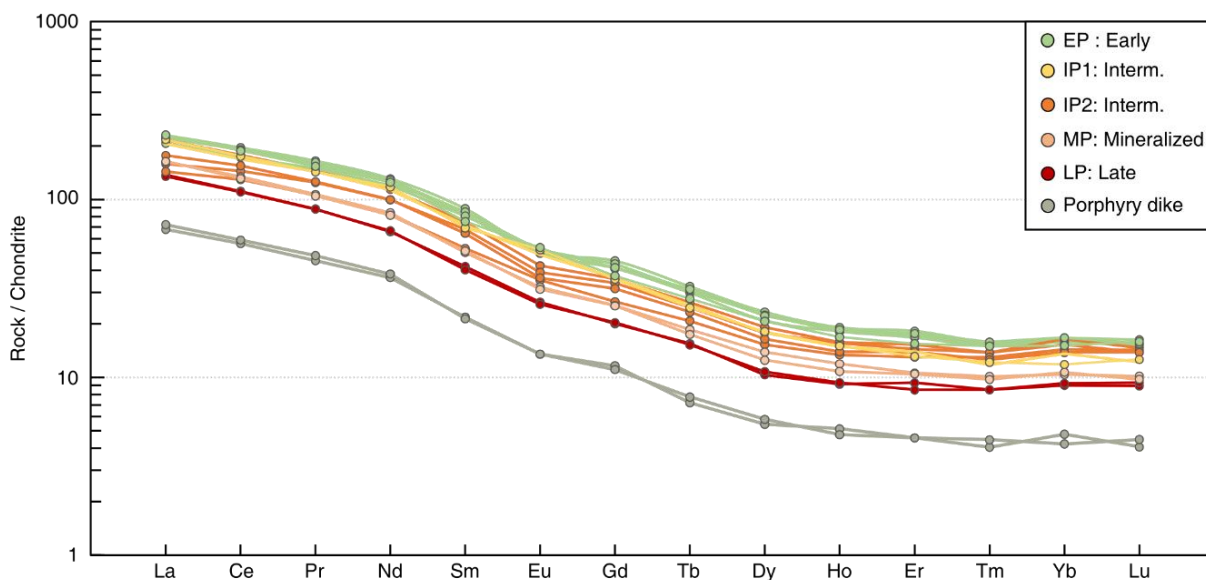


Figure 1.5 Major element geochemistry plots for the rock of the East-Sullivan intrusive suite: (A) Co-variation plots of $\text{Fe}_2\text{O}_3(\text{t})$ and TiO_2 vs SiO_2 (wt%); symbols for the facies are shown in (D); (B) Co-variation plots of Al_2O_3 and P_2O_5 vs SiO_2 (wt%); (C) alteration box plot from Large *et al.* (2001) with Hashimoto alteration (Saeki and Date, 1980; Date et al., 1983) plotted against chlorite-carbonate pyrite index [CCPI: $(\text{MgO} + \text{Fe}_2\text{O}_3(\text{t})) / (\text{MgO} + \text{Fe}_2\text{O}_3(\text{t}) + \text{Na}_2\text{O} + \text{CaO})$]; (D) $\text{Na}_2\text{O}/\text{Al}_2\text{O}_3$ vs $\text{K}_2\text{O}/\text{Al}_2\text{O}_3$ molar from Davies and Whitehead (2006); (E) Streckeisen plot of the ESS porphyries facies; the compositions range from Syenite to Monzonite; (F) SiO_2 vs Zr/TiO_2 petrological classification from Winchester and Floyd (1977). The host rock has a basaltic composition. Data from this study, Taner (1996), Mercier and Berthelot (2017).

A)



B)

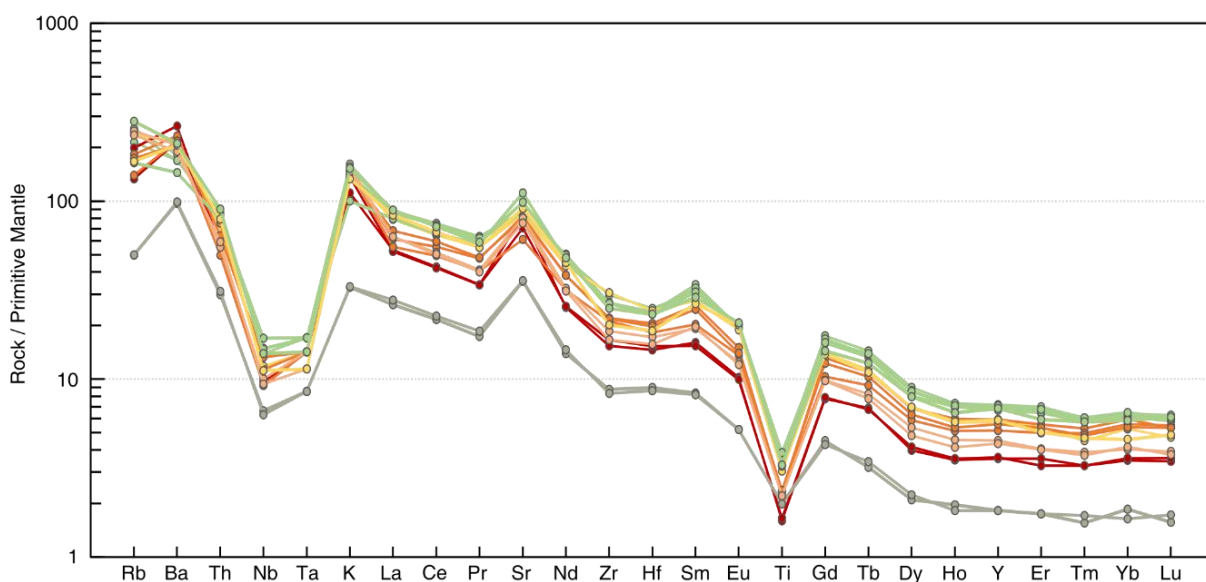


Figure 1.6 Normalized trace element abundances of the East-Sullivan facies: (A) REE profiles normalized to chondrite from McDonough and Sun (1995); (B) Extended trace element profiles normalized to primitive mantle from Hofmann (1988). All the samples exhibit enrichments in LREE relative to HREE and/or MREE, as well as characteristic negative Nb, Ta and Ti anomalies.

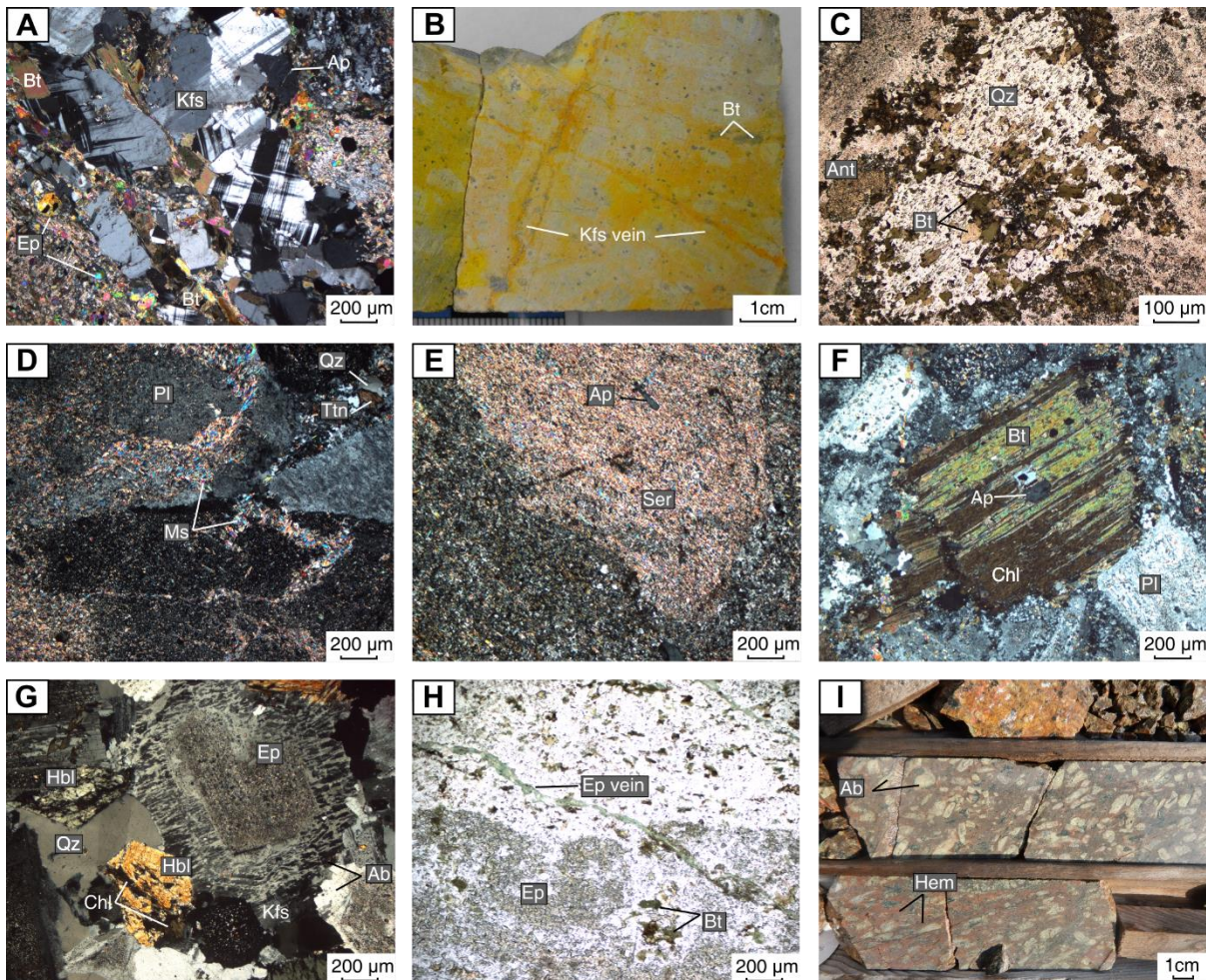


Figure 1.7 Hand specimen photographs and photomicrographs of the typical alterations in the East-Sullivan Stock: (A) K-feldspar, biotite, and apatite vein in a highly altered intermediate porphyry (IP) rock (drill hole AMCD-30); (B) Potassic staining of early porphyry stage (EP) to reveal K-feldspar (yellow), cut by secondary K-feldspar veins (drill hole AMCD-28); (C); Pseudomorphosis of quartz, biotite, and titanite (anatase) after primary Fe-Mg mineral in intermediate porphyry (IP); (D) Muscovite-sericite vein and impregnation of primary plagioclase and groundmass by sericite in the early porphyry phase (EP) (drill hole 17407-03); (E) Complete replacement of primary plagioclase phenocrysts by sericite in EP (drill hole AMCD-29); (F) Pervasive

alteration of magmatic biotite by brown chlorite following cleavages in an intermediate porphyry phase (IP2) (drill hole DAX-15-008); (G) Calcic core replacement by epidote of perthitic primary plagioclase and chlorite alteration of magmatic hornblende in late porphyry (LP) (drill hole AMCD-29); (H) Late epidote vein crosscutting the matrix and an epidotized plagioclase in EP (drill hole AMCD-28); (I) Intense pervasive hematization of EP facies (drill hole AMCD-29). Abbreviations : Ab = albite; Ant = anatase; Ap = apatite; Bt = biotite; Chl = chlorite; Ep= epidote; Hem = hematite; Hbl = hornblende; Kfs = K-feldspar; Mt = magnetite; Ms = muscovite; Ser= sericite; Ttn = titanite; Qz = quartz.

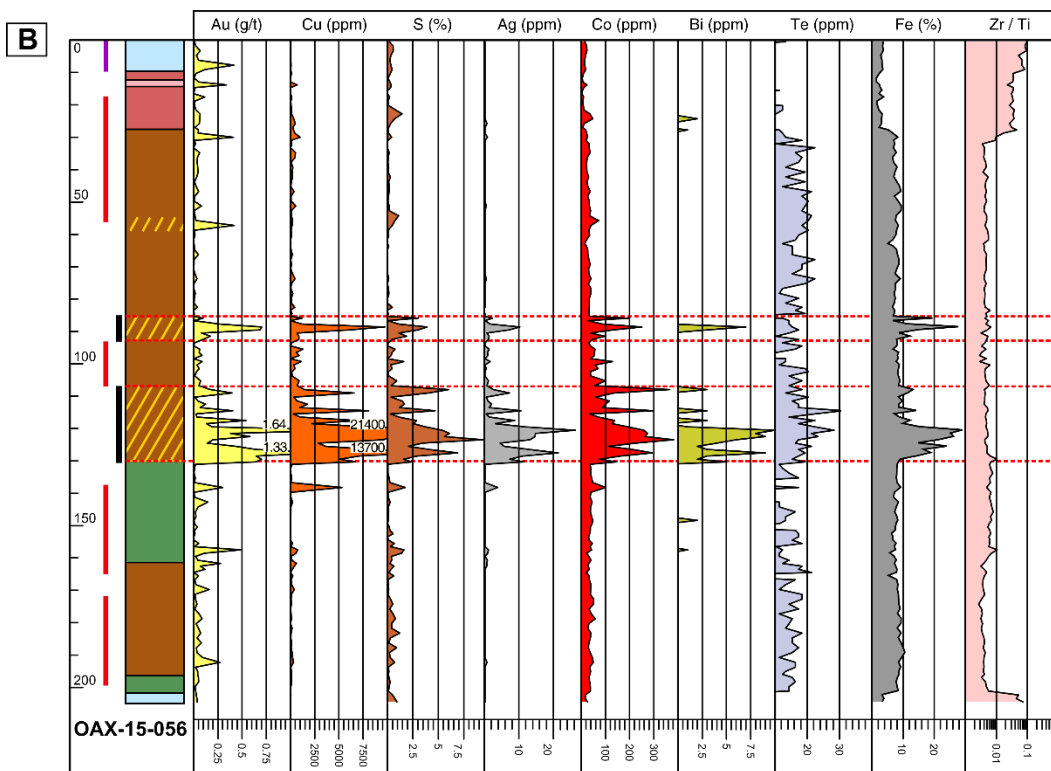
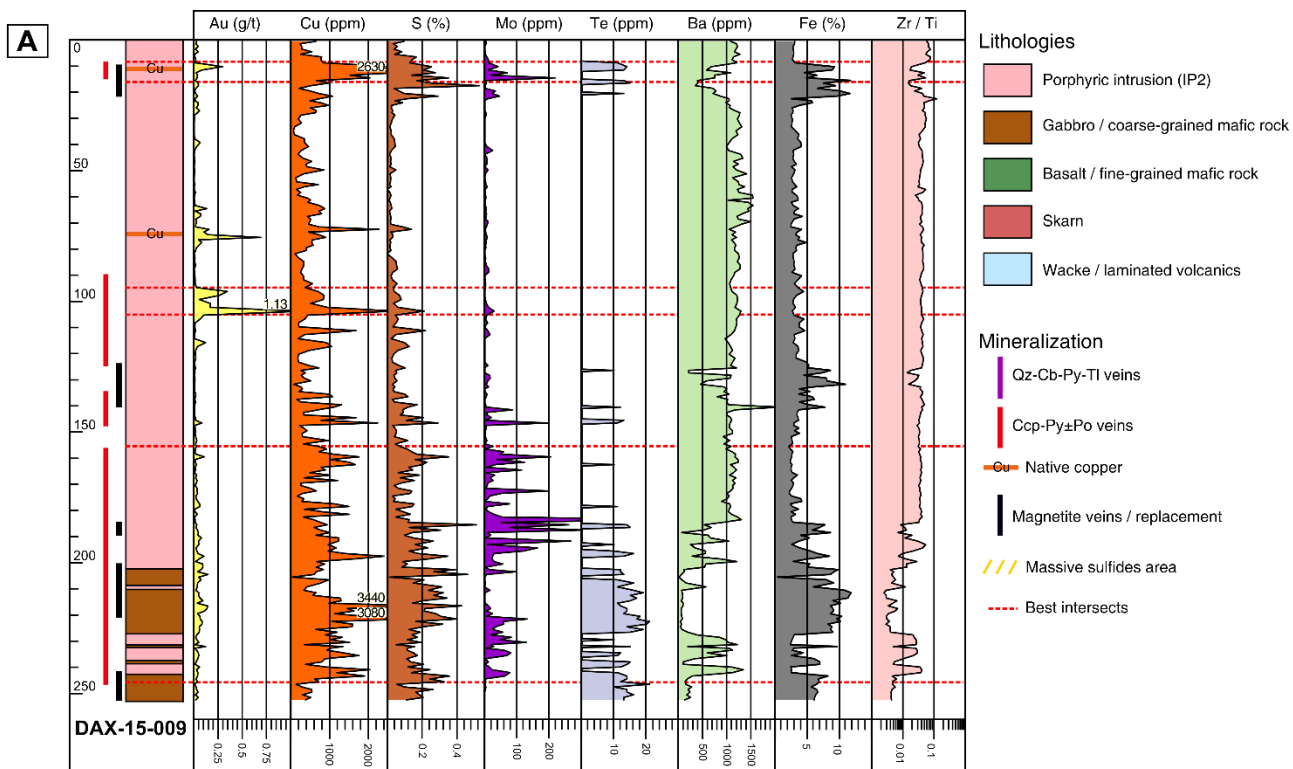


Figure 1.8 Drill core logs with geochemical profiles of selected elements and ratios for ore zone: (A) hole DAX-15-009 through Ducros Zone 1 (Cu-Au porphyry-style) in the East-Sullivan Stock and (B) hole OAX-15-056 through Zone 5 (Cu-Au-Ag skarn) in the Héva Formation. Values are assay data from Alexandria Minerals. See Figure 1.3A for location of drill holes. Abbreviations: Cu = native copper.

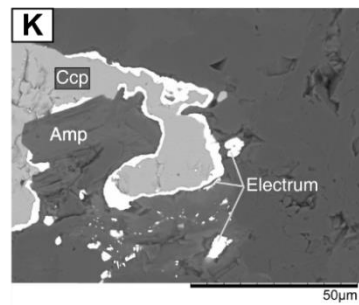
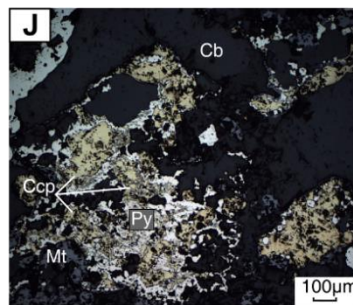
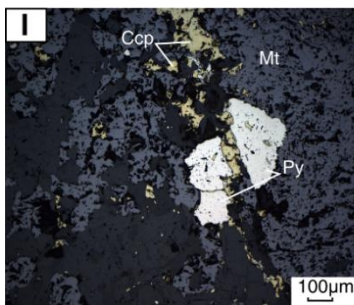
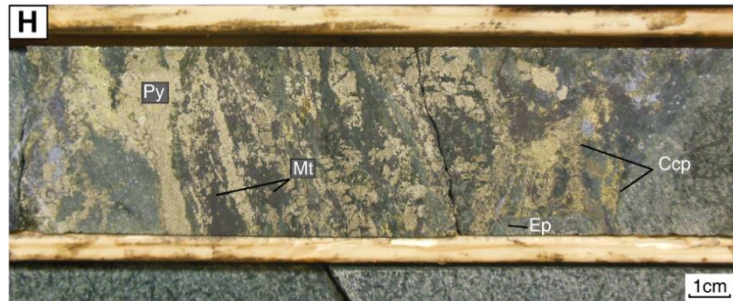
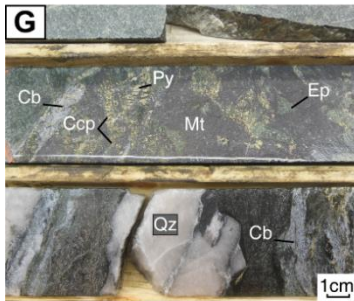
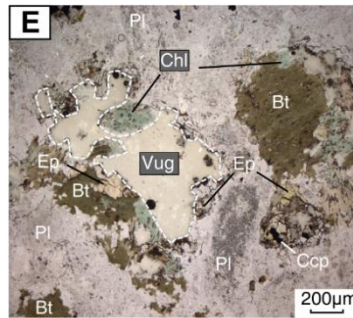
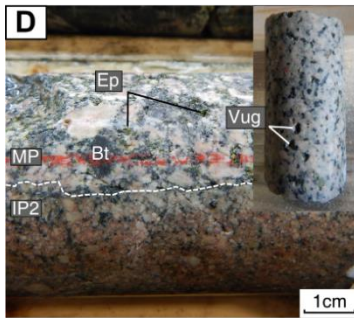
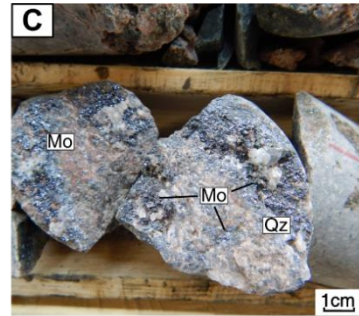
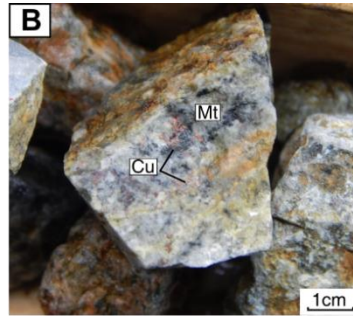


Figure 1.9 Hand specimen photographs and photomicrographs of mineralized phases and ore zone within the East Sullivan Stock and in the Héva Formation: (A) Quartz-molybdenite vein in K-altered intermediate porphyry (IP2) (drill hole DAX-15-009); (B) Dendritic native copper and magnetite in highly altered porphyry rock (DAX-15-010); (C) Contact between IP2 and historical mineralized porphyry (MP) (drill hole DAX-15-009); (D) Sample core of MP with characteristic vugs (drill hole D69-05); (E) Secondary filling of vug by biotite, chlorite, epidote, chalcopyrite surrounding by albite-plagioclase (drill hole D69-05); (F) Outcrop of Zone 5 showing pyrite-chalcopyrite-magnetite massive mineralization in a metasomatized basalt; (G) Chalcopyrite-pyrite-magnetite mineralization within an amphibole rich gabbro; a late quartz vein and calcite veinlets cross-cut the mineralization (drill hole OAX-15-056); (H) Zone 5 massive mineralization (drill hole OAX-15-056); (I) Chalcopyrite filling and cross-cutting a pyrite grain in magnetite fracture, reflected light (drill hole 17407-04); (J) Complex pyrite-chalcopyrite association in ore zone, reflected light (drill hole OAX-15-056); (K) Backscattered electron imaging (BSE) of electron microprobe around chalcopyrite in Zone 5 ore zone (drill hole OAX-15-056). Abbreviations: Amp = amphibole; Bt = biotite; Cb = carbonate; Ccp = chalcopyrite; Chl = chlorite; Cu = native copper; Ep = epidote; Mo = molybdenite; Mt = magnetite; Pl = plagioclase; Py = pyrite; Qz = quartz.

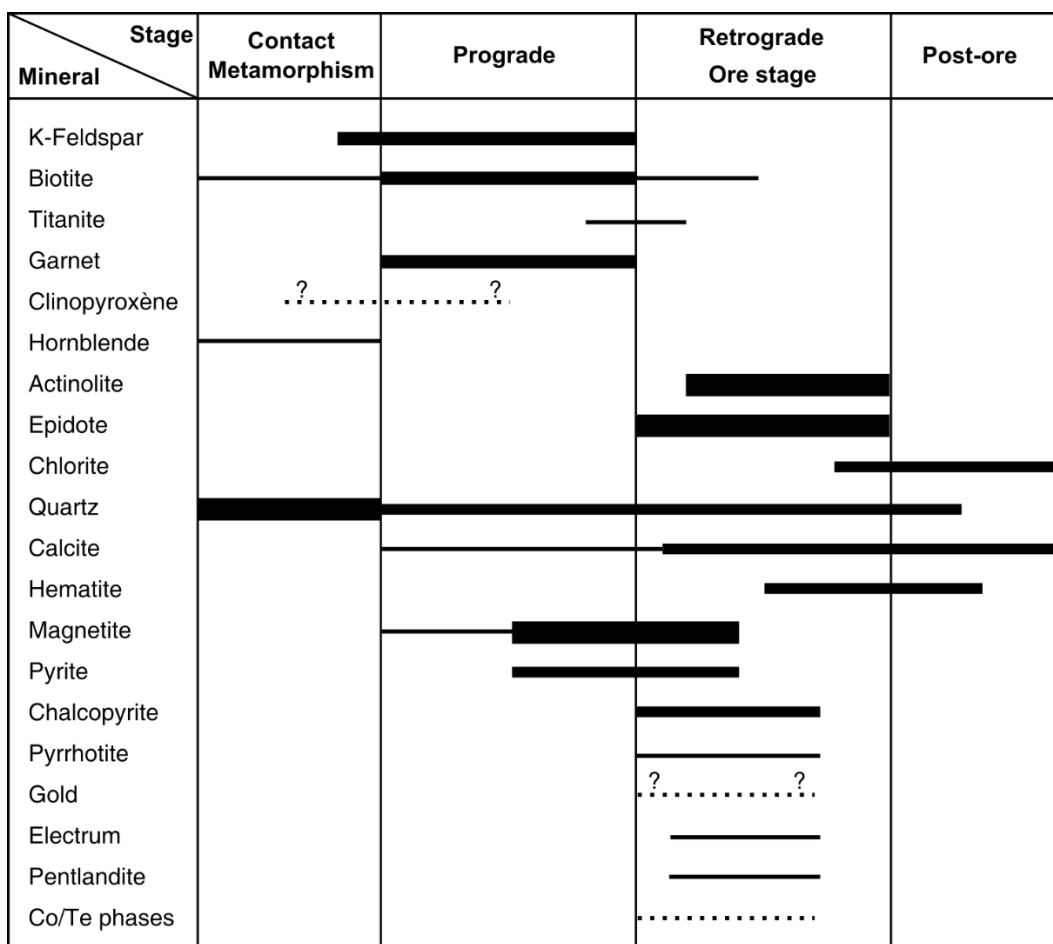


Figure 1.10 Paragenetic sequence diagram for East-Sullivan skarn assemblages. Relative abundances are indicated by width of lines. Dashed lines indicate uncertainty in timing of minor phases

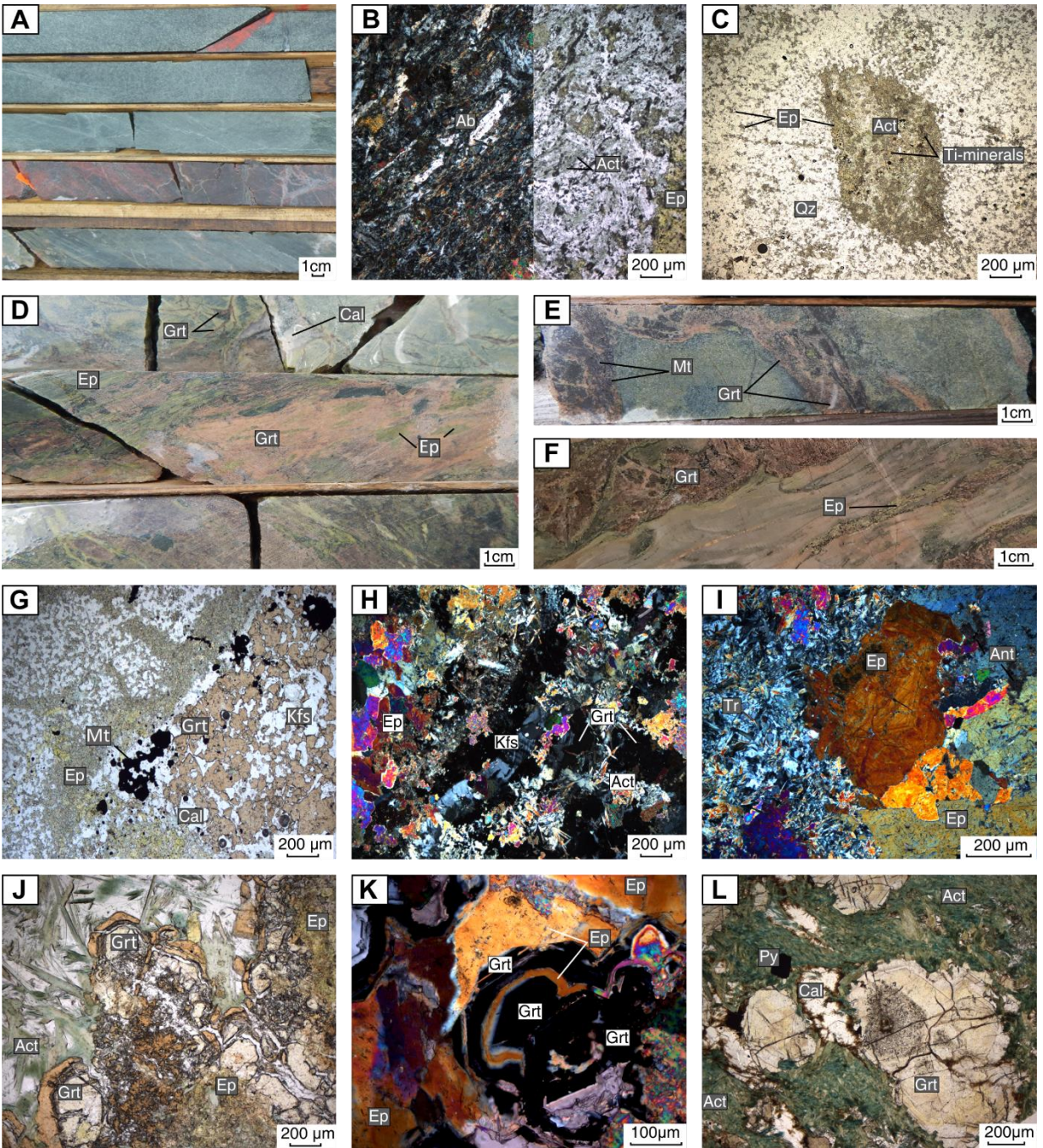


Figure 1.11 Hand specimen photographs and photomicrographs of host rock, hornfel and skarn area from the Héva Formation: (A) Gabbro displaying typical white patchy texture on top and fine tuff levels in the lower part; intense silicification of gabbro occurs in central part (drill hole 17407-04); (B) Albite laths, fibrous actinolite and epidote in a strongly altered basalt (drill hole D69-05); (C) Pseudomorphosis of Fe-Mg minerals by actinote-anatase-epidote surrounding by a quartz-epidote matrix in silicified area (drill hole 17407-03); (D) Complete replacement after volcanics by massive garnet, epidote and amphibole; small zoned veins of garnets and epidote are visible in the upper part (drill hole AAX-08-25); (E, F) Partial skarn replacement : pink to red garnet, green epidote-actinolite, magnetite, and calcite veinlets in leucoxene gabbro and in laminated unit (drill hole DAX-14-005); (G) Orange type 1 garnet in vein associated with \pm K-feldspar \pm quartz \pm calcite \pm magnetite and epidote on the walls (drill hole AMCD-28) (H) K-feldspar vein and garnet with epidote and actinolite cross-cutting and replacement (drill hole D69-05); (I) Radial and acicular actinolite-tremolite with coarse-grained epidote exhibiting optic sector zonings in metasomatized gabbro and fine titanium-iron oxide grain formed after ilmenite of the original protolith. (drill hole OAX-15-056); (J) Garnet and calcite vein with actinolite needles in skarn area (drill hole D69-05); (K) Epidote replacement after garnet in skarn area (drill hole D69-05); (L) Type 2 garnet exhibits inclusion-rich core and optical zoning in actinolite garnet skarn (drill hole 17407-03). Abbreviations: Ab = albite; Act = actinolite; Ant = anatase; Cal = calcite; Ep = epidote; Grt = garnet; Kfs =K-feldspar; Mt = magnetite; Py = pyrite; Qz = quartz.

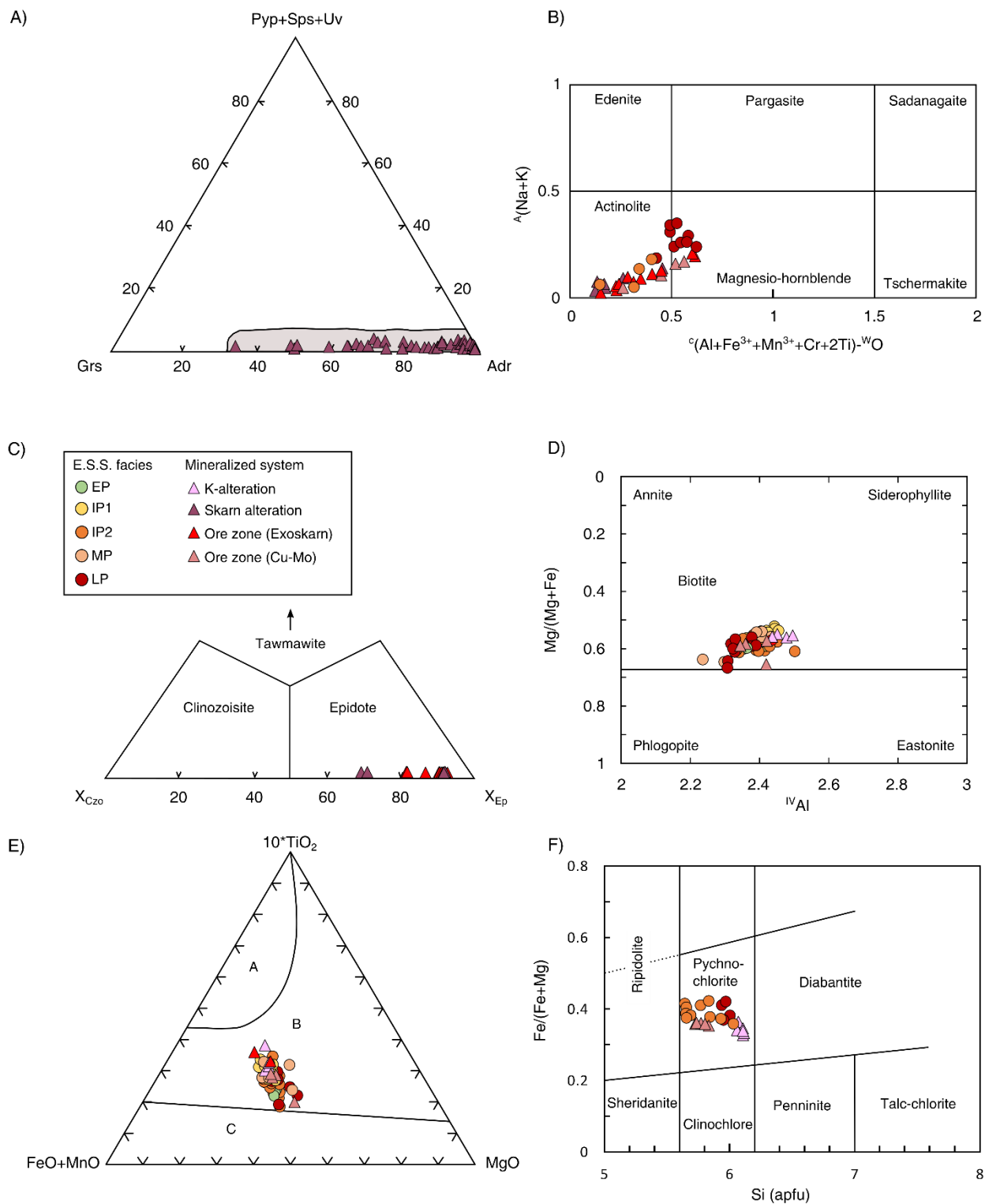


Figure 1.12 Composition of representative mineral from the South border of the East-Sullivan Stock : (A) Ternary plots of garnet compositions with garnet compositional field (gray) associated with Cu Skarn after Meinert *et al.* (2005); (B) Classification diagram for calcic amphibole according to Hawthorne *et al.* (2012) following the IMA 2012 guidelines using the spreadsheet of Locock (2014); (C) Epidote classification diagram according to Franz and Liebscher (2004). The Cr (tawmanite) field was cut for better visualization; (D) Plot of Fe / (Fe +Mg) versus ^{IV}Al for biotite classification. Field boundaries from Rieder *et al.* (1998). The biotite-phlogopite field boundary is based of an Mg:Fe ratio of 2:1 from Deer *et al.* (2013); (E) (FeO +MnO)-10*TiO₂-MgO ternary diagram for biotite discrimination from Nachit *et al.* (2005) with field of : (A) Domain of the primary magmatic biotite, (B) domain of the reequilibrated biotite and (C) domain of the secondary biotite; (F) Fe/(Fe + Mg) versus Si classification diagram for chlorite according to Hey (1954). Abbreviations: apfu = atoms per formula unit; Adr = andradite; Grs = grossular; Pyp = pyrope; Sps = spessartine; Uv = uvarovite; $X_{Czo} = (Al-2)/(Fe^{3+}+Al+Cr^{3+}-2)$; $X_{Ep} = Fe^{3+}/(Fe^{3+}+Al+Cr^{3+}-2)$.

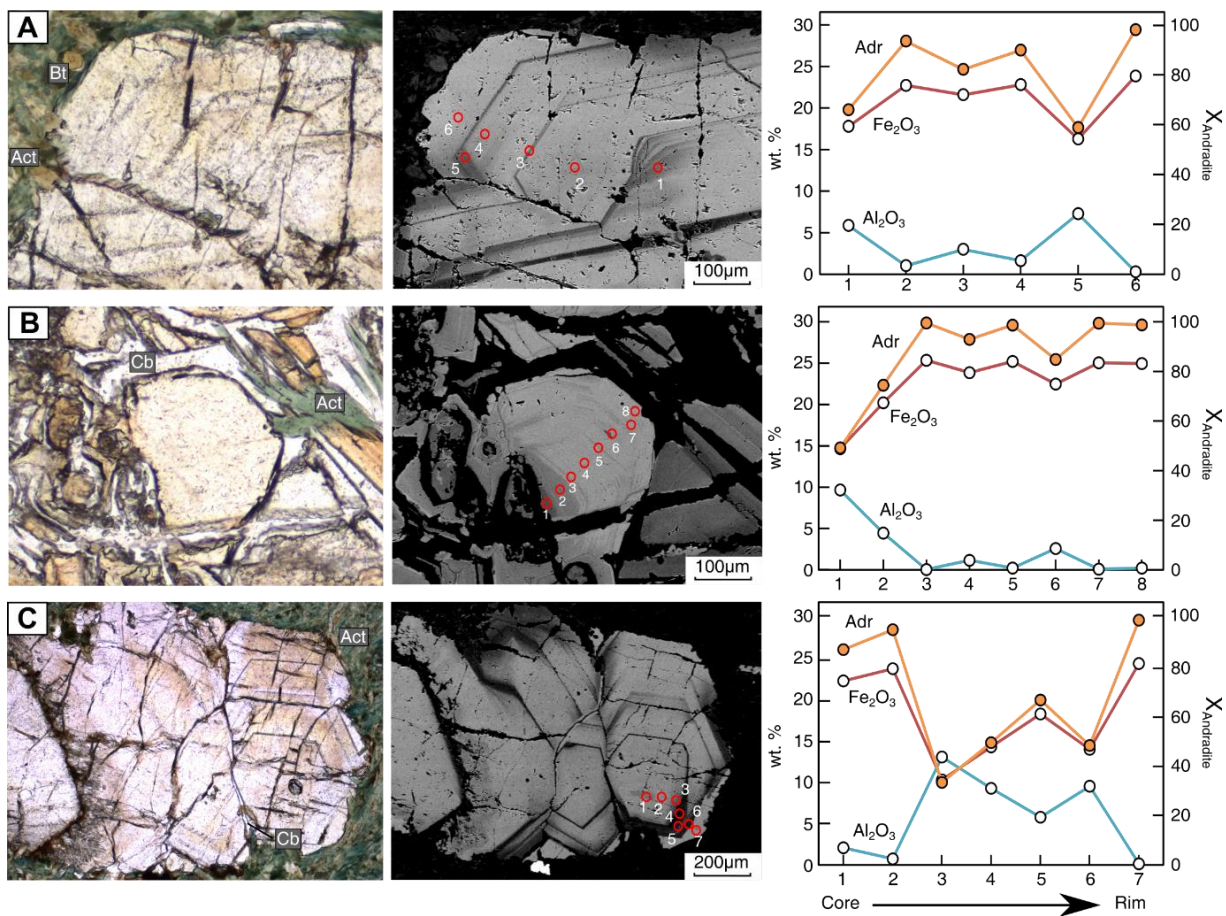
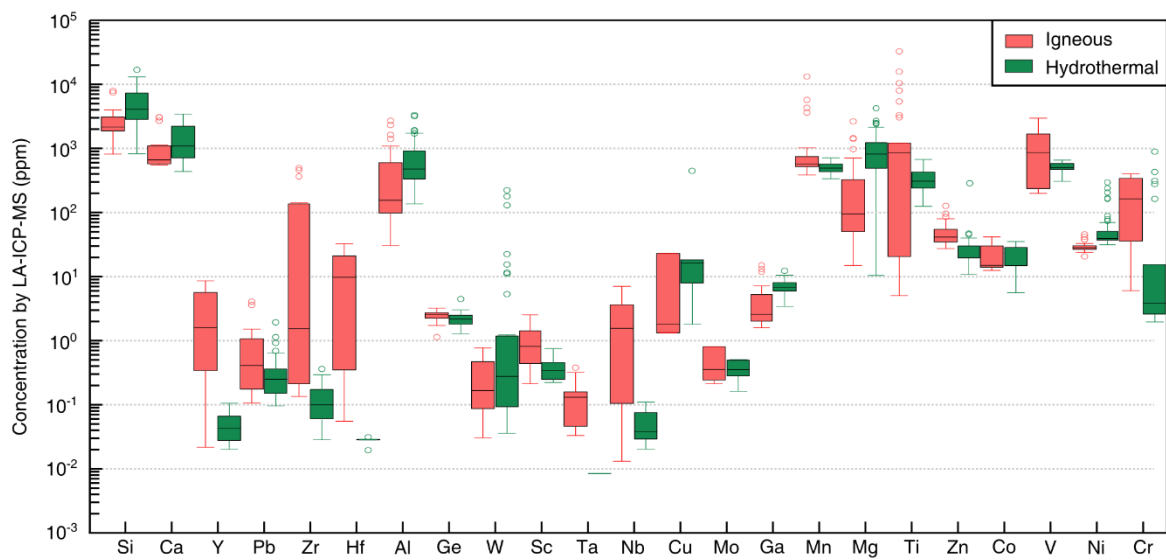


Figure 1.13 Photomicrographs (cross-polarized transmitted light), backscattered electron (BSE) images, and electron microprobe analysis profiles for andradite ($X_{\text{Andradite}}$, %), Fe_2O_3 and Al_2O_3 (wt%) proportion for three representative garnets of the skarn alteration area. Circles in photomicrographs and BSE represent the analyzed spots. Abbreviations: Adr = andradite; Act = actinolite; Cb = carbonate; Bt = Biotite.

A)



B)

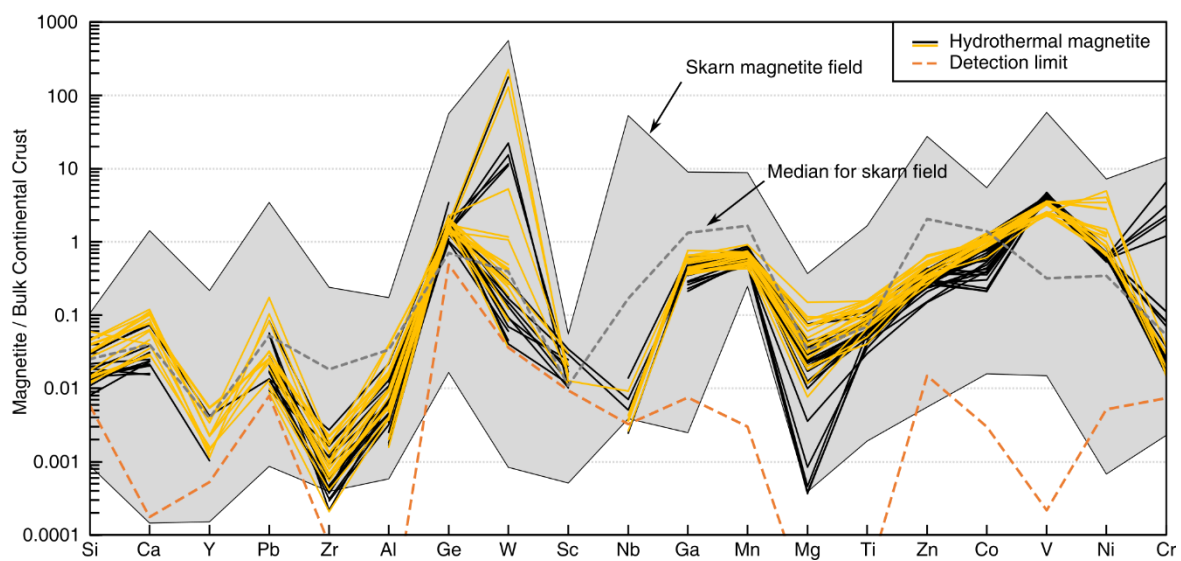


Figure 1.14 (A) Multi-element box and whisker plots of trace elements analyzed by LA-ICP-MS showing the compositional differences between igneous and hydrothermal magnetite. Boxes outline the 25th to 75th percentiles, and whiskers extend to the minimum and maximum values. Short lines within the boxes represent the median values and open circles represent outliers; (B) Multielement profiles for hydrothermal magnetite analyzed by LA-ICP-MS, normalized to bulk continental crust (Rudnick and Gao 2003); gray field data from worldwide skarn deposits (Huang 2019 and reference therein); elements are ordered by increasing compatibility in magnetite.

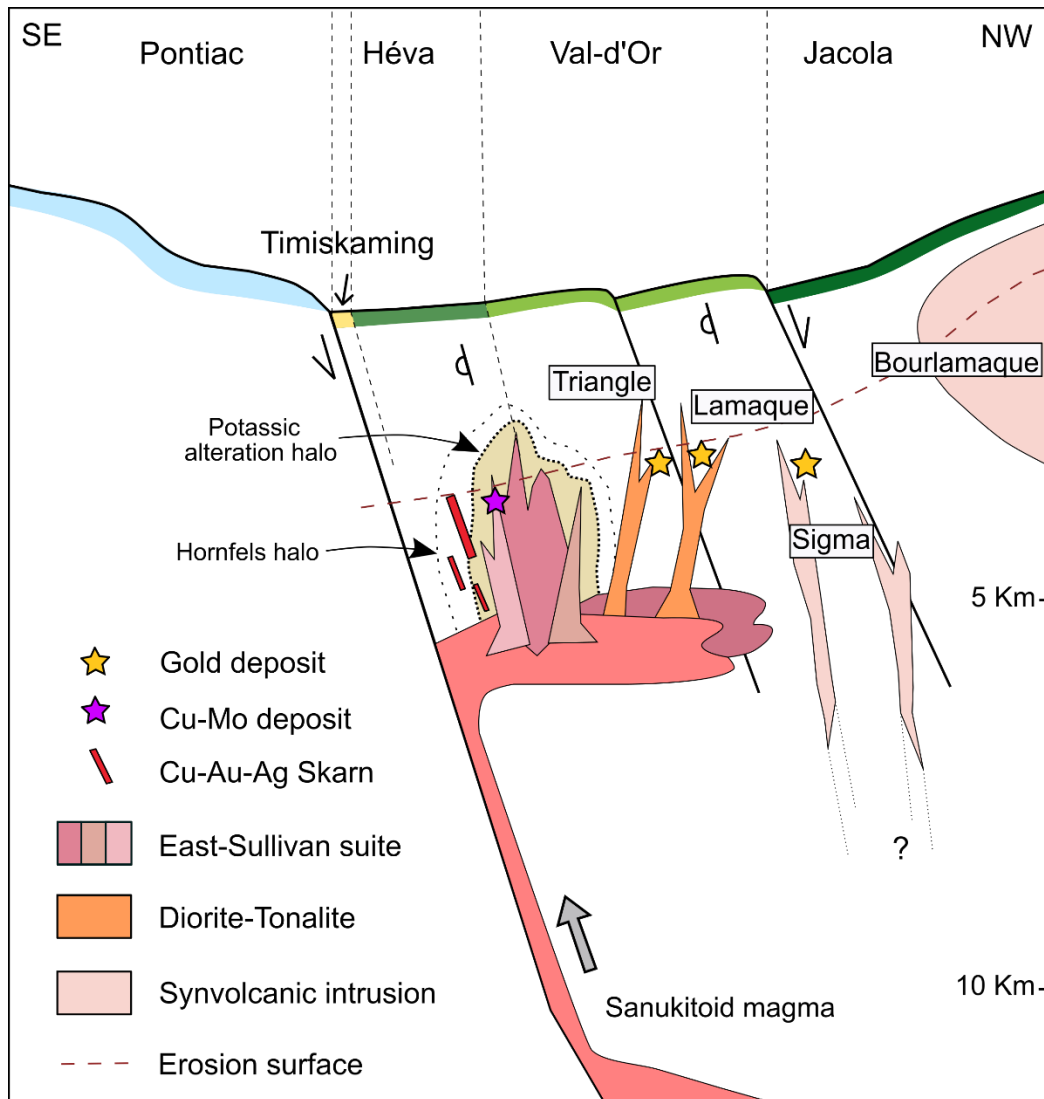


Figure 1.15 Schematic model of the East-Sullivan Stock and related intrusions emplacement in the Val-d'Or area.

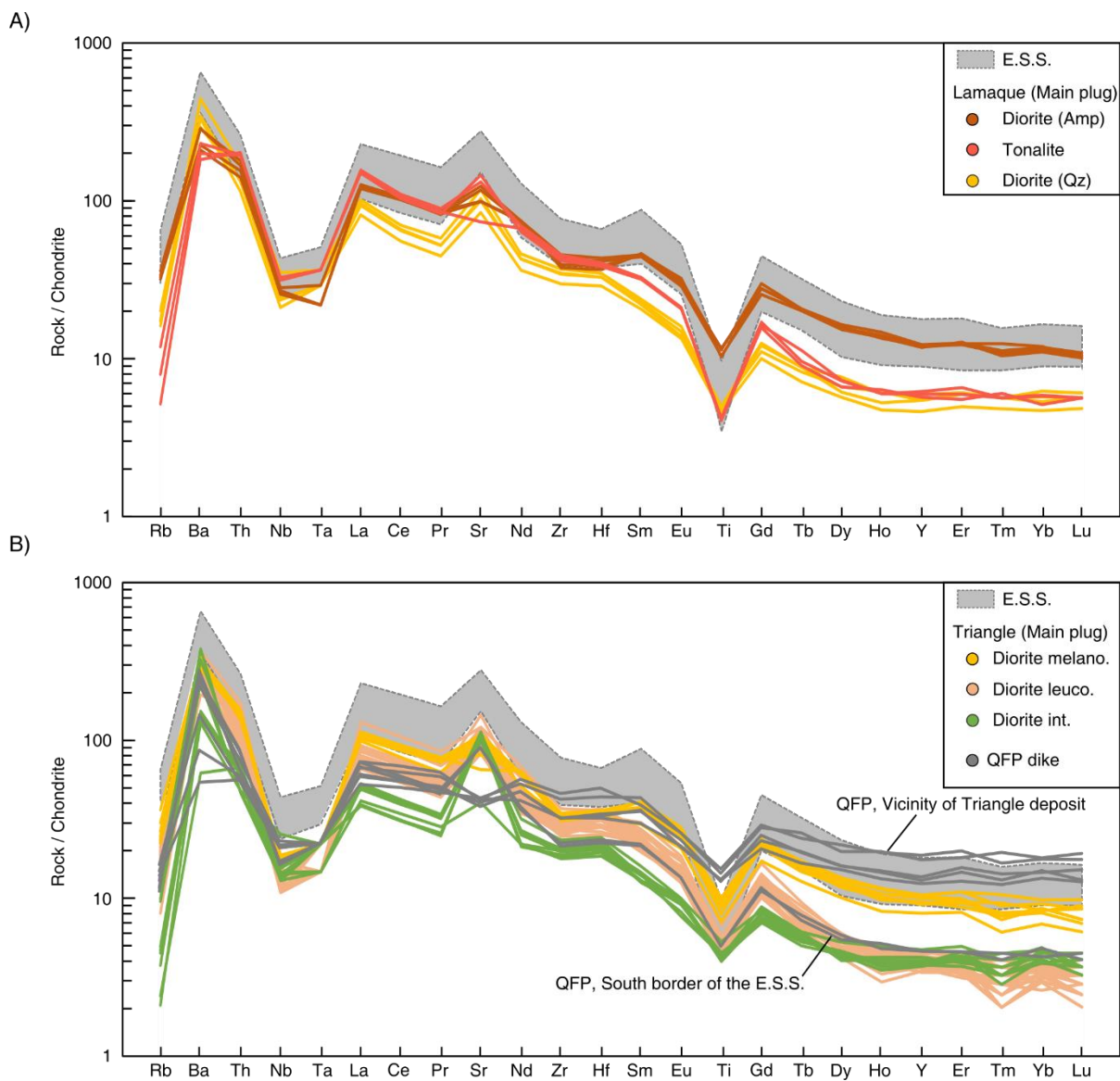


Figure 1.16 Extended trace element profiles normalized to chondrites from McDonough and Sun (1995); (A) E.S.S compared to the Lamaque Main plug facies; (B) E.S.S compared to the Triangle facies and QFP dikes. Lamaque and Triangle data from J. Dubé, (2018)

Table 1.1 Whole-rock major elements composition for the East-Sullivan Stock and associated rocks.

Sample	Major Elements (wt. %)															
	SiO ₂	TiO ₂	Al ₂ O ₃	FeO*	Fe ₂ O ₃	MnO	MgO	CaO	Na ₂ O	K ₂ O	P ₂ O ₅	LOI	Total	S	C	F
D.L.	0,01	0,01	0,01	0,01	0,00	0,01	0,01	0,01	0,01	0,01	0,01	0,01	0,01	0,01	0,01	0,01
Early (PE)																
FB1604	56,74	0,61	19,12	n.a.	5,99	0,13	2,01	4,48	4,94	4,41	0,46	1,02	99,92	b.d.	0,04	n.a.
FB1607	55,63	0,66	18,50	n.a.	6,46	0,13	1,94	4,96	4,49	5,05	0,52	1,42	99,77	0,01	0,03	n.a.
FB1626	54,67	0,70	19,86	n.a.	6,59	0,13	1,69	5,89	4,53	3,13	0,51	1,67	99,37	b.d.	b.d.	n.a.
FB1627	56,06	0,67	18,77	n.a.	6,58	0,14	2,16	4,80	4,92	4,26	0,53	1,16	100,05	b.d.	0,04	n.a.
FB1805	56,40	0,58	18,85	3,53	7,22	0,24	1,26	4,92	4,32	3,96	0,47	1,35	99,55	n.a.	n.a.	0,09
Intermediate (IP1)																
FB1611	57,78	0,55	18,87	n.a.	6,16	0,08	1,79	3,47	5,19	4,36	0,40	1,41	100,05	0,02	0,15	n.a.
QMX01	54,78	0,57	19,72	n.a.	5,51	0,06	1,71	4,88	5,11	4,04	0,50	2,88	99,77	n.a.	n.a.	n.a.
QMX02	56,10	0,59	19,77	n.a.	5,61	0,12	1,58	4,60	4,97	4,72	0,42	0,80	99,28	n.a.	n.a.	n.a.
FB1804	56,88	0,58	18,57	2,35	5,71	0,08	1,65	4,18	6,08	2,66	0,44	2,02	98,85	n.a.	n.a.	0,09
Intermediate (IP2)																
FB1610	61,02	0,47	18,10	n.a.	5,00	0,07	1,32	2,94	5,39	4,36	0,26	1,11	100,05	0,01	0,09	n.a.
FB1618	61,20	0,42	18,22	n.a.	4,07	0,06	1,21	2,75	5,86	4,65	0,21	0,71	99,36	0,01	0,08	n.a.
FB1619	61,81	0,43	18,50	n.a.	3,68	0,08	1,22	3,30	5,73	3,95	0,21	0,88	99,79	b.d.	b.d.	n.a.
FB1620	61,04	0,42	18,02	n.a.	2,92	0,05	1,05	2,62	6,43	4,64	0,22	1,83	99,23	0,07	0,42	n.a.
FB1624	60,50	0,43	17,94	n.a.	5,13	0,10	1,31	3,72	5,46	4,44	0,23	0,69	99,95	0,02	0,05	n.a.
FB1802	62,22	0,42	18,16	1,57	3,64	0,09	1,15	3,59	5,61	3,87	0,22	1,10	100,07	n.a.	n.a.	0,05
FB1803	61,80	0,47	17,66	2,10	4,74	0,07	1,27	2,99	5,32	4,45	0,27	1,09	100,11	n.a.	n.a.	0,08
Late (LP)																
FB1605	64,40	0,29	17,42	n.a.	2,96	0,05	1,11	2,61	6,07	3,47	0,14	0,74	99,27	b.d.	0,07	n.a.
FB1606	64,27	0,30	17,66	n.a.	2,95	0,06	1,16	2,31	5,98	4,28	0,15	0,86	100,00	0,01	0,10	n.a.
FB1801	64,86	0,30	17,41	1,31	2,84	0,05	1,06	2,58	6,17	3,87	0,16	0,84	100,13	n.a.	n.a.	0,06
Mineralized (MP)																
FB1614	61,76	0,40	18,15	n.a.	4,14	0,02	1,21	2,26	5,38	4,89	0,21	0,84	99,26	0,08	0,05	n.a.
FB1615	61,54	0,40	18,13	n.a.	4,15	0,02	1,26	2,21	5,60	4,60	0,22	0,93	99,05	0,07	0,07	n.a.
Porphyritic dike																
FB1608	63,26	0,36	16,63	n.a.	4,06	0,06	3,18	5,71	4,89	1,03	0,14	0,63	99,95	0,16	0,04	n.a.
FB1609	63,34	0,36	16,74	n.a.	3,92	0,06	3,20	5,70	4,94	1,04	0,14	0,77	100,20	0,14	0,03	n.a.
Alteration																
FB1616	64,42	0,44	13,57	n.a.	6,01	0,09	0,64	2,81	2,70	7,79	0,11	1,67	100,25	0,49	0,37	n.a.
Héva Formation																
FB1612	49,29	1,44	13,46	n.a.	13,70	0,27	6,83	11,28	2,26	0,19	0,11	1,66	100,50	0,03	0,04	n.a.
FB1613	48,94	1,75	13,89	n.a.	14,46	0,24	5,20	10,34	3,73	0,58	0,10	1,02	100,25	0,04	0,01	n.a.
FB1617	47,11	1,44	14,39	n.a.	13,27	0,27	6,15	12,73	2,30	0,48	0,11	1,38	99,65	0,01	0,01	n.a.
Hornfel in Héva F.																
FB1621	76,72	0,20	9,36	n.a.	4,56	0,04	0,31	1,91	2,83	2,27	0,05	1,24	99,49	0,07	0,30	n.a.
FB1622	79,34	0,23	8,60	n.a.	2,73	0,06	0,80	1,54	1,10	5,43	0,05	0,04	99,93	0,06	0,03	n.a.
FB1623	79,39	0,23	8,58	n.a.	2,83	0,07	0,79	1,53	1,11	5,43	0,05	-0,12	99,90	0,07	0,03	n.a.
FB1625	77,43	0,26	11,17	n.a.	1,55	0,05	0,32	1,76	3,54	3,81	0,05	0,20	100,15	0,02	0,05	n.a.

NOTES:

Abbreviations: D.L. = detection limit; n.a. = not analysed; LOI= loss on ignition (3 h at 1000°C) .

See Appendix Table A1 for sample locations.

Table 1.2 Trace element abundances determined by solution ICP-MS for rocks of the area.

(ppm)	L.D.	East-Sullivan Stock											
		Early (EP)				Intermediate (IP1)			Intermediate (IP2)				
		F1604	F1607	F1626	F1627	F1611	QMX1	QMX2	F1610	F1618	F1619	F1620	F1624
Li	10	20	20	20	20	30	n.a.	n.a.	10	10	10	10	b.d.
Sc	1	8	10	9	9	7	n.a.	n.a.	5	5	5	5	5
V	5	90	147	143	137	88	103	90	74	69	66	45	76
Cr	10	20	20	20	10	20	10	10	10	20	20	20	30
Co	1	11	11	12	12	8	10	11	5	5	4	3	8
Ni	1	11	9	8	8	6	9	5	4	9	7	5	8
Cu	1	46	2	63	28	132	22	70	72	85	73	312	187
Zn	2	95	77	70	103	58	41	87	49	41	63	29	57
Ga	0,1	22	22	23	22	22	21	21	23	22	20	20	21
As	0,1	1	3	1	0,9	5	n.a.	n.a.	3	1	1	0,5	1
Se	0,2	b.d.	0,3	0,3	b.d.	b.d.	n.a.	n.a.	0,2	b.d.	0,2	0,4	0,2
Rb	0,2	132	137	88	115	127	90	151	111	98	74	93	75
Sr	0,1	1590	1600	2030	1515	1535	1665	1795	1495	1500	1490		1455
Y	0,5	26	28	28	28	23	23	27	25	23	16	20	22
Zr	2	288	262	259	259	297	196	243	270	214	205	206	212
Nb	0,2	9,2	8,6	11	9,1	7,3	6,9	8,6	8,3	8,2	5,8	5,7	7,0
Mo	1	2	2	1	1	4	1	2	3	1	2	1	2
In	0,005	0,007	0,014	0,007	0,007	0,011	n.a.	n.a.	0,008	0,010	0,005	0,016	0,013
Sn	1	2	2	2	2	2	1	2	2	2	1	2	2
Sb	0,05	0,08	0,27	0,08	b.d.	0,52	n.a.	n.a.	0,33	0,14	0,25	0,14	0,12
Te	0,01	b.d.	0,01	0,01	b.d.	0,01	n.a.	n.a.	0,02	0,01	b.d.	0,05	0,01
Cs	0,01	3,1	1,04	2,2	2,7	4,4	0,74	2,3	1,8	0,90	0,54	0,99	0,31
Ba	0,5	1025	1105	876	1025	1315	1250	1275	1215	1405	1295	1255	1315
La	0,1	53	54	49	52	49	51	55	51	38	25	34	42
Ce	0,1	117	120	106	117	104	108	115	109	89	52	79	95
Pr	0,03	14,5	15,3	13,9	15,0	13,3	13	14	13,5	11,6	6,64	9,82	11,7
Nd	0,1	57	60	55	59	52	54	57	52	46	27	38	46
Sm	0,03	12	13	12	13	11	10	11	11	10	6,3	7,9	9,5
Eu	0,03	2,8	2,9	3,0	2,9	2,8	2,9	3,0	2,39	2,2	1,8	2,0	2,0
Gd	0,05	8,2	9,0	8,3	8,6	7,2	7,1	7,4	7,1	6,7	4,3	5,3	6,3
Tb	0,01	1,1	1,2	1,1	1,1	0,92	0,89	1,0	0,95	0,89	0,56	0,75	0,84
Dy	0,05	5,1	5,7	5,5	5,5	4,4	4,5	5,1	5	4,4	2,9	3,8	4,0
Ho	0,01	0,99	1,04	1,01	0,99	0,81	0,82	0,92	0,86	0,85	0,56	0,73	0,76
Er	0,03	2,7	2,9	2,8	2,7	2,2	2,1	2,5	2,4	2,3	1,6	2,1	2,2
Tm	0,01	0,37	0,39	0,39	0,38	0,29	0,30	0,37	0,34	0,34	0,22	0,32	0,31
Yb	0,03	2,5	2,7	2,7	2,6	2,2	1,9	2,4	2,6	2,5	1,7	2,3	2,2

(ppm)	East-Sullivan Stock						Héva Formation		
	(MP)		Late (LP)		Porphyritic dike		Volcanic rock		
	F1614	F1615	F1605	F1606	F1608	F1609	F1612	F1613	F1617
Li	20	20	10	10	10	10	10	10	10
Sc	1.2	1.2	4	4	8	8	46	50	43
V	78	75	55	54	77	79	460	607	457
Cr	20	20	30	30	110	110	130	30	300
Co	6	6	4	3	13	12	43	46	39
Ni	8	10	11	12	46	45	72	40	107
Cu	724	504	1	1	96	89	74	135	16
Zn	20	17	16	37	43	41	73	116	88
Ga	22	21	20	21	20	20	17	21	18
As	3	3	0.6	0.7	8	7	3	10	0.9
Se	0.4	0.5	0.2	b.d.	0.3	0.3	0.3	0.2	b.d.
Rb	133	126	72	107	27	29	4.3	39	19
Sr	1465	1375	1500	1290	647	650	103	152	166
Y	18	17	14	14	7.2	7.2	20	25	20
Zr	181	162	149	162	85	81	56	75	63
Nb	6.2	5.8	6.0	5.7	4.1	3.9	2.8	3.3	2.8
Mo	58	128	1	b.d.	b.d.	b.d.	1	3	6
In	b.d.	b.d.	b.d.	b.d.	0.005	b.d.	0.006	0.008	0.013
Sn	1	1	1	1	1	1	1	1	1
Sb	1.28	1.15	0.11	0.13	0.24	0.21	0.38	0.46	0.63
Te	0.02	0.02	b.d.	b.d.	0.05	0.05	0.01	b.d.	0.01
Cs	1.43	1.3	0.65	0.95	0.96	1.12	0.21	3.8	1.4
Ba	1250	1150	1310	1600	588	599	27.0	60.4	59.8
La	39	39	33	32	16	17	3.0	4.5	3.0
Ce	82	81	68	68	35	36	8.3	12	8.5
Pr	9.93	9.72	8.21	8.19	4.20	4.49	1.31	1.82	1.33
Nd	39	37	30	31	17	16	6.8	9.0	7.0
Sm	7.4	7.6	6.2	6.0	3.2	3.4	2.5	3.2	2.7
Eu	1.8	1.8	1.5	1.5	0.76	0.84	0.87	1.1	0.87
Gd	5.1	5.0	4.0	4.0	2.3	2.2	3.0	3.9	3.3
Tb	0.67	0.63	0.56	0.55	0.26	0.28	0.57	0.74	0.56
Dy	3.4	3.1	2.5	2.7	1.3	1.4	3.6	4.7	3.5
Ho	0.65	0.59	0.50	0.51	0.28	0.26	0.79	0.98	0.79
Er	1.7	1.7	1.5	1.4	0.73	0.71	2.4	2.8	2.2
Tm	0.25	0.24	0.21	0.21	0.10	0.11	0.35	0.39	0.34
Yb	1.7	1.7	1.5	1.5	0.77	0.68	2.3	2.7	2.3

Lu	0.25	0.24	0.22	0.23	0.10	0.11	0.34	0.40	0.33
Hf	4.6	4.2	3.9	4.1	2.4	2.3	1.6	2.2	1.6
Ta	0.5	0.4	0.5	0.5	0.3	0.3	0.3	0.3	0.3
W	2	2	b.d.	b.d.	1	1	3	1	2
Re	0.012	0.03	b.d.	b.d.	0.001	b.d.	0.003	0.009	0.01
Hg	0.401	0.206	0.013	0.027	0.015	0.013	0.043	0.243	0.168
Tl	0.08	0.08	0.02	0.04	0.14	0.14	b.d.	0.2	0.06
Pb	6	8	2	2	2	b.d.	b.d.	b.d.	b.d.
Bi	0.03	0.04	0.01	0.01	0.02	0.02	0.02	0.01	0.03
Th	4.5	4.8	4.5	4.5	2.4	2.5	0.26	0.38	0.28
U	1.3	1.3	2.1	1.2	0.69	0.73	0.07	0.12	0.15
Σ REE	192	189	158	157	81	85	36	48	37
Eu*	0.90	0.87	0.91	0.90	0.85	0.88	0.98	0.95	0.90
(La/Yb) _N	15.7	15.3	15.3	14.6	14.2	17.1	0.9	1.1	0.9

NOTES: Abbreviation : b.d. = below detection; n.a. = not analysed
Ag, Cd, Ge above detection. See Appendix Table A1 for sample locations.

Table 1.3 Re-Os data and model ages for molybdenite from E.S.S Cu-Mo-Au porphyry mineralization

Drill Core	North	East	Host Rock	Sample description	Re (ppm)	$\pm 2\sigma$	^{187}Re (ppm)	$\pm 2\sigma$	^{187}Os (ppb)	$\pm 2\sigma$	Model Age (Ma)	$\pm 2\sigma$ (Ma)
DAX-15-009 273m	300272.2	5325533.4	Intermediate facies (IP2)	Qz-mo vein in potassic alteration	491.8	1.4	309.1	0.9	14191	12	2695	12

Table 1.4 Microprobe Analyses of Amphiboles.

%	Héva Formation				East-Sullivan Stock					
	Ore zone (n=20)		Skarn alteration (n=7)		Cu-Mo Ore zone (n=4)		Intermediate (IP2) (n=5)		Late (LP) (n=10)	
	Avg	Std	Avg	Std	Avg	Std	Avg	Std	Avg	Std
SiO₂	53,76	1,54	54,18	0,28	50,31	1,21	52,36	0,72	51,17	0,72
TiO₂	0,00	0,04	0,05	0,05	0,02	0,03	0,12	0,12	0,70	0,12
Al₂O₃	1,41	1,50	1,23	0,23	2,41	0,68	2,99	0,49	4,01	0,49
FeO	14,02	1,94	12,70	1,11	20,61	1,18	12,04	0,42	11,32	0,42
Cr₂O₃	0,08	0,03	0,01	0,01	0,07	0,07	0,01	0,01	0,01	0,01
MnO	0,35	0,10	0,87	0,33	0,74	0,04	0,55	0,06	0,66	0,06
MgO	14,27	1,46	15,32	0,37	10,30	0,54	15,46	0,49	16,09	0,49
CaO	12,52	0,26	12,40	0,17	11,88	0,07	12,40	0,13	11,57	0,13
Na₂O	0,16	0,20	0,24	0,04	0,38	0,07	0,46	0,21	1,17	0,21
K₂O	0,02	0,10	0,06	0,03	0,19	0,09	0,18	0,03	0,45	0,03
CoO	0,02	0,01	0,01	0,02	0,00	0,00	0,01	0,01	0,01	0,01
NiO	0,38	0,11	0,01	0,01	0,00	0,00	0,01	0,02	0,03	0,02
F	0,00	0,07	0,07	0,07	0,07	0,10	0,16	0,09	0,37	0,09
Cl	0,00	0,01	0,01	0,01	0,03	0,00	0,03	0,01	0,03	0,01
O=F, C	0,00	0,03	0,03	0,03	0,04	0,04	0,07	0,04	0,16	0,04
H₂O	2,05	0,05	2,03	0,05	1,93	0,06	1,97	0,05	1,87	0,05
Total	99,04	1,13	99,15	1,01	98,90	0,20	98,68	0,38	99,28	0,38
Number of cations on the basis of 23 (O)										
Si	7,85	0,20	7,86	0,03	7,59	0,16	7,61	0,07	7,39	0,07
Al^{IV}	0,15	0,20	0,14	0,03	0,41	0,15	0,39	0,07	0,61	0,07
T_Σ	8,00	0,00	8,00	0,00	8,00	0,00	8,00	0,00	8,00	0,00
Al^{VI}	0,09	0,07	0,07	0,02	0,02	0,03	0,08	0,03	0,13	0,07
Ti⁴⁺	0,00	0,00	0,01	0,01	0,00	0,00	0,08	0,01	0,01	0,01
Cr	0,01	0,00	0,00	0,00	0,01	0,01	0,00	0,00	0,00	0,00
Fe³⁺	0,07	0,10	0,07	0,02	0,33	0,17	0,16	0,03	0,25	0,03
Co	0,00	0,00	0,00	0,00	0,00	0,00	0,00	0,00	0,00	0,00
Ni	0,04	0,01	0,00	0,00	0,00	0,00	0,00	0,00	0,00	0,00
Mg²⁺	3,11	0,28	3,31	0,10	2,31	0,12	3,35	0,09	3,47	0,09
Fe²⁺	1,64	0,26	1,47	0,12	2,27	0,02	1,30	0,08	1,11	0,08
Mn²⁺	0,04	0,02	0,07	0,03	0,06	0,01	0,04	0,01	0,01	0,01
C_Σ	5,00	0,00	5,00	0,00	5,00	0,00	5,00	0,00	5,00	0,00

Mn²⁺	0,01	0,02	0,03	0,02	0,04	0,00	0,03	0,01	0,07	0,01
Ca²⁺	1,96	0,03	1,93	0,02	1,92	0,01	1,93	0,02	1,79	0,02
Na⁺	0,03	0,01	0,04	0,01	0,04	0,00	0,04	0,02	0,14	0,02
B_Σ	2,00	0,00	2,00	0,00	2,00	0,00	2,00	0,00	2,00	0,00
Na⁺	0,01	0,05	0,03	0,01	0,07	0,02	0,09	0,05	0,19	0,05
K⁺	0,00	0,02	0,01	0,00	0,04	0,02	0,03	0,01	0,08	0,01
A_Σ	0,02	0,06	0,04	0,01	0,11	0,04	0,12	0,05	0,27	0,05
F⁻	0,00	0,03	0,03	0,03	0,03	0,05	0,07	0,04	0,17	0,04
Cl⁻	0,00	0,00	0,00	0,00	0,01	0,00	0,01	0,00	0,01	0,00
O	0,00	0,00	0,00	0,00	0,02	0,01	0,01	0,00	0,02	0,00
OH⁻	2,00	0,04	1,96	0,03	1,95	0,06	1,91	0,05	1,81	0,05
W_Σ	2,00	0,00	2,00	0,00	2,00	0,00	2,00	0,00	2,00	0,00
Total	15,02	0,06	15,04	0,01	15,10	0,03	15,12	0,05	15,28	0,05

NOTES: Abbreviations: Avg = average; Std = standard deviation

Analyses with high or low totals (>101 or <96 wt.%) or poor stoichiometries are omitted.

Formula using the spreadsheet given from Locock (2014).

Table 1.5 Microprobe Analyses of Epidote.

%	Héva				ESS	
	Ore zone (n=13)		Skarn alt. (n=6)		Mineralized (MP) (n=5)	
	Avg	Std	Avg	Std	Avg	Std
SiO₂	37,49	0,33	37,34	0,18	37,36	0,08
TiO₂	0,17	0,12	0,04	0,04	0,16	0,12
Al₂O₃	22,15	0,65	22,71	1,11	22,17	0,59
FeO(t)	13,13	0,53	12,65	1,57	13,11	0,78
MnO	0,08	0,04	0,34	0,35	0,09	0,09
MgO	0,05	0,10	0,02	0,02	0,02	0,02
CaO	23,14	0,19	22,57	0,51	22,76	0,37
K₂O	0,01	0,02	0,00	0,00	0,00	0,00
H₂O	1,80	0,01	1,80	0,01	1,79	0,01
Cl	0,01	0,01	0,01	0,01	0,00	0,00
Total	98,04	0,50	97,49	0,55	97,50	0,37
Number of cations on the basis of 12.5 (O)						
Si	3,01	0,03	3,01	0,01	3,02	0,01
Ti	0,01	0,01	0,00	0,00	0,01	0,01
Al	2,10	0,06	2,16	0,10	2,11	0,05
Fe	0,88	0,47	0,85	0,14	0,89	0,07
Mn	0,01	0,00	0,02	0,02	0,01	0,01
Mg	0,01	0,01	0,00	0,00	0,00	0,00
Ca	1,99	0,01	1,95	0,04	1,97	0,02
K	0,00	0,00	0,00	0,00	0,00	0,00
Cl	0,00	0,00	0,00	0,00	0,00	0,00
OH	0,96	0,00	0,97	0,00	0,97	0,00
Total	8,00	0,00	8,00	0,00	8,00	0,00

NOTES:

Abbreviations: Avg = average; Std = standard deviation

Analyses with high or low totals (>101 or <96 wt.%) or poor stoichiometries are omitted.

Table 1.6 Microprobe Analysis of Mica.

%	Héva F.		East-Sullivan Stock													
	Ore zone		K-alteration		Cu-Mo		Early (EP)		IP1		IP2		MP		Late (PL)	
	(n=2)		(n=4)		(n=4)		(n=6)		(n=11)		(n=19)		(n=6)		(n=10)	
	Avg	Std	Avg	Std	Avg	Std	Avg	Std	Avg	Std	Avg	Std	Avg	Std	Avg	Std
SiO₂	36,92	0,50	36,65	0,22	37,70	0,45	36,85	0,43	36,70	0,38	36,88	0,62	37,50	0,94	37,58	0,56
TiO₂	1,52	0,02	1,50	0,24	1,12	0,22	1,00	0,06	1,36	0,16	1,19	0,21	1,29	0,22	1,12	0,19
Al₂O₃	15,67	0,23	15,90	0,17	15,09	0,07	14,51	0,24	15,58	0,22	14,75	0,32	15,09	0,80	14,39	0,37
FeO	17,42	0,07	17,67	0,30	16,66	1,19	16,65	0,31	17,92	0,83	17,35	0,53	17,01	1,70	16,64	1,24
MnO	0,42	0,01	0,43	0,05	0,36	0,04	0,52	0,04	0,42	0,08	0,48	0,06	0,12	0,02	0,58	0,14
MgO	11,23	2,36	12,52	0,13	14,16	1,32	13,72	0,38	12,19	0,58	13,51	0,92	13,24	1,32	13,93	0,97
CaO	0,02	0,03	0,01	0,01	0,01	0,01	0,05	0,02	0,03	0,02	0,05	0,09	0,03	0,02	0,02	0,02
Na₂O	0,09	0,04	0,06	0,02	0,04	0,02	0,08	0,01	0,04	0,01	0,05	0,02	0,07	0,02	0,05	0,04
K₂O	9,49	0,17	9,69	0,11	9,53	0,22	9,20	0,11	9,40	0,22	9,29	0,36	9,47	0,16	9,57	0,21
Cr₂O₃	0,00	0,00	0,01	0,02	0,01	0,02	0,03	0,01	0,01	0,02	0,01	0,02	0,03	0,04	0,02	0,03
NiO	0,02	0,02	0,01	0,01	0,00	0,01	0,01	0,01	0,01	0,01	0,01	0,01	0,01	0,01	0,01	0,02
BaO	0,00	0,00	0,00	0,00	0,00	0,00	0,00	0,00	0,00	0,01	0,02	0,06	0,04	0,07	0,00	0,00
H₂O	3,50	0,20	3,49	0,09	3,72	0,05	3,44	0,07	3,57	0,08	3,45	0,10	3,29	0,16	3,41	0,15
Rb₂O	0,04	0,01	0,06	0,03	0,02	0,03	0,09	0,01	0,02	0,03	0,02	0,02	0,04	0,05	0,06	0,03
F	0,63	0,14	0,74	0,13	0,40	0,08	0,76	0,11	0,55	0,15	0,81	0,23	1,20	0,36	0,95	0,34
Cl	0,16	0,00	0,15	0,02	0,12	0,01	0,10	0,02	0,09	0,03	0,08	0,04	0,05	0,01	0,05	0,03
Total	97,13	2,91	98,90	0,60	98,95	0,52	97,00	0,49	97,90	1,19	97,94	1,20	98,47	0,68	98,39	0,77
O=F,Cl	0,30	0,06	0,35	0,06	0,20	0,03	0,34	0,05	0,25	0,07	0,36	0,09	0,52	0,15	0,41	0,14
Total	96,83	2,97	98,55	0,63	98,75	0,49	96,66	0,50	97,65	1,16	97,58	1,15	97,96	0,67	97,98	0,75

Number of cations on the basis of 22 (O)

Si	5,73	0,12	5,73	0,05	5,61	0,02	5,72	0,02	5,66	0,03	5,68	0,05	5,73	0,10	5,75	0,04
Al^{IV}	2,27	0,12	2,27	0,05	2,39	0,02	2,28	0,02	2,34	0,03	2,32	0,05	2,27	0,10	2,25	0,04
Al^{VI}	0,60	0,17	0,36	0,05	0,48	0,04	0,38	0,05	0,50	0,06	0,37	0,07	0,45	0,06	0,35	0,05
Ti⁴⁺	0,18	0,01	0,12	0,01	0,17	0,03	0,12	0,01	0,16	0,02	0,14	0,02	0,15	0,03	0,13	0,02
Fe²⁺	2,26	0,08	2,14	0,10	2,26	0,04	2,15	0,05	2,29	0,12	2,24	0,08	2,18	0,23	2,13	0,17
Cr²⁺	0,00	0,00	0,00	0,00	0,00	0,00	0,00	0,00	0,00	0,00	0,00	0,00	0,00	0,01	0,00	0,00
Mn²⁺	0,06	0,00	0,07	0,00	0,06	0,01	0,07	0,00	0,05	0,01	0,06	0,01	0,02	0,00	0,08	0,02
Mg²⁺	2,59	0,46	3,21	0,03	2,86	0,01	3,18	0,08	2,81	0,12	3,10	0,19	3,02	0,28	3,18	0,20
Ca²⁺	0,00	0,00	0,01	0,01	0,00	0,00	0,01	0,00	0,01	0,00	0,01	0,02	0,00	0,00	0,00	0,00
Na⁺	0,03	0,01	0,02	0,00	0,02	0,01	0,02	0,00	0,01	0,00	0,01	0,01	0,02	0,01	0,02	0,01
K⁺	1,88	0,10	1,82	0,02	1,89	0,02	1,82	0,01	1,85	0,04	1,83	0,07	1,85	0,03	1,87	0,04
Ni	0,00	0,00	0,00	0,00	0,00	0,00	0,00	0,00	0,00	0,00	0,00	0,00	0,00	0,00	0,00	0,00
OH	3,65	0,08	3,59	0,09	3,60	0,07	3,60	0,06	3,71	0,08	3,59	0,11	3,41	0,17	3,53	0,16
Total	15,61	0,11	15,75	0,05	15,74	0,01	15,75	0,03	15,69	0,03	15,76	0,05	15,69	0,03	15,76	0,04
F	0,31	0,08	0,39	0,08	0,36	0,07	0,37	0,06	0,27	0,07	0,39	0,11	0,58	0,17	0,46	0,16
Cl	0,04	0,00	0,03	0,01	0,04	0,01	0,03	0,00	0,02	0,01	0,02	0,01	0,01	0,00	0,01	0,01
XMg	0,53	0,05	0,56	0,01	0,56	0,01	0,60	0,01	0,55	0,02	0,58	0,02	0,58	0,05	0,60	0,03

NOTES:

Analyses with high or low totals (>101 or <96 wt.%) or poor stoichiometries are omitted.

Abbreviations: Avg = average; Std = standard deviation

Table 1.7 Microprobe Analyses of Chlorite.

%	Héva				E.S.S.							
	Ore zone (n=7)		Ore zone (n=8)		K-Alteration (n=9)		Inter. (IP) (n=2)		Inter. (IP2) (n=8)		Late (LP) (n=4)	
	Avg	Std	Avg	Std	Avg	Std	Avg	Std	Avg	Std	Avg	Std
SiO₂	29,51	0,07	29,46	0,19	27,98	0,24	28,90	0,60	27,21	0,26	28,54	0,60
TiO₂	0,02	0,02	0,06	0,03	0,02	0,01	0,02	0,01	0,02	0,02	0,03	0,03
Al₂O₃	16,34	0,19	16,80	0,13	18,77	0,15	16,86	0,59	19,06	0,57	17,14	0,64
FeO	18,43	0,11	19,14	0,14	19,69	0,09	20,68	0,13	21,35	0,78	21,73	0,81
MnO	0,71	0,05	0,71	0,01	0,63	0,07	0,80	0,06	0,88	0,10	0,96	0,25
MgO	20,58	0,24	19,77	0,52	19,59	0,08	19,89	0,73	17,77	0,72	18,43	1,26
CaO	0,02	0,01	0,07	0,06	0,04	0,01	0,05	0,03	0,02	0,03	0,04	0,03
Na₂O	0,04	0,01	0,05	0,02	0,02	0,01	0,02	0,00	0,03	0,02	0,04	0,05
K₂O	0,22	0,11	0,44	0,11	0,10	0,03	0,10	0,08	0,06	0,05	0,14	0,19
Cr₂O₃	0,01	0,01	0,00	0,00	0,02	0,02	0,00	0,00	0,01	0,02	0,01	0,02
NiO	0,02	0,01	0,00	0,00	0,02	0,01	0,00	0,00	0,01	0,01	0,03	0,00
H₂O calc	11,55	0,05	11,58	0,06	11,61	0,04	11,60	0,10	11,40	0,12	11,49	0,25
Total	97,51	0,44	98,12	0,39	98,51	0,34	98,94	0,73	97,81	1,34	98,58	1,91
Number of cations on the basis of 28 (O)												
Si	6,11	0,02	6,09	0,03	5,77	0,03	5,98	0,07	5,72	0,08	5,96	0,03
Al^{IV}	1,89	0,02	1,92	0,03	2,23	0,03	2,03	0,08	2,29	0,08	2,05	0,03
Al^{VI}	2,11	0,04	2,18	0,04	2,34	0,02	2,08	0,10	2,42	0,08	2,17	0,07
Ti⁴⁺	0,00	0,00	0,01	0,00	0,00	0,00	0,00	0,00	0,00	0,00	0,00	0,00
Fe²⁺	3,10	0,03	3,25	0,07	3,35	0,05	3,58	0,05	3,75	0,11	3,80	0,18
Cr²⁺	0,00	0,00	0,00	0,00	0,00	0,00	0,00	0,00	0,00	0,00	0,00	0,00
Mn²⁺	0,12	0,01	0,12	0,00	0,11	0,01	0,14	0,01	0,16	0,02	0,17	0,05
Mg²⁺	6,35	0,06	6,09	0,13	6,02	0,02	6,13	0,17	5,56	0,22	5,73	0,33
Ca²⁺	0,00	0,00	0,02	0,01	0,01	0,00	0,01	0,01	0,01	0,01	0,01	0,01
Na⁺	0,03	0,01	0,03	0,01	0,01	0,01	0,01	0,00	0,01	0,01	0,02	0,02
K⁺	0,12	0,06	0,18	0,07	0,04	0,01	0,03	0,02	0,02	0,01	0,04	0,05
Ni	0,00	0,00	0,00	0,00	0,00	0,00	0,00	0,00	0,00	0,00	0,00	0,00
XFe	0,33	0,00	0,35	0,01	0,36	0,00	0,37	0,01	0,40	0,02	0,40	0,02

NOTES:

Abbreviations: Avg = average; Std = standard deviation

Analyses with high or low totals (>101 or <95 wt.%) or poor stoichiometries are omitted.

Formula for chlorite using the spreadsheet WinEp program from Yavuz (2018).

Table 1.8 Carbon and oxygen isotopic composition of calcite veins from ESS skarn.

Sample	UTM(N)	UTM(E)	Drill hole #	Depth (m)	$\delta^{13}\text{C}\%$, PDB	$\delta^{18}\text{O}\%$, PDB	$\delta^{18}\text{O}\%$, SMOW
GAR1	216225,8	5323953	AAX-08-25	419	-5,32	-18,94	11,33
GAR2			AAX-08-25		-5,16	-19,36	10,90
GAR3			AAX-08-25		-5,22	-19,08	11,20
GAR4			AAX-08-25		-5,32	-19,07	11,20
MT1	299803,1	5325598	17407-04	468	-3,63	-18,48	11,81
MT2			17407-04		-3,67	-18,71	11,57
MT3			17407-04		-3,69	-18,79	11,49
MT4			17407-04		-3,63	-18,76	11,52
AAX1	216225,8	5323953	AAX-08-25	280	-4,30	-19,15	11,12
AAX2			AAX-08-25		-4,29	-18,99	11,28

Table 1.9 Estimation of temperature for different phases of the ESS and the skarn associated

Temperature (°C)	East-Sullivan Stock														Héva F.	
	Early (EP)		Inter. (IP1)		Inter. (IP2)		Min (MP)		Late (PL)		K. alt		Cu-Mo ore		Ore zone	
	Avg	Std	Avg	Std	Avg	Std	Avg	Std	Avg	Std	Avg	Std	Avg	Std	Avg	Std
Zircon																
Miller et al (2003)	774	9,0	774	24,8	774	14,2	758	4,7	764	7,0	n.a.	n.a.	n.a.	n.a.	n.a.	n.a.
Amphibole																
Ridolfi et al (2010)	n.a.	n.a.	n.a.	n.a.	n.a.	n.a.	n.a.	n.a.	730	11,6	n.a.	n.a.	n.a.	n.a.	n.a.	n.a.
Putirka (2016)	n.a.	n.a.	n.a.	n.a.	n.a.	n.a.	n.a.	n.a.	752	14,2	n.a.	n.a.	n.a.	n.a.	n.a.	n.a.
Biotite																
Henry (2005)	490	15,8	556	14,0	523	37,0	533	33,0	530	20,0	570	31,0	534	7,4	570	6,8
Chlorite																
Kranidiotis (1987)	n.a.	n.a.	260	8,8	291	8,5	n.a.	n.a.	265	4,6	246	4,6	280	3,5	n.a.	n.a.
Cathelineau (1988)	n.a.	n.a.	265	12,2	307	12,7	n.a.	n.a.	268	5,2	245	6,2	296	5,2	n.a.	n.a.
Jowett (1991)	n.a.	n.a.	266	12,4	310	12,7	n.a.	n.a.	271	5,6	246	6,4	297	5,3	n.a.	n.a.

NOTES:

Abbreviations: Avg = average; Std = standard deviation; n.a. not analysed or not applicable

Table 1.10 Comparison with other skarn occurrences.

	Archean			Phanerozoic
	ESS	Akasaba deposit	Shea prospects and Hannan South	Galore Creek
Location	Abitibi Subprovince	Abitibi Subprovince	Yilgam craton Eastern Goldfields Orogen	Stikine Terrane British Columbia
Proximal fault zone	CLLFZ	CLLFZ	Boulder Lefroy and Golden Mile (1st order)	First order faults
Associated metals	Cu (Au-Ag)	Au, Ag (Cu)	Cu (Au±Ag)	Cu-Au(Ag)
Host rocks	Intermediate to mafic volcanics (Héva For.)	Intermediate to mafic volcanics (Héva For.)	2658±3 to 2642±6 Ma Intrusive	Basalt-andesite, volcanoclastic sediments, tuffs
Associated Intrusion	Monzonite-syenite porphyry stock	Monzonite-syenite ?	Qz monzodiorite-granodiorite	Syenite to monzonite porphyry stock
Intrusion Geochemistry	Slightly alkaline Metaluminous Oxydized Sanukitoid	n.a.	Calc-alkaline - Oxydized Sanukitoid	Alkaline Metaluminous Oxydized
Intrusion age	2684 ± 1 Ma	< 2680 Ma	2658±3 to 2662±3 Ma	211-206 Ma
Alteration in intrusive	Potassic, phyllic, propylitic	No igneous rocks near skarn	Propylitic, sodic-calcic, minor potassic	Potassic, propylitic, phyllic
Skarn Gangue minerals	Grt(Adr40-100) Ep-Act-Qz-Chl	Grt(Adr40-100), Cpx(Hd40-60)-Ep-Hbl-Act-Bt-Chl-Qz	Ep-Cal or Ep-Act ± Chl-Bt-Ab	Grt(Adr75-100) - Cpx (Di) Ep-Ser-Cb-Chl
Opaque minerals	Mag-Ccp-Py-Po Electrum	Mag-Po-Py-Ccp	Mag (±Hem)-Py-Ccy gold, electrum, silver	Mt-Ccp-Py-Bn ± Hem-Sp -Gn ±Mo, silver and gold
References	This study	Vorobiev (1998)	Mueller (2007,2012)	Enns et al.(1995), Micko (2014)

NOTES:

Abbreviations: Avg = average; Std = standard deviation; n.a. not analysed or not applicable

Minerals: Ab=albite; Act=actinolite; Adr=andradite; Alm=almandine; Bn=bornite; Bt=biotite; Cal=calcite;

Ccp=chalcopyrite; Chl=chlorite; Di=diopside; Ep=epidote; Gn=galena; Hbl=hornblende; Hd=hedenbergite;

Hem=hematite; Mag=magnetite; Py=pyrite; Po=pyrrhotite; Qz=quartz; Sp=sphalerite

CLLFZ=Cadillac-Larder Lake fault zone

BIBLIOGRAPHIE

- Assad, R.J. (1958). *The geology of the East Sullivan Deposit Val-d'Or Quebec*. (unpublished Ph.D. thesis). McGill University, Montreal.
- Ayer, J.A., Amelin, Y., Corfu, F., Kamo, S., Ketchum, J., Kwok, K. and Trowell, N. (2002). Evolution of the southern Abitibi greenstone belt based on U-Pb geochronology : autochthonous volcanic construction followed by plutonism, regional deformation and sedimentation. *Precambrian Research*, 115, 69-95.
- Bailey, J.C. (1977). Fluorine in granitic rocks and melts: A review. *Chemical Geology*, 19(1-4), 1-42. doi: 10.1016/0009-2541(77)90002-X
- Baker, T., Van Achterberg, E., Ryan, C.G. and Lang, J.R. (2004). Composition and evolution of ore fluids in a magmatic-hydrothermal skarn deposit. *Geology*, 32(2), 117-120. doi: 10.1130/g19950.1
- Bayne, A.S. (1985). *Report on Bourlamaque property*. (GM49911 Ministère de l'Energie et Ressources naturelles du Québec). Mid-Canada Gold & Copper Mines LTD.
- Beaudoin, G. and Pitre, D. (2005). Stable isotope geochemistry of the Archean Val-d'Or (Canada) orogenic gold vein field. *Mineralium Deposita*, 40(1), 59-75. doi: 10.1007/s00126-005-0474-z
- Bedeaux, P., Pilote, P., Daigneault, R. and Rafini, S. (2017). Synthesis of the structural evolution and associated gold mineralization of the Cadillac Fault, Abitibi, Canada. *Ore Geology Reviews*, 82, 49-69. doi: 10.1016/j.oregeorev.2016.11.029

- Bérubé, M. (1969). *Diamond drill record*. (GM24709-GM25750, Ministère de l'Énergie et des Ressources naturelles du Québec). Ducros Mines Limited.
- Bérubé, M. (1974). *Rapport géologique sommaire du pluton Central et des roches encaissantes, canton de Bourlamaque, Abitibi, Québec*. (GM 29960, Ministère de l'Énergie et des Ressources naturelles du Québec). Ducros Mines Ltd.
- Bigot, L. and Jébrak, M. (2015). Gold Mineralization at the syenite-hosted Beattie Gold deposit, Duparquet, Neoproterozoic Abitibi belt, Canada. *Economic Geology*, 110, 315-335.
- Boucher, S.M., Hannington, M.D. and Dubé, B. (2010). Primary and secondary ore textures in the West Ansil volcanic-hosted massive-sulphide deposit, Noranda mining camp, Rouyn-Noranda, Quebec. *Geological Survey of Canada, Current Research, 2010-10*, 16.
- Bowman, J.R. (1998). Stable isotope systematics of skarn. In D.R. Lentz (ed.), *Mineralized intrusion-related skarn system* (vol. 26, p. 99-145). Mineralogical Association of Canada.
- Brimhall, G., Agee, C. and Stoffregen, R.E. (1984). The hydrothermal conversion of hornblende to biotite. *Canadian Mineralogist*, 23(3), 369-379.
- Bubar, D.S. and Beaudry, C. (1986). *Geological Compilation Report, Oramaque Property, Bourlamaque Twp., Québec*. Unpublished private report for Aur Resources Inc.
- Bubar, D.S. and Cooke, D.R. (1987). *Report on the 1987 Diamond drilling program, Oramaque Property, Project 410, Bourlamaque Tp, Québec*. (GM47650 Ministère de l'Énergie et des Ressources naturelles du Québec). Aur Resources Inc.

- Burnham, C.W. (1997). Magmas and hydrothermal fluids. In H.L. Barnes (ed.), *Geochemistry of Hydrothermal Ore Deposits* (vol. 3rd edition., p. 63–123). New York: John Wiley and Sons.
- Burt, D.M. (1977). Mineralogy and Petrology of Skarn Deposits. *Rendiconti Società Italiana di Mineralogia e Petrologia*, 33(2), 859-873.
- Cameron, E.M. and Hattori, K. (1987). Archean gold mineralization and oxidized hydrothermal fluids. *Economic Geology*, 82(5), 1177-1191. doi: 10.2113/gsecongeo.82.5.1177
- Campiglio, C. and Darling, R. (1976). The geochemistry of the Archean Bourlamaque batholith, Abitib, Quebec. *Canadian Journal of Earth Sciences*, 13, 972-986.
- Card, K.D. (1990). A review of the Superior Province of the Canadian Shield, a product of Archean accretion. *Precambrian Research*, 48, 99-156.
- Card, K.D. and Ciesielski, A. (1986). Subdivisions of the Superior Province of the Canadian Shield. *Geosciences Canada*, 13, 5-13.
- Caritat, P., Hutcheon, I. and Walshe, J.L. (1993). Chlorite Geothermometry : a review. *Clays and Clay Minerals*, 41(2), 219-239.
- Carrier, A., Savard, C. and Berthelot, P. (2004). *Resultats de la campagne d'exploration, Hiver 2003-2004, propriété Orenada, projet 17407, Canton Bourlamaque, Québec*. (Vol. GM462121 Ministère de l'Energie et des Ressources naturelles du Québec). Alexis Minerals Corporation.
- Cashman, K.V., Sparks, R.S. and Blundy, J.D. (2017). Vertically extensive and unstable magmatic systems: A unified view of igneous processes. *Science*, 355(6331). doi: 10.1126/science.aag3055

- Cathelineau, M. (1986). The Hydrothermal Alkali Metasomatism Effects on Granitic Rocks: Quartz Dissolution and Related Subsolvus Changes. *Journal of Petrology*, 27(4), 945-965. doi: 10.1093/petrology/27.4.945
- Cathelineau, M. and Nieva, D. (1985). A chlorite solid solution geothermometer. The Los Azufres (Mexico) geothermal system. *Contributions to Mineralogy and Petrology*, 91, 235-244.
- Chang, Z. and Meinert, L.D. (2004). The magmatic–hydrothermal transition—evidence from quartz phenocryst textures and endoskarn abundance in Cu–Zn skarns at the Empire Mine, Idaho, USA. *Chemical Geology*, 210(1-4), 149-171. doi: 10.1016/j.chemgeo.2004.06.018
- Chown, E.H., Daigneault, R., Mueller, W.U. and Mortensen, J.K. (1992). Tectonic evolution of the Northern volcanic zone, Abitibi belt, Quebec. *Canadian Journal of Earth Sciences*, 29, 2211-2225.
- Couture, J.-F., Pilote, P., Machado, N. and Desrochers, J.-P. (1994). Timing of gold mineralization in the Val-d'Or District, southern Abitibi Belt; evidence for two distinct mineralizing events. *Economic Geology*, 89(7), 1542-1551. doi: 10.2113/gsecongeo.89.7.1542
- Daigneault, R., Mueller, W.U. and Chown, E.H. (2002). Oblique Archean subduction : accretion and exhumation of an oceanic arc during dextral transpression, Southern Volcanic Zone, Abitibi, Subprovince Canada. *Precambrian Research*, 115, 261-290. doi: 10.1016/S0304-3871(02)00115-1
- Davidson, J., Turner, S., Handley, H., Macpherson, C. and Dosseto, A. (2007). Amphibole “sponge” in arc crust? *Geology*, 35(9), 787-790. doi: 10.1130/G23637a.1

- Davies, J.F. and Whitehead, R.E. (2006). Alkali-Alumina and MgO-Alumina Molar Ratios of Altered and Unaltered Rhyolites. *Exploration and Mining Geology*, 15(1-2), 75-88.
- Davies, J.F. and Whitehead, R.E. (2010). Alkali/Alumina Molar Ratio Trends in Altered Granitoid Rocks Hosting Porphyry and Related Deposits. *Exploration and Mining Geology*, 19(1-2), 13-22.
- Davis, D.W. (1991). Age constraints on deposition and provenance of Archean sediments in the Southern Abitibi and Pontiac Subprovinces from U-Pb analyses of detrital zircons. Abitibi-Grenville transect. *Lithoprobe workshop*, 25, 147-150.
- Davis, D.W. (2002). U–Pb geochronology of Archean metasedimentary rocks in the Pontiac and Abitibi subprovinces, Quebec, constraints on timing, provenance and regional tectonics. *Precambrian Research*, 115, 97-117.
- Dawson, K.M., Gross, G.A. and Kirkham, R.V. (1995). Skarn Deposits. In O.R. Eckstrand, W.D. Sinclair et R.I. Thorpe (ed.), *Géologie des types de gîtes minéraux du Canada* (vol. P-1, chap. 20). Geological Society of Canada.
- De Souza, S., Dubé, B., McNicoll, V.J., Dupuis, C., Mercier-Langevin, P., Creaser, R.A. and Kjarsgaard, I.M. (2017). Geology and hydrothermal alteration of the world-class Canadian Malartic gold deposit: Genesis of an Archean stockwork-disseminated gold deposit in the Abitibi Greenstone Belt, Québec. *Reviews in Economic Geology*, 19, 263–291.
- Deer, W.A., FRS, Howie, R.A. and Zussman, J. (2013). *An Introduction to the Rock-Forming Minerals*. Mineralogical Society of Great Britain and Ireland. doi: 10.1180/dhz

- Desrochers, J.-P., Hubert, C. and Pilote, P. (1996). Géologie de la région de Val-d'Or-Malartic (Abitibi-Est). *Ministère des Ressources naturelles du Québec, ET 96-01*, p. 123.
- Dimroth, E., Imreh, L., Rocheleau, M. and Goulet, N. (1983). Evolution of the south-central segment of the Archean Abitibi Belt, Quebec. Part III: plutonic and metamorphic evolution and geotectonic model. *Canadian Journal of Earth Sciences*, 20, 1374-1388.
- Drake, M.J. and Weill, D.F. (1975). Partition of Sr, Ba, Ca, Y, Eu²⁺, Eu³⁺, and other REE between plagioclase feldspar and magmatic liquid: an experimental study. *Geochimica et Cosmochimica Acta*, 39, 689-712.
- Dubé, B. and Gosselin, P. (2007). Greenstone-hosted quartz-carbonate vein deposits. In W.D. Goodfellow (ed.), *Mineral deposits of Canada: A synthesis of major deposit-types, district metallogeny, the evolution of geological provinces, and exploration methods* (vol. Special Publication no.5, p. 49-73). Geological Association of Canada, Mineral Deposits Division
- Dubé, B., Mercier-Langevin, P., Castonguay, S., McNicoll, V.J., Bleeker, W., Lawley, C.J.M., . . . Lauzière, K. (2015). TGI4: Contributions to the understanding of Precambrian Lode Gold deposits and implications for exploration. *Geological Survey of Canada*, 7852, 297. doi: 10.4095/296624
- Dubé, J. (2018). *Caractérisation métallogénique et structurale de la minéralisation aurifère des gisements Triangle et Cheminée No. 4, Val-d'Or, Abitibi, Québec*. (MSc thesis online : <https://constellation.uqac.ca/4695/>). Université du Québec à Chicoutimi.
- Einaudi, M.T. (1981). General features and origin of skarns associated with porphyry copper plutons. In S.R. Titley (ed.), *Advances in geology of the porphyry copper deposits* (p. 185–209). The University of Arizona Press, Tucson.

- Einaudi, M.T. and Burt, D.M. (1982). Introduction Terminology, Classification, and Composition of Skarn Deposits. *Economic Geology*, 77, 745-754.
- Einaudi, M.T., Meinert, L.D. and Newberry, R.J. (1981). Skarn deposits. *Economic Geology, 75th Anniversary Volume*, 317-391.
- Enns, S.G., Thompson, J.F.H., Stanley, C.R. and Yarrow, E.W. (1995). The Galore Creek porphyry copper-gold deposits, northwestern British Columbia. In T.G. Schroeter (ed.), *Porphyry deposits of the northwestern Cordillera of North America* (vol. Special Volume 46, p. 630-644). Canadian Institute of Mining, Metallurgy and Petroleum
- Erdmann, S., Martel, C., Pichavant, M. and Kushnir, A. (2014). Amphibole as an archivist of magmatic crystallization conditions: problems, potential, and implications for inferring magma storage prior to the paroxysmal 2010 eruption of Mount Merapi, Indonesia. *Contributions to Mineralogy and Petrology*, 167(6). doi: 10.1007/s00410-014-1016-4
- Faure, S. (2015). *Relations entre les minéralisations aurifères et les isogrades métamorphiques en Abitibi*. (Vol. Projet CONSOREM 2013-03).
- Fayol, N. and Jébrak, M. (2017). Archean Sanukitoid Gold Porphyry Deposits: A New Understanding and Genetic Model from the Lac Bachelor Gold Deposit, Abitibi, Canada. *Economic Geology*, 112(8), 1913-1936. doi: 10.5382/econgeo.2017.4534
- Feng, R. and Kerrich, R. (1992). Geochemical evolution of granitoids from the Archean Abitibi Southern Volcanic Zone and the Pontiac subprovince, Superior Province, Canada: Implications for tectonic history and source regions. *Chemical Geology*, 98, 23-70.

- Franz, G. and Liebscher, A. (2004). Physical and Chemical Properties of the Epidote Minerals-An Introduction. *Reviews in Mineralogy and Geochemistry*, 56(1), 1-81. doi: 10.2138/gsrmg.56.1.1
- Frost, B.R., Barnes, C.G., Collins, W.J., Arculus, R.J., Ellis, D.J. and Frost, C.D. (2001). A Geochemical Classification for Granitic Rocks. *Journal of Petrology*, 42(11), 2033-2048.
- Frost, B.R. and Frost, C.D. (2008). A Geochemical Classification for Feldspathic Igneous Rocks. *Journal of Petrology*, 49(11), 1955-1969. doi: 10.1093/petrology/egn054
- Gagnon, J.-M. and David, J. (1982). *Echantillonnage en vrac, propriété first Orenada, projet zone 4*. (GM42867 Ministère de l'Énergie et des Ressources naturelles du Québec).
- Galley, A.G., Jonasson, I.R. and Watkinson, D.H. (2000a). Magnetite-rich calc-silicate alteration in relation to synvolcanic intrusion at the Ansil volcanogenic massive sulfide deposit, Rouyn-Noranda, Quebec, Canada. *Mineralium Deposita*, 35, 619-637.
- Galley, A.G., van Breemen, O. and Franklin, J.M. (2000b). The relationship between intrusion-hosted Cu-Mo mineralization and deposits of the Archean Sturgeon Lake mining camp, northwestern Ontario. *Economic Geology*, 95(7), 1543-1550.
- Goldfarb, R.J., Baker, T., Dubé, B. and Groves, D.I. (2005). Distribution, character and genesis of gold deposits in metamorphic terranes. *Economic Geology, 100th Anniversary Volume*, 407-450.
- Gosselin, P. and Dubé, B. (2005). *Gold deposits of Canada: distribution, geological parameters and gold content*. [CD-ROM]. *Open File 4896*: Geological Survey of Canada.

- Groves, D.I., Goldfarb, R.J., Gebre-Mariam, M., Hagemann, S.G. and Robert, F. (1998). Orogenic gold deposits : A proposed classification in the context of their crustal distribution and relationship to other gold deposit types. *Ore Geology Reviews*, 13, 7-20.
- Groves, D.I., Goldfarb, R.J., Robert, F. and Hart, C.J.R. (2003). Gold Deposits in Metamorphic Belts : Overview of Current Understanding, Outstanding Problems, Future Research, and Exploration Significance. *Economic Geology*, 98, 1-29.
- Groves, D.I., Golding, S.D., Rock, N.M.S., Barley, M.E. and McNaughton, N.J. (1988). Archaean carbon reservoirs and their relevance to the fluid source for gold deposits. *Nature*, 331(6153), 254-257. doi: 10.1038/331254a0
- Hanchar, J.M. and Hoskin, P.W.O. (2003). Zircon Saturation Thermometry. In J.M. Hanchar et P.W.O. Hoskin (ed.), *Zircon* (vol. 53, Reviews in Mineralogy and Geochemistry, chap. 4, p. 518). Mineralogical Society of America.
- Hanes, J.A., Archibald, D.A., Hodgson, C.J. and Robert, F. (1992). Dating of Archean Auriferous Quartz Vein Deposits in the Abitibi Greenstone Belt, Canada: $^{40}\text{Ar}/^{39}\text{Ar}$ Evidence for a 70- to 100-m.y.-Time Gap between Plutonism-Metamorphism and Mineralization. *Economic Geology*, 87(7), 1849-1861.
- Hawthorne, F.C., Oberti, R., Harlow, G.E., Maresch, W.V., Martin, R.F., Schumacher, J.C. and Welch, M.D. (2012). Nomenclature of the amphibole supergroup. *American Mineralogist*, 97(11-12), 2031-2048. doi: 10.2138/am.2012.4276
- Henry, D.J., Guidotti, C.V. and Thomson, J.A. (2005). The Ti-saturation surface for low-to-medium pressure metapelitic biotites: Implications for geothermometry and Ti-substitution mechanisms. *American Mineralogist*, 90(2-3), 316-328. doi: 10.2138/am.2005.1498

- Hey, M.H. (1954). A new review of the chlorites. *Mineralogical Magazine*, 30, 272-292.
- Hofmann, A.W. (1988). Chemical differentiation of the Earth: the relationship between mantle, continental crust, and oceanic crust. *Earth and Planetary Science Letters*, 90, 297-314. doi: 10.1016/0012-821X(88)90132-X
- Huang, X.-W., Sappin, A.-A., Boutroy, E., Beaudoin, G. and S., M. (2019). Trace element composition of igneous and hydrothermal magnetite from porphyry deposits: relationship to deposit subtypes and magmatic affinity. *Economic Geology*, 114(5), 917-952.
- Imreh, L. (1984). Sillon de la Motte-Vassan et son avant-pays méridional : synthèse volcanologique, lithostratigraphique et gîtologique. *Ministère des Ressources naturelles du Québec, MM 82-04*, 72.
- Ishihara, S. (1998). Granitoid Series and Mineralization in the Circum-Pacific Phanerozoic Granitic Belt. *Resource Geology*, 48(4), 219-224.
- Jamtveit, B., Wogelius, R.A. and Fraser, D.G. (1993). Zonation patterns of skarn garnets: Records of hydrothermal system evolution. *Geology*, 21(2). doi: 10.1130/0091-7613(1993)021<0113:Zposgr>2.3.Co;2
- Jébrak, M. (1997). Hydrothermal breccias in vein-type ore deposits: A review of mechanisms, morphology and size distribution. *12*(3), 111-134. doi: 10.1016/S0169-1368(97)00009-7
- Jébrak, M. and Doucet, P. (2002). Geology and gold-molbydenum porphyry mineralisation of the Archean Taschereau-Launay plutons, Abitibi, Quebec. *Precambrian Research*, 115, 20.

- Jébrak, M., LeQuentrec, M.F., Mareschal, J.C. and Blais, D. (1991). A gravity survey across the Bourlamaque massif, southeastern Abitibi greenstone belt, Quebec, Canada : the relationship between the geometry of tonalite plutons and associated gold mineralization. *Precambrian Research*, 50, 261-268.
- Jemielita, R., Davis, D.W., Krogh, T. and Spooner, E. (1989). Chronological constraints on the origin of Archean lode gold deposits in the southern Superior Province from U/Pb isotopic analyses of hydrothermal rutile and titanite., *Geological Society of America:1989 Annual Meeting* (vol. Abstract with Programs, p. A351).
- Jowett, E.C. (1991). *Fitting iron and magnesium into the hydrothermal chlorite geothermometer*. GAC/MAC/SEG Joint Annual Meeting, Toronto (May 27-29, 1991) Program with Abstracts 16, A62.
- Kerrick, R. (1990). Carbon-isotope systematics of Archean Au–Ag vein deposits in the Superior Province. *Canadian Journal of Earth Sciences*, 27(1), 40-56. doi: 10.1139/e90-004
- Kerrick, R. and Wyman, D.A. (1996). The trace element systematics of igneous rocks in mineral exploration: an overview. In D.A. Wyman (ed.), *Trace element geochemistry of volcanic rocks: applications for massive sulphide exploration* (vol. Short Course Notes, Vol.12, p. 1-50). Geological Association of Canada.
- Khobzi, A., Beauregard, A.J. and Sullivan, D.L. (1986). *Evaluation report*. (GM4337 Ministère de l'Énergie et Ressources naturelles du Québec). [Evaluation Report]. Geologica groupe Conseil.
- Kranidiotis, P. and MacLean, W.H. (1987). Systematics of chlorite alteration at the Phelps Dodge massive sulfide deposit, Matagami, Quebec. *Economic Geology*, 82, 1898-1911.

- Lameyre, J. and Bowden, P. (1982). Plutonic rock type series: discrimination of various granitoid series and related rocks. *Journal of Volcanology and Geothermal Research*, 14(1-2), 169-186. doi: 10.1016/0377-0273(82)90047-6
- Large, R.R., Gemmill, J.B. and Paulick, H. (2001). The Alteration Box Plot: A Simple Approach to Understanding the Relationship between Alteration Mineralogy and Lithochemistry Associated with Volcanic-Hosted Massive Sulfide Deposits. *Economic Geology*, 96, 957-971.
- Laurent, O., Doucelance, R., Martin, H. and Moyen, J.-F. (2013). Differentiation of the late-Archaean sanukitoid series and some implications for crustal growth: Insights from geochemical modelling on the Bulai pluton, Central Limpopo Belt, South Africa. *Precambrian Research*, 227, 186-203. doi: 10.1016/j.precamres.2012.07.004
- Laurent, O., Martin, H., Moyen, J.-F. and Doucelance, R. (2014). The diversity and evolution of late-Archaean granitoids: Evidence for the onset of “modern-style” plate tectonics between 3.0 and 2.5Ga. *Lithos*, 205, 208-235. doi: 10.1016/j.lithos.2014.06.012
- Lavoie, S. (2003). *Geologie de la mine East-Sullivan, Abitibi-Est, Val d'Or, Québec*. (MSc thesis online : <https://constellation.uqac.ca/788/>). Université du Québec à Chicoutimi.
- Le Maitre, R.W. (1976). Some problems of the projection of chemical data into mineralogical classifications. *Contributions to Mineralogy and Petrology*, 56, 181-189.
- Leake, B.E., A.R., W., Arps, C.E.S., Birch, W.D., Gilbert, M.C., Grice, J.D., . . . Youzhi, G. (1997). Nomenclature of amphiboles: report of the subcommittee on amphiboles of the International Mineralogical Association Commission on New Minerals and Mineral Names. *European Journal of Mineralogy*, 9(3), 623-652.

- Lebel, J. (1987). *Gîtologie de la mine d'or Akasaba, Abitibi, Québec*. (unpublished Msc thesis). Ecole Polytechnique, Montréal.
- Lemarchand, J. (2012). *Les mineralisations filoniennes aurifères du pluton de Bourlamaque (Val d'Or, Abitibi) : Synthèse structurale et apports de la datation Ar/Ar*. (PhD thesis online: <https://archipel.uqam.ca/5208/>). Rennes1, UQAM.
- Locock, A.J. (2014). An Excel spreadsheet to classify chemical analyses of amphiboles following the IMA 2012 recommendations. *Computers & Geosciences*, 62, 1-11. doi: 10.1016/j.cageo.2013.09.011
- Machado, N. and Gariépy, C. (1992). *Geochronologie U-Pb du territoire québécois. Partie I : les sous-province de l'Abitibi et du Pontiac*. (GM 66921, Ministère des Ressources naturelles du Québec).
- Manning, D.A.C. (1981). The effect of fluorine on liquidus phase relationships in the system Qz-Ab-Or with excess water at 1kb. *Contributions to Mineralogy and Petrology*, 76, 206-215. doi: 10.1007/BF00371960
- Martin, H., Smithies, R.H., Rapp, R., Moyen, J.-F. and Champion, D. (2005). An overview of adakite, tonalite–trondhjemite–granodiorite (TTG), and sanukitoid: relationships and some implications for crustal evolution. *Lithos*, 79(1-2), 1-24. doi: 10.1016/j.lithos.2004.04.048
- McDonough, M.F. and Sun, S.-s. (1995). The composition of the Earth. *Chemical Geology*, 120, 223-253.
- McQueen, K.G. and Cross, A.J. (1998). Magnetite as a geochemical sampling medium: application to skarn deposits. *Geological Society, Australia, Special Publications*, 20, 194-199.

- Meinert, L.D. (1995). Compositional variation of igneous rocks associated with skarn deposits - Chemical evidence for a genetic connection between petrogenesis and mineralization. In J.F.H. Thompson (ed.), *Magma, Fluids, and ore deposits* (vol. Short Course Volume 23, chap. 18, p. 401-418). Victoria, British Columbia: Mineralogical Association of Canada.
- Meinert, L.D., Dipple, G.M. and Nicolescu, S. (2005). World Skarn Deposits. *Economic Geology, 100th Anniversary Volume*, 299-336.
- Mercer, C.N. and Reed, M.H. (2013). Porphyry Cu-Mo Stockwork Formation by Dynamic, Transient Hydrothermal Pulses: Mineralogic Insights from the Deposit at Butte, Montana. *Economic Geology*, 108, 1347-1377. doi: 0361-0128/13/4143/1347-31
- Mercier-Langevin, P., Gibson, H.L., Hannington, M.D., Goutier, J., Monecke, T., Dubé, B. and G., H.M. (2014). A Special Issue on Archean Magmatism, Volcanism, and Ore Deposits: Part 2. Volcanogenic Massive Sulfide Deposits. *Economic Geology*, 109, 1-9. doi: 0361-0128/14/4177/1-9
- Mercier, P.-E. and Berthelot, P. (2017). *Drilling Campaign Fall 2014-Winter 2015, Orenada Group*. (GM 70071 Ministère de l'Énergie et Ressources naturelles du Québec). Alexandria Minerals.
- Mériaud, N. and Jébrak, M. (2017). From intrusion-related to orogenic mineralization: The Wasamac deposit, Abitibi Greenstone Belt, Canada. *Ore Geology Reviews*, 84, 289-308. doi: 10.1016/j.oregeorev.2017.01.021
- Micko, J., Tosdal, R.M., Bissig, T., Chamberlain, C.M. and Simpson, K.A. (2014). Hydrothermal Alteration and Mineralization of the Galore Creek Alkalic Cu-Au Porphyry Deposit, Northwestern British Columbia, Canada. *Economic Geology*, 109(4), 891-914. doi: 10.2113/econgeo.109.4.891

- Miller, C.F., McDowell, S.M. and Mapes, R.W. (2003). Hot and cold granites? Implications of zircon saturation temperatures and preservation of inheritance. *Geology*, 31(6), p.529-532. doi: 10.1130/0091-7613(2003)031
- Monecke, T., Mercier-Langevin, P., Dubé, B. and Frieman, B.M. (2017). Geology of the Abitibi Greenstone Belt. *Reviews in Economic Geology*, 19, 7-49.
- Monecke, T., Monecke, J., Reynolds, T.J., Tsuruoka, S., Bennett, M.M., Skewes, W.B. and Palin, R.M. (2018). Quartz Solubility in the H₂O-NaCl System: A Framework for Understanding Vein Formation in Porphyry Copper Deposits. *Economic Geology*, 113(5), 1007-1046. doi: 10.5382/econgeo.2018.4580
- Mortensen, J.K. and Card, K.D. (1993). U-Pb age constraints for the magmatic and tectonic evolution of the Pontiac Subprovince, Quebec. *Canadian Journal of Earth Sciences*, 30, 1970-1980.
- Moyen, J.-F. (2019). Archean granitoids: classification, petrology, geochemistry and origin. *Geological Society, London, Special Publications*, 489, 34. doi: 10.1144/sp489-2018-34
- Moyen, J.-F., Martin, H. and Jayananda, M. (2001). Multi-element geochemical modelling of crust – mantle interactions during late-Archaean crustal growth: the Closepet granite (South India). *Precambrian Research*, 112, 87-105.
- Mueller, A.G. (1997). The Nevoia Gold Skarn Deposit in Archean Iron-Formation, Southern Cross Greenstone Belt, Western Australia : I. Tectonic Setting, Petrography, and Classification. *Economic Geology*, 92, 181-209.
- Mueller, A.G. (2007). Copper-gold endoskarns and high-Mg monzodiorite–tonalite intrusions at Mt. Shea, Kalgoorlie, Australia: implications for the origin of gold–pyrite–tennantite mineralization in the Golden Mile. *Mineralium Deposita*, 42(7), 737-769. doi: 10.1007/s00126-007-0132-8

- Mueller, A.G., Hall, G.C., Nemchin, A.A., Stein, H.J., Creaser, R.A. and Mason, D.R. (2007). Archean high-Mg monzodiorite–syenite, epidote skarn, and biotite–sericite gold lodes in the Granny Smith–Wallaby district, Australia: U–Pb and Re–Os chronometry of two intrusion-related hydrothermal systems. *Mineralium Deposita*, 43(3), 337-362. doi: 10.1007/s00126-007-0164-0
- Mueller, A.G., Lawrance, L.M., Muhling, J. and Pooley, G.D. (2012). Mineralogy and PTX Relationships of the Archean Hannan South Au-Cu (Co-Bi) Deposit, Kalgoorlie, Western Australia: Thermodynamic Constraints on the Formation of a Zoned Intrusion-Related Skarn. *Economic Geology*, 107(1), 1-24. doi: 10.2113/econgeo.107.1.1
- Mueller, A.G., Nemchin, A.A. and Frei, R. (2004). The Nevorio Gold Skarn Deposit, Southern Cross Greenstone Belt, Western Australia: II. Pressure-Temperature-Time Path and Relationship to Postorogenic Granites. *Economic Geology*, 99(3), 453-478. doi: 10.2113/gsecongeo.99.3.453
- Munoz, J.L. (1984). F–OH and Cl–OH exchange in micas with applications to hydrothermal ore deposits. In S.W. Bailey (ed.), *Micas*. (vol. 13, p. 469-494). Reviews in Mineralogy.
- Nachit, H., Ibhi, A., Abia, E.H. and Ben Ohoud, M. (2005). Discrimination between primary magmatic biotites, reequilibrated biotites and neofomed biotites. *Comptes Rendus Geoscience*, 337(16), 1415-1420. doi: 10.1016/j.crte.2005.09.002
- Nadeau, O. (2019). Sources of fluids in Archean hydrothermal stockwork-disseminated gold deposits of Abitibi, Canada: Insights from Duquesne, Dolodau, Lac Shortt and Canadian Malartic. *Ore Geology Reviews*, 111. doi: 10.1016/j.oregeorev.2019.102975
- Nadoll, P., Angerer, T., Mauk, J.L., French, D. and Walshe, J. (2014). The chemistry of hydrothermal magnetite: A review. *Ore Geology Reviews*, 61, 1-32. doi: 10.1016/j.oregeorev.2013.12.013

- Nadoll, P., Mauk, J.L., Leveille, R.A. and Koenig, A.E. (2015). Geochemistry of magnetite from porphyry Cu and skarn deposits in the southwestern United States. *Mineralium Deposita*, 50(4), 493-515. doi: 10.1007/s00126-014-0539-y
- Nakamura, K. and Kato, Y. (2004). Carbonatization of oceanic crust by the seafloor hydrothermal activity and its significance as a CO₂ sink in the Early Archean. *Geochimica et Cosmochimica Acta*, 68(22), 4595-4618. doi: 10.1016/j.gca.2004.05.023
- Naney, M.T. (1983). Phase equilibria of rock-forming ferromagnesian silicates in granitic systems. *American Journal of Science*, 283, 993–1033.
- Neumayr, P., Hagemann, S.G. and Couture, J.-F. (2000). Structural setting, textures, and timing of hydrothermal vein systems in the Val d'Or camp, Abitibi, Canada: implications for the evolution of transcrustal, second- and third-order fault zones and gold mineralization. *Canadian Journal of Earth Sciences*, 37(1), 95-114.
- Norman, G.W.H. (1943). Bourlamaque, Abitibi County, Quebec. *Geological Survey of Canada, Paper 43-2*.
- Pilote, P. (2000). *Géologie de la région de Val-d'Or, Sous-province de l'Abitibi volcanologie physique et évolution métallogénique*. (Ministère des Ressources naturelles du Québec) (MB 2000-09).
- Pilote, P., Daigneault, R., David, J. and McNicoll, V. (2014). L'architecture des groupes de Malartic, de Piché et de Cadillac et de la Faille de Cadillac, Abitibi : révision géologique, nouvelles datations et interprétations., *Ministère de l'Énergie et des Ressources Naturelles du Québec* (DV 2015-03, p. 37).

- Pilote, P., Lacoste, P., Bedeaux, P. and Lienard, A. (2017). *Compilation Géologique - Rivière Bourlamaque*. CG-2016-2012. Ministère de l'Énergie et des Ressources naturelles.
- Pilote, P., Lacoste, P., David, J., Daigneault, R., McNicoll, V. and Moorhead, J. (2015). La région de Val-d'Or – Malartic: volcanologie et évolution métallogénique. In *Stratigraphy, volcanology and metallogenic evolution of Val-d'Or – Malartic (Québec), Kirkland Lake, and Timmins (Ontario) areas, Abitibi Subprovince*. (p. 147). Edited by Pilote, P & Prefontaine, S.: Ministère de l'énergie et des Ressources naturelles du Québec and Ontario Geological Survey.
- Pilote, P., Mueller, W.U., Scott, C., Champagne, C., Lavoie, S. and Moorhead, J. (1998). Volcanologie de la Formation Val-d'Or et du Groupe de Malartic, sous-Province de l'Abitibi : contraintes géochimiques et géochronologiques., *Ministère des Ressources naturelles du Québec* (DV 98-05, p. 48-49).
- Pilote, P., Scott, C., Mueller, W.U., Lavoie, S. and Riopel, P. (1999). Géologie des formations Val-d'Or, Héva et Jacola -nouvelle interprétation du bloc de Malartic. *Ministère des Ressources naturelles du Québec* (DV 99-03, p. 19-20).
- Pollok, K., Jamtveit, B. and Putnis, A. (2001). Analytical transmission electron microscopy of oscillatory zoned grandite garnets. *Contributions to Mineralogy and Petrology*, 141(3), 358-366. doi: 10.1007/s004100100248
- Poulsen, K.H. (2017). The Larder Lake-Cadillac break and its gold districts. *Reviews in Economic Geology*, 19, 133-167.
- Poulsen, K.H., Robert, F. and Dubé, B. (2000). *Geological classification of Canadian gold deposits* (Geological survey of Canada éd., vol. 540).
- Putirka, K. (2016). Amphibole thermometers and barometers for igneous systems and some implications for eruption mechanisms of felsic magmas at arc volcanoes. *American Mineralogist*, 101(4), 841-858. doi: 10.2138/am-2016-5506

- Rafini, S. (2014). *Typologie des minéralisations aurifères dans Faille Cadillac*. CONSOREM project reports 2011–01.
- Redmond, P.B. and Einaudi, M.T. (2010). The Bingham Canyon Porphyry Cu-Mo-Au Deposit. I. Sequence of Intrusions, Vein Formation, and Sulfide Deposition. *Economic Geology*, 105(1), 43-68. doi: 10.2113/gsecongeo.105.1.43
- Rezaei, M. and Zarasvandi, A. (2020). Titanium-in-biotite thermometry in porphyry copper systems: Challenges to application of the thermometer. *Resource Geology*, 70(2), 157-168. doi: 10.1111/rge.12227
- Richards, J.P. (2011). Magmatic to hydrothermal metal fluxes in convergent and collided margins. *Ore Geology Reviews*, 40(1), 1-26. doi: 10.1016/j.oregeorev.2011.05.006
- Ridolfi, F. and Renzulli, A. (2011). Calcic amphiboles in calc-alkaline and alkaline magmas: thermobarometric and chemometric empirical equations valid up to 1,130°C and 2.2 GPa. *Contributions to Mineralogy and Petrology*, 163(5), 877-895. doi: 10.1007/s00410-011-0704-6
- Ridolfi, F., Renzulli, A. and Puerini, M. (2009). Stability and chemical equilibrium of amphibole in calc-alkaline magmas: an overview, new thermobarometric formulations and application to subduction-related volcanoes. *Contributions to Mineralogy and Petrology*, 160(1), 45-66. doi: 10.1007/s00410-009-0465-7
- Rieder, M., Cavazzini, G. and D'yakov, Y. (1998). Nomenclature of the Micas. *The Canadian Mineralogist*, 36, 41-48.
- Robert, F. (1989). Internal structure of the Cadillac tectonic zone southeast of Val d'Or, Abitibi greenstone belt, Quebec. *Canadian Journal of Earth Sciences*, 26, 2661-2675.

- Robert, F. (1994). Vein fields in gold districts: the example of Val-d'Or, southeastern Abitibi subprovince, Quebec. In Geological Survey of Canada (ed.), *Canadian Shield, Current Research no. 1994-C* (p. 295-302). Natural Resources Canada.
- Robert, F. (2001). Syenite-associated disseminated gold deposits in the Abitibi greenstone belt, Canada. *Mineralium Deposita*, 36, 503-516.
- Robert, F., Brommecker, R.S. and Bubar, D. (1990). The Orenada Zone 4 Deposit: Deformed veine-type gold mineralization within the Cadillac tectonic zone, SE of Val-d'Or. *Institut Canadien des mines et de la métallurgie, Spécial 43*, 255-268.
- Robert, F. and Brown, A.C. (1986a). Archean gold-bearing quartz veins at the Sigma Mine, Abitibi Greenstone belt, Quebec. Part I. Geologic relations and formation of the veins system. . *Economic Geology*, 81, 578-592.
- Robert, F. and Brown, A.C. (1986b). Archean Gold-Bearing Quartz Veins at the Sigma Mine, Abitibi Greenstone Belt, Quebec: Part II. Vein Paragenesis and Hydrothermal Alteration. *Economic Geology*, 81, 593-616. doi: 0361-0128/86/524/593-24
- Robert, F. and Poulsen, K.H. (1997). World - class Archaean gold deposits in Canada: An overview. *Australian Journal of Earth Sciences*, 44(3), 329-351. doi: 10.1080/08120099708728316
- Robert, F., Poulsen, K.H., Cassidy, K.F. and Hodgson, C.J. (2005). Gold Metallogeny of the Superior and Yilgarn Cratons. *Economic Geology, 100th Anniversary Volume*, 1001-1033.
- Ross, P.-S. and Bédard, J.H. (2009). Magmatic affinity of modern and ancient subalkaline volcanic rocks determined from trace-element discriminant

diagrams. *Canadian Journal of Earth Sciences*, 46(11), 823-839. doi: 10.1139/e09-054

Sauvé, P., Imreh, L. and Trudel, P. (1993). *Description des gîtes d'or de la région de Val-d'Or* (vol. MM 91-03). Ministère des Ressources Naturelles du Québec

Savard, C., Carrier, A. and Durieux, G. (2018). *NI 43-101 technical report and updated mineral resource estimate for the Orenada zones 2 and 4 project, Orenada group properties*. InnovExplo.

Scott, C.R., Mueller, W.U., Pilote, P. and Mueller, A.G. (2002). Physical volcanology, stratigraphy, and lithogeochemistry of an Archean volcanic arc : evolution from plume-related volcanism to arc rifting of SE Abitibi Greenstone Belt, Val d'Or, Canada. *Precambrian Research*, 115, 223-260.

Seedorf, E., Dilles, J.H., Profett, J.M. and Einaudi, M.T. (2005). Porphyry Deposits : Characteristics and Origin of Hypogene Features. *Economic Geology*, 100, 251-298.

Seedorf, E. and Einaudi, M.T. (2004). Henderson Porphyry Molybdenum System, Colorado: I. Sequence and Abundance of Hydrothermal Mineral Assemblages, Flow Paths of Evolving Fluids, and Evolutionary Style. *Economic Geology*, 99, 3-37. doi: 0361-0128/01/3400/3-35

Selby, D. and Nesbitt, B.E. (2000). Chemical composition of biotite from the Casino porphyry Cu–Au–Mo mineralization, Yukon, Canada: evaluation of magmatic and hydrothermal fluid chemistry. *Chemical Geology*, 171(1-2), 77-93. doi: 10.1016/S0009-2541(00)00248-5

Sillitoe, R.H. (1991). Intrusion related gold deposits. In Springer (ed.), *Gold Metallogeny and Exploration* (chap. 6, p. 165-209).

- Sillitoe, R.H. (2000). Gold-Rich Porphyry Deposits: Descriptive and Genetic Models and Their Role in Exploration and Discovery. *Reviews in Economic Geology*, 13, 315-345. doi: 10.5382/Rev.13.09
- Sillitoe, R.H. (2010). Porphyry Copper Systems. *Economic Geology*, 105(1), 3-41. doi: 10.2113/gsecongeo.105.1.3
- Sinclair, W.D., Jonasson, I.R., Kirkham, R.V. and Soregaroli, A.E. (2016). *Rhenium in Canadian mineral deposits, Open File 7780*: Geological Survey of Canada.
- Sisson, T.W. and Grove, T.L. (1993). Experimental investigations of the role of H₂O in calc-alkaline differentiation and subduction zone magmatism. *Contributions to Mineralogy and Petrology*, 113, 143–166.
- Smith, D.J. (2014). Clinopyroxene precursors to amphibole sponge in arc crust. *Nat Commun*, 5, 4329. doi: 10.1038/ncomms5329
- Stern, R.A. and Hanson, G. (1991). Archean High-Mg Granodiorite : A Derivative of Light Rare Earth Element-enriched Monzodiorite of Mantle Origin. *Journal of Petrology*, 32(1), 201-238.
- Stevenson, R., Henry, P. and Gariépy, C. (1999). Assimilation–fractional crystallization origin of Archean Sanukitoid Suites: Western Superior Province, Canada. *Precambrian Research*, 96, 83-99.
- Streckeisen, A. (1974). Classification and Nomenclature of Plutonic Rocks Recommendations of the IUGS Subcommittee on the Systematics of Igneous Rocks. *Geologische Rundschau*, 63(2), 773-786.
- Suikkanen, E. and Rämö, O.T. (2019). Episyenites—Characteristics, Genetic Constraints, and Mineral Potential. *Mining, Metallurgy & Exploration*, 36(5), 861-878. doi: 10.1007/s42461-019-00120-9

- Sun, W., Huang, R.-f., Li, H., Hu, Y.-b., Zhang, C.-c., Sun, S.-j., . . . Ling, M.-x. (2015). Porphyry deposits and oxidized magmas. *Ore Geology Reviews*, 65, 97-131. doi: 10.1016/j.oregeorev.2014.09.004
- Taner, M.F. (1996). The East Sullivan Stock and its Gold-Copper Potential, Val d'Or, Quebec, Canada. *Exploration Mining Geology*, 5(1).
- Taner, M.F., Trudel, P. and Perreault, G. (1986). Geochimie de la biotite associée à certains gisements d'or de Val d'Or, Malartic et Chibougamau, Québec. *Canadian Mineralogist*, 24, 13.
- Thurston, P.C., Ayer, J.A., Goutier, J. and Hamilton, M.A. (2008). Depositional Gaps in Abitibi Greenstone belt stratigraphy : a key to exploration for syngenetic mineralization. *Economic Geology*, 103, 1097-1124.
- Tremblay, A., Ruffet, G. and Lemarchand, J. (2020). Timing and duration of Archean orogenic gold deposits in the Bourlamaque pluton, Val d'Or mining camp, Abitibi, Canada. *Ore Geology Reviews*, 127. doi: 10.1016/j.oregeorev.2020.103812
- Veizer, J., Hofs, J., Ridler, R.H., Jensen, L.S. and Lowe, D.R. (1989). Geochemistry of Precambrian carbonates: I. Archean hydrothermal systems. *Geochimica et Cosmochimica Acta*, 53(4), 845-857. doi: 0.1016/0016-7037(89)90030-6
- Vlasova, D.K., Podlesskiy, K.V., Kudrya, P.F., Boronikhin, V.A. and Muravitskaya, G.N. (1985). Zoning in garnet from Skarn deposits. *International Geology Review*, 27(4), 465-482. doi: 10.1080/00206818509466434
- Vorobiev, L. (1998). *Réévaluation de la nature et de l'origine de la minéralisation Au-Ag-Cu d'Akasaba, District de Val d'Or, Québec*. (unpublished MSc thesis). Université de Montréal, Montréal.

- Watson, E.B. and Harrison, T.M. (1983). Zircon saturation revisited: temperature and composition effects in a variety of crustal magma types. *Earth and Planetary Science Letters*, 64(2), p.295-304. doi: 10.1016/0012-821X(83)90211-X
- Whitney, D.L. and Evans, B.W. (2009). Abbreviations for names of rock-forming minerals. *American Mineralogist*, 95(1), 185-187. doi: 10.2138/am.2010.3371
- Winchester, J.A. and Floyd, P.A. (1977). Geochemical discrimination of different magma series and their differentiation products using immobile elements. *Chemical geology*, 20, 325-343.
- Witt, W.K., Cassidy, K., Lu, Y.-J. and Hagemann, S. (2018). Syenitic Group intrusions of the Archean Kurnalpi Terrane, Yilgarn Craton: Hosts to ancient alkali porphyry gold deposits? *Ore Geology Reviews*, 96, 262-268. doi: 10.1016/j.oregeorev.2017.08.037
- Wong, L., Davis, D.W., Krogh, T.E. and Robert, F. (1991). U-Pb zircon and rutile chronology of Archean greenstone formation and gold mineralization in the Val d'Or region, Quebec. *Earth and Planetary Science Letters*, 104, 325-336.

CONCLUSION GENERALE

Le Stock d'East-Sullivan représente une suite intrusive porphyrique archéenne de composition monzonitique à syénitique, constitué de trois faciès distinctifs majeurs: précoce, intermédiaire et tardif. L'intrusion partage des caractéristiques spécifiques avec le groupe des sanukitoïdes syn-Timiskaming associés aux minéralisations en or. La mise en place du stock s'est produite vers 2684 Ma à faible profondeur, à la suite du basculement de la Formation Héva et de Val d'Or, formées respectivement entre 2705 et 2702 Ma. L'affinité alcaline de l'intrusion, associé à un état d'oxydation élevé et à la forte teneur en eau du magma initial, explique son potentiel à former une minéralisation de type porphyre à Cu-(Au-Mo). Trois principaux assemblages d'altérations caractéristiques associés à la minéralisation porphyrique ont été identifiés: (1) potassique avec un assemblage à biotite-microcline-quartz-magnétite; (2) phyllique avec un assemblage à séricite-quartz ± pyrite; et (3) propylitique représenté par un assemblage à épidote ± chlorite ± calcite.

De plus, les roches volcaniques carbonatées entourant et abritant l'intrusion ont permis le développement d'une minéralisation de type skarn à Cu-(Au-Ag). Le développement de la minéralisation a été contraint par le plissement et la verticalisation des formations volcaniques avant la mise en place de l'intrusion. Ce paramètre a restreint la zonation du système habituellement observée dans les skarns à cuivre du Phanérozoïque. La formation de skarn s'est déroulée en trois étapes principales: 1) un métamorphisme de contact à haute température induit par la mise en place du pluton; 2) un stade prograde dominé par le grenat, et potentiellement le pyroxène; et 3) un stade rétrograde abondant associé au dépôt de la minéralisation à Cu-Au-Ag, à la destruction du stade prograde, et à diminution de la température du système. Un phénomène d'épisyénitisation du

faciès intermédiaire a permis un enrichissement local en Cu-Mo conduisant à une formation d'endoskarn. L'endoskarn peut avoir été favorisé par la forte teneur en fluor du faciès intermédiaire, mis en évidence notamment dans la composition des biotites et dans la géochimie des faciès du Stock de East Sullivan. La majeure partie du dépôt de cuivre coïncide avec la transition entre les stades prograde et rétrograde dans l'exoskarn ainsi que la fin de l'altération potassique au sein de l'intrusion.

Bien que leur présence soit exceptionnelle, cette étude démontre avec celui d'Akasaba l'existence de gisements de type skarn à Cu-Au à l'archéen dans la ceinture de roches vertes de l'Abitibi.

Le Stock de East Sullivan et la minéralisation de type skarn associée sont contemporains des intrusions Lamaque et Triangle qui hébergent des gisements de plusieurs millions d'onces et qui sont actuellement exploités. Ces intrusions forment un vaste et prolifique système igné situé entre la faille Cadillac et la ville de Val-d'Or. Cette partie du district de Val-d'Or présente donc deux événements aurifères distincts, le premier de type plutonique développé au sein du pluton et de sa zone de contact, le second lié à un événement hydrothermal orogénique associé au métamorphisme régional. Un tel schéma soulève la question de l'origine de l'or dans ce district soit d'une origine commune de l'or, soit d'une possible remobilisation de l'or plutonique par des fluides orogéniques.

APPENDICE A

DETAILED ANALYTICAL METHODS

To characterize and identify textural variations in the rocks, alteration and ore, a set of 29 samples was investigated in thin section using a Leica DMLP transmitted-reflected light polarizing microscope and a Hitachi TM3000 (LV-SEM) with energy-dispersive X-ray spectrometry (EDS) and backscattered electron (BSE) imaging at the SEM laboratory of UQAM, Montréal, Canada. Images were captured in backscatter electron mode with an accelerating voltage of 20kV, a 5 μm beam, and a working distance of about 10 mm. The samples were prepared by Vancouver Geotech Labs, Canada.

Whole-rock geochemistry

Whole-rock major and trace elements analyses were performed by ALS Chemicals, in Val-d'Or. Representative selection of the least altered samples was pulverized (particle size less than 75 μm) and analyzed by XRF spectrometry (X-Ray-Fluorescence) to obtain the major elements composition. The process consists in fusing 0.66g of sample powder with a solution composed of lithium tetraborate and lithium metaborate (12:22), also adding an oxidizing agent (Lithium Nitrate), then poured into a platinum mold. The resulting disk is then analyzed by spectrometry. The rock powders were ignited for 3 h at 1000°C to expel volatile elements. The following elements were obtained with a detection limit of 0,01%: Al_2O_3 , CaO , Cr_2O_3 , Fe_2O_3 , K_2O , MgO , MnO , Na_2O , P_2O_5 , SiO_2 , and TiO_2 (Table 1.1).

Reference samples were used as external standards. These reference samples SY-4 (diorite) and NCSDC73303 (carbonates) were analyzed as unknown to control accuracy with results close to the recommended values. Duplicates of three samples (FB1604, FB1608, FB1622) were reproduced in a limit of 0.1% by weight for LOI and SiO₂, 0.02% by weight for CaO, Al₂O₃ and Na₂O, 0.01% by weight for MgO, TiO₂, MnO, K₂O and P₂O₅. Chemical blanks were also analyzed, giving concentrations of 0.9 ppm for Ba, 0.01-0.1 ppm for Li, Sr, Zr and Rb, 0.01 ppm for Y, Nb, Cs, Th, Ce, Hf, Th and below the detection limits for the other elements. C and S were also analyzed as Total Sulfur and Carbon. The sulfur dioxide and carbon dioxide released by the sample using a stream of oxygen flows through 0.05g of sample, heated at 1350°C were measured by an infrared detection system with a detection limit of 0.01%.

To obtain the rare earth and trace elements (Ba, Ce, Cr, Cs, Dy, Er, Eu, Ga, Gd, Hf, Ho, La, Lu, Nb, Nd, Pr, Rb, Sm, Sn, Sr, Ta, Tb, Th, Tm, U, V, W, Y, Yb, Zr), the sample powders (0.100 g) were mixed with a solution of lithium metaborate and tetraborate (LiBO₂ / Li₂B₄O₇) and fused at 1025°C. The resulting liquid is then cooled and dissolved in an acidic mixture containing nitric, hydrochloric and fluoric acids. The final solution obtained is then analyzed by ICP-MS (Inductively Coupled Plasma - Mass Spectrometry). For the base metals (Ag, Co, Cu, Li, Mo, Ni, Pb, Sc, Tl), specific elements such as cadmium and zinc and some minerals not completely dissolved using lithium borate fusion such as zircon, some metal oxides, rare earth phosphates and some sulfides were analyzed by ICP-AES (plasma coupled to an atomic emission spectroscope) after a 4-acid dissolution. The process consists to dissolve 0.25 g of samples in a mixture of perchloric acid, nitric acid, fluorine and hydrochloric acid, the results being corrected by spectral interference. The remaining trace elements (As, Bi, Hg, In, Re, Sb, Sc, Se, Te, Tl) were analyzed by ICP-MS preceded by Aqua Regia dissolution. 0.50g of sample is digested with aqua regia for 45 minutes. After cooling, the resulting solution is diluted to 12.5 ml with deionized water, mixed and analyzed.

Fluor content of five intrusive rocks was obtained by Na_2O_2 fusion, citric acid leach and ion selective electrode. The iron of these five samples was also analyzed by titration to obtain the FeO content. FeO and F were obtained with a detection limit of 0,01%. The range of detection limits for each element is reported in Table 1.1

Electron Probe Micro-Analysis (EPMA)

Major and minor elements composition in minerals were acquired with a CAMECA SX-100 electron probe equipped with five WDS spectrometers at the Université Laval, Québec. All the data was acquired using the following conditions: a 5 μm beam diameter, 15kV accelerating voltage, 20nA beam current, counting 10s on both sides for background and 15-20s at peak.

Compositional data of chlorite and amphibole grains were obtained for twelve elements (Na, Mg, Al, Si, K, Ca, Ti, Fe, Mn, Cr, Co, Ni) with additional F and Cl for amphibole. For epidote, micas and plagioclase compositions, ten elements (Na, Mg, Al, Si, K, Ca, Ti, Fe, Mn, Cl) were measured, with additional Cr, Ni, Rb, Ba and F for mica and Sr and Ba for plagioclase grains. The same ten elements, except K, were acquired for garnet with the addition of Zn and Zr.

Oxygen was calculated by stoichiometry and included in the data reduction, as was the correction for oxygen equivalence of the halogens (F and Cl). The calibration of the instrument was achieved using a range of natural and synthetic minerals. Complete geochemical data are available in the Appendices Table B2 to B6.

Re-Os molybdenite dating

The Re-Os analyses were performed at the Canadian Centre for Isotopic analysis, Re-Os Crustal Geochronology Laboratory, University of Alberta. The Qz-Cb-Bt-Cpy-Mo

vein sample was processed by metal-free crushing and then by gravity and magnetic concentration methods, to obtain a pure molybdenite concentrate for Re-Os age dating. The ^{187}Re and ^{187}Os concentrations in molybdenite were determined by isotope dilution mass spectrometry using Carius-tube, solvent extraction, anion chromatography and negative thermal ionization mass spectrometry techniques. For this work, a mixed double spike containing known amounts of isotopically enriched ^{185}Re , ^{190}Os , and ^{188}Os analysis was used (Markey et al., 2007). Isotopic analysis used a ThermoScientific Triton mass spectrometer with a Faraday collector. Total procedural blanks for Re and Os were less than <3 picograms and 2 picograms, respectively. The molybdenite powder HLP-5 (Markey et al., 1998) was analyzed as a standard, and during the analysis returned a Re-Os date of 220.5 ± 1.0 Ma, indistinguishable from that reported by Markey et al. (1998) of 221.0 ± 1.0 Ma. The age model and uncertainty were quoted at $\pm 2\sigma$ level and include all known analytical uncertainty. Detailed methods for the molybdenite analysis can be found in Markey et al. (2007) and Selby and Creaser (2004).

Carbon and oxygen isotopes

The carbon and oxygen isotopes analyses were performed at the Light stable isotope geochemistry Laboratory, Geotop-UQAM, Université du Québec à Montréal. The samples were weighted in micro glass crucibles to obtain 100 mg of CaCO_3 . The samples were then inserted in a 90°C heated rack. After 1 hour, the samples were analyzed with a Micromass model Isoprime isotope ratio mass spectrometer coupled to a MultiCarb system in dual inlet mode.

Two internal reference materials (CaCO_3 $\delta^{13}\text{C}=2,21\pm 0,03\text{‰}$ & $-40,78\pm 0,05\text{‰}$; $\delta^{18}\text{O}=-1,48\pm 0,03 \text{‰}$ & $-14,25\pm 0,05 \text{‰}$) were used to normalize the results on the NBS19-LSVEC scale. When the expected values of the samples were close to 0‰, only one

reference material was used (CaCO_3 $\delta^{13}\text{C}=2,21\pm 0,03\%$; $\delta^{18}\text{O}=-1,48\pm 0,03 \%$). Results are given in delta units (δ) in ‰ vs VPDB.

The overall analytical uncertainty (1s) is better than $\pm 0.05\%$ for $\delta^{18}\text{O}$ and $\pm 0.08 \%$ for $\delta^{13}\text{C}$. These uncertainties are based on the propagation of uncertainties of the normalization of the internal reference materials and the samples but do not include the homogeneity nor the representativity of the sample.

LA-ICP-MS analyses on magnetite

The in-situ determination of trace elements in magnetite was performed on polished thin sections by a laser ablation system coupled to a mass spectrometer (LA-ICP-MS) at the LabMaTer laboratory of the Université du Québec à Chicoutimi (UQAC, Canada). The following elements were analyzed: 23Na, 25Mg, 27Al, 29Si, 39K, 44Ca, 45Sc, 49Ti, 51V, 52Cr, 55Mn, 57Fe, 59Co, 60Ni, 65Cu, 66Zn, 71Ga, 74Ge, 88Sr, 89Y, 90Zr, 93Nb, 95Mo, 81Ta, 182W, 208Pb, 232Th and 238U based on the method from Dare et al. (2014). The LA-ICP-MS system used is Resonetics RESolution M-50 Excimer 193 nm laser equipped with a S155 ablation cell (Laurin Technic) coupled to an Agilent 7900 Model ICP-MS. The analyzes were performed with 30 seconds of background acquisition to define the blank following by 20 seconds of sample data acquisition. A spot size dependent of the mineral grain size and ranged between 25 and 33 μm was used with a frequency of 15 Hz and an energy density of 3 J / cm^2 . The USGS certified reference material GSE-1g, a synthetic glass containing 10% Fe and doped with approximately 500 ppm of each trace element was used for instrument and mass calibration. Three reference materials were used for external calibration: BC28 (natural Ti-rich magnetite derived from the Bushveld complex; Dare et al., 2012), GSD-1g (synthetic basalt glass), and Gprob6 (matrix artificial basalt glass). Material analyzes were performed before each scan cycle to correct the deviation and calibrate the equipment. The results obtained are in good agreement with the working values

(see appendice Table B8). Si, Ca, V and Ti were monitored to ensure that the measured signal was pure magnetite. All acquired data was then reduced using the Iolite software (Paton et al., 2011). LA-ICP-MS analyses of reference material used for calibration is provided in the Appendices Table B6.

Références

- Dare, S., Barnes, S.-J. and Beaudoin, G. (2012). Variation in trace element content of magnetite crystallized from a fractionating sulfide liquid, Sudbury, Canada: Implications for provenance discrimination. *Geochimica et Cosmochimica Acta*, 88, 27-50. doi: 10.1016/j.gca.2012.04.032
- Dare, S., Barnes, S.-J., Beaudoin, G., Méric, J. and Boutroy, E. (2014). Trace elements in magnetite as petrogenetic indicators. *Mineralium Deposita*, 49, 785–796. doi: 10.1007/s00126-014-0529-0
- Markey, R., Stein, H. and Morgan, J. (1998). Highly precise Re–Os dating for molybdenite using alkaline fusion and NTIMS. *Talanta*, 45, 935–946.
- Markey, R., Stein, H. J., Hannah, J. L., Zimmerman, A., Selby, D. and Creaser, R. A. (2007). Standardizing Re–Os geochronology: A new molybdenite reference material (Henderson, USA) and the stoichiometry of Os salts. *Chemical Geology*, 244, 74-87.
- Paton, C., Hellstrom, J., Paul, B., Woodhead, J. and Hergt, J. (2011). Iolite: Freeware for the visualisation and processing of mass spectrometric data. *Journal of Analytical Atomic Spectrometry*, 26(12), 2508-2518. doi: 10.1039/c1ja10172b
- Selby, D. and Creaser, R. A. (2004). Macroscale NTIMS and microscale LA-MC-ICP-MS Re-Os isotopic analysis of molybdenite: Testing spatial restrictions for reliable Re-Os age determinations, and implications for the decoupling of Re and Os within molybdenite. *Geochimica et Cosmochimica Acta*, 68, 3897–3908.

APPENDICE B

SUPPLEMENTARY DATA

Appendix Table B1. Localisation des échantillons et description

Sample #	Drill hole #	UTM (E)	UTM (N)	Azimuth (°)	Dip (°)	Depth (m)	Facies	Geochemical analyses
Thin section								
SUL1	AMCD28	301379,98	5326433,19	25	-48	128	Early (EP)	Biotite, plagioclase EPMA
SUL2	AMCD28	301379,98	5326433,19	25	-48	126,9	Contact EP-LP	LA-ICP-MS analyses on magnetite
SUL3	AMCD29	300881,70	5326296,55	25	-48	70	Early (EP)	Biotite, amphibole, plagioclase EPMA
SUL4	AMCD28	301379,98	5326433,19	25	-48	169,8	Late (LP)	Biotite, plagioclase, chlorite EPMA
SUL5	AMCD30	299976,23	5325975,17	25	-48	18,7	Late (LP)	
SUL6	AMCD29	300881,70	5326296,55	25	-48	112,6	Early (EP)	
SUL7	17407-03	299483,95	5325716,57	170	-55	66,5	Intermediate (IP2)	LA-ICP-MS analyses on magnetite and Biotite, plagioclase, chlorite EPMA
SUL8	17407-03	299483,95	5325716,57	170	-55	110,4	Intermediate (IP1)	Biotite, plagioclase EPMA
SUL9	17407-03	299483,95	5325716,57	170	-55	143	Porphyritic dike	
SUL10	DAX-15-008	300272,22	5325533,42	197	-50	127	Early (EP)	
SUL11	DAX-15-008	300272,22	5325533,42	197	-50	167	Intermediate (IP2)	
SUL12	DAX-15-008	300272,22	5325533,42	197	-50	227,6	Contact IP2-Héva	Biotite, amphibole EPMA
SUL13	DAX-15-008	300272,22	5325533,42	197	-50	161,3	Intermediate (IP2)	Biotite, plagioclase, chlorite EPMA
TRACH	AMCD28	301379,98	5326433,19	25	-48	98,5	Early (EP)	Biotite, plagioclase EPMA
VUG	D69-05	300048,40	5325368,52	42	-50	222	Mineralized (MIP)	Biotite, epidote, plagioclase EPMA
GLOM	DAX-14-001	300040,81	5325720,98	196	-53	69,1	Intermediate (IP2)	Plagioclase, Chlorite EPMA
MIX	AMCD29	300881,70	5326296,55	25	-48	132	Intermediate (IP)	Biotite, chlorite EPMA
GAR1	17407-03	299483,95	5325716,57	170	-55	332,8	Skarn alteration	
GAR2	D69-05	300048,40	5325368,52	42	-50	53,3	Skarn alteration	
GAR3	DAX-15-008	300272,22	5325533,42	197	-50	243,1	Skarn alteration	
GAR4	DAX-15-008	300272,22	5325533,42	197	-50	240,5	Skarn alteration	LA-ICP-MS analyses on magnetite
MIN1	AMCD30	299976,23	5325975,17	25	-48	245	K-alt in ESS	
MIN2	OAX-15-056	299490,90	5325476,60	180	-50	174,5	Ore zone (Exoskam)	LA-ICP-MS analyses on magnetite
MIN3	OAX-15-056	299490,90	5325476,60	180	-50	175	Ore zone (Exoskam)	
MIN4	OAX-15-056	299490,90	5325476,60	180	-50	175,5	Ore zone (Exoskam)	
MIN5	17407-04	299803,08	5325597,87	170	-55	467,8	Ore zone (Exoskam)	LA-ICP-MS analyses on magnetite
MIN6	17407-04	299803,08	5325597,87	170	-55	263,5	Ore zone (Exoskam)	
MIN7	DAX-15-008	300272,22	5325533,42	197	-50	287	Ore zone (Endoskam)	
MIN8	DAX-15-008	300272,22	5325533,42	197	-50	254,6	Ore zone (Endoskam)	

Whole Rock														
FB1604	AMCD28	301379,98	5326433,19	25	-48	128	Early (EP)	Whole-rock major and trace elements						
FB1605	AMCD28	301379,98	5326433,19	25	-48	169,8	Late (LP)	Whole-rock major and trace elements						
FB1606	AMCD28	301379,98	5326433,19	25	-48	BX30	Late (LP)	Whole-rock major and trace elements						
FB1607	AMCD29	300881,70	5326296,55	25	-48	112,6	Early (EP)	Whole-rock major and trace elements						
FB1608	17407-04	299803,08	5325597,87	170	-55	181	Porphyritic dike (QFP)	Whole-rock major and trace elements						
FB1609	17407-04	299803,08	5325597,87	170	-55	181,5	Porphyritic dike (QFP)	Whole-rock major and trace elements						
FB1610	17407-03	299483,95	5325716,57	170	-55	110,4	Intermediate (IP2)	Whole-rock major and trace elements						
FB1611	17407-03	299483,95	5325716,57	170	-55	66	Intermediate (IP1)	Whole-rock major and trace elements						
FB1612	17407-03	299483,95	5325716,57	170	-55	488	Héva Formation	Whole-rock major and trace elements						
FB1613	D69-05	300048,40	5325368,52	42	-50	27	Héva Formation	Whole-rock major and trace elements						
FB1614	D69-05	300048,40	5325368,52	42	-50	223,1	Mineralized (MP)	Whole-rock major and trace elements						
FB1615	D69-05	300048,40	5325368,52	42	-50	245	Mineralized (MP)	Whole-rock major and trace elements						
FB1616	17407-04	299803,08	5325597,87	170	-55	461,5	Héva Formation	Whole-rock major and trace elements						
FB1617	17407-04	299803,08	5325597,87	170	-55	467,5	Héva Formation	Whole-rock major and trace elements						
FB1618	DAX-15-007	300272,22	5325533,42	197	-50	103,5	Intermediate (IP2)	Whole-rock major and trace elements						
FB1619	DAX-15-008	300272,22	5325533,42	197	-50	180,5	Intermediate (IP2)	Whole-rock major and trace elements						
FB1620	DAX-15-008	300272,22	5325533,42	197	-50	222	Intermediate (IP2)	Whole-rock major and trace elements						
FB1621	DAX-15-008	300272,22	5325533,42	197	-50	289,5	Hornfel in Héva F.	Whole-rock major and trace elements						
FB1622	DAX-15-008	300272,22	5325533,42	197	-50	290	Hornfel in Héva F.	Whole-rock major and trace elements						
FB1623	DAX-15-008	300272,22	5325533,42	197	-50	268	Alteration	Whole-rock major and trace elements						
FB1624	DAX-15-008	300272,22	5325533,42	197	-50	207,3	Intermediate (IP2)	Whole-rock major and trace elements						
FB1625	DAX-15-008	300272,22	5325533,42	197	-50	234,7	Hornfel in Héva F.	Whole-rock major and trace elements						
FB1626	Outcrop	300963,90	5326498,65				Early (EP)	Whole-rock major and trace elements						
FB1627	Outcrop	300963,90	5326498,65				Early (EP)	Whole-rock major and trace elements						
FB1801	AMCD28	301379,981	5326433,19	25	-48	175	Late (LP)	Whole-rock major, fluor and FeO						
FB1802	DA X-14-001	300040,81	5325720,98	196	-53	72,5	Intermediate (IP2)	Whole-rock major, fluor and FeO						
FB1803	DAX-14-001	300040,81	5325720,98	196	-53	77,1	Intermediate (IP2)	Whole-rock major, fluor and FeO						
FB1804	17407-03	299483,95	5325716,57	170	-55	71	Intermediate (IP1)	Whole-rock major, fluor and FeO						
FB1805	AMCD28	301379,98	5326433,19	26	-47	108	Early (EP)	Whole-rock major, fluor and FeO						
QMX01	17402-01	300665,60	5329395,90	170	-55	45	Intermediate (IP1)	Whole-rock major and trace elements						
QMX02	17402-01	300665,60	5329395,90	170	-55	33,2	Intermediate (IP1)	Whole-rock major and trace elements						

NOTES:

Abbreviations: EPM-A = Electron Probe Micro-Analysis; UTM = Universal Transverse Mercator

Appendice Table B2. Analyses des plagioclases à la sonde

SAMPLE	SiO ₂	TiO ₂	Al ₂ O ₃	FeO(t)	MgO	CaO	MnO	BaO	Na ₂ O	K ₂ O	Total
Héva Formation (Ore zone)											
MIN6 2-1	68,60	0,00	20,01	0,46	0,05	0,19	0,00	0,00	11,51	0,07	100,88
MIN6 2-2	68,50	0,01	19,83	0,26	0,01	0,22	0,02	0,00	11,30	0,18	100,32
MIN6 2-3	67,73	0,02	20,43	0,00	0,03	0,48	0,00	0,01	11,26	0,11	100,06
MIN6 2-4	67,62	0,03	19,95	0,02	0,00	0,36	0,00	0,03	11,31	0,14	99,46
Early (EP)											
TRACH1 1-1	68,00	0,00	20,23	0,07	0,04	0,57	0,03	0,03	11,38	0,06	100,41
TRACH1 2-2	67,75	0,00	20,01	0,07	0,03	0,35	0,00	0,06	11,39	0,17	99,82
TRACH1 2-3	66,72	0,00	20,14	0,09	0,01	0,54	0,02	0,00	11,24	0,06	98,83
TRACH1 2-4	68,33	0,00	20,27	0,01	0,01	0,22	0,02	0,01	11,50	0,06	100,43
TRACH1 3-1	67,69	0,00	20,10	0,07	0,00	0,40	0,01	0,00	11,42	0,07	99,80
Mineralized (MP)											
VUG 2-1	65,93	0,06	21,13	0,54	0,15	0,62	0,00	0,04	10,30	1,18	100,01
VUG 2-2	68,35	0,00	20,28	0,04	0,03	0,32	0,02	0,00	11,43	0,05	100,51
VUG 2-3	67,57	0,00	20,46	0,03	0,01	0,30	0,00	0,05	11,53	0,07	100,00
VUG 3-2	67,35	0,00	20,25	0,06	0,01	0,57	0,00	0,00	11,42	0,06	99,77
Intermediate (IP1)											
SUL7 1-1	63,65	0,02	21,15	0,25	0,17	2,45	0,02	0,00	10,25	0,20	98,26
SUL7 1-2	66,17	0,01	20,48	0,04	0,03	0,63	0,01	0,04	10,92	0,11	98,43
SUL7 2-1	66,78	0,00	20,51	0,03	0,02	0,69	0,00	0,01	11,04	0,13	99,22
SUL8 4-1	68,42	0,01	20,13	0,08	0,02	0,24	0,00	0,00	11,52	0,10	100,52
SUL8 4-2	67,78	0,02	20,45	0,08	0,04	0,55	0,01	0,00	11,20	0,15	100,27
Intermediate (IP2)											
GLOM 7-1	67,77	0,03	19,85	0,52	0,52	0,09	0,00	0,01	11,29	0,07	100,15
GLOM 5-1	66,29	0,00	20,09	0,09	0,01	0,64	0,00	0,00	11,33	0,05	98,48
GLOM 5-2	67,21	0,00	19,82	0,12	0,01	0,38	0,03	0,00	11,42	0,04	99,03
GLOM 4-1	66,23	0,00	20,47	0,07	0,02	0,70	0,00	0,00	11,05	0,08	98,63
GLOM 4-2	66,71	0,03	20,25	0,06	0,00	0,83	0,00	0,00	11,06	0,06	98,99
GLOM 1-5	66,31	0,05	20,15	1,22	0,80	0,71	0,04	0,00	10,50	0,56	100,34
SUL12 4-3	65,17	0,02	21,74	0,39	0,01	2,80	0,00	0,00	10,40	0,05	100,59
SUL12 1-3	67,06	0,00	20,34	0,12	0,03	0,80	0,00	0,04	11,41	0,06	99,85
SUL13 2-1	67,72	0,03	20,06	0,01	0,00	0,27	0,00	0,00	11,52	0,04	99,65
SUL13 2-2	67,93	0,03	19,98	0,04	0,01	0,20	0,00	0,00	11,64	0,04	99,86

Late (LP)

SUL4 4-1	1	62,84	0,00	18,92	0,09	0,01	0,00	0,02	1,70	0,36	15,36	99,30
SUL4 4-2	2	65,70	0,00	21,57	0,19	0,00	2,20	0,01	0,10	10,21	0,09	100,15
SUL4 4-3	3	63,86	0,05	22,33	0,05	0,02	2,99	0,00	0,00	9,90	0,08	99,48
SUL4 4-4	4	65,17	0,00	21,66	0,18	0,06	2,11	0,00	0,06	10,06	0,08	99,46
SUL4 4-5	5	63,06	0,02	23,67	0,19	0,04	4,21	0,00	0,00	9,09	0,11	100,52
SUL4 4-6		68,52	0,01	20,20	0,04	0,01	0,20	0,03	0,00	11,59	0,06	100,66
SUL4 4-7		66,06	0,01	21,47	0,19	0,10	2,06	0,05	0,04	10,38	0,09	100,44
SUL4 6-1	1	66,72	0,00	21,02	0,08	0,05	0,56	0,00	0,00	10,98	0,48	99,87
SUL4 6-2	2	67,73	0,02	20,43	0,00	0,03	0,48	0,00	0,01	11,26	0,11	100,06
SUL4 7-1		68,13	0,01	20,17	0,02	0,02	0,16	0,03	0,00	11,54	0,07	100,15
SUL4 7-2		68,52	0,00	20,36	0,00	0,01	0,27	0,00	0,02	11,46	0,05	100,71
SUL4 9-1	1	63,21	0,04	23,05	0,10	0,01	3,76	0,01	0,06	9,33	0,06	99,77
SUL4 9-2	2	63,38	0,00	22,98	0,06	0,00	3,74	0,05	0,00	9,40	0,05	99,77
SUL4 9-3	3	63,25	0,00	22,98	0,10	0,06	3,36	0,05	0,05	9,13	0,40	99,48
SUL4 9-4	4	63,65	0,00	22,80	0,05	0,02	3,18	0,04	0,08	9,51	0,24	99,75
SUL4 9-5	1	67,53	0,02	20,52	0,04	0,00	0,77	0,00	0,07	11,15	0,04	100,17
SUL4 9-6	2	63,71	0,01	22,57	0,11	0,00	3,38	0,02	0,04	9,55	0,09	99,62
SUL4 9-7	3	63,17	0,00	22,84	0,07	0,02	3,66	0,00	0,09	9,51	0,08	99,67
SUL4 9-8	4	62,87	0,01	22,99	0,11	0,01	3,90	0,00	0,14	9,31	0,08	99,61
SUL4 9-9	5	66,17	0,07	21,01	0,00	0,00	1,48	0,03	0,00	10,74	0,05	99,61
SUL2 5-1		67,68	0,00	20,17	0,11	0,00	0,46	0,03	0,00	11,40	0,05	99,91
SUL2 4-2		67,70	0,00	20,04	0,03	0,00	0,35	0,00	0,01	11,45	0,08	99,69
SUL2 2-1		63,39	0,00	23,21	0,17	0,03	2,04	0,01	0,06	8,95	1,08	99,13
SUL2 2-2		63,51	0,02	22,80	0,19	0,01	3,39	0,02	0,02	9,25	0,33	99,64
SUL2 2-3		65,36	0,00	21,97	0,00	0,01	2,27	0,00	0,04	10,23	0,06	100,21
SUL2 1-1	1	62,81	0,08	18,97	0,00	0,01	0,02	0,00	1,76	0,23	15,52	99,49
SUL2 1-2	2	67,39	0,01	20,13	0,04	0,03	0,26	0,00	0,01	11,36	0,08	99,31
SUL2 1-3	3	67,90	0,04	20,38	0,05	0,00	0,44	0,00	0,01	11,45	0,06	100,35
SUL5 6-1		66,96	0,00	19,71	0,06	0,04	0,23	0,00	0,01	11,60	0,07	98,68
SUL5 6-2		62,33	0,01	18,48	0,00	0,02	0,01	0,00	0,97	0,26	15,39	97,54
SUL5 6-3		67,22	0,00	19,82	0,02	0,01	0,32	0,04	0,00	11,39	0,07	98,90
SUL5 5-1		66,86	0,01	20,34	0,02	0,05	0,34	0,00	0,07	11,42	0,09	99,20
SUL5 5-2		62,69	0,03	18,63	0,00	0,01	0,00	0,00	1,45	0,29	15,38	98,60
SUL5 5-3		63,72	0,02	18,69	0,02	0,01	0,00	0,01	0,30	0,20	15,89	98,85
SUL5 5-4		63,40	0,01	22,46	0,01	0,03	0,02	0,00	1,24	0,28	15,42	102,90
SUL5 5-5		63,73	0,00	18,48	0,07	0,05	0,07	0,02	0,48	0,26	15,92	99,07
SUL5 3-1		66,36	0,00	20,23	0,04	0,08	0,42	0,00	0,00	11,31	0,07	98,51
SUL5 2-3		68,32	0,00	20,12	0,00	0,01	0,28	0,00	0,00	11,71	0,06	100,51
SUL5 1-1		67,62	0,03	19,95	0,02	0,00	0,36	0,00	0,03	11,31	0,14	99,46
SUL5 1-2		63,78	0,00	18,54	0,16	0,00	0,01	0,00	0,08	0,18	16,12	98,88

NOTES:

Analyses with high or low totals (>103 or <98 wt.%) or poor stoichiometries are omitted.

Numbers in second column are analysis points in one lath

SAMPLE	Si	Al	Fe	Ti	Mg	Mn	Na	Ca	K	Ba	Total	An	Ab	Or
Héva Formation (Ore zone)														
MIN6 2-1	2,98	1,02	0,02	0,00	0,00	0,00	0,97	0,01	0,00	0,00	5,00	0,4	98,7	0,4
MIN6 2-2	2,98	1,02	0,01	0,00	0,00	0,00	0,95	0,01	0,01	0,00	4,99	1,0	97,9	1,0
MIN6 2-3	2,96	1,05	0,00	0,00	0,00	0,00	0,95	0,02	0,01	0,00	4,99	2,3	97,1	0,6
MIN6 2-4	2,97	1,03	0,00	0,00	0,00	0,00	0,96	0,02	0,01	0,00	5,00	1,7	97,5	0,8
Early (EP)														
TRACH1 1-1	2,96	1,04	0,00	0,00	0,00	0,00	0,96	0,03	0,00	0,00	5,00	2,7	97,0	0,4
TRACH1 2-2	2,97	1,03	0,00	0,00	0,00	0,00	0,97	0,02	0,01	0,00	5,00	1,6	97,4	1,0
TRACH1 2-3	2,95	1,05	0,00	0,00	0,00	0,00	0,96	0,03	0,00	0,00	5,00	2,6	97,1	0,3
TRACH1 2-4	2,97	1,04	0,00	0,00	0,00	0,00	0,97	0,01	0,00	0,00	5,00	1,0	98,7	0,3
TRACH1 3-1	2,97	1,04	0,00	0,00	0,00	0,00	0,97	0,02	0,00	0,00	5,00	1,9	97,7	0,4
Mineralized (MP)														
VUG 2-1	2,91	1,10	0,02	0,00	0,01	0,00	0,88	0,03	0,07	0,00	5,01	3,0	90,2	6,8
VUG 2-2	2,97	1,04	0,00	0,00	0,00	0,00	0,96	0,02	0,00	0,00	4,99	1,5	98,2	0,3
VUG 2-3	2,96	1,05	0,00	0,00	0,00	0,00	0,98	0,01	0,00	0,00	5,01	1,4	98,2	0,4
VUG 3-2	2,96	1,05	0,00	0,00	0,00	0,00	0,97	0,03	0,00	0,00	5,01	2,7	97,0	0,4
Intermediate (IP1)														
SUL7 1-1	2,86	1,12	0,01	0,00	0,01	0,00	0,89	0,12	0,01	0,00	5,03	11,6	87,4	1,1
SUL7 1-2	2,94	1,07	0,00	0,00	0,00	0,00	0,94	0,03	0,01	0,00	5,00	3,1	96,3	0,7
SUL7 2-1	2,95	1,07	0,00	0,00	0,00	0,00	0,94	0,03	0,01	0,00	5,00	3,3	96,0	0,7
SUL8 4-1	2,97	1,03	0,00	0,00	0,00	0,00	0,97	0,01	0,01	0,00	5,00	1,1	98,3	0,6
SUL8 4-2	2,96	1,05	0,00	0,00	0,00	0,00	0,95	0,03	0,01	0,00	5,00	2,6	96,6	0,8
Intermediate (IP2)														
GLOM 7-1	2,96	1,02	0,02	0,00	0,03	0,00	0,96	0,00	0,00	0,00	5,01	0,4	99,2	0,4
GLOM 5-1	2,95	1,05	0,00	0,00	0,00	0,00	0,98	0,03	0,00	0,00	5,01	3,0	96,7	0,3
GLOM 5-2	2,97	1,03	0,00	0,00	0,00	0,00	0,98	0,02	0,00	0,00	5,01	1,8	98,0	0,2
GLOM 4-1	2,94	1,07	0,00	0,00	0,00	0,00	0,95	0,03	0,00	0,00	5,00	3,3	96,2	0,4
GLOM 4-2	2,95	1,06	0,00	0,00	0,00	0,00	0,95	0,04	0,00	0,00	5,00	4,0	95,7	0,3
GLOM 1-5	2,92	1,04	0,04	0,00	0,05	0,00	0,90	0,03	0,03	0,00	5,02	3,5	93,2	3,3
SUL12 4-3	2,86	1,12	0,01	0,00	0,00	0,00	0,89	0,13	0,00	0,00	5,02	12,9	86,8	0,3
SUL12 1-3	2,94	1,05	0,00	0,00	0,00	0,00	0,97	0,04	0,00	0,00	5,02	3,7	96,0	0,3
SUL13 2-1	2,97	1,04	0,00	0,00	0,00	0,00	0,98	0,01	0,00	0,00	5,00	1,3	98,5	0,2
SUL13 2-2	2,97	1,03	0,00	0,00	0,00	0,00	0,99	0,01	0,00	0,00	5,01	0,9	98,8	0,2

Late (LP)

SUL4 4-1	1	2,96	1,05	0,00	0,00	0,00	0,00	0,03	0,00	0,92	0,03	5,00	0,0	3,4	96,6
SUL4 4-2	2	2,89	1,12	0,01	0,00	0,00	0,00	0,87	0,10	0,00	0,00	4,99	10,6	88,9	0,5
SUL4 4-3	3	2,84	1,17	0,00	0,00	0,00	0,00	0,85	0,14	0,00	0,00	5,01	14,2	85,3	0,5
SUL4 4-4	4	2,88	1,13	0,01	0,00	0,00	0,00	0,86	0,10	0,00	0,00	4,99	10,3	89,2	0,5
SUL4 4-5	5	2,78	1,23	0,01	0,00	0,00	0,00	0,78	0,20	0,01	0,00	5,00	20,2	79,1	0,6
SUL4 4-6		2,97	1,03	0,00	0,00	0,00	0,00	0,98	0,01	0,00	0,00	5,00	0,9	98,7	0,3
SUL4 4-7		2,89	1,11	0,01	0,00	0,01	0,00	0,88	0,10	0,00	0,00	5,00	9,8	89,7	0,5
SUL4 6-1	1	2,93	1,09	0,00	0,00	0,00	0,00	0,93	0,03	0,03	0,00	5,01	2,6	94,6	2,7
SUL4 6-2	2	2,96	1,05	0,00	0,00	0,00	0,00	0,95	0,02	0,01	0,00	4,99	2,3	97,1	0,6
SUL4 7-1		2,97	1,04	0,00	0,00	0,00	0,00	0,98	0,01	0,00	0,00	5,00	0,8	98,9	0,4
SUL4 7-2		2,97	1,04	0,00	0,00	0,00	0,00	0,96	0,01	0,00	0,00	4,99	1,3	98,5	0,3
SUL4 9-1	1	2,80	1,20	0,00	0,00	0,00	0,00	0,80	0,18	0,00	0,00	5,00	18,2	81,5	0,3
SUL4 9-2	2	2,81	1,20	0,00	0,00	0,00	0,00	0,81	0,18	0,00	0,00	5,00	18,0	81,8	0,3
SUL4 9-3	3	2,81	1,20	0,00	0,00	0,00	0,00	0,79	0,16	0,02	0,00	4,99	16,5	81,1	2,4
SUL4 9-4	4	2,82	1,19	0,00	0,00	0,00	0,00	0,82	0,15	0,01	0,00	5,00	15,4	83,3	1,4
SUL4 9-5	1	2,95	1,06	0,00	0,00	0,00	0,00	0,94	0,04	0,00	0,00	4,99	3,7	96,1	0,2
SUL4 9-6	2	2,83	1,18	0,00	0,00	0,00	0,00	0,82	0,16	0,01	0,00	5,00	16,3	83,2	0,5
SUL4 9-7	3	2,81	1,20	0,00	0,00	0,00	0,00	0,82	0,17	0,00	0,00	5,01	17,5	82,1	0,4
SUL4 9-8	4	2,80	1,21	0,00	0,00	0,00	0,00	0,80	0,19	0,00	0,00	5,00	18,7	80,8	0,5
SUL4 9-9	5	2,91	1,09	0,00	0,00	0,00	0,00	0,92	0,07	0,00	0,00	5,00	7,1	92,7	0,3
SUL2 5-1		2,96	1,04	0,00	0,00	0,00	0,00	0,97	0,02	0,00	0,00	5,00	2,2	97,6	0,3
SUL2 4-2		2,97	1,04	0,00	0,00	0,00	0,00	0,97	0,02	0,00	0,00	5,00	1,6	97,9	0,5
SUL2 2-1		2,82	1,22	0,01	0,00	0,00	0,00	0,77	0,10	0,06	0,00	4,98	10,5	82,9	6,6
SUL2 2-2		2,82	1,19	0,01	0,00	0,00	0,00	0,80	0,16	0,02	0,00	4,99	16,5	81,6	1,9
SUL2 2-3		2,87	1,14	0,00	0,00	0,00	0,00	0,87	0,11	0,00	0,00	5,00	10,9	88,7	0,4
SUL2 1-1	1	2,95	1,05	0,00	0,00	0,00	0,00	0,02	0,00	0,93	0,03	4,99	0,1	2,2	97,7
SUL2 1-2	2	2,97	1,04	0,00	0,00	0,00	0,00	0,97	0,01	0,00	0,00	5,00	1,2	98,3	0,4
SUL2 1-3	3	2,96	1,05	0,00	0,00	0,00	0,00	0,97	0,02	0,00	0,00	5,00	2,1	97,6	0,3
SUL5 6-1		2,97	1,03	0,00	0,00	0,00	0,00	1,00	0,01	0,00	0,00	5,02	1,1	98,6	0,4
SUL5 6-2		2,97	1,04	0,00	0,00	0,00	0,00	0,02	0,00	0,94	0,02	4,99	0,0	2,5	97,5
SUL5 6-3		2,97	1,03	0,00	0,00	0,00	0,00	0,98	0,01	0,00	0,00	5,00	1,5	98,1	0,4
SUL5 5-1		2,95	1,06	0,00	0,00	0,00	0,00	0,98	0,02	0,01	0,00	5,01	1,6	97,9	0,5
SUL5 5-2		2,97	1,04	0,00	0,00	0,00	0,00	0,03	0,00	0,93	0,03	4,99	0,0	2,7	97,3
SUL5 5-3		2,98	1,03	0,00	0,00	0,00	0,00	0,02	0,00	0,95	0,01	4,99	0,0	1,9	98,1
SUL5 5-4		2,86	1,20	0,00	0,00	0,00	0,00	0,02	0,00	0,89	0,02	5,00	0,1	2,6	97,3
SUL5 5-5		2,98	1,02	0,00	0,00	0,00	0,00	0,02	0,00	0,95	0,01	4,99	0,3	2,4	97,3
SUL5 3-1		2,95	1,06	0,00	0,00	0,01	0,00	0,97	0,02	0,00	0,00	5,01	2,0	97,6	0,4
SUL5 2-3		2,97	1,03	0,00	0,00	0,00	0,00	0,99	0,01	0,00	0,00	5,01	1,3	98,4	0,3
SUL5 1-1		2,97	1,03	0,00	0,00	0,00	0,00	0,96	0,02	0,01	0,00	5,00	1,7	97,5	0,8
SUL5 1-2		2,98	1,02	0,01	0,00	0,00	0,00	0,02	0,00	0,96	0,00	4,99	0,0	1,7	98,2

NOTES:

Analyses with high or low totals (>103 or <98 wt.%) or poor stoichiometries are omitted.

Numbers in second column are analysis points in one lath

Appendice Table B3. Analyses des grenats à la microsonde

SAMPLE		SiO ₂	TiO ₂	Al ₂ O ₃	Cr ₂ O ₃	Fe ₂ O ₃	FeO	MnO	MgO	ZnO	CaO	Total
GAR3 3-1		35.55	0.00	1.42	0.00	23.31	7.71	0.63	0.03	0.00	31.04	99.69
GAR3 3-2		34.81	0.03	0.89	0.00	23.82	6.89	1.06	0.02	0.00	31.05	98.57
GAR2 2-5		33.27	0.00	0.38	0.00	24.86	5.84	0.18	0.00	0.01	32.52	97.07
GAR2 2-6		34.33	0.07	6.43	0.02	18.37	4.09	0.23	0.03	0.02	33.85	97.43
GAR2 2-7		33.86	0.24	3.78	0.00	20.96	5.82	0.79	0.09	0.02	31.76	97.32
GAR2 3-1a	Core	33.80	0.24	3.25	0.00	21.56	5.13	0.44	0.08	0.00	32.65	97.15
GAR2 3-2b		32.87	0.05	0.15	0.00	25.26	5.74	0.32	0.03	0.00	32.49	96.91
GAR2 3-3c		32.98	0.01	0.10	0.05	25.49	5.99	0.36	0.04	0.00	32.49	97.50
GAR2 3-4d	Rim	33.41	0.00	0.00	0.00	25.36	6.27	0.36	0.03	0.00	32.20	97.61
GAR2 3-5		34.62	0.44	4.98	0.00	19.24	4.65	0.90	0.05	0.01	32.46	97.35
GAR2 3-6		33.36	0.03	0.03	0.00	25.42	6.05	0.34	0.02	0.00	32.48	97.72
GAR2 3-7		33.69	0.33	3.56	0.05	20.85	5.32	1.84	0.06	0.01	31.03	96.73
GAR2 4-1		33.99	0.03	0.13	0.00	25.18	6.00	0.30	0.00	0.00	32.67	98.32
GAR2 4-2		34.41	0.00	0.03	0.00	25.25	6.06	0.24	0.05	0.00	32.71	98.75
GAR2 4-3		34.82	0.00	5.46	0.00	19.28	5.30	0.58	0.04	0.00	32.71	98.20
GAR2 4-4		34.82	0.11	1.86	0.00	23.05	5.94	0.50	0.04	0.04	32.43	98.78
GAR2 4-5		34.73	0.80	5.19	0.04	19.07	4.92	1.00	0.09	0.03	32.32	98.19
GAR2 4-6		34.86	0.00	0.40	0.06	24.79	5.99	0.17	0.03	0.00	32.97	99.26
GAR2 4-7		34.38	0.00	1.93	0.00	23.16	5.96	0.45	0.00	0.02	32.49	98.40
GAR2 4-8		34.12	0.90	4.63	0.06	19.60	4.44	0.97	0.08	0.04	32.52	97.35
GAR1 5-1		35.68	0.04	0.58	0.00	24.62	6.64	0.20	0.01	0.02	32.75	100.53
GAR1 5-2		35.25	0.00	2.34	0.02	22.79	6.17	0.25	0.02	0.00	32.86	99.71
GAR1 5-3		35.99	0.00	0.31	0.03	24.55	5.96	0.15	0.11	0.00	32.97	100.07
GAR1 4-1a	Core	36.25	0.00	0.03	0.02	24.84	5.88	0.05	0.07	0.00	33.28	100.41
GAR1 4-1b		35.55	0.00	0.52	0.00	24.39	6.01	0.25	0.19	0.00	32.60	99.52
GAR1 4-1c		35.71	0.00	0.35	0.01	24.76	6.03	0.25	0.09	0.02	32.98	100.19
GAR1 4-1d		36.67	0.05	3.69	0.00	21.08	5.24	0.33	0.07	0.03	33.63	100.79
GAR1 4-1e	Rim	35.84	0.00	0.24	0.00	24.85	6.26	0.27	0.01	0.00	32.93	100.40
GAR1 4-2		36.75	0.07	6.45	0.00	17.98	4.24	0.39	0.03	0.00	34.14	100.06

GAR1 3-1a	Core	37.23	0.12	9.67	0.00	14.66	3.47	0.27	0.03	0.04	34.93	100.41
GAR1 3-1b		36.90	0.00	4.44	0.00	20.20	5.19	0.27	0.06	0.00	33.69	100.74
GAR1 3-1c		35.34	0.04	0.04	0.07	25.35	5.98	0.13	0.09	0.01	33.31	100.34
GAR1 3-1d		36.33	0.04	1.14	0.03	23.84	5.98	0.31	0.10	0.00	33.12	100.88
GAR1 3-1e		34.69	0.00	0.21	0.01	25.20	5.88	0.21	0.15	0.05	32.94	99.33
GAR1 3-1f		36.11	0.04	2.57	0.00	22.47	5.35	0.22	0.08	0.06	33.62	100.51
GAR1 3-1g		36.03	0.11	0.08	0.00	25.05	5.94	0.19	0.14	0.00	33.22	100.76
GAR1 3-1h	Rim	35.43	0.00	0.21	0.00	24.94	6.11	0.29	0.02	0.00	32.94	99.93
GAR1 2-1a	Rim	34.18	0.03	0.29	0.02	23.83	5.36	0.23	0.11	0.01	31.97	96.02
GAR1 2-2b		36.19	0.03	7.27	0.01	16.26	4.04	0.29	0.08	0.05	33.19	97.41
GAR1 2-3c		34.06	0.00	1.63	0.04	22.80	5.24	0.30	0.13	0.00	32.26	96.44
GAR1 2-4d		34.42	0.01	2.99	0.02	21.59	4.95	0.32	0.09	0.04	32.79	97.21
GAR1 2-5e		34.46	0.04	1.02	0.00	22.71	6.40	0.47	0.21	0.00	30.55	95.86
GAR1 2-6f	Core	35.30	0.00	5.86	0.00	17.78	5.15	0.45	0.16	0.00	31.86	96.56
GAR1 1-1a	Rim	33.12	0.00	0.04	0.02	24.59	5.88	0.20	0.06	0.00	31.77	95.68
GAR1 1-2b		36.65	0.01	9.55	0.03	14.08	3.25	0.42	0.06	0.03	34.01	98.09
GAR1 1-3c		35.34	0.01	5.76	0.04	18.42	4.34	0.39	0.08	0.03	33.20	97.61
GAR1 1-4d		36.22	0.00	9.31	0.01	14.39	3.49	0.62	0.05	0.00	33.62	97.70
GAR1 1-5e		36.85	0.00	13.14	0.03	10.34	2.97	0.59	0.02	0.01	34.13	98.08
GAR1 1-6f		34.25	0.00	0.66	0.03	23.96	5.67	0.23	0.01	0.00	32.40	97.20
GAR1 1-7g	Core	34.62	0.03	2.02	0.00	22.45	5.50	0.16	0.02	0.00	32.56	97.35
GAR4 3-2		34.78	0.07	0.57	0.00	24.41	7.43	0.71	0.02	0.00	31.17	99.16
GAR4 3-3		34.24	0.10	0.76	0.03	24.38	7.54	0.69	0.03	0.02	31.06	98.85
GAR4 3-4		34.19	0.07	0.92	0.00	24.02	7.45	0.73	0.02	0.00	30.89	98.29
GAR4 2-1		35.73	0.11	1.83	0.00	22.86	6.92	0.93	0.03	0.00	31.49	99.88
GAR4 2-2		35.45	0.11	1.83	0.00	22.80	7.55	0.87	0.01	0.00	30.89	99.51

NOTES:

Analyses with high or low totals (>101 or <96 wt.%) or poor stoichiometries are omitted.

Second column indicate points from core to rim in one garnet cristal

SAMPLE	Si	Al ^{IV}	Al ^{VI}	Ti ⁴⁺	Cr ²⁺	Fe ³⁺	Fe ²⁺	Mn ²⁺	Mg ²⁺	Zn	Ca ²⁺	Total	And	Gr ^s	Pyr	Sps	Uva
GAR3 3-1	3,04	0,00	0,15	0,00	0,00	1,50	0,55	0,05	0,00	0,00	2,85	8,14	91,28	6,70	0,16	1,85	0,00
GAR3 3-2	3,03	0,00	0,10	0,00	0,00	1,56	0,50	0,08	0,00	0,00	2,89	8,16	94,49	2,22	0,13	3,16	0,00
GAR2 2-5	2,95	0,04	0,00	0,00	0,00	1,66	0,43	0,01	0,00	0,00	3,09	8,20	97,67	1,77	0,02	0,54	0,00
GAR2 2-6	2,92	0,08	0,60	0,00	0,00	1,18	0,29	0,02	0,00	0,00	3,09	8,19	64,54	34,64	0,15	0,59	0,07
GAR2 2-7	2,94	0,06	0,35	0,02	0,00	1,37	0,42	0,06	0,01	0,00	2,96	8,19	77,97	19,39	0,43	2,21	0,00
GAR2 3-1a Core	2,94	0,06	0,30	0,02	0,00	1,41	0,37	0,03	0,01	0,00	3,05	8,19	80,88	17,49	0,38	1,23	0,01
GAR2 3-2b	2,93	0,02	0,00	0,00	0,00	1,70	0,43	0,02	0,00	0,00	3,11	8,21	99,08	0,00	0,15	0,77	0,00
GAR2 3-3c	2,93	0,01	0,00	0,00	0,00	1,70	0,44	0,03	0,01	0,00	3,09	8,21	99,22	0,00	0,20	0,38	0,20
GAR2 3-4d Rim	2,96	0,00	0,00	0,00	0,00	1,69	0,46	0,03	0,00	0,00	3,05	8,20	100,0	0,00	0,00	0,00	0,00
GAR2 3-5	2,97	0,03	0,50	0,03	0,00	1,24	0,33	0,07	0,01	0,00	2,98	8,16	71,16	26,07	0,26	2,51	0,00
GAR2 3-6	2,95	0,00	0,00	0,00	0,00	1,69	0,45	0,03	0,00	0,00	3,08	8,20	99,84	0,00	0,09	0,07	0,00
GAR2 3-7	2,95	0,05	0,34	0,02	0,00	1,37	0,39	0,14	0,01	0,00	2,91	8,18	78,75	15,54	0,30	5,22	0,19
GAR2 4-1	2,98	0,01	0,00	0,00	0,00	1,66	0,44	0,02	0,00	0,00	3,07	8,18	99,18	0,00	0,00	0,82	0,00
GAR2 4-2	3,00	0,00	0,00	0,00	0,00	1,66	0,44	0,02	0,01	0,00	3,05	8,17	99,82	0,00	0,17	0,00	0,01
GAR2 4-3	2,96	0,04	0,54	0,00	0,00	1,23	0,38	0,04	0,00	0,00	2,98	8,18	69,29	28,97	0,18	1,57	0,00
GAR2 4-4	3,00	0,00	0,20	0,01	0,00	1,49	0,43	0,04	0,00	0,00	2,99	8,17	88,79	9,60	0,18	1,43	0,00
GAR2 4-5	2,95	0,05	0,50	0,05	0,00	1,22	0,35	0,07	0,01	0,00	2,94	8,15	70,03	26,62	0,46	2,74	0,15
GAR2 4-6	3,01	0,00	0,04	0,00	0,00	1,61	0,43	0,01	0,00	0,00	3,05	8,17	97,30	1,78	0,17	0,51	0,24
GAR2 4-7	2,98	0,02	0,19	0,00	0,00	1,51	0,43	0,03	0,00	0,00	3,02	8,18	88,46	10,24	0,00	1,30	0,00
GAR2 4-8	2,93	0,07	0,43	0,06	0,00	1,27	0,32	0,07	0,01	0,00	3,00	8,16	72,83	23,83	0,39	2,71	0,24
GAR1 5-1	3,03	0,00	0,06	0,00	0,00	1,58	0,47	0,01	0,00	0,00	2,98	8,15	96,44	2,91	0,06	0,59	0,00
GAR1 5-2	3,00	0,00	0,25	0,00	0,00	1,46	0,44	0,02	0,00	0,00	3,00	8,17	86,05	13,04	0,11	0,71	0,09
GAR1 5-3	3,07	0,00	0,03	0,00	0,00	1,57	0,42	0,01	0,01	0,00	3,01	8,13	97,95	0,90	0,60	0,44	0,11
GAR1 4-1a Core	3,08	0,00	0,00	0,00	0,00	1,59	0,42	0,00	0,01	0,00	3,03	8,13	99,71	0,00	0,21	0,00	0,08
GAR1 4-1b	3,05	0,00	0,06	0,00	0,00	1,57	0,43	0,02	0,02	0,00	2,99	8,14	96,79	1,45	1,00	0,76	0,00
GAR1 4-1c	3,04	0,00	0,04	0,00	0,00	1,59	0,43	0,02	0,01	0,00	3,01	8,15	97,82	0,93	0,49	0,74	0,02
GAR1 4-1d	3,04	0,00	0,38	0,00	0,00	1,32	0,36	0,02	0,01	0,00	2,99	8,13	78,47	20,28	0,32	0,92	0,00
GAR1 4-1e Rim	3,05	0,00	0,03	0,00	0,00	1,59	0,45	0,02	0,00	0,00	3,00	8,14	98,54	0,59	0,07	0,81	0,00
GAR1 4-2	3,02	0,00	0,66	0,00	0,00	1,11	0,29	0,03	0,00	0,00	3,01	8,13	64,05	34,78	0,12	1,05	0,00

GARI 3-1a	Core	3,00	0,00	0,95	0,01	0,00	0,89	0,23	0,02	0,00	0,00	3,02	8,12	49,20	50,01	0,12	0,68	0,00
GARI 3-1b		3,05	0,00	0,46	0,00	0,00	1,26	0,36	0,02	0,01	0,00	2,98	8,13	74,40	24,59	0,28	0,73	0,00
GARI 3-1c		3,02	0,00	0,00	0,00	0,00	1,63	0,43	0,01	0,01	0,00	3,05	8,16	99,51	0,00	0,22	0,00	0,27
GARI 3-1d		3,06	0,00	0,12	0,00	0,00	1,51	0,42	0,02	0,01	0,00	2,99	8,13	92,92	5,56	0,52	0,90	0,11
GARI 3-1e		3,00	0,00	0,02	0,00	0,00	1,64	0,43	0,02	0,02	0,00	3,05	8,17	98,68	0,00	0,80	0,47	0,05
GARI 3-1f		3,03	0,00	0,27	0,00	0,00	1,42	0,38	0,02	0,01	0,00	3,02	8,15	84,82	14,15	0,41	0,62	0,00
GARI 3-1g		3,05	0,00	0,01	0,01	0,00	1,60	0,42	0,01	0,02	0,00	3,02	8,14	99,48	0,00	0,52	0,00	0,00
GARI 3-1h	Rim	3,04	0,00	0,02	0,00	0,00	1,61	0,44	0,02	0,00	0,00	3,02	8,15	98,72	0,34	0,09	0,85	0,00
GARI 2-1a	Rim	3,04	0,00	0,03	0,00	0,00	1,59	0,40	0,02	0,01	0,00	3,05	8,15	98,04	0,59	0,58	0,72	0,07
GARI 2-2b		3,04	0,00	0,75	0,00	0,00	1,03	0,28	0,02	0,01	0,00	2,98	8,12	58,76	40,02	0,38	0,79	0,05
GARI 2-3c		3,00	0,00	0,18	0,00	0,00	1,51	0,39	0,02	0,02	0,00	3,05	8,17	89,81	8,48	0,68	0,87	0,16
GARI 2-4d		2,99	0,01	0,31	0,00	0,00	1,41	0,36	0,02	0,01	0,00	3,05	8,17	82,13	16,46	0,43	0,91	0,08
GARI 2-5e		3,06	0,00	0,11	0,00	0,00	1,52	0,48	0,04	0,03	0,00	2,91	8,13	93,43	3,97	1,14	1,46	0,00
GARI 2-6f	Core	3,02	0,00	0,62	0,00	0,00	1,15	0,37	0,03	0,02	0,00	2,92	8,14	65,94	31,99	0,80	1,26	0,00
GARI 1-1a	Rim	2,98	0,00	0,00	0,00	0,00	1,67	0,44	0,02	0,01	0,00	3,06	8,18	99,66	0,00	0,26	0,00	0,08
GARI 1-2b		3,02	0,00	0,96	0,00	0,00	0,87	0,22	0,03	0,01	0,00	3,00	8,12	48,46	50,06	0,29	1,09	0,09
GARI 1-3c		3,00	0,00	0,61	0,00	0,00	1,18	0,31	0,03	0,01	0,00	3,02	8,15	67,02	31,38	0,38	1,08	0,15
GARI 1-4d		3,00	0,00	0,95	0,00	0,00	0,90	0,24	0,04	0,01	0,00	2,99	8,13	49,64	48,49	0,23	1,59	0,05
GARI 1-5e		2,98	0,02	1,27	0,00	0,00	0,63	0,20	0,04	0,00	0,00	2,96	8,11	33,40	64,97	0,08	1,44	0,11
GARI 1-6f		3,01	0,00	0,07	0,00	0,00	1,59	0,42	0,02	0,00	0,00	3,05	8,16	95,75	3,41	0,07	0,67	0,10
GARI 1-7g	Core	3,01	0,00	0,22	0,00	0,00	1,47	0,40	0,01	0,00	0,00	3,04	8,16	87,67	11,78	0,08	0,47	0,00
GAR4 3-2		3,01	0,00	0,06	0,00	0,00	1,59	0,54	0,05	0,00	0,00	2,89	8,16	96,50	1,28	0,12	2,11	0,00
GAR4 3-3		2,98	0,02	0,07	0,01	0,00	1,60	0,55	0,05	0,00	0,00	2,90	8,18	95,23	2,46	0,17	2,03	0,11
GAR4 3-4		2,99	0,01	0,09	0,00	0,00	1,58	0,54	0,05	0,00	0,00	2,90	8,17	94,35	3,41	0,08	2,16	0,00
GAR4 2-1		3,04	0,00	0,19	0,01	0,00	1,46	0,49	0,07	0,00	0,00	2,87	8,14	88,89	8,29	0,13	2,70	0,00
GAR4 2-2		3,03	0,00	0,20	0,01	0,00	1,47	0,54	0,06	0,00	0,00	2,83	8,14	88,82	8,58	0,04	2,56	0,01

Appendice Table B4. Analyses par méthode LA-ICP-MS de la composition en éléments traces (ppm) des magétites de la zone d'étude

	Fe(%)	Na	Mg	Al	Si	K	Ca	Sc	Ti	V	Cr
D.L	4,60	2,79	0,329	0,301	1665	2,30	184	0,206	0,100	0,030	1,00
Magmatic											
TRACH-1-1	71,65	-	41,6	126	-	41,9	-	-	807	2848	315
TRACH-1-2	71,78	-	129	185	-	124	-	-	23,3	2955	347
TRACH-1-3	71,92	-	66,2	116	-	76,3	-	-	107	2688	340
TRACH-2-1	71,21	1395	258	2305	3042	227	659	0,213	364	1640	333
TRACH-2-3	71,72	-	273	494	-	345	-	-	1210	1674	361
TRACH-3-1	71,26	31,3	1403	1403	2744	1668	630	-	104	1543	397
TRACH-3-2	70,63	257	705	873	7901	724	-	-	54,7	1545	365
TRACH-4-1	69,95	13,9	1442	1622	-	1572	-	-	7984	1928	400
SUL3-1-1	72,11	114	84,5	98,1	-	90,0	572	-	14,7	329	71,7
SUL3-1-2	72,16	80,1	333	443	-	290	-	-	21,2	201	-
SUL3-1-3	72,06	9,43	43,7	241	-	161	-	-	-	279	115
SUL3-1-4	71,74	216	73,4	376	3091	75,7	-	-	10,9	207	6,01
SUL3-1-5	72,26	16,4	15,7	33,2	-	-	-	-	-	266	16,1
SUL3-1-6	71,81	14,1	14,8	57,6	2350	-	565	-	795	246	23,2
SUL3-1-7	72,03	14,0	52,5	71,5	1121	18,7	-	1,90	8,23	352	262
SUL3-2-1	71,51	-	19,4	121	2158	-	3047	0,584	3301	312	34,7
SUL3-2-2	71,42	-	672	761	3525	495	1040	0,482	1078	198	59,4
SUL3-2-3	71,94	-	134	119	2015	82,1	-	-	20,5	199	18,2
SUL3-3-1	71,27	-	24,3	125	3970	-	2694	0,932	3039	236	35,6
SUL3-3-2	72,10	19,6	30,9	39,6	815	33,6	660	1,42	272	292	41,6
SUL3-3-3	72,12	-	50,2	30,5	1036	-	-	-	5,02	198	22,5
SUL3-3-4	72,06	54,6	176	220	-	190	950	0,849	1112	295	112
SUL3-3-5	71,92	66,9	245	241	1891	268	-	0,439	30,4	250	51,8
SUL3-3-6	71,95	-	131	155	1871	-	-	-	17,6	231	20,0
SUL3-4-1	72,25	-	53,42	94,1	-	52,2	-	0,292	8,27	235	209
SUL3-4-2	71,84	15,7	94,4	141	1912	103	551	1,42	686	240	278
SUL7-1B	72,12	-	63,8	67,6	-	-	-	-	8,17	792	118
Hydrothermal											
MIN2-1-1	72,04	-	13,1	211	825	-	-	-	239	531	277
MIN2-1-2	72,11	-	10,9	152	-	-	-	-	167	604	428
MIN2-1-3	72,03	13,1	-	213	-	-	-	-	195	610	310
MIN2-1-4	71,78	-	101	316	2003	330	-	-	126	584	890
MIN2-2-1	71,21	67,4	1031	593	5059	148	1090	-	311	583	15,1
MIN2-2-2	71,27	31,5	822	909	4592	558	582	-	355	518	15,2
MIN2-2-3	71,49	41,4	686	531	3625	181	676	-	265	652	3,50
MIN2-2-4	70,30	342	2129	1847	8818	946	2095	0,642	461	629	3,61

MIN2-3-1	70,49	103	2091	1084	8362	508	2213	0,750	402	564	4,9146
MIN2-3-2	71,86	32,8	491	577	1347	295	-	0,269	240	564	163
MIN2-4-1	71,90	-	283	290	1537	28,9	-	-	272	561	-
MIN2-5-1	71,39	66,5	819	555	4140	120	455	0,373	303	511	2,15
MIN2-5-2	71,00	142	1059	853	6159	253	710	0,541	314	501	2,26
MIN2-5-3	71,62	50,4	488	415	3177	29,1	-	0,224	216	470	2,80
MIN2-5-4	71,53	20,7	628	382	3647	66,9	809	-	260	509	-
MIN2-6-1	71,60	16,6	502	449	3170	96,6	-	-	267	568	3,28
MIN2-6-2	71,09	117	1237	1024	5273	131	436	0,446	317	549	2,05
MIN2-6-3	71,75	11,9	572	365	2287	77,6	665	0,222	244	575	3,12
MIN2-6-4	71,59	20,8	692	388	3102	95,4	891	0,367	255	584	9,54
MIN2-7-1	71,45	34,6	656	332	4143	48,0	582	-	211	634	11,1
MIN2-7-2	72,18	-	24,0	141	-	-	-	-	148	656	10,9
MIN2-8-1	71,29	177	889	823	4421	311	610	0,253	309	625	2,41
MIN2-8-2	71,53	95,2	631	539	3473	235	866	-	211	644	-
MIN2-6-5	72,19	-	10,4	215	-	-	-	-	182	550	-
MIN2-6-6	71,89	20,9	333	267	1737	30,7	-	-	203	482	-
MIN2-6-7	71,78	55,0	355	404	2192	37,7	-	0,456	243	581	-
MIN5-1-1	70,37	144	2488	1265	8714	321	2546	0,326	510	451	-
MIN5-1-2	69,62	177	2403	1918	12850	681	2980	0,454	670	493	-
MIN5-1-3	70,18	535	1718	3177	8756	658	3198	0,662	611	471	-
MIN5-1-4	71,31	49,9	1175	769	4126	224	1320	-	427	491	-
MIN5-1-5	71,63	31,6	746	328	2970	40,7	-	-	345	486	-
MIN5-1-6	71,14	112	1391	797	4977	202	1735	-	539	477	-
MIN5-1-7	71,39	59,3	913	632	3909	216	834	-	527	491	-
MIN5-1-8	71,91	18,6	217	133	1779	-	-	-	278	499	-
MIN5-1-9	70,20	123	2479	1705	9270	635	2280	0,248	526	486	-
MIN5-2-1	70,77	91,7	719	492	-	77,4	-	-	398	448	-
MIN5-2-2	71,41	32,7	953	447	4138	168	792	-	306	473	-
MIN5-2-3	71,51	43,6	910	457	3331	119	1006	-	507	483	2,59
MIN5-2-4	71,53	52,2	880	404	3479	160	839	-	293	467	5,02
MIN5-3-1	71,42	33,4	860	346	4253	35,8	-	-	377	356	-
MIN5-3-2	71,85	-	511	173	2106	66,2	-	-	211	340	1,95
MIN5-4-1	69,37	119	1090	827	16826	213	1143	0,248	374	445	2,20
MIN5-4-2	69,15	153	4221	3315	13213	949	3433	0,341	650	477	-
MIN5-5-1	70,04	224	2039	1405	11158	165	2229	-	517	330	4,03
MIN5-5-2	70,32	104	2689	1228	9137	283	2871	-	373	329	-
MIN5-5-3	71,73	30,3	570	309	2773	56,6	-	-	170	313	-
MIN5-5-4	71,98	14,7	331	172	1270	-	-	-	342	333	2,57
MIN5-5-5	70,59	149	2042	1303	7553	233	1822	0,277	639	351	-
GAR4-1-1	71,97	-	37,99	23,3	1453	-	-	-	6,92	328	2,41
GAR4-1-2	72,22	-	13,20	35,2	-	18,3	-	-	4,43	306	-

NOTES: Abbreviation: D.L. = detection limit, (-) below detection limit

Detection limit (D.L.)= $3 \times \sigma_{\text{background}}$

Internal standard ^{57}Fe and the stoichiometric value of 72.36 wt % was used

	Mn	Co	Ni	Cu	Zn	Ga	Ge	As	Sr	Y
D.L	2.33	0.080	0.304	0.435	1.08	0.121	0.637	0.783	0.016	0.010
Magmatic										
TRACH-1-1	1016	14.7	45.4	-	47.5	3.65	2.69	0.987	0.203	-
TRACH-1-2	384	13.1	41.6	-	41.3	3.23	2.22	-	0.112	1.24
TRACH-1-3	496	13.0	37.7	-	42.0	3.34	2.42	-	0.919	0.215
TRACH-2-1	643	36.0	27.3	-	53.3	6.05	1.72	-	28.5	0.064
TRACH-2-3	721	40.9	30.1	-	39.9	5.15	1.90	1.08	0.489	-
TRACH-3-1	750	41.5	37.8	-	85.4	7.12	3.21	-	2.95	-
TRACH-3-2	743	35.4	31.5	-	43.4	5.33	2.57	-	5.89	-
TRACH-4-1		28.7	29.4	-	74.7	11.8	-	-	1.55	-
SUL3-1-1	594	14.6	28.1	-	57.5	2.18	2.73	0.954	-	-
SUL3-1-2	545	14.6	28.1	-	37.0	2.46	2.71	-	3.63	-
SUL3-1-3	571	15.4	26.5	-	41.7	2.54	3.08	-	1.40	-
SUL3-1-4	520	14.7	28.7	-	30.7	2.65	1.13	-	4.36	-
SUL3-1-5	557	15.1	27.3	-	34.6	1.89	2.03	-	0.075	0.164
SUL3-1-6	511	13.6	26.7	-	38.7	1.64	2.28	-	0.571	3.34
SUL3-1-7	668	15.2	32.1	1.79	54.6	2.58	2.73	-	0.298	1.93
SUL3-2-1	541	14.4	25.3	-	37.3	1.92	3.17	-	2.29	6.73
SUL3-2-2	527	14.2	28.5	-	35.6	2.52	2.23	-	1.45	5.58
SUL3-2-3	481	13.0	29.6	-	37.8	2.62	2.89	-	3.00	-
SUL3-3-1	539	13.4	27.8	-	32.4	1.58	2.54	-	1.85	8.55
SUL3-3-2	518	16.9	24.5	-	31.3	1.84	2.08	-	0.369	5.63
SUL3-3-3	460	14.0	23.7	-	27.3	1.84	2.56	-	0.393	0.408
SUL3-3-4	647	15.6	26.5	-	42.9	2.22	2.91	0.788	4.65	8.09
SUL3-3-5	520	14.2	27.9	-	30.9	2.16	2.64	1.24	0.103	2.01
SUL3-3-6	533	14.9	29.7	-	31.4	1.85	2.67	-	0.146	0.022
SUL3-4-1	585	12.7	24.8	-	31.2	2.01	2.57	-	0.210	0.674
SUL3-4-2	586	12.4	24.4	-	41.7	2.14	2.46	-	0.576	6.62
SUL7-1B	390	26.2	20.5	23.0	36.1	2.58	2.53	-	0.255	-
Hydrothermal										
MIN2-1-1	433	10.2	33.9	-	17.0	3.41	2.43	-	0.041	-
MIN2-1-2	397	16.9	35.1	-	21.0	3.70	2.5	-	-	-
MIN2-1-3	392	18.7	38.6	-	20.8	4.16	1.43	-	-	-
MIN2-1-4	360	10.5	37.0	-	10.8	4.54	1.94	-	0.037	-
MIN2-2-1	609	9.5	37.6	-	26.5	7.19	1.79	2.02	0.637	-
MIN2-2-2	516	11.4	37.1	-	24.0	10.2	2.18	2.01	0.666	-
MIN2-2-3	456	8.0	34.3	-	19.7	6.82	2.47	1.26	0.390	-
MIN2-2-4	631	10.1	37.1	2.25	31.4	8.02	2.73	4.69	2.38	0.080

MIN2-3-1	593	14,7	38,1	-	30,7	6,21	2,13	5,12	1,77	-
MIN2-3-2	441	11,7	34,4	-	17,1	4,66	1,80	1,14	0,167	-
MIN2-4-1	492	29,0	39,1	-	19,7	6,95	1,80	-	0,106	-
MIN2-5-1	626	22,2	36,7	-	17,6	5,92	1,33	1,18	0,19	-
MIN2-5-2	688	21,5	36,9	-	19,2	6,56	2,38	3,34	0,460	-
MIN2-5-3	529	20,3	35,4	-	30,2	6,27	2,56	0,85	0,092	-
MIN2-5-4	523	23,3	38,9	-	18,1	6,62	1,28	-	0,388	-
MIN2-6-1	525	24,0	38,8	-	27,4	6,93	2,18	1,29	0,179	-
MIN2-6-2	667	32,0	42,5	-	30,1	8,62	2,37	1,67	0,446	-
MIN2-6-3	441	24,6	38,7	-	18,1	6,98	1,88	-	0,232	-
MIN2-6-4	523	33,3	39,5	-	27,8	6,79	1,80	1,28	0,545	-
MIN2-7-1	490	5,6	34,4	-	20,6	7,80	1,96	1,75	0,319	-
MIN2-7-2	375	5,7	32,7	8,14	19,0	6,49	2,04	-	-	-
MIN2-8-1	548	6,1	49,5	-	22,1	8,04	3,02	4,40	0,587	0,020
MIN2-8-2	435	17,3	32,1	1,80	18,5	5,80	1,62	4,14	0,801	-
MIN2-6-5	366	14,2	37,5	-	10,9	6,92	-	-	-	-
MIN2-6-6	445	12,9	31,3	-	15,0	5,61	2,50	0,845	0,096	-
MIN2-6-7	454	15,9	40,7	-	20,6	6,80	4,45	2,14	0,289	-
MIN5-1-1	538	27,3	50,0	18,75	47,3	8,08	1,88	1,59	2,70	0,02
MIN5-1-2	579	28,1	40,3	18,15	45,0	8,55	2,95	1,76	4,17	0,04
MIN5-1-3	534	28,3	39,3	-	29,3	9,22	1,85	3,92	3,49	0,04
MIN5-1-4	525	29,7	37,8	-	29,4	8,95	2,00	1,58	0,988	-
MIN5-1-5	409	24,7	162,6	-	22,8	6,03	2,61	-	0,208	-
MIN5-1-6	512	27,3	51,3	-	25,9	7,16	2,52	2,22	1,16	0,027
MIN5-1-7	537	24,7	41,4	-	19,5	6,89	2,55	1,48	0,736	-
MIN5-1-8	378	34,1	167	-	18,2	5,75	2,48	-	-	-
MIN5-1-9	569	32,6	42,7	446	286	8,22	2,09	1,75	3,81	0,04
MIN5-2-1	404	22,7	73,5	-	23,5	5,75	2,24	1,58	0,46	-
MIN5-2-2	389	24,8	204,3	-	23,1	5,90	1,95	-	0,636	-
MIN5-2-3	494	26,6	59,2	-	25,3	6,38	2,61	1,00	0,595	-
MIN5-2-4	398	23,3	239,5	-	21,6	5,74	1,71	-	0,563	0,031
MIN5-3-1	475	22,5	78,7	-	22,0	6,80	1,72	0,84	0,293	-
MIN5-3-2	353	16,3	294	16,3	25,4	6,21	2,75	-	0,168	-
MIN5-4-1	436	22,5	50,7	16,2	21,6	6,62	1,96	1,60	1,04	0,025
MIN5-4-2	709	30,2	38,6	-	39,6	10,3	1,80	1,61	4,49	0,044
MIN5-5-1	559	30,4	41,2	-	34,5	10,4	1,99	4,10	2,21	0,103
MIN5-5-2	562	35,1	41,7	-	34,6	12,3	2,22	2,11	2,54	0,073
MIN5-5-3	335	24,0	69,6	-	22,2	6,56	2,21	0,884	0,221	0,029
MIN5-5-4	433	27,7	88,0	-	29,0	6,75	2,34	-	-	-
MIN5-5-5	559	31,6	40,9	-	37,1	9,49	2,35	2,16	2,18	0,065
GAR4-1-1	1263	77,4	54,7	-	59,2	2,67	2,49	-	0,083	-
GAR4-1-2	1048	70,1	50,3	-	54,5	2,47	2,19	-	0,118	0,030

	Zr	Nb	Mo	Sb	Hf	Ta	W	Pb	Th	U
D.L	0.010	0.010	0.013	0.132	0.012	0.007	0.036	0.086	0.014	0.009
Magmatic										
TRACH-1-1	0.182	0.105	-	-	-	-	0.123	-	0.030	0.060
TRACH-1-2	-	-	0.213	-	2.25	-	-	0.126	0.087	2.527
TRACH-1-3	-	-	-	-	0.055	-	-	-	0.132	0.033
TRACH-2-1	-	0.099	0.465	-	0.349	-	0.079	0.388	0.124	0.052
TRACH-2-3	-	0.257	-	-	-	-	-	0.198	0.044	0.028
TRACH-3-1	0.874	-	-	0.246	-	-	-	0.752	0.295	0.037
TRACH-3-2	-	0.047	0.801	-	-	-	0.138	-	-	-
TRACH-4-1	-	1.67	-	0.670	-	-	0.695	1.262	0.283	-
SUL3-1-1	-	-	-	0.142	-	-	-	3.60	-	-
SUL3-1-2	-	0.018	-	-	-	-	-	0.135	0.017	0.013
SUL3-1-3	0.134	-	-	0.290	-	-	-	0.198	-	-
SUL3-1-4	-	-	-	-	-	-	-	-	0.033	-
SUL3-1-5	3.32	-	-	-	0.112	-	-	-	0.021	-
SUL3-1-6	0.583	2.17	-	0.173	-	0.131	-	0.175	0.228	0.058
SUL3-1-7	1335	0.013	-	0.203	24.7	-	-	1.11	2.62	2.122
SUL3-2-1	457	6.86	-	0.686	11.7	0.317	-	0.432	1.00	1.473
SUL3-2-2	495	3.42	-	0.431	13.7	0.137	0.030	0.520	1.05	1.255
SUL3-2-3	1.71	-	-	-	-	-	-	0.125	0.014	0.014
SUL3-3-1	677	7.02	-	0.587	20.9	0.100	-	0.345	1.06	2.21
SUL3-3-2	1203	0.815	-	-	32.6	0.033	-	0.446	1.30	3.13
SUL3-3-3	55.0	-	-	-	1.57	-	-	0.118	0.408	0.204
SUL3-3-4	627	3.64	-	0.344	13.5	0.378	0.087	4.063	1.33	2.22
SUL3-3-5	363	-	-	-	9.743	-	-	0.151	0.535	0.955
SUL3-3-6	0.144	-	-	-	-	-	-	-	-	0.020
SUL3-4-1	136	-	-	-	3.815	-	-	0.106	0.382	0.509
SUL3-4-2	1017	1.43	-	0.196	27.0	0.158	-	1.51	2.21	3.92
SUL7-1B	-	-	-	-	-	-	0.166	-	0.022	-
Hydrothermal										
MIN2-1-1	-	-	-	-	-	-	-	-	-	-
MIN2-1-2	-	-	-	-	-	-	-	0.148	-	-
MIN2-1-3	-	-	-	-	-	-	-	0.677	-	-
MIN2-1-4	0.060	-	-	0.137	-	-	-	-	-	-
MIN2-2-1	0.055	-	-	3.06	-	-	11.0	0.625	-	-
MIN2-2-2	0.230	0.111	0.279	4.14	-	-	178	0.921	-	-
MIN2-2-3	0.029	-	-	1.88	-	-	11.6	0.598	-	-
MIN2-2-4	0.360	0.041	-	2.39	0.028	-	0.169	0.149	-	-

Appendix Table B5. Analyse de l'amphibole à la microsonde

SAMPLE	SiO ₂	TiO ₂	Al ₂ O ₃	FeO	Cr ₂ O ₃	MnO	MgO	CaO	Na ₂ O	K ₂ O	CoO	NiO	F	Cl	O=F,Cl	H ₂ O	Total
Ore zone (Exoskarn)																	
MIN4 2-1	53,76	0,00	1,41	14,02	0,08	0,35	14,27	12,52	0,16	0,02	0,02	0,38	0,00	0,00	0,00	2,05	99,04
MIN4 2-2	48,50	0,09	6,55	16,83	0,05	0,39	11,43	12,06	0,67	0,40	0,02	0,00	0,00	0,01	0,00	2,01	98,99
MIN3 2-4	49,43	0,08	4,48	17,72	0,03	0,59	11,53	11,91	0,57	0,22	0,02	0,03	0,00	0,00	0,00	1,99	98,59
MIN3 2-5	50,71	0,05	3,43	17,14	0,00	0,64	12,41	12,12	0,40	0,17	0,00	0,00	0,00	0,00	0,00	2,01	99,07
MIN3 2-6	48,14	0,11	5,47	18,58	0,00	0,67	10,60	11,83	0,61	0,38	0,00	0,00	0,01	0,02	0,01	1,97	98,38
MIN3 1-2	51,03	0,11	3,21	16,03	0,00	0,66	12,39	11,98	0,34	0,16	0,03	0,03	0,09	0,02	0,04	1,95	98,00
MIN4B 2-1	52,11	0,04	2,15	15,60	0,01	0,62	13,02	11,93	0,25	0,13	0,00	0,00	0,00	0,01	0,00	2,01	97,87
MIN4B 2-2	51,62	0,00	2,60	16,16	0,00	0,67	12,84	11,93	0,29	0,14	0,01	0,00	0,11	0,01	0,05	1,95	98,28
MIN4B 2-3	51,23	0,04	2,41	16,33	0,00	0,66	12,50	11,70	0,30	0,14	0,00	0,00	0,05	0,02	0,02	1,96	97,30
MIN4B 2-4	50,30	0,00	3,55	16,42	0,00	0,59	12,22	11,89	0,38	0,22	0,02	0,00	0,17	0,01	0,07	1,90	97,60
MIN4B 2-5	51,08	0,05	2,82	15,72	0,03	0,65	12,53	11,98	0,34	0,14	0,00	0,01	0,00	0,01	0,00	1,99	97,34
MIN4B 2-6	51,97	0,07	2,12	15,43	0,00	0,65	13,05	12,03	0,27	0,09	0,03	0,01	0,07	0,01	0,03	1,97	97,74
MIN4B 3-2	50,62	0,04	2,52	16,48	0,09	0,69	11,79	11,53	0,27	0,12	0,00	0,00	0,09	0,03	0,04	1,91	96,14
MIN4B 3-3	51,08	0,01	2,24	14,57	0,05	0,63	12,82	11,75	0,24	0,11	0,03	0,02	0,01	0,02	0,01	1,96	95,52
MIN4B 3-4	51,53	0,07	2,17	15,40	0,08	0,68	12,90	11,59	0,26	0,13	0,03	0,00	0,00	0,02	0,01	1,98	96,83
MIN6 2-4	52,34	0,12	2,07	17,36	0,00	0,63	12,30	12,07	0,35	0,12	0,03	0,02	0,00	0,02	0,01	2,02	99,45
Ore zone (Endoskarn)																	
MIN8 3-1	53,92	0,07	2,46	10,65	0,00	0,69	16,83	12,27	0,35	0,05	0,00	0,01	0,00	0,02	0,01	2,09	99,40
MIN8 3-2	52,22	0,04	3,89	12,07	0,00	0,58	15,74	12,21	0,62	0,07	0,00	0,00	0,11	0,01	0,05	2,02	99,53
MIN8 2-1	49,93	0,15	5,94	13,39	0,00	0,58	13,99	11,88	0,86	0,15	0,01	0,03	0,20	0,04	0,09	1,93	98,98
MIN8 2-2	50,85	0,09	5,35	13,30	0,00	0,63	14,37	11,92	0,79	0,13	0,00	0,00	0,21	0,02	0,09	1,95	99,50

Skarn alteration																
GAR3 2-1	54,06	0,05	1,16	11,64	0,00	1,24	15,62	12,26	0,24	0,10	0,00	0,13	0,01	0,06	1,99	98,43
GAR3 2-2	53,83	0,00	1,01	11,01	0,00	1,19	15,76	12,25	0,18	0,04	0,05	0,17	0,00	0,07	1,96	97,38
GAR3 2-3	54,17	0,14	1,09	12,09	0,00	1,23	15,63	12,22	0,23	0,07	0,00	0,13	0,00	0,05	2,00	98,94
GAR2 2-1	53,94	0,03	1,46	13,28	0,00	0,61	15,10	12,38	0,23	0,08	0,00	0,01	0,00	0,00	2,06	99,18
GAR2 2-2	54,68	0,04	0,93	13,68	0,04	0,61	15,34	12,56	0,23	0,03	0,00	0,00	0,02	0,00	2,08	100,21
GAR2 2-3	54,31	0,09	1,51	13,42	0,00	0,55	15,06	12,56	0,31	0,06	0,02	0,04	0,05	0,02	2,05	100,01
GAR2 2-4	54,24	0,00	1,42	13,81	0,00	0,65	14,75	12,61	0,28	0,09	0,01	0,00	0,00	0,00	2,07	99,92
GAR1 4-5	51,17	0,04	1,93	19,78	0,02	0,77	10,68	11,93	0,34	0,12	0,00	0,00	0,03	0,01	1,98	98,76
GAR1 1-8	49,46	0,00	2,89	21,44	0,12	0,72	9,91	11,83	0,43	0,25	0,00	0,14	0,03	0,06	1,89	99,05
Intermediate (IP2)																
SUL12 4-1	51,92	0,18	3,23	12,55	0,00	0,40	15,75	12,36	0,64	0,24	0,00	0,11	0,04	0,05	2,00	99,37
SUL12 4-2	53,14	0,21	2,72	11,49	0,00	0,56	16,37	12,47	0,50	0,23	0,02	0,09	0,07	0,05	2,02	99,85
SUL12 3-1	49,01	0,03	6,30	12,51	0,04	0,56	13,14	12,41	0,46	0,23	0,00	0,17	0,03	0,08	1,91	96,72
SUL12 3-2	53,64	0,20	1,86	11,49	0,01	0,63	16,23	12,44	0,31	0,13	0,02	0,16	0,00	0,07	1,99	99,04
SUL12 1-1	54,12	0,00	0,83	12,19	0,00	0,62	15,82	12,32	0,37	0,04	0,00	0,27	0,00	0,12	1,92	98,43
Late (LP)																
SUL4 1-1	50,99	0,62	4,60	10,67	0,00	0,71	16,44	11,56	1,00	0,47	0,03	0,45	0,04	0,20	1,84	99,25
SUL4 1-2	51,22	0,71	3,91	11,03	0,00	0,67	16,15	11,50	1,43	0,42	0,00	0,40	0,02	0,17	1,86	99,20
SUL4 2-1	52,78	0,45	2,84	10,97	0,00	0,57	16,97	11,90	0,79	0,39	0,01	0,44	0,01	0,19	1,86	99,83
SUL4 2-2	51,30	0,77	4,08	11,50	0,01	0,62	15,91	11,56	1,17	0,44	0,00	0,24	0,03	0,11	1,94	99,48
SUL4 3-1	50,70	0,83	4,26	11,80	0,00	0,62	15,60	11,50	1,12	0,48	0,00	0,34	0,03	0,15	1,88	99,05
SUL4 3-2	50,63	0,82	4,19	11,23	0,03	0,65	16,02	11,46	1,46	0,46	0,00	0,38	0,03	0,17	1,86	99,05
SUL4 5-1	50,38	0,73	4,28	12,13	0,00	0,71	15,16	11,66	1,00	0,46	0,00	0,28	0,03	0,13	1,89	98,57
SUL4 5-2	51,98	0,60	3,56	11,16	0,01	0,58	16,47	11,50	1,13	0,46	0,00	0,32	0,02	0,14	1,91	99,55
SUL4 7-3	50,93	0,81	4,27	11,47	0,00	0,74	16,17	11,56	1,22	0,44	0,03	0,30	0,03	0,13	1,92	99,76
SUL4 7-4	50,81	0,66	4,08	11,24	0,00	0,69	16,04	11,56	1,38	0,45	0,01	0,56	0,03	0,24	1,77	99,07

NOTES: Analyses with high or low totals (>101 or <95 wt.%) or poor stoichiometries are omitted.

Formula on the basis of 13 cations using the spreadsheet given by Locock (2014).

SAMPLE	Si	Al ^{IV}	T _Σ	Al ^{VI}	Ti ⁴⁺	Cr	Fe ³⁺	Co	Ni	Mg ²⁺	Fe ²⁺	Mn ²⁺	C _Σ	Mn ²⁺	Ca ²⁺	Na ⁺	B _Σ	Na ⁺
Ore zone (Exoskarn)																		
MIN4 2-1	7,85	0,15	8	0,09	0,00	0,01	0,07	0,00	0,04	3,11	1,64	0,04	5	0,01	1,96	0,03	2	0,01
MIN4 2-2	7,20	0,80	8	0,35	0,01	0,01	0,25	0,00	0,00	2,53	1,84	0,01	5	0,04	1,92	0,04	2	0,15
MIN3 2-4	7,38	0,62	8	0,17	0,01	0,00	0,33	0,00	0,00	2,57	1,88	0,03	5	0,04	1,91	0,05	2	0,11
MIN3 2-5	7,50	0,50	8	0,10	0,01	0,00	0,35	0,00	0,00	2,74	1,77	0,04	5	0,04	1,92	0,04	2	0,07
MIN3 2-6	7,25	0,75	8	0,22	0,01	0,00	0,36	0,00	0,00	2,38	1,98	0,04	5	0,04	1,91	0,05	2	0,13
MIN3 1-2	7,61	0,39	8	0,18	0,01	0,00	0,15	0,00	0,00	2,76	1,85	0,04	5	0,04	1,92	0,05	2	0,05
MIN4B 2-1	7,76	0,24	8	0,14	0,00	0,00	0,09	0,00	0,00	2,89	1,86	0,02	5	0,05	1,90	0,04	2	0,03
MIN4B 2-2	7,67	0,33	8	0,12	0,00	0,00	0,19	0,00	0,00	2,84	1,82	0,02	5	0,06	1,90	0,04	2	0,04
MIN4B 2-3	7,70	0,30	8	0,13	0,00	0,00	0,14	0,00	0,00	2,80	1,91	0,01	5	0,07	1,89	0,04	2	0,04
MIN4B 2-4	7,55	0,46	8	0,17	0,00	0,00	0,24	0,00	0,00	2,73	1,82	0,03	5	0,04	1,91	0,05	2	0,06
MIN4B 2-5	7,67	0,33	8	0,17	0,01	0,00	0,12	0,00	0,00	2,80	1,86	0,05	5	0,03	1,93	0,04	2	0,06
MIN4B 2-6	7,75	0,25	8	0,12	0,01	0,00	0,11	0,00	0,00	2,90	1,81	0,05	5	0,04	1,92	0,04	2	0,04
MIN4B 3-2	7,72	0,28	8	0,18	0,01	0,01	0,09	0,00	0,00	2,68	2,02	0,02	5	0,07	1,89	0,05	2	0,03
MIN4B 3-3	7,77	0,23	8	0,18	0,00	0,01	0,06	0,00	0,00	2,91	1,80	0,05	5	0,03	1,92	0,05	2	0,02
MIN4B 3-4	7,76	0,24	8	0,14	0,01	0,01	0,08	0,00	0,00	2,90	1,86	0,01	5	0,08	1,87	0,05	2	0,03
MIN6 2-4	7,72	0,28	8	0,08	0,01	0,00	0,19	0,00	0,00	2,70	1,95	0,05	5	0,03	1,91	0,07	2	0,03
Ore zone (Endoskarn)																		
MIN8 3-1	7,71	0,29	8	0,12	0,01	0,00	0,16	0,00	0,00	3,59	1,12	0,01	5	0,07	1,88	0,05	2	0,05
MIN8 3-2	7,50	0,50	8	0,16	0,00	0,00	0,29	0,00	0,00	3,37	1,16	0,01	5	0,06	1,88	0,07	2	0,11
MIN8 2-1	7,28	0,72	8	0,30	0,02	0,00	0,28	0,00	0,00	3,04	1,35	0,00	5	0,07	1,86	0,08	2	0,17
MIN8 2-2	7,36	0,64	8	0,27	0,01	0,00	0,28	0,00	0,00	3,10	1,33	0,01	5	0,07	1,85	0,08	2	0,14

Skarn alteration																			
GAR3 2-1	7,87	0,13	8	0,07	0,01	0,00	0,06	0,00	0,00	0,00	3,39	1,36	0,11	5	0,04	1,91	0,05	2	0,02
GAR3 2-2	7,90	0,10	8	0,08	0,00	0,00	0,04	0,01	0,00	0,00	3,45	1,31	0,11	5	0,03	1,93	0,04	2	0,01
GAR3 2-3	7,86	0,14	8	0,05	0,02	0,00	0,08	0,00	0,00	0,00	3,38	1,39	0,09	5	0,06	1,90	0,04	2	0,03
GAR2 2-1	7,83	0,17	8	0,08	0,00	0,00	0,08	0,00	0,00	0,00	3,27	1,53	0,04	5	0,04	1,93	0,04	2	0,03
GAR2 2-2	7,86	0,14	8	0,02	0,00	0,00	0,11	0,00	0,00	0,00	3,29	1,54	0,04	5	0,03	1,94	0,03	2	0,03
GAR2 2-3	7,83	0,17	8	0,08	0,01	0,00	0,06	0,00	0,00	0,00	3,24	1,55	0,05	5	0,02	1,94	0,04	2	0,04
GAR2 2-4	7,84	0,16	8	0,08	0,00	0,00	0,05	0,00	0,00	0,00	3,18	1,62	0,07	5	0,01	1,95	0,03	2	0,04
GAR1 4-5	7,70	0,30	8	0,05	0,00	0,00	0,21	0,00	0,00	0,00	2,40	2,28	0,06	5	0,04	1,93	0,04	2	0,06
GAR1 1-8	7,47	0,51	8	0,00	0,00	0,01	0,45	0,00	0,00	0,00	2,23	2,25	0,05	5	0,04	1,92	0,05	2	0,08
Intermediate (IP2)																			
SUL12 4-1	7,51	0,49	8	0,06	0,02	0,00	0,27	0,00	0,00	0,00	3,40	1,24	0,01	5	0,04	1,92	0,05	2	0,14
SUL12 4-2	7,61	0,39	8	0,07	0,02	0,00	0,19	0,00	0,00	0,00	3,50	1,19	0,03	5	0,04	1,92	0,05	2	0,09
SUL12 3-1	7,33	0,67	8	0,44	0,00	0,00	0,07	0,00	0,00	0,00	2,93	1,49	0,07	5	0,01	1,99	0,01	2	0,13
SUL12 3-2	7,73	0,27	8	0,05	0,02	0,00	0,19	0,00	0,00	0,00	3,49	1,20	0,06	5	0,02	1,92	0,06	2	0,03
SUL12 1-1	7,88	0,12	8	0,02	0,00	0,00	0,09	0,00	0,00	0,00	3,44	1,39	0,05	5	0,03	1,92	0,05	2	0,05
Late (LP)																			
SUL4 1-1	7,34	0,66	8	0,12	0,07	0,00	0,32	0,00	0,00	0,00	3,53	0,96		5	0,09	1,78	0,13	2	0,15
SUL4 1-2	7,41	0,59	8	0,08	0,08	0,00	0,21	0,00	0,00	0,00	3,48	1,12	0,02	5	0,06	1,78	0,16	2	0,24
SUL4 2-1	7,55	0,45	8	0,02	0,05	0,00	0,27	0,00	0,01	0,01	3,62	1,04		5	0,07	1,82	0,10	2	0,12
SUL4 2-2	7,40	0,60	8	0,09	0,08	0,00	0,24	0,00	0,01	0,01	3,42	1,15	0,01	5	0,07	1,79	0,15	2	0,18
SUL4 3-1	7,36	0,64	8	0,09	0,09	0,00	0,26	0,00	0,00	0,00	3,38	1,18	0,00	5	0,07	1,79	0,14	2	0,18
SUL4 3-2	7,35	0,65	8	0,06	0,09	0,00	0,23	0,00	0,00	0,00	3,47	1,13	0,01	5	0,07	1,78	0,15	2	0,26
SUL4 5-1	7,37	0,63	8	0,11	0,08	0,00	0,23	0,00	0,00	0,00	3,31	1,26	0,02	5	0,07	1,83	0,11	2	0,17
SUL4 5-2	7,47	0,53	8	0,07	0,06	0,00	0,26	0,00	0,00	0,00	3,53	1,08		5	0,07	1,77	0,16	2	0,16
SUL4 7-3	7,33	0,67	8	0,05	0,09	0,00	0,30	0,00	0,00	0,00	3,47	1,08	0,00	5	0,09	1,78	0,13	2	0,21
SUL4 7-4	7,37	0,63	8	0,07	0,07	0,00	0,23	0,00	0,00	0,00	3,47	1,13	0,02	5	0,07	1,80	0,14	2	0,25

SAMPLE	K ⁺	^A Σ	F ⁻	Cl ⁻	O	OH ⁻	^W Σ	Total	XMg
Ore zone (Exoskarn)									
MIN4 2-1	0.00	0.02	0.00	0.00	0.00	2.00	2	15.02	0.65
MIN4 2-2	0.08	0.23	0.00	0.00	0.01	1.99	2	15.23	0.58
MIN3 2-4	0.04	0.16	0.00	0.00	0.01	1.99	2	15.16	0.58
MIN3 2-5	0.03	0.10	0.00	0.00	0.01	1.99	2	15.10	0.61
MIN3 2-6	0.07	0.20	0.00	0.01	0.02	1.98	2	15.20	0.55
MIN3 1-2	0.03	0.08	0.04	0.00	0.01	1.94	2	15.08	0.60
MIN4B 2-1	0.02	0.05	0.00	0.00	0.00	1.99	2	15.05	0.61
MIN4B 2-2	0.03	0.07	0.05	0.00	0.01	1.93	2	15.07	0.61
MIN4B 2-3	0.03	0.07	0.02	0.01	0.01	1.97	2	15.07	0.59
MIN4B 2-4	0.04	0.10	0.08	0.00	0.01	1.90	2	15.10	0.60
MIN4B 2-5	0.03	0.09	0.00	0.00	0.01	1.99	2	15.09	0.60
MIN4B 2-6	0.02	0.05	0.03	0.00	0.01	1.96	2	15.05	0.62
MIN4B 3-2	0.02	0.05	0.04	0.01	0.01	1.95	2	15.05	0.57
MIN4B 3-3	0.02	0.04	0.01	0.01	0.00	1.99	2	15.04	0.62
MIN4B 3-4	0.03	0.05	0.00	0.01	0.00	1.99	2	15.05	0.61
MIN6 2-4	0.02	0.06	0.00	0.01	0.01	1.99	2	15.06	0.58
Ore zone (Endoskarn)									
MIN8 3-1	0.01	0.06	0.00	0.01	0.01	1.99	2	15.06	0.76
MIN8 3-2	0.01	0.12	0.05	0.00	0.01	1.94	2	15.12	0.74
MIN8 2-1	0.03	0.19	0.09	0.01	0.02	1.88	2	15.19	0.69
MIN8 2-2	0.02	0.17	0.10	0.01	0.02	1.88	2	15.16	0.70
Skarn alteration									
GAR3 2-1	0.02	0.04	0.06	0.00	0.01	1.93	2	15.04	0.71
GAR3 2-2	0.01	0.02	0.08	0.00	0.00	1.92	2	15.02	0.72
GAR3 2-3	0.01	0.04	0.06	0.00	0.01	1.94	2	15.04	0.71
GAR2 2-1	0.01	0.04	0.01	0.00	0.00	1.99	2	15.04	0.68
GAR2 2-2	0.01	0.04	0.00	0.00	0.01	1.99	2	15.04	0.68
GAR2 2-3	0.01	0.05	0.02	0.00	0.00	1.97	2	15.05	0.68
GAR2 2-4	0.02	0.06	0.00	0.00	0.00	2.00	2	15.06	0.66
GAR1 4-5	0.02	0.08	0.00	0.01	0.01	1.99	2	15.08	0.51
GAR1 1-8	0.05	0.13	0.07	0.01	0.02	1.91	2	15.13	0.50
Intermediate (IP2)									
SUL12 4-1	0.05	0.18	0.05	0.01	0.01	1.93	2	15.18	0.73
SUL12 4-2	0.04	0.14	0.04	0.02	0.01	1.93	2	15.14	0.75
SUL12 3-1	0.04	0.17	0.08	0.01	0.01	1.91	2	15.17	0.66
SUL12 3-2	0.02	0.06	0.07	0.00	0.01	1.92	2	15.06	0.74
SUL12 1-1	0.01	0.06	0.13	0.00	0.01	1.87	2	15.06	0.71

Late (LP)

SUL4 1-1	0.09	0.24	0.21	0.01	0.02	1.76	2	15.24	0.79
SUL4 1-2	0.08	0.32	0.18	0.01	0.02	1.80	2	15.32	0.76
SUL4 2-1	0.07	0.19	0.20	0.00	0.02	1.78	2	15.19	0.78
SUL4 2-2	0.08	0.26	0.11	0.01	0.02	1.87	2	15.26	0.75
SUL4 3-1	0.09	0.27	0.16	0.01	0.02	1.82	2	15.27	0.74
SUL4 3-2	0.09	0.35	0.18	0.01	0.02	1.80	2	15.35	0.75
SUL4 5-1	0.09	0.26	0.13	0.01	0.02	1.85	2	15.26	0.72
SUL4 5-2	0.08	0.24	0.15	0.01	0.02	1.83	2	15.24	0.77
SUL4 7-3	0.08	0.29	0.14	0.01	0.02	1.84	2	15.29	0.76
SUL4 7-4	0.08	0.34	0.26	0.01	0.02	1.72	2	15.34	0.75

Appendix Table B6. Analyse des Biotites à la microsonde

Sample	SiO ₂	TiO ₂	Al ₂ O ₃	FeO	MnO	MgO	CaO	Na ₂ O	K ₂ O	Cr ₂ O ₃	NiO	BaO	H ₂ O	Rb ₂ O	F	Cl	Total	
Héva Formation (Ore zone)																		
MIN 2-3	37,27	1,51	15,84	17,38	0,41	12,90	0,04	0,12	9,37	0,00	0,00	0,00	3,64	0,03	0,53	0,15	99,18	
MIN 2-4	36,57	1,53	15,51	17,47	0,43	9,56	0,00	0,07	9,61	0,00	0,04	0,00	3,35	0,05	0,73	0,16	95,07	
K-alteration in E.S.S.																		
MIN 1-1	36,90	1,40	15,83	17,51	0,44	12,58	0,01	0,05	9,72	0,00	0,03	0,00	3,57	0,05	0,60	0,14	98,83	
MIN 1-2	36,74	1,86	15,86	17,92	0,46	12,61	0,00	0,09	9,59	0,05	0,00	0,00	3,55	0,07	0,68	0,16	99,64	
MIN 1-3	36,39	1,30	15,75	17,91	0,37	12,32	0,02	0,07	9,61	0,00	0,00	0,00	3,37	0,03	0,91	0,13	98,19	
MIN 1-4	36,60	1,46	16,14	17,33	0,46	12,55	0,01	0,05	9,82	0,00	0,00	0,00	3,47	0,09	0,78	0,18	98,94	
Ore zone (Endoskarn)																		
MIN8 1-1	37,83	0,79	15,04	15,01	0,36	16,13	0,03	0,03	9,57	0,00	0,01	0,00	3,78	0,04	0,35	0,12	99,08	
MIN8 1-2	38,21	1,22	15,03	16,89	0,32	13,70	0,00	0,05	9,82	0,00	0,00	0,00	3,69	0,00	0,50	0,10	99,53	
MIN8 1-3	37,64	1,19	15,16	16,90	0,35	13,36	0,00	0,05	9,37	0,04	0,00	0,00	3,73	0,06	0,32	0,12	98,28	
MIN8 1-4	37,13	1,28	15,14	17,86	0,42	13,46	0,01	0,02	9,35	0,00	0,00	0,00	3,68	0,00	0,43	0,13	98,91	
Late (PL)																		
SUL4 6-3	38,39	1,01	14,30	15,01	0,38	15,14	0,00	0,14	9,67	0,07	0,00	0,00	3,30	0,05	1,29	0,01	98,75	
SUL4 6-4	38,56	0,88	14,28	14,16	0,36	15,90	0,01	0,02	9,94	0,04	0,00	0,00	3,07	0,06	1,74	0,02	99,05	
SUL2 4-1	36,92	0,74	13,95	16,20	0,57	14,27	0,02	0,03	9,55	0,00	0,04	0,00	3,34	0,04	0,94	0,08	96,68	
SUL2 3-1	37,90	1,16	14,27	16,62	0,59	13,96	0,02	0,03	9,65	0,02	0,03	0,00	3,47	0,01	0,87	0,03	98,62	
SUL2 3-2	37,12	1,33	14,17	17,25	0,52	13,97	0,00	0,03	9,40	0,00	0,00	0,00	3,62	0,10	0,49	0,08	98,08	
SUL2 3-3	37,44	1,12	15,17	16,84	0,56	13,49	0,05	0,08	9,73	0,00	0,00	0,00	3,48	0,08	0,84	0,07	98,95	
SUL5 4-1	37,22	1,29	14,05	16,85	0,73	13,19	0,04	0,03	9,57	0,00	0,03	0,00	3,39	0,09	0,90	0,05	97,43	
SUL5 4-2	37,26	1,24	14,30	17,81	0,70	13,57	0,01	0,04	9,52	0,00	0,00	0,00	3,43	0,05	0,90	0,06	98,88	
SUL5 2-1	37,81	1,29	14,72	17,54	0,72	12,88	0,05	0,08	9,15	0,05	0,00	0,00	3,54	0,04	0,73	0,04	98,63	
SUL5 2-2	37,21	1,13	14,70	18,11	0,71	12,92	0,02	0,05	9,56	0,03	0,00	0,00	3,45	0,05	0,84	0,07	98,84	

Intermediate (IP1)																		
SUL8 1-1	36,05	1,10	15,52	17,38	0,35	12,03	0,02	0,04	9,28	0,00	0,00	0,00	0,00	0,00	3,60	0,12	0,35	0,05
SUL8 1-2	36,51	1,32	15,28	17,19	0,33	11,73	0,02	0,05	9,24	0,01	0,00	0,00	0,00	0,00	3,45	0,02	0,54	0,06
SUL8 3-2	37,43	1,51	15,49	18,29	0,33	12,42	0,00	0,06	9,76	0,00	0,01	0,00	0,00	0,00	3,64	0,00	0,57	0,05
SUL8 5-1	36,51	1,50	15,56	18,12	0,40	11,80	0,03	0,04	9,62	0,00	0,01	0,00	0,00	0,00	3,67	0,01	0,35	0,07
SUL8 5-2	36,98	1,21	16,03	18,11	0,32	12,07	0,01	0,02	9,65	0,04	0,03	0,00	0,00	0,00	3,57	0,03	0,64	0,07
MIX1 1-1	36,42	1,44	15,45	19,28	0,43	11,81	0,06	0,07	9,05	0,03	0,00	0,01	0,01	0,01	3,53	0,04	0,61	0,15
MIX1 1-2	36,58	1,54	15,61	18,77	0,48	11,90	0,04	0,04	9,28	0,00	0,00	0,00	0,00	0,00	3,63	0,01	0,46	0,10
MIX1 2-1	37,14	1,33	15,78	16,74	0,52	12,97	0,06	0,05	9,16	0,00	0,01	0,02	0,02	0,02	3,49	0,03	0,77	0,11
MIX1 2-2	36,82	1,16	15,28	16,70	0,47	13,54	0,04	0,03	9,47	0,01	0,00	0,02	0,02	0,02	3,48	0,01	0,75	0,13
MIX1 3-1	36,60	1,37	15,63	17,93	0,50	11,78	0,03	0,04	9,47	0,00	0,00	0,00	0,00	0,00	3,64	0,00	0,39	0,11
MIX1 3-2	36,67	1,53	15,72	18,57	0,48	12,07	0,02	0,05	9,45	0,06	0,00	0,00	0,00	0,00	3,54	0,00	0,65	0,12
Mineralized (MP)																		
VUG3-1	37,32	1,47	15,97	17,91	0,15	12,66	0,05	0,11	9,29	0,02	0,00	0,19	0,19	0,19	3,41	0,02	1,03	0,07
VUG3-2	36,96	1,18	15,48	17,87	0,14	12,73	0,01	0,07	9,47	0,00	0,02	0,00	0,00	0,00	3,32	0,00	1,11	0,05
VUG4-1	36,71	1,51	15,37	18,38	0,12	12,09	0,03	0,08	9,30	0,00	0,02	0,04	0,04	0,04	3,43	0,02	0,85	0,05
VUG4-2	36,70	1,20	15,36	18,25	0,13	12,13	0,02	0,06	9,44	0,05	0,00	0,00	0,00	0,00	3,37	0,00	0,93	0,06
VUG5-1	38,34	0,95	14,70	14,61	0,08	14,96	0,05	0,05	9,70	0,00	0,00	0,00	0,00	0,00	3,06	0,10	1,71	0,04
VUG5-2	38,97	1,43	13,69	15,06	0,11	14,85	0,02	0,05	9,60	0,11	0,00	0,00	0,00	0,00	3,13	0,10	1,60	0,04

NOTES:

Analyses with high or low totals (> 101 or < 95 wt.%) or poor stoichiometries are omitted.

Sample	O=F,Cl	Total	Si	Al ^{IV}	Al ^{VI}	Ti ⁴⁺	Fe ²⁺	Cr ²⁺	Mn ²⁺	Mg ²⁺	Ca ²⁺	Na ⁺	K ⁺	Ni	OH	Total	F	Cl	XMg
Héva Formation (Ore zone)																			
MIN 2-3	0,26	98,93	5,65	2,35	0,48	0,17	2,20	0,00	0,05	2,92	0,01	0,04	1,81	0,00	3,71	15,68	0,25	0,04	0,57
MIN 2-4	0,34	94,73	5,82	2,18	0,72	0,18	2,32	0,00	0,06	2,27	0,00	0,02	1,95	0,00	3,59	15,53	0,37	0,04	0,49
K-alteration in E.S.S.																			
MIN 1-1	0,29	98,54	5,64	2,36	0,49	0,16	2,24	0,00	0,06	2,87	0,00	0,01	1,90	0,00	3,67	15,73	0,29	0,04	0,56
MIN 1-2	0,32	99,32	5,58	2,42	0,42	0,21	2,28	0,01	0,06	2,86	0,00	0,03	1,86	0,00	3,63	15,72	0,33	0,04	0,56
MIN 1-3	0,41	97,77	5,62	2,38	0,49	0,15	2,31	0,00	0,05	2,84	0,00	0,02	1,89	0,00	3,52	15,75	0,45	0,03	0,55
MIN 1-4	0,37	98,57	5,60	2,40	0,51	0,17	2,22	0,00	0,06	2,86	0,00	0,01	1,92	0,00	3,58	15,74	0,38	0,05	0,56
Ore zone (Endoskarn)																			
MIN8 1-1	0,17	98,91	5,68	2,32	0,34	0,09	1,88	0,00	0,05	3,61	0,00	0,01	1,83	0,00	3,80	15,82	0,17	0,03	0,66
MIN8 1-2	0,23	99,29	5,76	2,24	0,43	0,14	2,13	0,00	0,04	3,08	0,00	0,02	1,89	0,00	3,74	15,72	0,24	0,03	0,59
MIN8 1-3	0,16	98,11	5,74	2,26	0,46	0,14	2,15	0,00	0,04	3,04	0,00	0,01	1,82	0,00	3,81	15,68	0,16	0,03	0,58
MIN8 1-4	0,21	98,70	5,66	2,34	0,38	0,15	2,28	0,00	0,05	3,06	0,00	0,01	1,82	0,00	3,76	15,74	0,21	0,03	0,57
Late (PL)																			
SUL4 6-3	0,55	98,20	5,81	2,19	0,36	0,12	1,90	0,01	0,05	3,41	0,00	0,04	1,87	0,00	3,38	15,75	0,62	0,00	0,64
SUL4 6-4	0,74	98,31	5,81	2,19	0,35	0,10	1,78	0,00	0,05	3,57	0,00	0,01	1,91	0,00	3,16	15,77	0,83	0,01	0,67
SUL2 4-1	0,41	96,27	5,76	2,24	0,32	0,09	2,11	0,00	0,08	3,32	0,00	0,01	1,90	0,00	3,52	15,83	0,46	0,02	0,61
SUL2 3-1	0,37	98,25	5,78	2,22	0,35	0,13	2,12	0,00	0,08	3,17	0,00	0,01	1,88	0,00	3,57	15,74	0,42	0,01	0,60
SUL2 3-2	0,23	97,85	5,71	2,29	0,28	0,15	2,22	0,00	0,07	3,20	0,00	0,01	1,84	0,00	3,74	15,77	0,24	0,02	0,59
SUL2 3-3	0,37	98,58	5,70	2,30	0,43	0,13	2,14	0,00	0,07	3,06	0,01	0,02	1,89	0,00	3,58	15,76	0,40	0,02	0,59
SUL5 4-1	0,39	97,04	5,77	2,23	0,34	0,15	2,19	0,00	0,10	3,05	0,01	0,01	1,89	0,00	3,55	15,74	0,44	0,01	0,58
SUL5 4-2	0,39	98,49	5,71	2,29	0,29	0,14	2,28	0,00	0,09	3,10	0,00	0,01	1,86	0,00	3,55	15,79	0,44	0,02	0,58
SUL5 2-1	0,32	98,31	5,77	2,23	0,42	0,15	2,24	0,01	0,09	2,93	0,01	0,02	1,78	0,00	3,64	15,65	0,35	0,01	0,57
SUL5 2-2	0,37	98,47	5,71	2,29	0,37	0,13	2,32	0,00	0,09	2,96	0,00	0,01	1,87	0,00	3,57	15,77	0,41	0,02	0,56

Intermediate (IP2)																			
GLOM 6-1	0,36	97,32	5,66	2,34	0,31	0,19	2,22	0,01	0,07	3,02	0,07	0,01	1,84	0,00	3,58	15,74	0,38	0,04	0,58
GLOM 6-2	0,46	97,72	5,68	2,32	0,38	0,16	2,26	0,00	0,07	2,98	0,01	0,02	1,86	0,00	3,47	15,75	0,50	0,04	0,57
GLOM 2-1	0,35	95,52	5,67	2,33	0,40	0,13	2,36	0,00	0,07	2,94	0,01	0,02	1,82	0,00	3,58	15,75	0,38	0,03	0,56
GLOM 2-2	0,30	95,85	5,69	2,31	0,45	0,13	2,23	0,00	0,07	2,98	0,00	0,01	1,88	0,00	3,64	15,75	0,33	0,03	0,57
GLOM 1-1	0,46	98,95	5,63	2,37	0,30	0,13	2,32	0,00	0,07	3,15	0,00	0,01	1,88	0,00	3,48	15,85	0,49	0,03	0,58
GLOM 1-2	0,32	98,88	5,68	2,32	0,41	0,16	2,26	0,00	0,06	2,96	0,00	0,01	1,87	0,00	3,63	15,73	0,34	0,03	0,57
GLOM 1-6	0,41	98,37	5,76	2,24	0,29	0,09	2,13	0,00	0,06	3,38	0,00	0,00	1,85	0,00	3,53	15,81	0,45	0,02	0,61
SUL12 2-1	0,28	96,67	5,69	2,31	0,35	0,14	2,40	0,00	0,05	2,96	0,01	0,03	1,81	0,00	3,67	15,76	0,31	0,02	0,55
SUL12 2-2	0,25	96,48	5,65	2,35	0,34	0,15	2,36	0,00	0,07	3,01	0,02	0,02	1,79	0,01	3,71	15,76	0,27	0,02	0,56
SUL7 3-1	0,47	97,90	5,65	2,35	0,35	0,11	2,22	0,00	0,05	3,21	0,01	0,01	1,85	0,00	3,46	15,82	0,53	0,01	0,59
SUL7 3-2	0,47	98,02	5,67	2,33	0,35	0,11	2,14	0,00	0,05	3,31	0,00	0,01	1,81	0,00	3,47	15,79	0,53	0,01	0,61
SUL7 4-2	0,50	99,60	5,78	2,22	0,39	0,14	2,07	0,00	0,05	3,18	0,00	0,02	1,87	0,00	3,44	15,72	0,56	0,00	0,61
SUL7 4-3	0,48	98,06	5,57	2,43	0,25	0,14	2,23	0,01	0,05	3,47	0,00	0,01	1,58	0,00	3,45	15,75	0,54	0,01	0,61
SUL13 5-1	0,17	97,92	5,70	2,30	0,44	0,17	2,26	0,00	0,07	2,87	0,01	0,02	1,84	0,00	3,81	15,69	0,17	0,02	0,56
SUL13 5-2	0,28	98,67	5,69	2,31	0,42	0,14	2,27	0,00	0,06	2,98	0,00	0,01	1,85	0,00	3,67	15,74	0,31	0,02	0,57
SUL13 5-3	0,33	98,09	5,70	2,30	0,32	0,14	2,13	0,00	0,06	3,27	0,00	0,02	1,82	0,00	3,62	15,76	0,36	0,01	0,60
SUL13 3-1	0,36	97,71	5,69	2,31	0,26	0,11	2,18	0,00	0,06	3,39	0,00	0,01	1,83	0,00	3,58	15,84	0,40	0,02	0,61
SUL13 1-1	0,26	96,18	5,71	2,29	0,43	0,16	2,21	0,00	0,07	2,96	0,00	0,02	1,84	0,00	3,69	15,70	0,29	0,02	0,57
SUL13 1-2	0,31	96,11	5,73	2,27	0,48	0,13	2,24	0,00	0,07	2,91	0,00	0,02	1,81	0,00	3,64	15,68	0,34	0,02	0,57
Early (EP)																			
TRACHI 4-1	0,31	97,47	5,76	2,24	0,40	0,12	2,07	0,00	0,07	3,19	0,00	0,03	1,83	0,00	3,65	15,72	0,33	0,02	0,61
TRACHI 4-2	0,41	96,13	5,69	2,31	0,33	0,11	2,22	0,00	0,07	3,22	0,01	0,02	1,80	0,00	3,52	15,79	0,44	0,03	0,59
TRACHI 4-3	0,36	96,80	5,73	2,27	0,36	0,12	2,14	0,00	0,07	3,21	0,01	0,02	1,82	0,00	3,59	15,75	0,39	0,03	0,60
TRACHI 5-1	0,36	96,80	5,73	2,27	0,36	0,12	2,14	0,00	0,07	3,21	0,01	0,02	1,82	0,00	3,59	15,75	0,39	0,03	0,60
TRACHI 5-2	0,26	96,16	5,71	2,29	0,47	0,12	2,17	0,00	0,06	3,02	0,01	0,02	1,84	0,00	3,69	15,71	0,29	0,02	0,58
TRACHI 2-1	0,37	96,58	5,72	2,28	0,35	0,11	2,17	0,00	0,07	3,21	0,01	0,02	1,81	0,00	3,56	15,77	0,41	0,03	0,60

Intermediate (IP1)																			
SUL8 1-1	0,16	95,74	5,70	2,30	0,59	0,13	2,17	0,00	0,05	2,84	0,00	0,01	1,87	0,00	3,81	15,66	0,17	0,01	0,57
SUL8 1-2	0,24	95,49	5,69	2,31	0,58	0,16	2,17	0,00	0,04	2,80	0,00	0,01	1,89	0,00	3,71	15,66	0,27	0,02	0,56
SUL8 3-2	0,25	99,30	5,68	2,32	0,46	0,17	2,32	0,00	0,04	2,81	0,00	0,02	1,89	0,00	3,71	15,71	0,27	0,01	0,55
SUL8 5-1	0,16	97,51	5,65	2,35	0,49	0,18	2,35	0,00	0,05	2,72	0,01	0,01	1,90	0,00	3,81	15,71	0,17	0,02	0,54
SUL8 5-2	0,29	98,50	5,66	2,34	0,55	0,14	2,32	0,00	0,04	2,75	0,00	0,01	1,88	0,00	3,67	15,70	0,31	0,02	0,54
MIX1 1-1	0,29	98,08	5,63	2,37	0,44	0,17	2,49	0,00	0,06	2,72	0,01	0,02	1,78	0,00	3,67	15,70	0,30	0,04	0,52
MIX1 1-2	0,22	98,23	5,63	2,37	0,46	0,18	2,42	0,00	0,06	2,73	0,01	0,01	1,82	0,00	3,75	15,69	0,22	0,03	0,53
MIX1 2-1	0,35	97,83	5,68	2,32	0,52	0,15	2,14	0,00	0,07	2,96	0,01	0,02	1,79	0,00	3,60	15,65	0,37	0,03	0,58
MIX1 2-2	0,34	97,57	5,66	2,34	0,43	0,13	2,15	0,00	0,06	3,10	0,01	0,01	1,86	0,00	3,60	15,75	0,36	0,03	0,59
MIX1 3-1	0,19	97,29	5,67	2,33	0,53	0,16	2,32	0,00	0,07	2,72	0,00	0,01	1,87	0,00	3,78	15,68	0,19	0,03	0,54
MIX1 3-2	0,30	98,62	5,62	2,38	0,46	0,18	2,38	0,01	0,06	2,76	0,00	0,02	1,85	0,00	3,65	15,71	0,32	0,03	0,54
Mineralized (MP)																			
VUG 3-1	0,45	99,22	5,66	2,34	0,51	0,17	2,27	0,00	0,02	2,86	0,01	0,03	1,80	0,00	3,49	15,66	0,49	0,02	0,56
VUG 3-2	0,48	97,92	5,68	2,32	0,48	0,14	2,30	0,00	0,02	2,92	0,00	0,02	1,85	0,00	3,45	15,72	0,54	0,01	0,56
VUG 4-1	0,37	97,62	5,67	2,33	0,47	0,18	2,37	0,00	0,02	2,78	0,00	0,02	1,83	0,00	3,57	15,68	0,41	0,01	0,54
VUG 4-2	0,41	97,29	5,69	2,31	0,49	0,14	2,37	0,01	0,02	2,80	0,00	0,02	1,87	0,00	3,53	15,71	0,46	0,02	0,54
VUG 5-1	0,73	97,62	5,82	2,18	0,45	0,11	1,85	0,00	0,01	3,38	0,01	0,01	1,88	0,00	3,17	15,70	0,82	0,01	0,65
VUG 5-2	0,68	98,06	5,89	2,11	0,33	0,16	1,90	0,01	0,01	3,35	0,00	0,01	1,85	0,00	3,23	15,64	0,76	0,01	0,64

Appendix Table B7. Analyse des Chlorites à la microsonde

SAMPLE	SiO ₂	TiO ₂	Al ₂ O ₃	FeO	MnO	MgO	CaO	Na ₂ O	K ₂ O	Cr ₂ O ₃	NiO	H ₂ O*	Total
Héva Formation (Ore zone)													
MIN 2-1	29,55	0,04	16,23	18,36	0,74	20,60	0,02	0,04	0,31	0,00	0,03	11,55	97,52
MIN 2-2	29,50	0,00	16,33	18,42	0,71	20,32	0,02	0,04	0,22	0,02	0,01	11,51	97,18
MIN 2-3	29,38	0,04	16,28	18,39	0,69	20,46	0,02	0,04	0,29	0,00	0,03	11,51	97,17
MIN 2-4	29,44	0,02	16,30	18,35	0,70	20,39	0,04	0,03	0,01	0,01	0,02	11,49	96,90
MIN4 1-1	29,59	0,01	16,12	18,66	0,62	20,92	0,03	0,03	0,15	0,01	0,03	11,58	97,80
MIN4 1-2	29,53	0,02	16,72	18,44	0,76	20,50	0,03	0,03	0,32	0,00	0,02	11,61	98,04
MIN4 1-3	29,56	0,02	16,42	18,37	0,74	20,89	0,01	0,04	0,24	0,00	0,01	11,61	97,96
K alteration in E.S.S.													
MIN1-5	29,47	0,05	16,87	18,98	0,73	20,57	0,01	0,02	0,29	0,00	0,02	11,67	98,66
MIN1-6	29,13	0,09	16,95	19,38	0,70	18,87	0,18	0,08	0,55	0,00	0,00	11,47	97,41
MIN1-7	29,78	0,08	16,55	18,96	0,72	19,99	0,03	0,04	0,58	0,05	0,00	11,62	98,37
MIN1-8-2	29,46	0,07	16,79	19,17	0,72	19,43	0,07	0,05	0,57	0,00	0,01	11,55	97,95
MIN1-8-3	29,62	0,08	16,67	19,24	0,72	19,72	0,05	0,04	0,33	0,00	0,00	11,59	98,15
MIN1-8-4	29,30	0,00	16,91	19,18	0,70	20,12	0,10	0,05	0,42	0,00	0,01	11,61	98,42
MIN1-8	29,46	0,04	16,81	19,13	0,71	19,43	0,11	0,06	0,42	0,00	0,00	11,54	97,80
MIN1-9	29,47	0,04	16,84	19,06	0,72	19,99	0,02	0,05	0,35	0,00	0,00	11,60	98,19
Ore zone (Endoskarn)													
MIN8 1-5	27,53	0,00	18,91	19,81	0,52	19,48	0,05	0,05	0,04	0,00	0,00	11,54	97,91
MIN8 1-6	28,25	0,04	18,51	19,55	0,74	19,68	0,04	0,01	0,15	0,05	0,04	11,64	98,70
MIN8 1-7	27,89	0,02	18,72	19,68	0,63	19,57	0,04	0,01	0,09	0,03	0,02	11,58	98,31
MIN8 1-8	28,33	0,02	18,71	19,67	0,64	19,58	0,04	0,02	0,09	0,04	0,01	11,66	98,86
MIN8 2-2	27,89	0,02	18,61	19,68	0,63	19,49	0,04	0,02	0,09	0,01	0,01	11,56	98,08
MIN8 2-3	28,11	0,03	18,89	19,62	0,68	19,63	0,02	0,03	0,09	0,02	0,01	11,65	98,84
MIN8 3-1	28,00	0,02	18,75	19,65	0,66	19,58	0,04	0,01	0,10	0,00	0,03	11,61	98,47
MIN8 3-2	28,05	0,03	18,93	19,73	0,52	19,60	0,04	0,01	0,09	0,01	0,03	11,64	98,74
MIN8 3-3	27,81	0,02	18,92	19,84	0,66	19,73	0,03	0,02	0,12	0,04	0,03	11,62	98,69
Intermediate (IP)													
M1X1 2-3	28,48	0,03	17,28	20,77	0,75	19,38	0,03	0,02	0,16	0,00	0,00	11,53	98,42
M1X1 2-4	29,33	0,01	16,44	20,58	0,84	20,41	0,08	0,03	0,05	0,00	0,005	11,67	99,45
Intermediate (IP2)													
GLOM 6-3	27,19	0,02	19,13	21,70	0,93	18,25	0,01	0,01	0,02	0,00	0,01	11,48	98,75
GLOM 6-4	27,72	0,02	18,96	21,73	1,00	16,62	0,08	0,07	0,11	0,05	0,03	11,37	97,76
GLOM 4-3	26,89	0,00	19,34	20,92	0,96	18,16	0,00	0,01	0,00	0,00	0,00	11,39	97,66
GLOM 4-4	26,99	0,00	19,03	21,08	0,73	16,87	0,01	0,00	0,03	0,02	0,00	11,19	95,96
GLOM 1-3	27,25	0,03	19,68	22,11	0,87	17,74	0,02	0,02	0,05	0,00	0,00	11,54	99,31
GLOM 1-4	27,14	0,04	19,58	22,43	0,97	17,51	0,00	0,02	0,14	0,00	0,03	11,51	99,36
SUL13 5-4	27,13	0,05	18,90	20,74	0,81	18,59	0,02	0,03	0,04	0,00	0,00	11,44	97,76
SUL13 1-3	27,39	0,02	17,83	20,06	0,78	18,42	0,03	0,05	0,07	0,00	0,00	11,25	95,92
Late (LP)													
SUL4 2-3	28,79	0,00	17,12	20,94	0,60	19,84	0,04	0,01	0,03	0,00	0,04	11,61	99,02
SUL2 3-4	28,97	0,05	18,05	22,59	1,05	17,89	0,01	0,02	0,43	0,00	0,03	11,71	100,81
SUL2 3-5	28,74	0,00	16,78	21,16	1,01	19,00	0,02	0,00	0,05	0,00	0,03	11,49	98,30
SUL5 4-3	27,64	0,05	16,62	22,25	1,17	16,97	0,08	0,12	0,06	0,05	0,03	11,14	96,19

NOTES:

Analyses with high or low totals (>101 or <96 wt.%) or poor stoichiometries are omitted.

Si	Al ^{IV}	Al ^{VI}	Ti ⁴⁺	Fe ²⁺	Cr ²⁺	Mn ²⁺	Mg ²⁺	Ca ²⁺	Na ⁺	K ⁺	Ni	OH	O	XFe
6.12	1.88	2.09	0.01	3.10	0.00	0.13	6.36	0.00	0.03	0.17	0.01	16	36	0.33
6.13	1.87	2.13	0.00	3.08	0.00	0.13	6.29	0.00	0.03	0.11	0.00	16	36	0.34
6.11	1.89	2.11	0.01	3.11	0.00	0.12	6.34	0.00	0.03	0.15	0.00	16	36	0.34
6.13	1.87	2.14	0.00	3.05	0.00	0.12	6.32	0.01	0.02	0.01	0.00	16	36	0.34
6.11	1.89	2.05	0.00	3.15	0.00	0.11	6.44	0.01	0.03	0.08	0.00	16	36	0.33
6.08	1.92	2.15	0.00	3.08	0.00	0.13	6.29	0.01	0.02	0.17	0.00	16	36	0.34
6.09	1.91	2.09	0.00	3.10	0.00	0.13	6.42	0.00	0.03	0.12	0.00	16	36	0.33
6.06	1.96	2.13	0.01	3.26	0.00	0.13	6.30	0.00	0.01	0.08	0.00	16	36	0.34
6.09	1.94	2.24	0.01	3.39	0.00	0.12	5.88	0.04	0.03	0.15	0.00	16	36	0.37
6.15	1.88	2.14	0.01	3.27	0.00	0.13	6.15	0.01	0.02	0.15	0.00	16	36	0.35
6.09	1.91	2.20	0.01	3.21	0.00	0.13	5.99	0.02	0.04	0.30	0.00	16	36	0.36
6.11	1.89	2.17	0.01	3.19	0.00	0.12	6.06	0.01	0.03	0.18	0.00	16	36	0.35
6.03	1.97	2.15	0.00	3.26	0.00	0.12	6.18	0.02	0.04	0.22	0.00	16	36	0.35
6.10	1.90	2.21	0.01	3.19	0.00	0.12	5.99	0.02	0.05	0.22	0.00	16	36	0.36
6.07	1.93	2.18	0.01	3.19	0.00	0.12	6.14	0.00	0.04	0.19	0.00	16	36	0.35
5.72	2.28	2.35	0.00	3.45	0.00	0.09	6.04	0.01	0.02	0.01	0.00	16	36	0.36
5.82	2.19	2.31	0.01	3.37	0.01	0.13	6.05	0.01	0.00	0.04	0.01	16	36	0.36
5.77	2.23	2.34	0.00	3.36	0.00	0.11	6.03	0.01	0.01	0.05	0.00	16	36	0.36
5.82	2.18	2.35	0.00	3.29	0.00	0.11	5.99	0.01	0.02	0.05	0.00	16	36	0.36
5.78	2.22	2.33	0.00	3.36	0.00	0.11	6.02	0.01	0.01	0.05	0.00	16	36	0.36
5.77	2.23	2.36	0.00	3.31	0.00	0.12	6.01	0.01	0.02	0.05	0.00	16	36	0.36
5.78	2.22	2.34	0.00	3.33	0.00	0.11	6.02	0.01	0.01	0.05	0.00	16	36	0.36
5.77	2.23	2.36	0.00	3.33	0.00	0.09	6.01	0.01	0.01	0.05	0.01	16	36	0.36
5.74	2.26	2.34	0.00	3.39	0.01	0.11	6.01	0.01	0.01	0.06	0.00	16	36	0.36
5.92	2.08	2.15	0.00	3.61	0.00	0.13	6.01	0.01	0.01	0.04	0.00	16	36	0.38
6.03	1.98	2.01	0.00	3.54	0.00	0.15	6.25	0.02	0.01	0.01	0.00	16	36	0.36
5.66	2.34	2.36	0.00	3.78	0.00	0.16	5.67	0.00	0.01	0.00	0.00	16	36	0.40
5.83	2.19	2.51	0.00	3.82	0.01	0.18	5.21	0.02	0.03	0.03	0.00	16	36	0.42
5.65	2.36	2.43	0.00	3.67	0.00	0.17	5.69	0.00	0.00	0.00	0.00	16	36	0.39
5.76	2.25	2.54	0.00	3.77	0.00	0.13	5.37	0.00	0.00	0.01	0.00	16	36	0.41
5.65	2.36	2.45	0.00	3.83	0.00	0.15	5.48	0.01	0.01	0.01	0.00	16	36	0.41
5.64	2.37	2.43	0.01	3.90	0.00	0.17	5.42	0.00	0.01	0.04	0.00	16	36	0.42
5.69	2.32	2.35	0.01	3.64	0.00	0.14	5.81	0.01	0.01	0.01	0.00	16	36	0.38
5.84	2.17	2.31	0.00	3.58	0.00	0.14	5.85	0.01	0.02	0.02	0.00	16	36	0.38
5.95	2.06	2.11	0.00	3.62	0.00	0.10	6.11	0.01	0.00	0.01	0.01	16	36	0.37
5.93	2.08	2.27	0.01	3.87	0.00	0.18	5.46	0.00	0.01	0.11	0.00	16	36	0.41
6.00	2.01	2.12	0.00	3.69	0.00	0.18	5.91	0.00	0.00	0.01	0.01	16	36	0.38
5.96	2.06	2.16	0.01	4.01	0.01	0.21	5.45	0.02	0.05	0.02	0.00	16	36	0.42

Appendice Table B8. Matériaux de référence utilisés pour les analyses au LA-ICP-MS

Element	L.D	Gprob6				BC28			GSD-1			
		Working value	S.D.	This study Avg (n=4)	This study S.D.	Working value	This study Avg (n=5)	This study S.D.	Certified value	S.D.	This study Avg (n=4)	This study S.D.
Na	2,79	15506	1335	14415	434	n.a	8,90	3,39	26707	1484	27076	731
Mg	0,33	51318	6935	50062	967	11618	11751	398	21709	241	21143	486
Al	0,30	92145	12438	89395	1584	20787	18256	679	70922	1588	69426	1772
Si	1665	224259	9418	226771	9478	n.a	649	325	248657	3739	248368	8520
K	2,30	1577	166	1427	63	n.a	10,61	2,95	25300	300	25852	635
Ca	184	86787	4643	86053	1567	n.a	138,16	94,53	51429	714	50931	1227
Sc	0,21	36,8	2,6	39,7	0,7	31	25	1	52	2	53	1
Ti	0,10	7012	1319	6631	115	87615	71951	1515	7432	360	7303	161
V	0,03	238	27	292	7	9603	9555	254	44	2	49	2
Cr	1,00	300	22	341	8	1172	1358	51	42	3	45	2
Mn	2,33	1255	93	1273	18	2125	1907	63	220	20	219	5
Fe		72598	13310	73522	1189	571789	581927	13301	103422	20	102548	2346
Co	0,08	46,9	3,5	47,6	0,9	321	303	6	40	2	40	1
Ni	0,30	145,7	18,9	150,4	3,6	573	604	21	58	4	61	2
Cu	0,43	89,5	20,3	76,8	3,2	n.a	5	2	42	2	43	2
Zn	1,08	70,8	16,6	90,7	21,0	588	406	15	54	2	56	2
Ga	0,12	16	2	28	1	40	44	3	54	7	55	1
Ge	0,64	1,3	0,4	1,4	0,2	0,8	2,4	0,3	32	8	33	1
As	0,78	n.a	n.a	1,91	0,30	n.a	0,16	0,14	27	8	27	1
Sr	0,02	167	26	162	2	n.a	0,02	0,01	69,4	0,7	69,6	1,0
Y	0,01	19,3	1,8	18,3	0,3	0,10	0,01	0,00	42	2	40	1
Zr	0,01	55,1	2,4	52,8	0,8	20,0	19,1	1,1	42	2	42	1
Nb	0,01	4,16	0,41	3,81	0,13	1,7	1,5	0,1	42	3	41	1
Mo	0,01	n.a	n.a	0,40	0,10	0,5	0,4	0,1	39	3	39	1
Sn		1,33	0,71	1,61	0,25	2,0	1,1	0,1	29	6	29	1
Sb	0,13	0,13	0,01	0,18	0,05	0,02	0,04	0,03	43	7	46	1
Hf	0,01	1,52	0,15	1,44	0,09	1,00	0,75	0,06	39	2	38	1
Ta	0,01	0,28	0,03	0,24	0,02	0,07	0,13	0,01	40	4	38	0,5
W	0,04	n.a	n.a	0,30	0,06	0,51	0,01	0,01	43	4	43	1
Pb	0,09	3,3	0,8	3,6	0,1	1,98	0,02	0,01	50	2	49	1
Th	0,01	0,33	0,02	0,32	0,02	<0,1	0,01	0,00	41	2	41	1
U	0,01	0,29	0,03	0,34	0,03	n.a	0,01	0,00	41	2	42	1

NOTES:

Abbreviations: Avg = average; S.D. = standard deviation.

The internal standard used is the 57 Fe with the following values : 9.8 wt.% (GSE-1g), 10.3 wt.% (GSD-1g), 7.3 wt.% (Gprob6) and 57.2 wt.% (BC28). Working values for BC28 are taken from Dare et al. (2012).

Reference material : GSE-1-g

